Dissecting the molecular regulation of chromosome axis formation and sister chromatid cohesion during meiosis in *Arabidopsis thaliana*

A dissertation submitted in fulfillment of the requirements for a doctoral degree at the Faculty of Mathematics, Informatics and Natural Sciences

Department of Biology
Universität Hamburg

Submitted by

Chao Yang

2019 in Hamburg, Germany

Supervised by **Prof. Dr. Arp Schnittger**

1st Examiner: **Prof. Dr. Arp Schnittger**

2nd Examiner: **Prof. Dr. Sigrun Reumann**

Date of disputation: 25/10/2019

Index

Abstract

Meiosis is of central importance for sexually reproducing organisms as it allows for recombination of homologous chromosomes and halves the chromosome content of meiocytes, thus producing reduced gametes with different genetic make up. In plants, any aberration of meiosis could result in the production of aneuploid progeny, reduce plant fertility and thus decrease yield. Therefore, understanding the mechanisms and regulation of meiosis is essential for plant breeding and food supply. To warrant an accurate course of meiotic events, many unique meiotic features have evolved including the formation of a meiosis-specific type of sister chromatid cohesion and the assembly of a chromosome axis, which functions to ensure chromosome recombination and thus the faithful distribution of chromosomes to daughter cells. In this dissertation, I investigated the molecular regulation of chromosome axis formation and sister chromatid cohesion and could reveal new mechanisms of regulation.

First, the regulatory mechanism of sister chromatid cohesion in meiosis was studied. Cohesin, a conserved proteinaceous complex that creates cohesion, embraces the sister chromatids and establishes a physical structure on which other meiotic regulators can act, thus ensuring an accurate meiosis. The functional cohesin relies on its dynamic chromosome association that is under a spatiotemporal control. Here, combining biochemical, genetic and cytological approaches with live cell imaging, I demonstrate that SWITCH 1/DYAD, a cohesin regulator of yet unknown molecular function, identified two decades ago, defines a novel WINGS APART-LIKE (WAPL) antagonist that acts in the maintenance of sister chromatid cohesion in early meiotic prophase I.

Second, I focused on understanding the role of cyclin-dependent kinase CDKA;1 in meiosis, especially in the formation of the chromosome axis. In this study, I have identified ASYNAPTIC 1 (ASY1), a key component of chromosome axis, as a phospho-target of CDKA;1. I show that phosphorylation of ASY1 is required for its chromosome association by promoting its binding affinity towards ASYNAPTIC 3 (ASY3), another axial component, counteracting the disassembly activity of the AAA+ ATPase PACHYTENE CHECKPOINT 2 (PCH2). Furthermore, I have identified the closure motif in ASY1, typical for HORMA

domain-containing proteins, and provide evidence that the phosphorylation of ASY1 regulates the putative self-polymerization of ASY1 along the chromosome axis. Hence, the phosphorylation of ASY1 by CDKA;1 appears to be a two-pronged mechanism to initiate chromosome axis formation in meiosis.

Taken together, this work provides insights on understanding the complex regulation of meiosis in plants, especially on the regulation of meiotic chromosome axis formation and sister chromatid cohesion.

Zusammenfassung

Meiose ist von zentraler Wichtigkeit für sich sexuell reproduzierende Organismen, da sie die Rekombination homologer Chromosomen ermöglicht sowie den Chromosomensatz der Meiozyten halbiert und so die Produktion von Gameten mit unterschiedlicher genetischer Ausstattung ermöglicht. In Pflanzen können Fehler in der Meiose zur Erzeugung aneuploider Nachkommen führen, die verringerte Fertilität aufweisen und so den Ertrag mindern. Daher ist es für die Pflanzenzüchtung und somit auch die Nahrungsversorgung wichtig, die grundlegenden Mechanismen der Regulation der Meiose zu verstehen. Um einen korrekten Ablauf dieser besonderen Zellteilung zu garantieren, haben sich im Laufe der Evolution viele spezifische Charakteristika entwickelt, wie z.B. eine Meiose-eigene Kontrolle der Schwesterchromatidkohäsion sowie die Bildung einer Chromsomenachse, die die chromosomale Rekombination und damit die akkurate Verteilung der Chromosomen auf die Tochterzellen gewährleisten. In dieser Dissertation habe ich die molekularen Mechanismen der Ausbildung der Chromsomenachse und der meiotischen Schwesterchromatidkohäsion untersucht und konnte neue Regulationsmechanismen aufzeigen.

Zunächst habe ich den regulatorischen Mechanismus der Schwesterchromatidkohäsion in der Meiose analysiert. Kohäsin, ein konservierter Proteinkomplex, der die Kohäsion ermöglicht, umschließt die Schwesterchromatiden und dient als Strukturelement, das mit anderen meiotischen Regulatoren interagiert, um so den fehlerfreien Ablauf der Meiose sicherzustellen. Die Funktion von Kohäsin hängt von seiner dynamischen Chromosomenassoziation ab, die räumlich und zeitlich kontrolliert wird. Hier zeige ich, durch Kombination biochemischer, genetischer sowie zytologischer Methoden mit Live Cell Imaging, dass SWITCH 1/DYAD, ein Kohäsinregulator unbekannter molekularer Funktion, der vor zwei Jahrzehnten identifiziert wurde, einen neuen WINGS APART-LIKE (WAPL)-Antagonisten darstellt, der die Schwesterchromatidkohäsion in der frühen meiotischen Prophase I aufrechterhält.

Der zweite Teil meiner Arbeit befasst sich mit der Rolle der Cyclin-abhängigen Kinase CDKA;1 in der Meiose, insbesondere im Rahmen der Ausbildung der Chromosomenachse. In diesem Zusammenhang konnte ich zeigen, dass

ASYNAPTIC 1 (ASY1), eine Schlüsselkomponente der Chromsomenachse, ein Phosphorylierungssubstrat von CDKA;1 darstellt und dass die Phosphorylierung von ASY1 für dessen Chromosomenassoziation benötigt wird, indem es die Bindungsaffinität für das axiale Protein ASYNAPTIC 3 (ASY3), erhöht und so der Abbauaktivität der AAA+ ATPase PACHYTENE CHECKPOINT 2 (PCH2) entgegenwirkt. Darüber hinaus habe ich das sogenannte „Closure Motif“, das für Proteine mit HORMA-Domäne typisch ist, in ASY1 lokalisieren können und zeige, dass die Phosphorylierung von ASY1 dessen putative Selbstpolymerisation entlang der Chromosomenachse reguliert. Folglich scheint die Phosphorylierung von ASY1 durch CDKA;1 ein dualer Mechanismus zu sein, um die Ausbildung der Chromosomenachse in der Meiose zu initiieren.

Zusammenfassend gibt diese Arbeit Aufschluss über verschiedene Aspekte der komplexen Mechanismen der pflanzlichen Meiose, insbesondere über die Regulation der Ausbildung der Chromosomenachse und der Schwesterchromatidkohäsion.

INTRODUCTION

General introduction

Most eukaryotes are capable of sexual reproduction, which involves halving the chromosome sets during meiosis as a prerequisite for gamete formation and the restoration of the original ploidy during fertilization, i.e., the fusion of male and female gametes (Mercier *et al*, 2015; Bolcun-Filas & Handel, 2018). Meiosis, crucial for the sexual life cycle, is a specialized nuclear division, which consists of one round of DNA replication followed by two rounds of chromosome segregation: one reductional division in meiosis I where homologous chromosomes are segregated and one equational division in meiosis II, which leads to the separation of sister chromatids. During meiosis, homologous chromosomes of different parental origin are recombined and rearranged creating novel genetic combinations and thus the genetic diversity (Zickler & Kleckner, 2015; Lambing *et al*, 2017).

The integrity of these two rounds of DNA segregation relies on a series of innovations compared to mitosis. First, the reductional division which is conceptually different from mitosis, is characterized by homologous chromosome pairing, synapsis and the formation of crossovers (COs) between homologs (Wang & Copenhaver, 2018; Bolcun-Filas & Handel, 2018). Chromosome synapsis in early meiosis I links each pair of homologous chromosomes (homologs) and thereby facilitates the formation of COs that physically couple the homologs ensuring the faithful chromosome segregation at the end of meiosis I. The presence of at least one CO for every pair of homologs, known as CO insurance, is indispensable for the error-free separation and thus for halving the ploidy (Zickler & Kleckner, 2015; Osman *et al*, 2011). Second, the co-orientation of sister kinetochores during meiosis I and bi-orientation during meiosis II have to be achieved to ensure the balanced distribution of chromosomes during the first and second meiotic divisions (Watanabe, 2012). Third, the meiosis-specific type of sister chromatid cohesion which is subject to a special and sophisticated regulation, contributes to the precise chromosome segregation by influencing chromosome pairing, synapsis and recombination (Bolaños-Villegas *et al*, 2017; Morales & Losada, 2018; MIZPAH, 2018). Finally, the canonical rules of mitosis that ensure the integrity of cell cycle, e.g., DNA replication

prior to each nuclear division, have to be modified to prevent an intervening DNA replication between these two meiotic divisions (Mercier *et al*, 2015).

Overview of Meiosis

Meiosis I and II can each be further divided into four substages: prophase, metaphase, anaphase and telophase. In the genetic model plant *Arabidopsis thaliana*, complete meiosis takes approximate 32-35 h with about 23 h being dedicated to prophase I (Armstrong *et al*, 2003; Prusicki *et al*, 2018), which is a crucial phase for achieving many meiosis-specific events, e.g., homologous pairing, synapsis and recombination. According to morphological differences in chromosome appearance five steps of prophase I have been distinguished: leptotene, zygotene, pachytene, diplotene and diakinesis (Ma, 2006). Following DNA replication in interphase, chromosomes start to condense at very early prophase I, forming into the thin thread-like structures organized by the formation of the chromosome axes. This stage is called **leptotene**. In order to achieve the ploidy reduction in meiosis I, homologs must recognize each other and pair, preparing for separation afterwards. The process of homolog pairing (the temporal alignment of homologous chromosomes) represents a crucial and conserved process across sexually reproducing organisms but the mechanisms of homolog recognition still remains a puzzle. Finding of the right partner is likely facilitated by chromosome movement, especially by the formation of a structure called the telomere "bouquet" where telomeres cluster together near the nuclear envelope, and DNA homology is thought to be the key criteria for the evaluation of correct pairing. (Sybenga, 1999; Zickler & Kleckner, 2015; GENETICS OF MEIOTIC PROPHASE I IN PLANTS, 2016). As the chromosomes condense further, homologs start synapsing by the formation of a tripartite proteinaceous structure called the synaptonemal complex (SC). In **zygotene**, homologs are partially synapsed and thicker chromosomal structures (two homologous chromosomes connected together) can be observed under a light microscope. By the time synapsis is complete, fully synapsed homologs can be distinguished by a more linearized SC structure; this stage is called **pachytene**. During normal meiosis, the SC is formed exclusively between homologs coinciding with the progress of pairing. However, in some mutants of different organisms, e.g., yeast, wheat and maize, the SC is also assembled between non-homologs indicating that the formation of SC (synapsis) *per se* is not limited to

homologs and can be uncoupled from homologous pairing (Nairz & Klein, 1997; Ronceret *et al*, 2009; RILEY & CHAPMAN, 1958). During leptotene to pachytene homologous recombination takes place, becoming evident as chiasmata, which are crossovers (CO) between non-sister chromatids of homologs, in the next phase called **diplotene** (Mercier *et al*, 2015; Osman *et al*, 2011). In this phase the chromosomes become a bit de-condensed coinciding with the disassembly of the SC. Subsequently, the chromosomes re-condense tremendously, resulting in the formation of bivalents (paired, fully condensed chromosomes; five bivalents in the case of *Arabidopsis thaliana*) that can be clearly discerned under the light microscope, reaching the **diakinesis** stage at the end of prophase I (Fig. 1).

Following prophase I, the bivalents gradually move to and align at the center of the meiocyte, facilitated by the meiotic spindle, a cytoskeleton structure comprising microtubules and associated proteins. This stage is recognized as **metaphase I** (Fig.1). To ensure the balanced disjunction of homologs (each homolog moving to one of the opposite poles), the homologs can only be separated when all kinetochores of the chromosomes are attached correctly to spindle microtubules, which is monitored by the meiotic spindle assembly checkpoint (SAC) (Gorbsky, 2015; Marston & Wassmann, 2017; Watanabe, 2012). In meiosis I kinetochores of sister chromatids must be attached to microtubules emanating from the same spindle pole (co-orientation), which is regulated by different mechanisms including sister chromatid cohesion, kinetochore geometry and the tension generated between bivalents which is supervised the by Aurora B kinase being part of the SAC (Chelysheva *et al*, 2005; Watanabe, 2012; Monje-Casas *et al*, 2007). Once all the kinetochores are attached correctly by the microtubules, the SAC is shut off allowing homologs to be pulled to opposite poles while the sister chromatids co-segregate; this stage is called **anaphase I**. To avoid the premature separation of sister chromatids, only chromosome arm cohesin is released in meiosis I by the joint contribution of a prophase pathway and the endopeptidase separase while centromeric cohesin is protected. When the sets of chromosomes are well separated, the nuclear envelope briefly reforms marking **telophase I** (Fig.1).

Similarly to meiosis I, the second meiotic division (meiosis II) is also divided into four substages: prophase II, metaphase II, anaphase II and telophase II (Fig.1). In

comparison to meiosis I, meiosis II has a relatively short duration (about 4 h in *Arabidopsis*) and resembles a mitotic division. Prior to meiosis II, sister chromatids decondense at interkinesis, a short stage between meiosis I and meiosis II, and re-condense at **prophase II**. Subsequently, when chromosomes align at the metaphase plate in **metaphase II**, the kinetochores of the sister chromatids are attached by spindle microtubules emanating from opposite poles (bi-orientation) similar to mitosis. As soon as all kinetochores are correctly linked to the spindle microtubules, sister chromatids are separated, coinciding with the cleavage of centromeric cohesin, at the stage called **anaphase II**. Finally, when all chromatids have moved to the relevant poles, the nuclear envelope rebuilds **(telophase II)** and cytokinesis concludes the formation of four haploid daughter cells. Notably, in *Arabidopsis* cytokinesis in female meiocytes is executed twice, at the end of meiosis I and II (successive cytokinesis), while in male meiosis a simultaneous cytokinesis takes place at the end of meiosis II (Otegui & Staehelin, 2000).

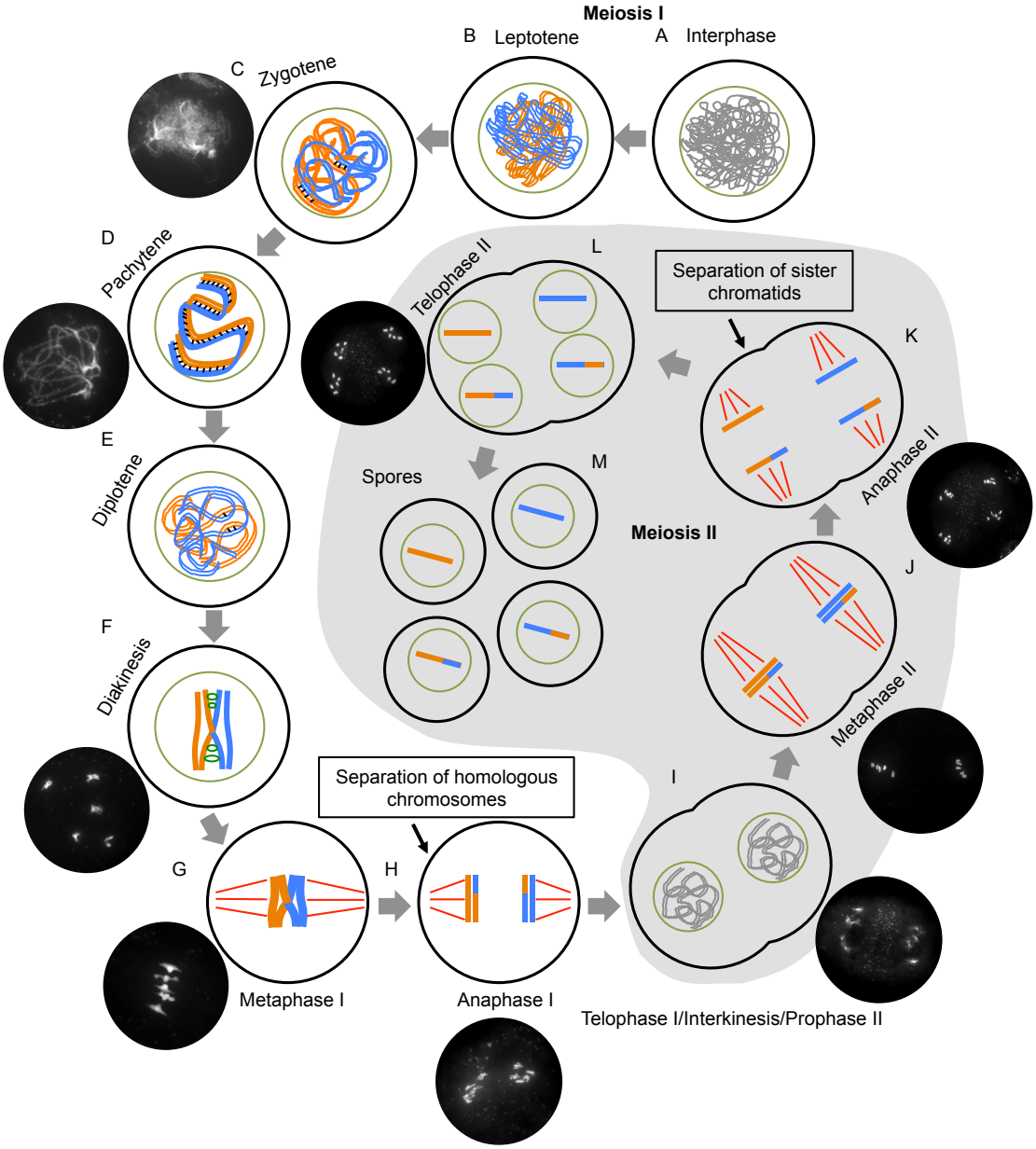

Figure 1. Schematic overview of male meiosis in *Arabidopsis*. (A) Interphase also called premeiosis consists of meiotic G1, S and G2 phases. (B) At leptotene, chromosome axes form and recombination initiates. (C) At zygotene, homologous chromosomes start pairing and synapsing mediated by the polymerization of a tripartite proteinaceous complex (synaptonemal complex, SC) and recombination progresses. (D) At pachytene, homologous chromosomes are fully synapsed and recombination continues. (E) At zygotene, the SC is disassembled and chromosomes partially decondense. Homologous chromosomes are linked through the crossovers. (F) At diakinesis, chromosomes further condense and bivalents connected by the chiasmata are visible. Prophase I ends followed by the nuclear envelope breaking down during prometaphase I. (G) At metaphase I, the spindle forms and aligns the bivalents in the metaphase plate. (H) At anaphase I, homologous chromosomes are distributed to two opposite poles following the release of cohesin complexes at chromosome arms while the pericentromeric cohesin is protected. (I) At interkinesis, meiosis I finishes and two nuclei are formed. Chromosomes experience a significant decondensation and meiosis II is prepared. (J) At metaphase II,

condensed univalent chromsomes are aligned in the respective metaphase plates facilitated by two spindles. (K) At anaphase II, sister chromatids are separated following the cleavage of cohesin at the pericentromeric regions. (L) At telophase II, four nuclei form and cytokinesis initiates. (M) At the end of meiosis, four haploid spores are formed after the cytokinesis. Chromosome spreads of the representative stages of the male meiosis in the wildtype are shown next to the cartoons.

Chromosome synapsis and the synaptonemal complex

Compared to mitosis, one of the most pronounced features of meiosis is chromosome synapsis, a very tight connection between chromosomes in comparison to the transient chromosome pairing occurring earlier. During leptotene, the chromatin of the sister chromatids is organized into loops by a proteinaceous axis known as the axial element (referred to as lateral element on synaptic chromosomes at later stages) that sits in the base of chromatin loops and serves as the framework to assemble the synaptonemal complex (SC) (Geelen, 2016; Mercier *et al*, 2015). The chromosome axis consists of sister chromatid cohesion components and other meiosis-specific axis proteins of which three have been characterized in plants: the coiled-coil domain-containing protein AtASY3 (Asynaptic3, corresponding to the Red1 homolog from yeast; PAIR3 in rice; DSY2 in maize), the HORMA domain-containing protein AtASY1 (Asynaptic1, the HOP1 homolog from yeast; PAIR2 in rice), and a small coiled-coil protein AtASY4 (Asynaptic4, the mammalian SYCP3/SCP3 homolog) (Armstrong, 2002; Ferdous *et al*, 2012; Wang *et al*, 2011; Lee *et al*, 2015) (Fig. 2).

Mutants deficient in any of these axial proteins show severe meiotic defects e.g., in chromosome synapsis, double strand break (DSB) formation and repair, inter-homolog biased recombination, and CO formation, highlighting the indispensable functions of the chromosome axis for those meiotic events (Armstrong, 2002; Ferdous *et al*, 2012; Wang *et al*, 2011; Lee *et al*, 2015). In *Arabidopsis*, ASY1 deficient mutants show drastic reduction of COs without obvious effect on DSB formation. This decrease in CO seems to be due to the unstable association of DMC1, a bacterial RecA ortholog functioning to promote the inter-homolog biased recombination. Thus the *asy1* mutant phenotype suggests that ASY1 plays a key role in coordinating the activity of DMC1 to create a bias in favor of using the homolog and not the sister chromatid as a template for the DSB repair (Sanchez-Moran *et al*, 2007). Similar to *asy1* mutants although less pronounced, COs are also reduced in *asy3* mutants, but in

this case the chromosome association of DMC1 is not affected and the phenotype is likely due to a decrease in DSBs (Ferdous *et al*, 2012). In both, *asy1* and *asy3* mutants, the vast majority of COs are found to be located to the ends of the chromosomes. Notably, despite a stronger defect in recombination, the chromosome association of ASY1 is found to be dependent on ASY3 in a non-reciprocal way, a relationship that seems conserved across the sexually reproducing organisms, including yeast, plants and animals (Ferdous *et al*, 2012; de los Santos & Hollingsworth, 1999; Wang *et al*, 2011; Lee *et al*, 2015).

More recently, Chambon and colleagues identified a new component of chromosome axis in *Arabidopsis*, Asynaptic4 (ASY4), that shows sequence similarity to the C-terminal coiled-coil domain of ASY3. It was interpreted to be a functional homologue of the mammalian axial component SYCP3/SCP3 despite limited sequence conservation (Chambon *et al*, 2018) (Fig. 2). Similar to ASY1 and ASY3, ASY4 is also an axis-associated protein detected by immunofluorescence analysis as a linear signal on chromatin from leptotene until pachytene. In the absence of *ASY4*, the plants show a slight but significant decrease in COs, which is less severe compared to that in *asy1* and *asy3* mutants (Chambon *et al*, 2018). ASY1, ASY3 and ASY4 seem to form into one complex crucial for the biogenesis of the meiotic chromosome axis and ASY4 is required for the normal ASY1 and ASY3 localization and for full synapsis to occur (Chambon *et al*, 2018).

Beginning in late leptotene, homologs recognize each other by largely not understood mechanisms and start synapsing in zygotene. The forming synaptonemal complex (SC) is composed of two lateral elements described above and one central element built by polymerizing transverse filament proteins (TF) that connect the two lateral elements (Fig. 2). Zip1 in budding yeast was the first TF protein identified and its homologs in other organisms have been characterized by different strategies. Although the exact function of the SC is still a mystery, its structure is very uniform across all sexually reproducing species analyzed to date. Despite the poor conservation of the central element proteins at the sequence level, they display a conserved secondary structure and assembly pattern, assembling reversely (N terminus of one molecule connects with the N-terminus of another molecule) in parallel with the N-terminal coiled-coil domain of the TF in the center and the C-

terminal globular domain associating with the lateral elements (Mercier *et al*, 2015; Higgins *et al*, 2005; Wang *et al*, 2010; Henderson & Keeney, 2005) (Fig. 2).

Zip1 homologs have been described in three plant species: Arabidopsis (AtZYP1a and AtZYP1b), rice (OsZEP1) and barley (ZYP1). In *Arabidopsis*, *ZYP1* knock-down lines by RNA interfering (RNAi) show only a slight reduction in the overall level of recombination, but extensive non-homologous recombination leading to the formation of multivalents (linking of several chromosomes) at metaphase I, suggesting that ZYP1 likely plays a role in preventing non-homologous recombination rather than promoting CO formation (Higgins *et al*, 2005). In comparison to Arabidopsis, rice ZEP1 deficient mutants show a slightly increased CO number, suggesting that ZEP1 in rice functions to limit CO formation (Wang *et al*, 2010). However, in barley, *ZYP1* knockdown plants show a drastic reduction of CO, which is similar to the observations in *zip1* mutants of budding yeast. This suggests ZYP1 in barley could promote the formation of CO as Zip1 does in yeast (Barakate *et al*, 2014). These observations indicate that besides the common structural role for the SC, the function of Zip1 homologs on recombination is quite diverse in different species.

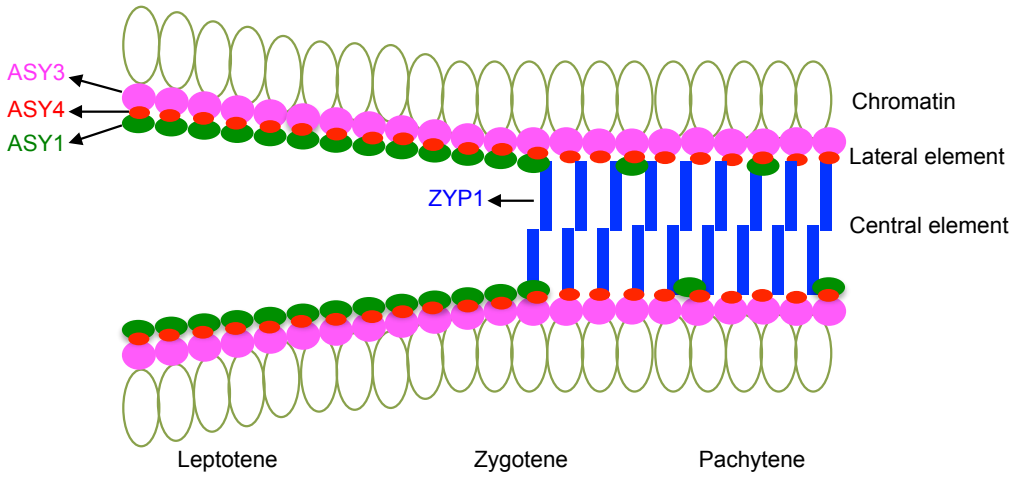

Figure 2. Schematic diagram of the synaptonemal complex (SC) in *Arabidopsis*. The SC comprises lateral and central elements. The lateral element is composed of the chromosome axis proteins including ASY1, ASY3 and ASY4; the central element is comprised of transverse filament proteins such as ZYP1, localizing in the central region..

Meiotic Recombination

DNA double-strand break formation

Meiotic recombination leading to the formation of COs between homologs is initiated by the programmed formation of DNA DSBs catalyzed by the conserved endonuclease SPOROLATION DEFECTIVE 11 (SPO11), a homologue of the A subunit of an archaeal topoisomerase VI (topo VI) (Wang & Copenhaver, 2018; Osman *et al*, 2011) (Fig. 3). SPO11 starts to localize on the chromatin in G2 and after DSB formation, SPO11 remains covalently associated with the 5' ends of the DNA on either side of the break sites until pachytene (Osman *et al*, 2011). In Arabidopsis, there are three SPO11 paralogs, two of which, SPO11-1 and SPO11-2, are required for meiotic recombination in a non-redundant manner; by contrast, SPO11-3 is involved in somatic endoreplication and does not play a role in meiosis. SPO11-1 and SPO11-2 function likely as a heterodimer and the catalytically active tyrosine residues of both proteins are required for DSB formation (Shingu *et al*, 2010; Stacey *et al*, 2006; Hartung *et al*, 2007). More recently, Vrielynck and colleagues identified a structural homologue of the topo VI B subunit in *Arabidopsis thaliana*, meiotic topoisomerase VIB-like (MTOPVIB), that is required for the formation of DSBs by mediating the formation of the SPO11-1/SPO11-2 heterodimer (Vrielynck *et al*, 2016).

In addition to SPO11, several regulatory and accessory proteins that are required for the DSB formation have been identified in plants by the classical genetic screens based on the fertility, e.g., AtPRD1, AtPRD2, AtPRD3 (OsPAIR1 in rice), AtDFO, OsCRC1 and OsP31^{comet} (Mercier *et al*, 2015; Osman *et al*, 2011; Lambing *et al*, 2017). These proteins tend to form distinct subcomplexes that interact to form a large recombination machinery by which DSBs are made. The N-terminal region of AtPRD1 interacts physically with AtSPO11-1, and thus could be a partner of AtSPO11 complexes. AtPRD1 shows sequence similarity to the mammalian MEI1, a protein required for the initiation of meiotic recombination, and thus seems to be a functional homologue of MEI1 (Wang & Copenhaver, 2018; Mercier *et al*, 2015). AtPRD2 shows limited sequence and secondary structure similarities to the yeast DSB formation proteins ScMei4/SpREC24. Such limited sequence and secondary structure similarities were also found between the yeast ScRec114/SpREC7 and the

plant meiotic protein PHS1. However, unlike the defects of DSB formation induced by the absence of *ScREC114/SpREC7*, the *phs1* mutants in neither maize nor *Arabidopsis* show any defective phenotype regarding DSB formation (Ronceret *et al*, 2009; Pawlowski *et al*, 2004). In contrast, AtPRD3/OsPAIR1 and AtDFO appear to be plant specific (Wang & Copenhaver, 2018). Moreover, rice CRC1, a homologue of yeast Pch2, is required for the DSB formation and was shown to interact with OsPAIR1. However, Pch2 is dispensable for the DSB formation in both yeast and *Arabidopsis*, suggesting a diverse regulation of DSB formation among species (Joshi *et al*, 2009; Lambing *et al*, 2015). Additionally, OsP31^{comet} was shown to form a complex with OsCRC1 in rice by which it contributes to the regulation of DSB formation (Ji *et al*, 2016).

DNA end processing and single-strand invasion

Following the formation of DSBs, 5' ends are resected yielding the 3' single-strand DNA (ssDNA) overhangs (Fig. 3). This process is catalyzed by a highly conserved Mre11-Rad50-Nbs1 (Xrs2 in yeast; MRN/X) complex together with Com1 (Sae2 in yeast) (Wang & Copenhaver, 2018). In Arabidopsis, AtMRE11 and AtRAD50 have been shown to be necessary for both mitotic and meiotic DSB repair while no function in meiotic DSB formation was identified (Puizina *et al*, 2004; Bleuyard *et al*, 2004). In contrast, AtNBS1 seems not to be essential for plant growth and meiosis under normal growth conditions, but the mutants show a hypersensitivity to DNA cross-linking reagents, suggesting a function of AtNBS1 in DNA repair under DNA damaging conditions. In addition, the depletion of *AtNBS1* exacerbates the meiotic and therefore fertility defects of plants without the DNA damage-response kinase ATM implying a role of AtNBS1 in DSB repair during the early stages of meiosis (Waterworth *et al*, 2007).

After the resection of the DSB ends, the resulting 3' ssDNA end invades one of the intact double-strand chromatids of the paired homologous chromosome by which a D-loop-like structure is formed (Fig. 3) (Wang & Copenhaver, 2018). This invasion process is mediated by RecA-related recombinases, e.g., RAD51 and DMC1 and facilitated by several cofactors such as XRCC3, RAD51B, RAD51C, RAD51D, and BRCA2 (Mercier *et al*, 2015). RAD51 plays roles in both mitotic and meiotic DNA repair, while DMC1 is exclusively involved in meiosis. The DMC1-mediated

inter-homologous (IH) repair is thought to be the main pathway, while RAD51 works in a backup pathway using the sister chromatid as a template for repair when DMC1 is absent (Kurzbauer *et al*, 2012; Mercier *et al*, 2015). Recent progress made by the analysis of transgenic *Arabidopsis* plants expressing a C-terminal GFP-tagged RAD51 that retains only the DNA-binding property, but has no catalytic activity in different mutant backgrounds, shows that the catalytic activity of RAD51 is dispensable for the DMC1-dependent IH repair, suggesting that RAD51 functions as an accessory factor of DMC1 during meiotic recombination (Da Ines *et al*, 2013).

Crossover formation

Following strand invasion and the formation of double holliday junctions (dHJs) dHJs are primarily resolved into either interference-sensitive class I or interference-insensitive class II COs. Theoretically dHJs can also resolve in NCOs, however there is no data on how often this occurs *in vivo* (Allers & Lichten, 2001; Wang & Copenhaver, 2018) (Fig. 3). Class I COs constitute the majority of COs (~85%) and are dependent on the ZMM group proteins (AtMSH4, AtMSH5, AtMER3, AtSHOC1, AtZIP4, AtHEI10, and AtPTD), as well as on AtMLH1 and AtMLH3. Single mutations in *AtMSH4, AtMSH5, AtSHOC1, ATZIP4 AtPTD, and AtHEI10* as well as different mutant combinations of these genes reduce the number of COs drastically to about 15% of the wildtype level (Mercier *et al*, 2015; Wang & Copenhaver, 2018). While *Atmer3* mutants show a slightly higher level of CO frequency (~25%), the combination of *Atmer3* with another *zmm*-type mutation results in a similar CO level (~15%) as seen for the other single *zmm* mutants. In *Atmlh1* and *Atmlh3* mutants CO frequency is reduced to only about 50% of the wild-type level, however similar to the co-depletion of *AtMER3* and one additional *ZMM* protein, the *Atmlh1 zmm* and *Atmlh1 zmm* double mutants resemble the single *zmm* mutants with about 15% wild-type level CO frequency.

These observations suggest that the ZMM-dependent CO pathway is the major one but that it is not unique (Mercier *et al*, 2015). In contrast, much less is known about the molecular players of the class II COs with AtMUS81 being the sole one identified so far. *Atmus81* mutants show a CO decrease by ~10% and eliminate ~33% of the residual COs when being combined with a *zmm* mutant. This suggests that

AtMUS81 only accounts for a part of the ZMM-independent COs, but which factors are responsible for the remaining COs is still unknown (Mercier *et al*, 2015).

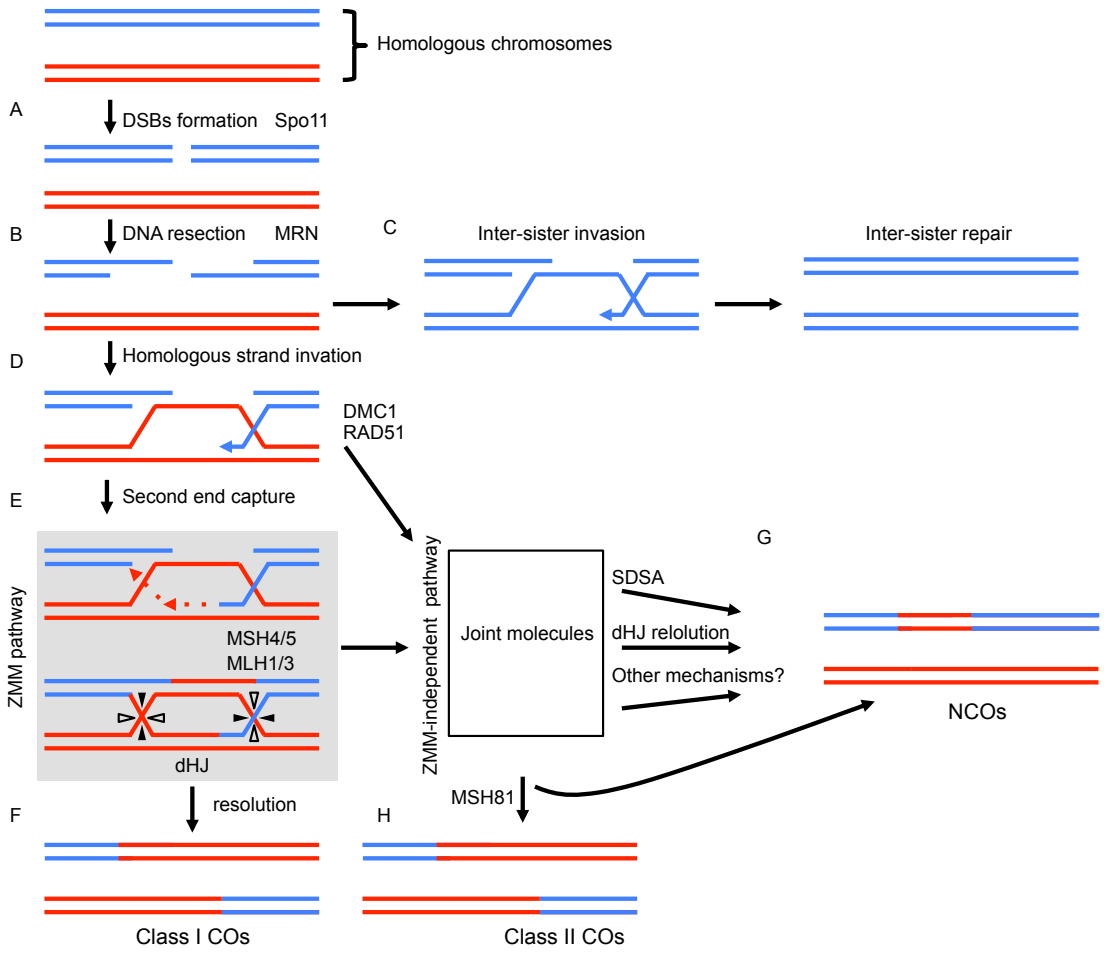

Figure 3. Model of meiotic recombination in *Arabidopsis*. Meiotic recombination is initiated by the formation of DSBs catalyzed by Spo11 (A), which are further resected into 3'-OH overhanging single-strand DNA by the MRN complex. The generated single-strand DNA then invades either the sister chromatid (C) or one of the non-sister chromatids of the homologous chromosome with the help of RAD51 and DMC1 recombinases, thereby forming a D-loop (D). The formed DNA intermediates are stabilized and further processed by the components of the ZMM pathway of crossover formation, resulting in the formation of double Holliday junctions (dHJs) (E). The intermediates including the dHJs are further resolved into either the class I crossovers (COs) or non-crossovers (NCOs) through different mechanisms (F,G). In addition, a portion of intermediates is resolved into class II COs by a ZMM-independent pathway (H).

Sister chromatid cohesion

In eukaryotic organisms, the genomic material is duplicated during the S phase forming sister chromatids which are held together by the cohesin complex until being segregated into daughter cells at anaphase. Sister chromatid cohesion mediated by the cohesin complex plays crucial roles in genome stability, DNA repair, chromatin structure organization, and gene expression in eukaryotes (Bolaños-Villegas *et al*, 2017; Makrantoni & Marston, 2018; Litwin *et al*, 2018).

Cohesin is an evolutionarily conserved complex, which consists of four core subunits: two ATPases of the structural maintenance of chromosome (SMC) type, SMC1 and SMC3, the heat-repeat domain protein SCC3/SA, and one α-kleisin called SCC1 which is replaced by REC8 in meiosis (Bolaños-Villegas *et al*, 2017). One widely accepted model for cohesin is that it forms a ring-shaped structure enwrapping two DNA molecules and thereby holding sister chromatids together.

The distribution of cohesin on chromosomes is very dynamic during the cell cycle comprising cohesin loading, establishment, maintenance and the final release from chromosomes (Fig. 4). Cohesin is loaded on chromosomes by the cohesin loader SCC2-SCC4 complex at G1 phase and cohesion is established as DNA replication progresses during the subsequent S phase (Bolaños-Villegas *et al*, 2017). Cohesin is then maintained on chromosomes until late G2 in the mitotic cell cycle and early prophase I in meiosis, respectively. As the cell cycle progresses, cohesin especially on chromosome arms, is first removed by a WAPL-mediated non-proteolytic prophase pathway, and the rest is then released by a separase-dependent proteolytic cleavage of the kleisin subunit SCC1/REC8 when the cell reaches anaphase (anaphase II in meiosis) (Bolaños-Villegas *et al*, 2017; Makrantoni & Marston, 2018). For more details on the regulation of cohesin see the manuscript in chapter 1.

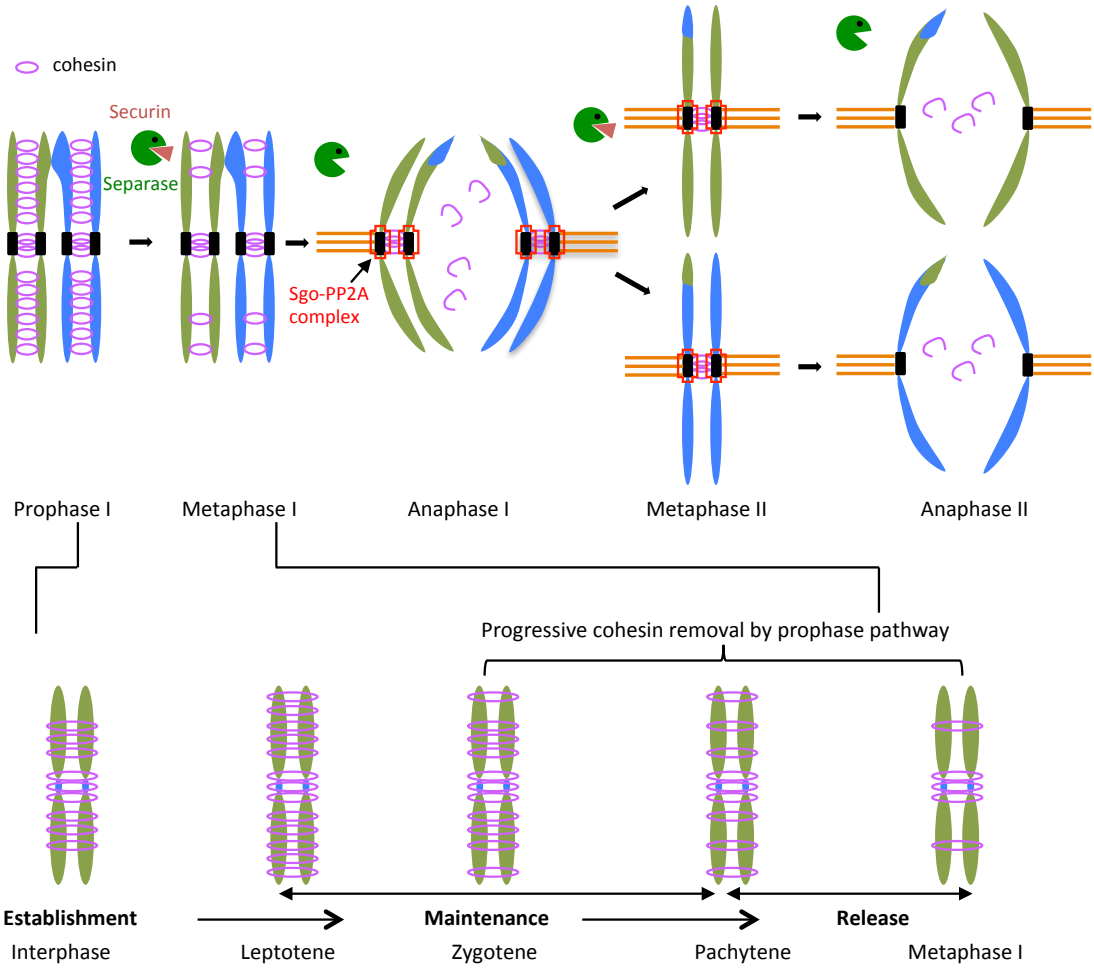

Figure 4. Schematic representation of the cohesin dynamics during meiosis. Sister chromatid cohesion is essential for the chromosome pairing, synapsis and recombination, thereby ensuring the faithful reduction and segregation of chromosomes. Cohesin rings are loaded and closed on chromosmes thus establishing sister chromatid cohesion during interphase, which is then largely maintained at leptotene and zygotene. Cohesin on chromosome arms then experiences a drastic removal by the prophase pathway during late prophase I. At the anaphase I onset, the rest cohesin on chromosome arms is cleaved completely by Separase, while the centromeric cohesin is protected until metaphase II by the Shugoshin-PP2A (Sgo-PP2A) complex. Afterwards, the remaining cohesin at centromeres is released by the cleavage of Separase at the anaphase II onset allowing the separation of sister chromatids.

Research aim

The reproduction of the majority of eukaryotes relies on meiosis, a highly regulated and intricate process, which is yet not fully understood. In comparison to mitosis, a unique feature of meiosis is the formation of the chromosome axis that organizes the duplicated sister chromatin into a linear array of DNA loops (Zickler & Kleckner, 2015) and builds the base for the synapsis and recombination. Thus, the faithful formation of a chromosome axis is fundamental to meiosis.

While the functions of the chromosome axis have been extensively characterized, the mechanisms underlying its assembly and disassembly, which requires a tight spatiotemporal regulation, are largely unknown. To understand these features would not only provide insights into the fundamental mechanisms of meiosis, but also open a door to modulate the meiotic crossover pattern via structural modification of the chromosome axis at will thus facilitating plant breeding.

In the course of my dissertation I first tackled the question of how meiotic cohesin is regulated and maintained on chromosomes in early prophase I leading to the discovery of a novel molecular mechanism. The results are presented in chapter 1 in the form of a recently published paper (Yang *et al*, 2019). Second, the regulation of chromosome axis formation, especially the chromosome assembly of ASY1, was studied, and also here a new mechanism was revealed, which I present in chapter 2 in the form of a manuscript currently under revision. Chapter 3 describes the exploration of the function of the here-identified closure motif of ASY1 and several results are presented, that shed light on the assembly mechanisms of the meiotic HORMA domain-containing proteins.

Chapter 1

1.1 Published paper

SWITCH 1/DYAD is a WINGS APART-LIKE antagonist that maintains sister chromatid cohesion in meiosis

Authors: Chao Yang[1], Yuki Hamamura[1], Kostika Sofroni[1], Franziska Böwer[1], Sara Christina Stolze[2], Hirofumi Nakagami[2] and Arp Schnittger[1,*]

Affiliations:

[1] Department of Developmental Biology, University of Hamburg, 22609 Hamburg, Germany.

[2] Max-Planck-Institute for Plant Breeding Research, 50829 Cologne, Germany.

*Correspondence to: arp.schnittger@uni-hamburg.de

Published on ***Nature Communications*** 10, 1755 (2019)

SWITCH 1/DYAD is a WINGS APART-LIKE antagonist that maintains sister chromatid cohesion in meiosis

Abstract

Mitosis and meiosis both rely on cohesin, which embraces the sister chromatids and plays a crucial role for the faithful distribution of chromosomes to daughter cells. Prior to the cleavage by Separase at anaphase onset, cohesin is largely removed from chromosomes by the non-proteolytic action of WINGS APART-LIKE (WAPL), a mechanism referred to as the prophase pathway. To prevent the premature loss of sister chromatid cohesion, WAPL is inhibited in early mitosis by Sororin. However, Sororin homologs have only been found to function as WAPL inhibitors during mitosis in vertebrates and Drosophila. Here we show that SWITCH 1/DYAD defines a novel WAPL antagonist that acts in meiosis of Arabidopsis. Crucially, SWI1 becomes dispensable for sister chromatid cohesion in the absence of *WAPL*. Despite the lack of any sequence similarities, we found that SWI1 is regulated and functions in a similar manner as Sororin hence likely representing a case of convergent molecular evolution across the eukaryotic kingdom.

Introduction

The tight regulation of sister chromatid cohesion is essential for accurate chromosome segregation during mitosis and meiosis. During S-phase, the genomic DNA is duplicated resulting in the formation of two sister chromatids per chromosomes. The newly formed sister chromatids are held together by the cohesin complex, which builds a ring-like structure embracing the chromatids. Besides sister chromatid cohesion, the cohesin complex is crucial for genome stability, DNA repair, chromatin structure organization, and gene expression (Bolaños-Villegas *et al*, 2017; Litwin *et al*, 2018; Makrantoni & Marston, 2018; Suja & Barbero, 2009).

The cohesin complex is highly conserved in the eukaryotic kingdom with homologs present from animals to plants comprising four core subunits: SMC1 and SMC3, two ATPases that belong to the family of structural maintenance of chromosomes (SMC) proteins, the heat-repeat domain protein SCC3/SA and one α-kleisin component RAD21/SCC1, which is replaced in meiosis by REC8/SYN1.

The presence of cohesin on chromosomes is very dynamic. Cohesin is already loaded onto chromosomes by the SCC2-SCC4 loader complex during the G1 phase of the cell cycle. Sister chromatid cohesion is established in the subsequent S-phase and regulated by several cohesin accessory proteins, including the PRECOCIOUS DISSOCIATION OF SISTER 5 (PDS5) and WINGS APART-LIKE (WAPL) (Ciosk *et al*, 2000; Watrin *et al*, 2006; Petela *et al*, 2018). PDS5 assists the acetylation of the SMC3 subunit by Establishment of cohesion 1 (Eco1)/Chromosome Transmission Fidelity 7 (CTF7), needed to close the cohesin ring (Lengronne *et al*, 2006; Ben-Shahar *et al*, 2008; Vaur *et al*, 2018). Cohesin is then maintained on chromosomes until late G2 in the mitotic cell cycle and early prophase I in meiosis, respectively. As cell division is approaching metaphase, cohesin, especially on chromosome arms, undergoes tremendous removal mediated by the cohesin dissociation factor WAPL, a process known as prophase pathway of cohesin removal (De *et al*, 2014; Gandhi *et al*, 2006; Sutani *et al*, 2009; Challa *et al*, 2019). At the centromeric regions, cohesin is largely protected by the Shugoshin-PP2A complex (Liu *et al*, 2013; Hara *et al*, 2014). This centromeric cohesin is released by a Separase-dependent proteolytic cleavage of the kleisin subunit RAD21/REC8, thereby allowing the separation of sister chromatids at anaphase onset (anaphase II in meiosis).

To prevent a premature release of sister chromatid cohesion in mitosis, especially on chromosome arms, Sororin counteracts the releasing force of WAPL by binding to PDS5 and displacing WAPL from PDS5 (Ladurner *et al*, 2016; Nishiyama *et al*, 2010; Kueng *et al*, 2006; De *et al*, 2014). However, Sororin has so far only been identified in vertebrates. More recently, an ortholog of Sororin, named Dalmatian, was found in *Drosophila*, which exert both Sororin's cohesin stabilizing and Shugoshin's cohesin protecting functions in mitosis (Yamada *et al*, 2017).

In late prophase, Sororin is recognized by the APC/C^{Cdh1} (Anaphase-promoting complex/cyclosome) and degraded by the ubiquitin-proteasome pathway, thereby releasing its repression of WAPL and activating the prophase removal of cohesin (Rankin *et al*, 2005; Nishiyama *et al*, 2010). Phosphorylation through Cdk1 (cyclin-dependent kinase 1) and Aurora B kinase serves thereby as a signal for the degradation of Sororin (Dreier *et al*, 2011; Nishiyama *et al*, 2013).

In contrast to mitosis, it is not clear how sister chromatid cohesion is protected during early meiotic prophase I. Notably, Sororin does not seem to play a role for the regulation of meiotic cohesion. Although Sororin is present in male meiosis in mouse,

it is exclusively localized on the central regions of the synaptonemal complex (SC) and not on the axial/lateral elements of SC where the cohesin complex is found (Gómez *et al*, 2016). This localization pattern makes Sororin unlikely, at least in mouse, be the protector of cohesin. This conclusion is substantiated by the finding that the localization of Sororin in the central region of the SC is not dependent on the meiosis-specific subunits REC8 and SMC1β (Gómez *et al*, 2016).

In contrast, WAPL has been found to remove meiotic cohesin at late prophase in most if not all organisms studied including Arabidopsis and other plants (De *et al*, 2014; Brieño-Enríquez *et al*, 2016; Challa *et al*, 2016; Crawley *et al*, 2016; Challa *et al*, 2019). Thus, it remains a puzzle how the activity of WAPL is inhibited in early meiotic prophase I especially since no obvious sequence homolog of Sororin or Dalmatian has been identified in the plant lineage and other major branches of the eukaryotic kingdom (Rankin, 2005).

Here, we report that the previously identified *SWI1* gene in *Arabidopsis* encodes a novel WAPL inhibitor. Despite any sequence similarities between SWI1 and Sororin, we further reveal that SWI1 antagonizes WAPL in prophase I of meiosis through a similar strategy as Sororin in mitosis. Moreover, SWI1 turned out to be amazingly similarly regulated in Arabidopsis as Sororin in vertebrates.

Results

Removal of meiotic cohesin is mediated to large extent by WAPL

To get an understanding of cohesin dynamics during meiosis, we followed the expression and localization of a previously generated functional REC8-GFP reporter in male meiocytes by live cell imaging (Prusicki *et al*, 2018). We observed that the majority of cohesin (~90%) in the wildtype, but not in the previously described *wapl1 wapl2* double mutant(De *et al*, 2014), is already largely released from chromatin prior to anaphase I indicating that the impact of the WAPL-dependent prophase pathway on cohesin removal is very strong in male meiosis of Arabidopsis (Fig. 1a-c, Supplementary Video S1, S2).

To follow WAPL1, we generated a WAPL1-GFP reporter, which fully complemented the *wapl1 wapl2* defects (Supplementary Fig. S1) and accumulated in somatic cells of the anther and in male meiocytes. In meiocytes, the WAPL1-GFP signal showed a homogeneous distribution in the nucleoplasm from pre-meiosis until

leptotene, suggesting no or only a very weak interaction of WAPL1 with chromatin (Fig. 1d i,ii). Subsequently, foci and/or short stretches of WAPL1-GFP appeared in the nucleus at late leptotene/early zygotene, coinciding with the eviction of cohesin from chromatin (Fig. 1d iii). The accumulation of WAPL1-GFP signal on chromatin became more prominent in zygotene and pachytene, which is consistent with the progressive release of cohesin (Fig. 1c, Fig. 1d iv,v). In metaphase I, WAPL1-GFP was found at condensed chromosomes (Fig.1d vi). While WAPL1-GFP signal is still present in the nucleus after the first meiotic division until tetrad stage, it was not localized to chromatin any longer (Fig. 1d vii,viii). This localization pattern was confirmed by immuno-localization of WAPL1-GFP using an antibody against GFP (Supplementary Fig. S1c).

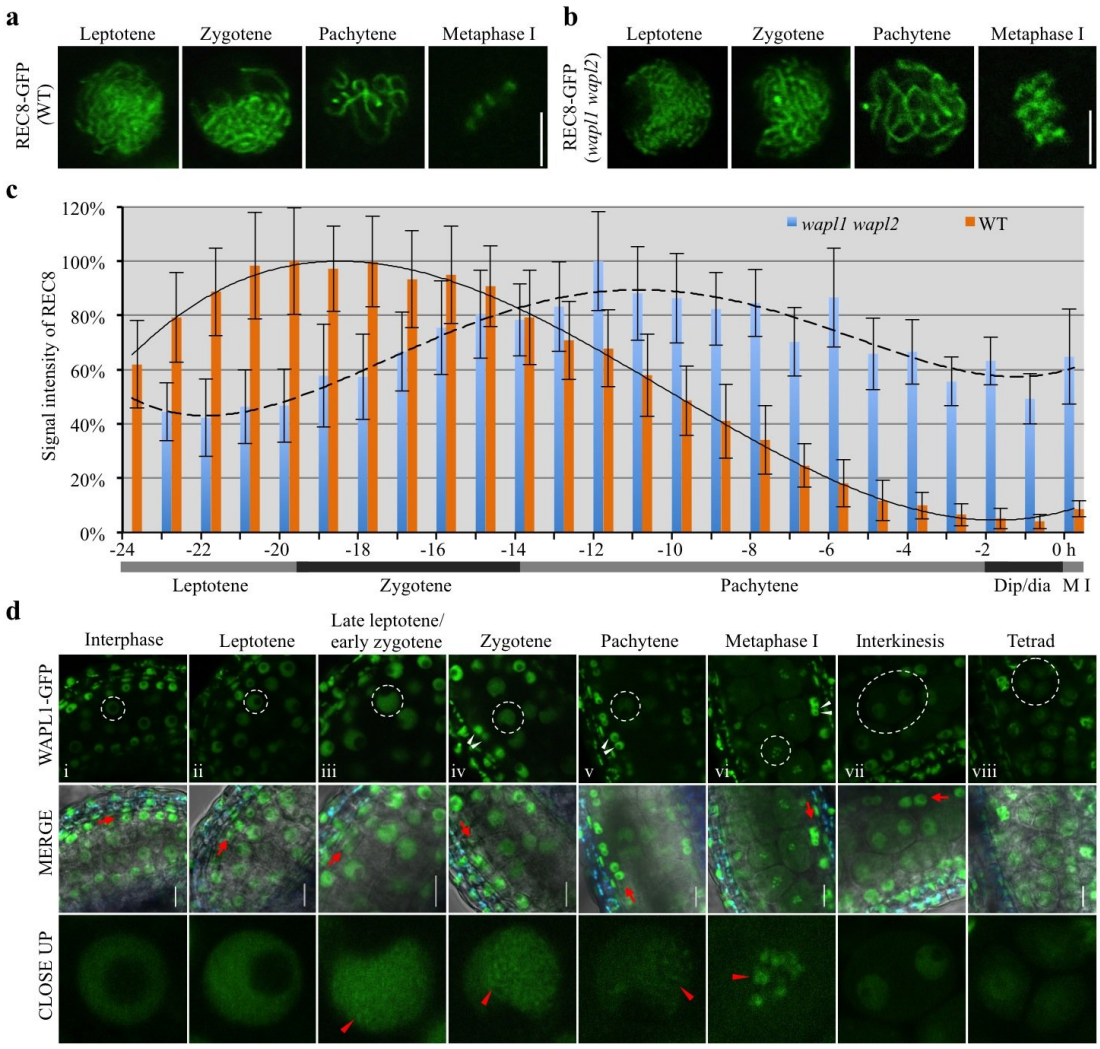

Figure 1. Dynamics of REC8 and WAPL in male meiocytes. (a, b) Confocal laser scanning micrographs of REC8-GFP localization in male meiocytes in the wildtype

(WT) (a) and in *wapl1 wapl2* double mutants (b). Bar: 5 μm. (c) Quantification of cohesin during meiosis I in male meiocytes of the wildtype (WT) and *wapl1 wapl2* mutants based on a REC8-GFP reporter. The graph represents the relative fluorescence intensity of the REC8-GFP signal; error bar represents standard deviation of at least 20 meiocytes analyzed. Dip/dia: diplotene/diakinesis, M I: metaphase I. Polynomial trendlines are shown (correlation coefficient R^2= 0.997 and 0.898 for the wildtype (solid line) and *wapl1 wapl2* (dashed line), respectively. (d) Confocal laser scanning micrographs of WAPL1-GFP in anthers of *wapl1 wpal2* double mutants. Dashed white cycles indicate the meiocytes magnified in the close-up panel in the bottom row. Red arrowheads denote the accumulated WAPL1-GFP signal at chromatin. Red arrows indicate the layer of tapetal cells that are used as one of the criteria for staging. White arrowheads depict bi-nuclear tapetal cells. Bar: 5 μm. **The figure (c) is kindly provided by Yuki Hamamura using the materials prepared by Chao Yang.**

SWI1 is expressed in early meiosis

The observation that WAPL1 is already present in early prophase at a time point when REC8 removal from chromatin has not started, suggested the existence of a WAPL repressor that might prevent WAPL from localizing to chromatin and unloading cohesin prematurely. However, no obvious sequence homolog of Sororin, the only known WAPL repressor in mitosis, exists in Arabidopsis (Rankin, 2005). We reasoned that a potential repressor of WAPL during meiosis should have all or least some of the following characteristics: First, mutants of this repressor should experience premature loss of sister chromatid cohesion and hence probably have a strong mutant phenotype in meiosis. In turn, this makes it likely that such a mutant has already been identified due to the extensive search for meiotic mutants in Arabidopsis. Second, this repressor would probably be a protein of unknown molecular function. Third, as a regulator of sister chromatid cohesion, this factor should interact with the cohesin complex and hence, its correct localization to chromatin may also depend on a functional cohesin complex.

The gene *SWITCH1* (*SWI1*), also known as *DYAD*, was previously identified based on its requirement for sister chromatid cohesion in meiosis (Mercier *et al*, 2001; Mercier, 2003; Ravi *et al*, 2008). SWI1 encodes for a protein of unknown biochemical function and its mechanism of action has been unresolved up to now.

However, SWI1 was previously reported to be exclusively expressed in interphase prior to meiosis and could neither be detected in leptotene nor in any subsequent meiotic stage (Mercier *et al*, 2001; Mercier, 2003). This expression pattern is difficult to reconcile with the *swi1* mutant phenotype, e.g., a failure to assemble the chromosome axis and to establish sister chromatid cohesion. Therefore, we revisited the expression pattern of *SWI1* in both male and female meiocytes by generating a genomic reporter in which the coding region of *GFP* was inserted directly before the STOP codon of *SWI1*. Expression of this reporter in *swi1* mutants could fully restore a wild-type meiotic program (Supplementary Fig. S2). To stage the expression of SWI1, we also generated a functional reporter line for the chromosome axis protein ASYNAPTIC 3 (ASY3), where RFP was used as a fluorescent protein (Supplementary Fig. S3).

Consistent with previous reports, SWI1 was first detected as numerous foci/short stretches in interphase nuclei of both male and female meiocytes (Fig. 2a; Supplementary Fig. S4). In addition, the SWI1-GFP signal was present in leptotene and became even stronger as cells progressed through leptotene as staged by the migration of the nucleolus to one side of the nucleus (Wang *et al*, 2004; Stronghill *et al*, 2014; Yang *et al*, 2006) and the appearance of an ASY3 signal on condensing chromosomes (Fig. 2a, Supplementary Fig. S4). This analysis also showed that SWI1 is chromatin associated. In zygotene, when chromosomes further condensed, highlighted by ASY3-RFP, the SWI1 signal strongly declined until it was not detectable any longer in late pachytene (Fig. 2a, Supplementary Fig. S4).

To confirm that SWI1 reaches its expression peak in late leptotene and decreases by zygotene, we constructed a reporter line for ZYP1b, a component of the central element of the synaptonemal complex. Since a fusion of ZYP1b to RFP resulted in only a very weak fluorescent signal, we generated a ZYP1b-GFP fusion along with a fusion of SWI1 to RFP, which could also restore full fertility and meiotic progression of *swi1* mutants (Supplementary Fig. S5, S6). In late leptotene, the SWI1-RFP signal is strongly present on chromosomes while no signal for ZYP1b was detected (Fig. 2b). From zygotene onwards, when short stretches of ZYP1b indicate partially synapsed chromosomes, the SWI1 signal was hardly detectable, corroborating that SWI1 is largely absent from chromosomes after zygotene corresponding to the removal of REC8 (Fig. 1a).

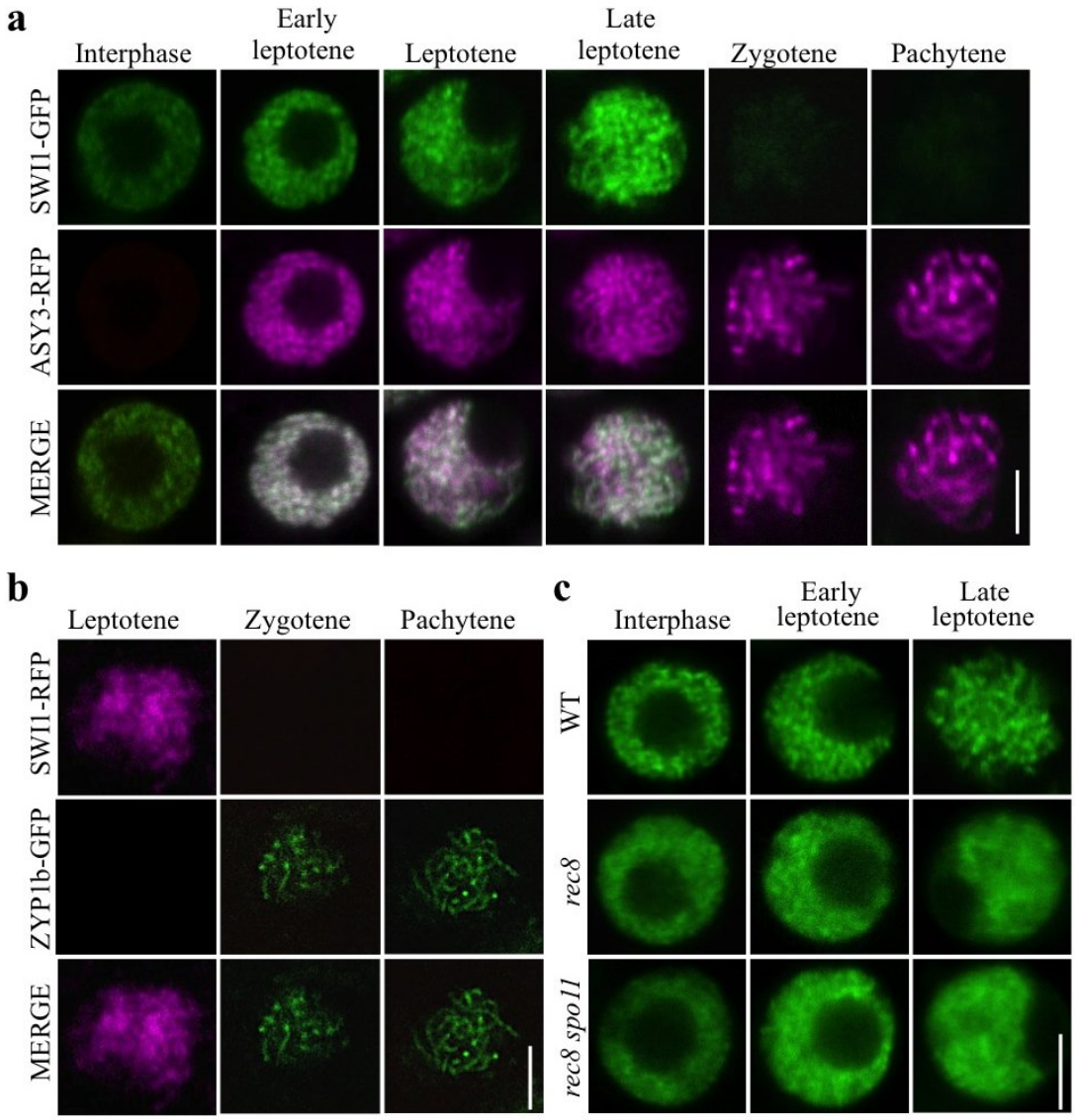

Figure 2. Localization pattern of SWI1. Co-localization analysis of SWI1-GFP with ASY3-RFP (a) and SWI1-RFP with ZYP1b-GFP (b) during interphase and prophase I of wild-type male meiocytes using confocal scanning laser microscopy. (c) SWI1-GFP in the male meiocytes of the wildtype (WT), *rec8* and *rec8 spo11* mutants during interphase and prophase I. Bar: 5 μm.

Chromatin association of SWI1 and REC8 is mutually dependent on each other

Establishment of sister chromatid cohesion has been shown to be compromised during meiosis in *swi1* and cohesin components, e.g., REC8 and SMC3, were found to be not properly bound to chromosomes in this mutant (Mercier *et al*, 2001). Using live cell imaging and immunodetection assays, we confirmed these cohesion defects by

studying REC8-GFP in three different mutant alleles, *swi1-2*, *swi1-3*, and *swi1-4*, that showed identical REC-GFP localization defects (Fig. 5a, Supplementary Fig. S7).

To address whether SWI1 localization also depends on cohesin, we introgressed the *SWI1-GFP* reporter into *rec8* mutants. While no obvious differences were found in interphase in comparison to *swi1* mutants complemented by the expression of *SWI1-GFP*, we found that SWI1 did not properly localize to chromatin in *rec8* mutants in prophase (Fig. 2c). This failure was not due to chromatin fragmentation present in *rec8* since we observed the same pattern when the *SWI1* reporter was introgressed into *rec8 spo11* double mutants in which the endonuclease SPORULATION DEFECTIVE 11 (SPO11) is not functional and hence no double strand breaks are formed.

However, immunolocalization experiments using an antibody against GFP corroborated that residual levels of SWI1 remain on chromatin in *rec8* mutants that expressed the SWI1-GFP reporter construct. This suggested that chromatin association of SWI1 also relies on other factors in addition to the REC8-containing cohesin (Supplementary Fig. S8a).

SWI1 interacts with PDS5 family proteins

A direct interaction of SWI1 with one of the cohesin components is a likely explanation for the observation that proper SWI1 localization is dependent on cohesin. To explore this possibility, we tested the interaction of SWI1 with all core cohesin subunits including SMC1, SMC3, REC8 and SCC3 by yeast two-hybrid assays. However, SWI1 did not interact with any of these proteins (Supplementary Fig. S9a). We further investigated the interaction of SWI1 with the cohesin accessory proteins PDS5A, one of the five *PDS5* genes in *Arabidopsis*, and WAPL1, one of the two WAPL homologs. While we did not find an interaction of SWI1 with WAPL1, SWI1 strongly interacted with the N-terminus but not the C-terminus of PDS5A (Fig. 3a, Supplementary Fig. S9b). The interaction domain of SWI1 was then determined to reside in the N-terminal 300 amino acids as the C-terminal domain from amino acid 301-639 failed to bind to N-terminus of PDS5A (Fig. 3a). This interaction was confirmed by GST pull down assay with recombinant proteins purified from *E. coli*, and by bimolecular fluorescence complementation (BiFC) assay in tobacco leaves (Fig. 3b,c). Whether SWI1 also interacts with the other four PDS5 paralogs present in Arabidopsis, was next addressed in BiFC assay. While PDS5B and PDS5D only

weakly bound to SWI1, an even stronger interaction of SWI1 with PDS5C and PD55E than with PDS5A was found, indicating that SWI1 has the potential to regulate all PDS5 proteins in Arabidopsis.

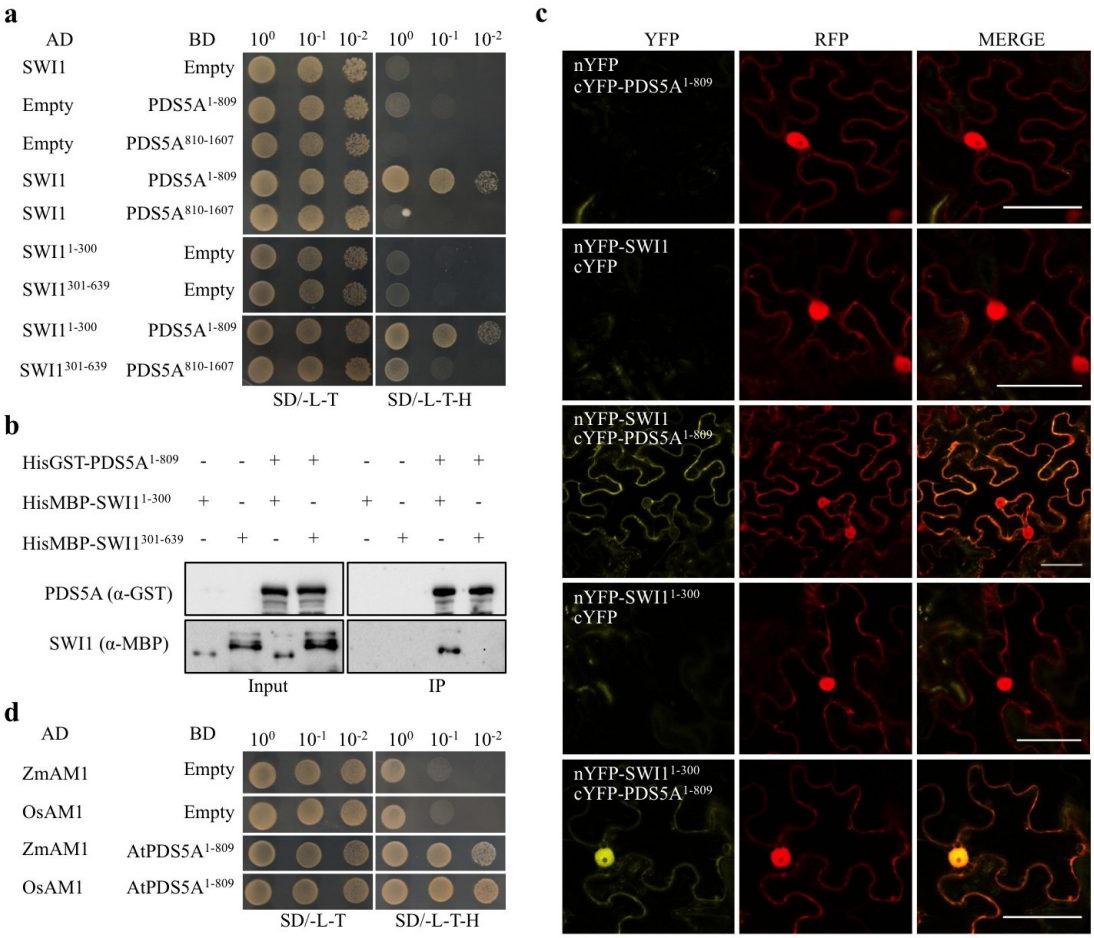

Figure 3. SWI1 interaction with cohesin components. (a) Yeast two-hybrid interaction assay of SWI1 with PDS5A. SWI1 and PDS5A were divided into an N-terminal part (SWI^{1-300}, $PDS5A^{1-809}$) and a C-terminal part ($SWI^{301-639}$, $PDS5A^{810-1607}$). Yeast cells harboring both the AD (activating domain) and BD (binding domain) were grown on synthetic medium supplied with dextrose (SD) in the absence of Leu and Trp (SD/ -L -T, left panel) and on SD medium in the absence of Leu, Trp, and His (SD/ -L -T -H, right panel). Yeast cells were incubated until OD_{600} = 1 and then diluted 10- and 100-fold for assays. (b) Co-immunoprecipitation assay of SWI1 with PDS5A. HisGST-$PDS5A^{1-809}$-bound or unoccupied agarose beads were incubated in the presence of HisMBP-$SWI1^{1-300}$ and HisMBP-$SWI1^{301-639}$. The pull-down fractions were analyzed by immunoblotting with anti-GST (upper panel) and anti-MBP (lower

panel) antibodies. (c) Interaction of SWI1 with PDS5A using bimolecular fluorescence complementation (BiFC) assays. YFP fluorescence indicates a successful complementation and hence interaction of the proteins tested. RFP is used as an indicator for the successful *Agrobacterium* infiltration. (d) Yeast two-hybrid interaction assay of SWI1 homologs in maize (ZmAM1) and rice (OsAM1) with Arabidopsis PDS5A (PDS5A).

SWI1 antagonizes WAPL

PDS5 has been shown to form a complex with WAPL in several vertebrates and yeast (Sutani *et al*, 2009; Kanke *et al*, 2016; Gandhi *et al*, 2006; Goto *et al*, 2017). Correspondingly, we found that Arabidopsis WAPL1 bound to the N- but not the C-terminus of PDS5A by yeast two-hybrid and BiFC assays (Supplementary Fig. S9b and c). Thus, WAPL1 and SWI1 interact, at least broadly, with the same region of PDS5. Sororin is known to bind to PDS5 and displace WAPL from the cohesin complex (Nishiyama *et al*, 2010). To assess whether SWI1 may act similarly as Sororin by dislodging WAPL from PDS5, we first compared the binding affinity of PDS5A with SWI1 and WAPL1 by using a ratiometric BiFC (rBiFC) system (Grefen & Blatt, 2012) that allows quantification of the interaction strength. The rBiFC assay revealed that the interaction between SWI1 and PDS5A is stronger than the interaction of WAPL1 with PDS5A (Fig. 4a,b). To further explore the relationship of these three proteins, we perform an *in vitro* competition experiment. To this end, we loaded recombinant WAPL1-PDS5A heterodimers co-purified from *E. coli* onto PDS5A-bound beads and incubated them with increasing concentrations of SWI1. With increasing concentrations of SWI1, more WAPL1 protein could be released from PDS5A into the supernatant (Fig. 4c). Conversely, more SWI1 was bound to PDS5 with increasing concentrations of SWI1.

The displacement of WAPL from PDS5 by SWI1 was further confirmed by a competitive binding assay in tobacco leaf cells (Fig. 4d). While the simultaneous presence of WAPL1 tagged with mTuquiose did not affect the interaction of SWI1 with PDS5A, the co-expression of SWI1-mTurquiose resulted in a strong reduction of the BiFC signal from WAPL1-PDS5A interaction (Fig. 4d). Thus, despite any sequence similarities, SWI1 appears to act in a similar fashion as Sororin in animals.

Therefore, we speculated that the absence of WAPL should restore the presence of REC8 on chromatin in *swi1* mutants. To this end, we generated the triple

mutant *swi1 wapl1 wapl2* containing in addition the *REC8-GFP* reporter. REC8 localization was then analyzed in male meiocytes at different meiotic stages of this triple mutant in comparison to the wildtype, *swi1* and *wapl1 wapl2* double mutants. In contrast to *swi1* mutants (Fig. 5a,b, Supplementary Fig. S7, Video S3), REC8 localization in *swi1 wapl1 wapl2* mutants was nearly identical to the pattern found in *wapl1 wapl2* double mutants, i.e., residing on chromosomes till metaphase I (Fig. 1a,b, 5c,d, Supplementary Video S4). Note that due to the failure of chromosome axis formation and of the aberrant migration of nucleolus in *swi1* mutants, the meiotic stages in *swi1* mutants were determined by the morphology of meiocytes in combination with the number of nuclei in tapetal cells (Prusicki *et al*, 2018; Stronghill *et al*, 2014). The restoration of cohesion in the *swi1 wapl1 wapl2* and the resemblance to the *wapl1 wapl2* mutant phenotype was further confirmed by chromosome spread analysis (Fig. 5c). Since *swi1* mutants do not have an obvious growth defect and since we also could not detect SWI1 outside of meiocytes, we conclude that SWI1 specifically maintains cohesion in meiosis by antagonizing WAPL. We also found that the putative SWI1 homologs from maize and rice, *AMEIOTIC 1* (*AM1*), which likewise are required for meiotic progression and cohesion establishment (Che *et al*, 2011; Pawlowski *et al*, 2009), both interacted with Arabidopsis PDS5A in a yeast two-hybrid interaction assay (Fig. 3d). Thus, it is likely that the SWI1 function as a WAPL antagonist in meiosis is conserved in flowering plants and, given the presence of SWI1 homologs in moss, possibly in all land plants.

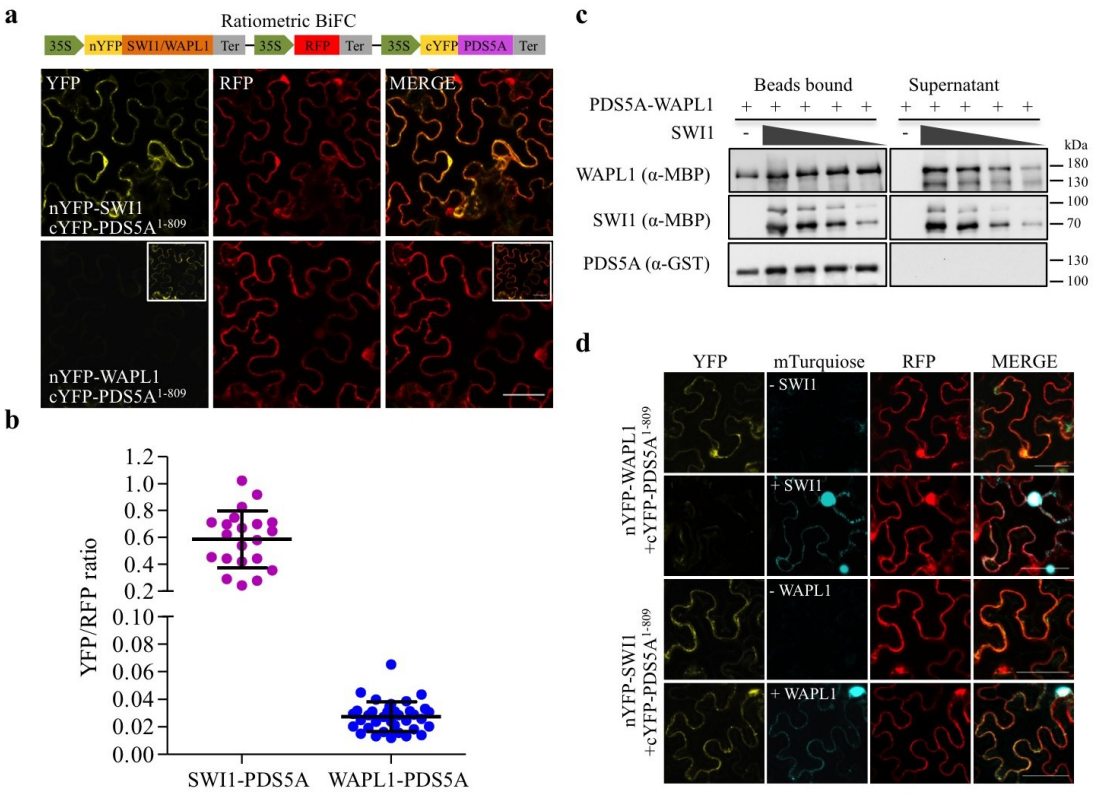

Figure 4. SWI1 dissociates WAPL1 from PDS5A. (a) Ratiometric BiFC (rBiFC) assays of PDS5A with SWI1 and WAPL1. The upper panel depicts the ratiometric gene expression cassette, and the below panels show representative images of the assay that were captured with the same settings at a confocal laser scanning microscope. The level of YFP fluorescence indicates the interaction strength with the RFP fluorescence used as a reference. The images in the white boxes represent the same pictures as the ones shown the respective panel but taken with increased sensitivity revieling an interaction between WAPl1 and PDS5A. Bar: 50 µm. (b) Quantification of the rBiFC assay by calculating the ratio between YFP and RFP signal intensity shown in (a). (c) SWI1 causes the dissociation of WAPL from PDS5. Anti-GST beads were incubated with or without SWI1$^{1-300}$ in the presence or absence of PDS5A$^{1-809}$-WAPL1 heterodimers. PDS5A$^{1-809}$ is His-GST tagged. WAPL1 and SWI1$^{1-300}$ are His-MBP tagged. Beads bound proteins were separated from the supernatant and analyzed by immunoblotting. Different amounts of SWI1$^{1-300}$ were used for the experiment. The empty beads control was shown in Supplementary Fig. S9e. (d) Co-expression of SWI1-mTurquiose inhibits the interaction of WAPL1 with PDS5A in tobacco leaf cells while the presence of WAPL1-mTurquiose has no obvious impact on the interaction of SWI1 with PDS5A. Bar: 50 µm.

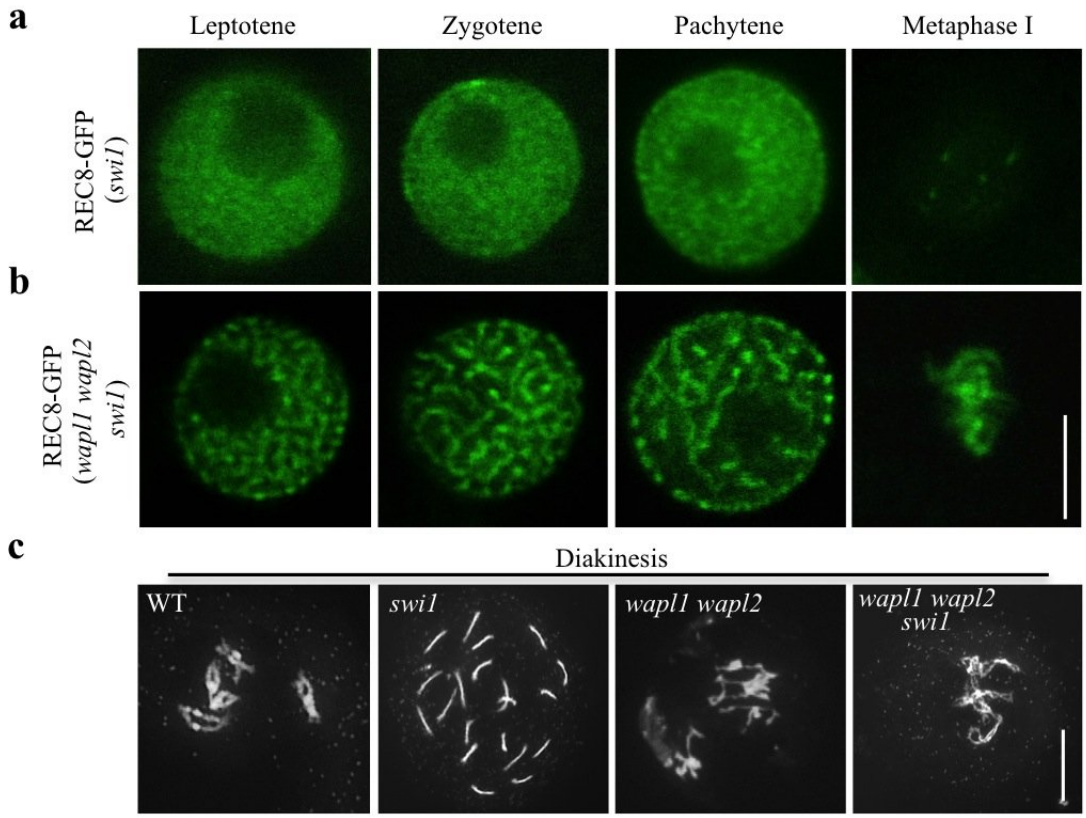

Figure 5. SWI1 is dispensable for the sister chromatid cohesion in the absence of WAPL. (a, b) Confocal laser scanning micrographs of REC8-GFP localization in male meiocytes in *swi1* (a) and in *swi1 wapl1 wapl2* (b). Bar: 5 µm. (c) Chromosome spreads of the wildtype (WT), *swi1*, *wapl1 wapl2* and *swi1 wapl1 wapl2* mutants in diakinesis. Bar: 10 µm.

SWI1 presence on chromatin is controlled by Cdk-cyclin activity

A crucial question is how WAPL is liberated from the inhibition by SWI1 in late prophase to mediate the release of cohesin (Fig. 1a-c). In vertebrate mitosis, this problem is solved by the phosphorylation dependent release of Sororin from chromatin. Two kinases have been observed to participate in this regulation, Cyclin-dependent kinase 1 (Cdk1) and Aurora B (Dreier *et al*, 2011; Nishiyama *et al*, 2013). We observed that SWI1 contains 13 consensus Cdk phosphorylation sites, 12 [S/T]P and 1 [S/T]Px[R/K] sites. We found that at least 7 of these sites can be phosphorylated in an *in vitro* kinase assay by CDKA;1, the Arabidopsis Cdk1/Cdk2 homolog, together with the meiotic cyclin SOLO DANCERS (SDS) (Fig. 6a, Supplementary Table S1).

To address whether the analogies between SWI1 and Sororin would extend to phospho-regulation, we introgressed the *SWI1-GFP* reporter, together with the *ASY3-RFP* reporter for staging, into weak loss-of-function alleles of *cdka;1* (*CDKA;1*^{T161D}) (Dissmeyer *et al*, 2007). Similar to the wildtype, SWI1 is present on chromatin in *CDKA;1*^{T161D} plants until leptotene (Fig. 6b). However, the SWI1 signal does not decline as strongly in *CDKA;1*^{T161D} plants as in the complemented *swi1* mutants. Remarkably, SWI1 stayed associated with chromosomes even until pachytene (Fig. 6b). Similarly, SWI1-GFP was also prolonged present in meiocytes of *sds* mutants (Fig. 6c).

To test whether the phosphorylation of SWI1 is essential for its release from chromosomes at late prophase I, we generated de-phospho mutant constructs. The localization pattern of SWI1 with four mutated CDK phosphorylation sites in the N-terminus of SWI1 (SWI1^{4A}-GFP), was indistinguishable from wildtype SWI1 protein (Fig. 6c). However, mutating all 13 or only the C-terminal nine phosphorylation sites in SWI1 (SWI1^{13A}-GFP and SWI1^{9A}-GFP), resulted in extended occupancy of SWI1 on chromosomes, reminiscent of the pattern found in *CDKA;1*^{T161D} and *sds* mutants (Fig. 6c, Supplementary Fig. S8b). Note that SWI1^{13A}-GFP and SWI1^{9A}-GFP seems to be functional since the cohesion defects in early prophase I were completely rescued in *swi1* mutants harboring either version (Supplementary Fig. S10d,e; for effects in later stages of meiosis, see below).

To complement this analysis, we also generated a phosphomimic version of SWI1 in which the Serine or Threonine of all 13 CDK phosphorylation sites were mutated to the negatively charged amino acid Aspartate (SWI1^{13D}-GFP) and introduced this construct into wild-type plants. SWI1^{13D}-GFP showed the same localization pattern as the wild-type version, indicating that the phosphomimic SWI1 version is recognized by its releasing factors (Fig. 7). Moreover, we did not find any reduction in fertility of these plants (Supplementary Fig. S11).

Taken together, these findings corroborated that mitosis in vertebrates and meiosis in plants (Arabidopsis) utilize a similar mechanism to control the presence of the WAPL inhibitors on chromatin through phosphorylation by CDK-cyclin complexes. However, the observation that SWI1 was not prematurely removed from chromatin by mimicking its phosphorylation indicates that phosphorylation is necessary but not sufficient for SWI1 removal hinting at a higher order coordination of SWI1 phosphorylation and the machinery involved in controlling its stability.

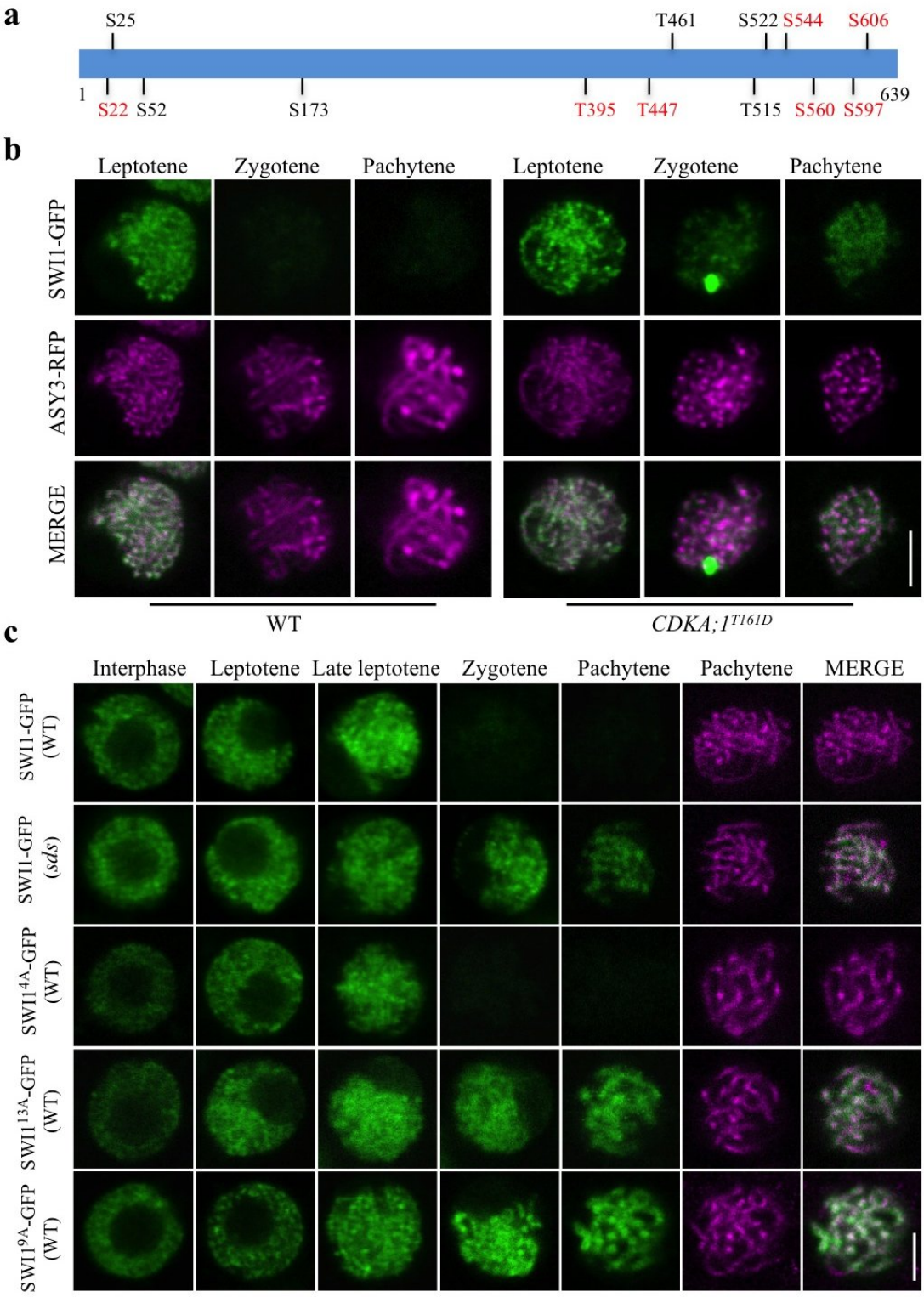

Figure 6. Phospho-control of SWI1 localization. (a) Schematic representation of SWI1 with the position of the 13 [S/T]P motifs. Phosphorylated sites identified by mass spectrometry are labeled in red. S: serine, T: threonine. (b) Confocal laser scanning micrographs of SWI1-GFP in comparison with ASY3-RFP as a meiosis staging marker in the wildtype (WT) and *CDKA;1*^{T161D} male meiocytes. (c) The

expression of SWI1-GFP and the de-phospho mutants SWI1^{4A}-GFP, SWI1^{9A}-GFP and SWI1^{13A}-GFP were analyzed in interphase and prophase I of male meiocytes of *sds* mutants and wild-type plants (WT), respectively. ASY3-RFP localization is only shown for pachytene. Bar: 5 µm.

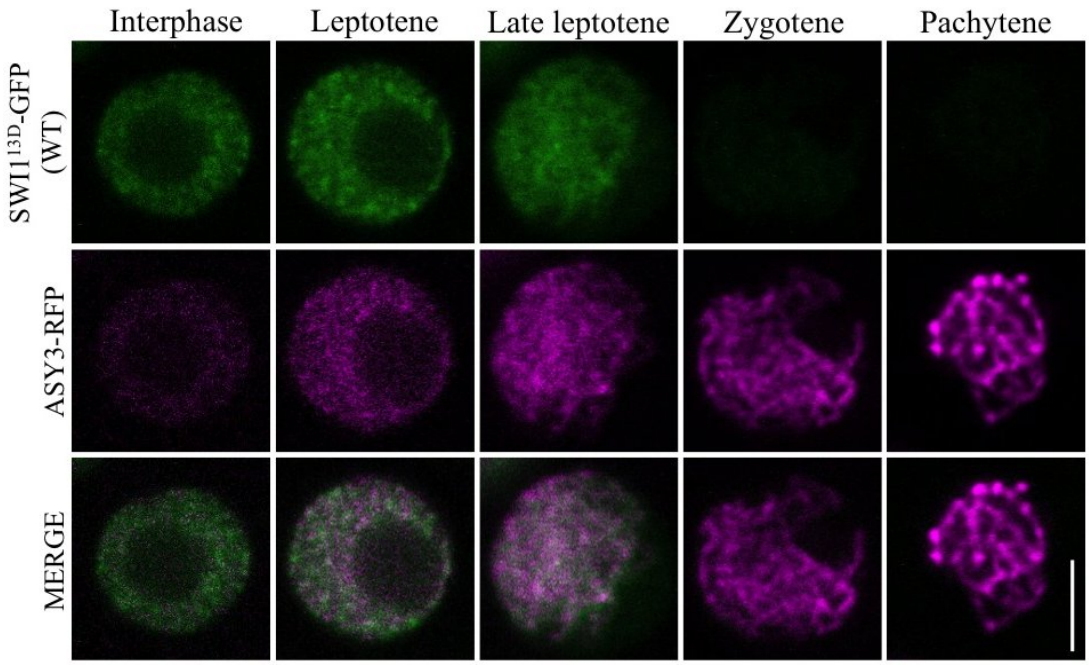

Figure 7. Localization of the phosphomimic version of SWI1. The localization of the phosphomimic version SWI1^{13D}-GFP is indistinguishable from the wild-type SWI1-GFP version (compare with Fig. 2a). ASY3-RFP is used for staging. Bar: 5 µm.

Chromatin release of SWI1 is important for WAPL action

Our above presented cytological and biochemical data suggested that the timely release of SWI1 is needed for WAPL to remove cohesin. To test this *in vivo*, we made use of the dephospho-mutant version of SWI1^{13A}-GFP that complemented the early defects of *swi1* mutants (Supplementary Fig. S10d, see above). Notably, *swi1* mutant harboring SWI1^{13A}-GFP were to a large degree infertile as seen by their short siliques and strongly reduced pollen viability (Supplementary Fig. S10a-c,i). Since these defects precluded discerning between a dominant effect as expected from interfering with WAPL versus a partial functionality of SWI1^{13A}-GFP, we switched to wild-type plants harboring the SWI1^{13A}-GFP construct (*SWI1^{13A}-GFP*/WT) for the following analysis. While the vegetative growth of these plants was not affected, they also suffered from a drastic fertility reduction in 51 out of 55 T1 transformants similar to

swi1 mutants expressing the *SWI1*^{13A}*-GFP* mutant version (Supplementary Fig. S10a-c,i), indicating that it is not the lack of a functional version that causes this phenotype.

Chromosome spread analysis showed that chromosome pairing and synapsis was not altered in *SWI1*^{13A}*-GFP*/WT (n=88) consistent with the restoration of these defects in *swi1* mutants by the same construct (Fig. 8a i). The first obvious defects were found at diakinesis. Whereas 5 clearly discernable bivilents are then present in the wildtype, chromosomes were entangled and clustered in *SWI1*^{13A}*-GFP*/WT (51 out of 101 meiocytes analyzed) (Fig. 8a ii,xvi). Intertwined chromosomes of *SWI1*^{13A}*-GFP*/WT persisted until metaphase I (87 out of 190 meiocytes analyzed) (Fig. 8a iii,ix,x,xvii). After metaphase I, chromosome fragmentation was observed (Fig. 8a iv,xi,xviii). Entangled chromosomes were even found at metaphase II (30 out of 71 meiocytes analyzed). (Fig. 8a vi,xiii,xx). Finally, tetrads with an unequal amount of DNA and triads were frequently observed in *SWI1*^{13A}*-GFP*/WT (84 out of 156 meiocytes analyzed) (Fig. 8a vii,xiv,xxi, Supplementary Fig. S12). Taken together, *SWI1*^{13A}*-GFP*/WT plants have an over cohesive phenotype which closely resembled the defects of the *wapl1 wapl2* mutants.

We therefore speculated that the prolonged retention of SWI1 might result in an extended abundance of cohesin on chromatin. To address this question, plants expressing a SWI1^{13A} version without a fluorescent tag were generated and combined with plants harboring the *REC8-GFP* reporter. Based on the time-resolved quantification of REC8-GFP signal in male meiocytes, we found that in comparison to wildtype, REC8-GFP signal showed a decreased speed of removal in *SWI1*^{13A} plants (1/2 removal time, 14.66 ± 0.58h, n=3 in *SWI1*^{13A} versus 11.33 ± 1.15h, n=3 in wildtype) (Fig. 8b, Supplementary Video S5, S6). At metaphase I, instead of ~10% (n=3) REC8-GFP signal retained in the wildtype, twice the signal, i.e., ~20% (n=3) was observed in *SWI1*^{13A} plants (student's t-test $P<0.0001$) partially resembling the retention of REC8-GFP in *wapl1 wapl2* mutants. However, it has to be noted that the level of REC8-GFP withholding in *wapl1 wapl2* is higher than in *SWI1*^{13A} plants (~55% versus ~20%) (Fig. 1a, 8b, Supplementary Video S2, S5, S6). The reason for this is not clear and we cannot exclude a slightly altered biochemical property of *SWI1*^{13A} due to the substitution of 13 amino acids possibly resulting in a less efficient inhibition of WAPL. Consistent with such a scenario is the observation that the eviction of REC8 starts apparently earlier in *SWI1*^{13A} versus the wildtype (Fig. 8b). In any case, our data strongly suggest that a vast (more than 90%) removal of REC8 is

crucial for meiosis and even an increase from 10 to 20% is sufficient to cause an over cohesive effect underlining the importance of the WAPL-PDS5-SWI1 regulatory triangle.

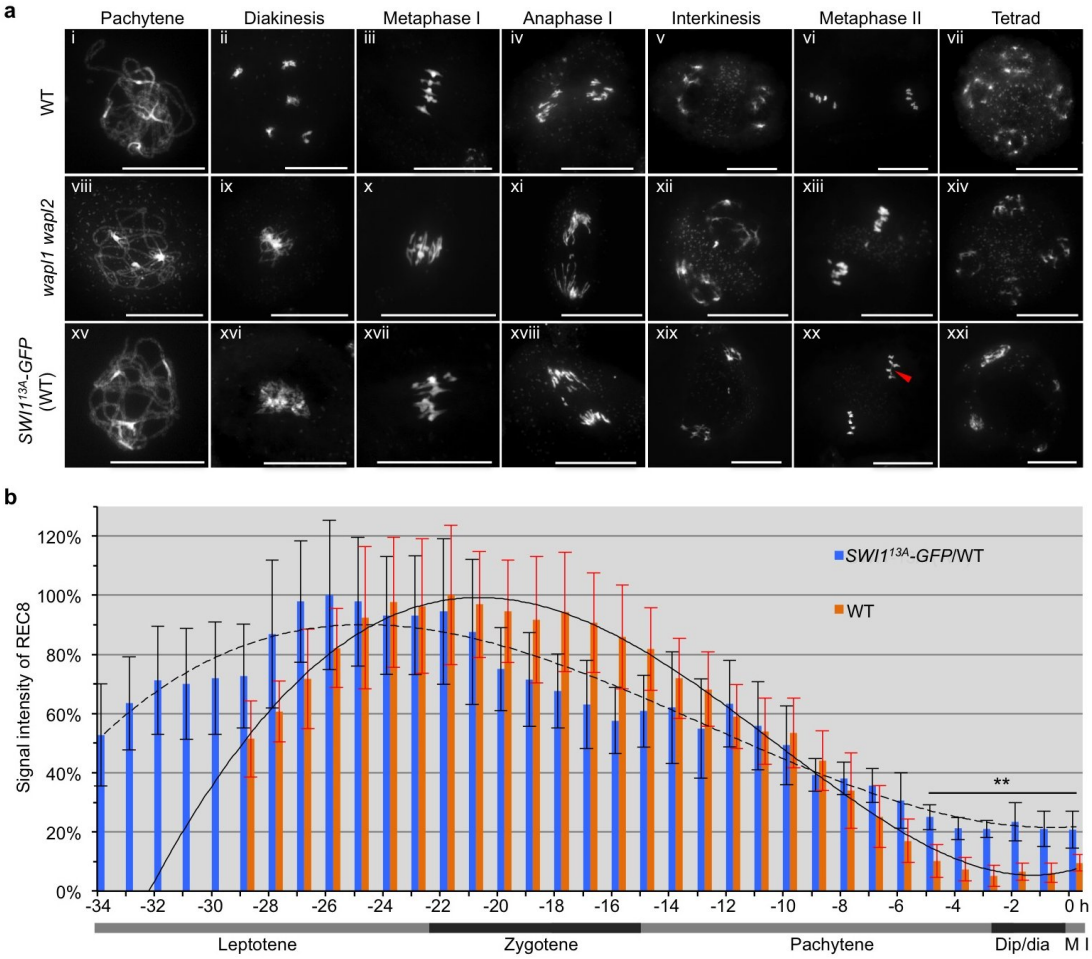

Figure 8. De-phosphomimic SWI1^{13A}-GFP interferes with the removal of cohesin. (a) Chromosome spreads of male meiocytes of the wildtype (WT), *wapl1 wapl2* mutants, and *SWI1^{13A}-GFP* in wild-type plants (*SWI1^{13A}-GFP*/WT). Bar: 20 µm. Red arrowhead in xx highlights intertwined chromosomes. (b) Quantification of cohesin during meiosis I in male meiocytes of the wildtype (WT) and *SWI1^{13A}-GFP*/WT based on the analysis of a REC8-GFP reporter. The graph represents the relative intensity of the REC8-GFP signal; error bar represents standard deviation of at least 10 meiocytes analyzed. **, Student's t-test, $p<0.01$. Dip/dia: diplotene/diakinesis, M I: metaphase I. A solid polynomial trendline is shown for the wildtype and a dashed line for *SWI1^{13A}-GFP*/WT (correlation coefficient $R^2= 0.993$ for the wildtype and 0.942 for *SWI113A-GFP*/WT). **The figures (a) and (b) are**

kindly provided by Kostika Sofroni and Yuki Hamamura respectively, using the materials prepared by Chao Yang.

SWI1 abundance is controlled by the APC/C

Our results show that the release of SWI1 from chromosomes is regulated by CDKA;1-mediated phosphorylation. However, the degradation pathway for SWI1 is still obscure. An analysis of SWI1 by the GPS-ARM algorithm (Liu *et al*, 2012) revealed 5 putative destruction boxes (D-box) in the C-terminus of SWI1, including 2 canonical and 3 less conserved D-boxes, hinting at a potential regulation of SWI1 by the APC/C (Supplementary Fig. S13a).

To address the functional relevance of the predicated D-boxes, we first mutated the two conserved D-boxes at position 306-309 and 559-562 (RXXL to AXXA) and generated plants expressing this *SWI1* mutant version (*SWI1-Δ2D-box-GFP*). Since plants harboring *SWI1-Δ2D-box-GFP* had no any obviously altered SWI1 protein expression and localization pattern (Supplementary Fig. S13b), we mutated all 5 D-boxes (SWI1-Δ5D-box-GFP). Plant expressing *SWI1-Δ5D-box-GFP* showed an extremely prolonged abundance of SWI1 that only disappeared in tetrads, suggesting that SWI1 is targeted by the APC/C for degradation from zygotene onwards (Fig. 9a, Supplementary Fig. S10 f-i). We also observed reduced fertility of SWI1-Δ5D-box-GFP expressing plants consistent with the prolonged presence of SWI1 on chromatin. However, the reduction in fertility was less severe in plants expressing *SWI1-Δ5D-box-GFP* than in *wapl1 wapl2* mutants or in *SWI1*^{13A}*-GFP* expressing plants (Supplementary Fig. S10 f-i). Again, we cannot exclude a compromised function of SWI1-Δ5D-box-GFP due to the many point mutations introduced and, consistent with an affected functionality, we also observed that SWI1-Δ5D-box-GFP had a slightly less pronounced chromosome association than the non-mutated SWI1-GFP version (compare Fig. 9a with Fig. 2a).

To hence seek further evidence for a possible proteolytic control of SWI1, we performed a cell free degradation assay by incubating protein extracts from flower buds with the purified C-terminal half of the SWI1 protein (His-GST-SWI1$^{301-639}$). We found that SWI1$^{301-639}$ degradation started in mock-treated samples after 15 min of incubation time and the majority of the protein (80%) was not detectable any longer by 90 min. In contrast, SWI1$^{301-639}$ disappeared at a much slower rate in

samples treated with the proteasome inhibitor MG132 and after 90 min, more than 50% of the protein was still present (Fig. 9b i,ii, 9c).

Since we found that phosphorylation is required for the release of SWI1 from chromatin, we next compared the degradation kinetics of wild-type $SWI1^{301-639}$ with the mutated $SWI1^{301-639/9A}$ version. Indeed, the non-phosphorylatable version $SWI1^{301-639/9A}$ was stabilized in comparison to the phosphorylatable version and showed similar turnover kinetics as MG132-treated extracts (Fig. 9b iii, 9c). To further assess whether the degradation of SWI1 is mediated through the phosphorylation of SWI1 by CDKs, we treated the protein extracts with Roscovitine, a potent CDK inhibitor (Taylor *et al*, 2004). In comparison to the mock-treated sample, $SWI1^{301-639}$ was also stabilized under Roscovitine treatment, substantiating that CDK-dependent phosphorylation marks SWI1 for 26S proteasome-dependent degradation which relies on D-boxes and thus, is likely mediated by the APC/C.

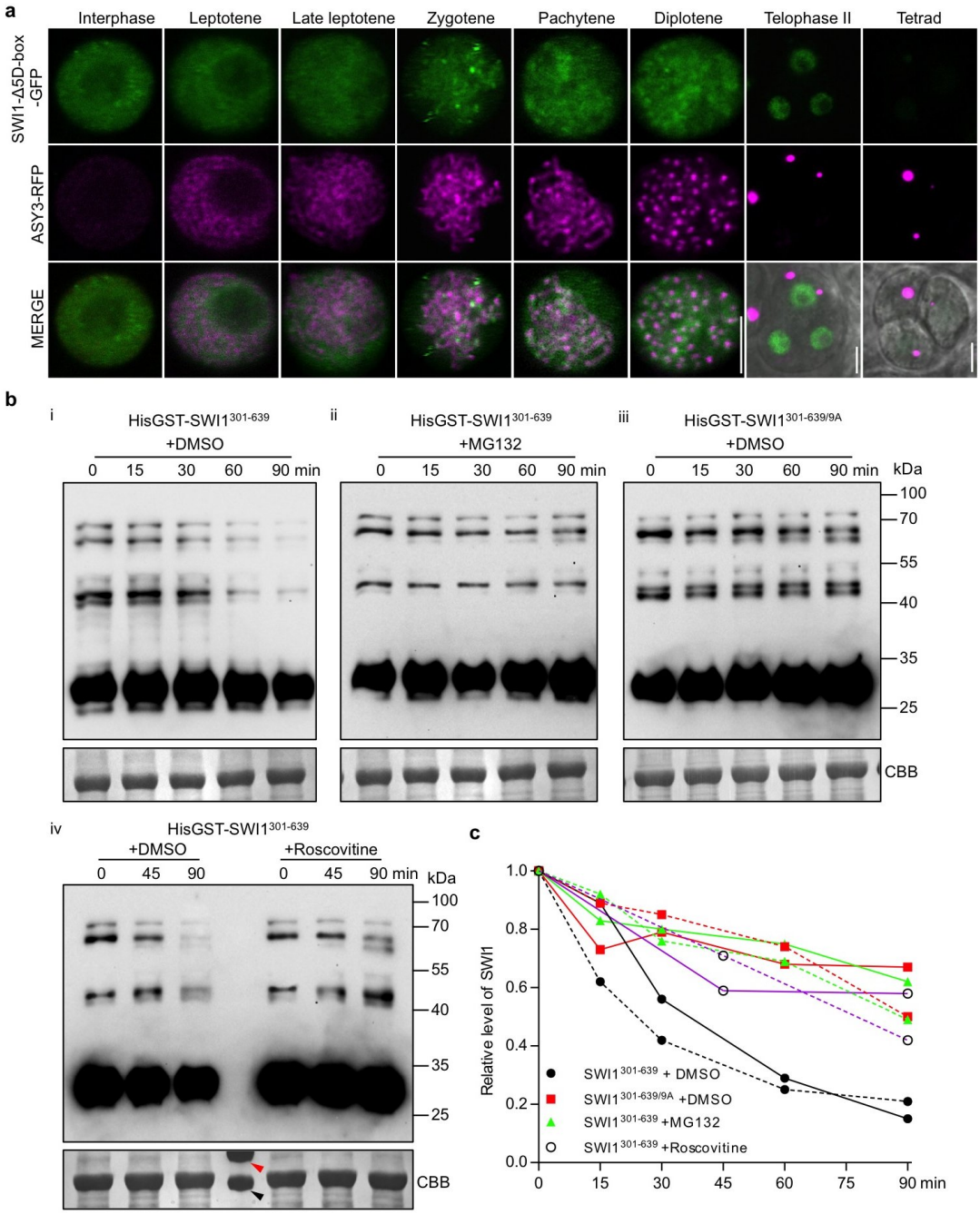

Figure 9. APC/C-mediated degradation of SWI1. (a) Deletion of the five predicted destruction boxes (D-box) in SWI1 (SWI1-Δ5D-box-GFP) results in prolonged occupancy along chromatin in comparison with SWI1-GFP (see Fig. 2a). ASY3-RFP is shown for staging. (b) Cell free degradation assay of HisGST-SWI$^{301-639}$ and HisGST-SWI$^{310-639}$ in the presence of DMSO (solvent control), 50 µm MG132, or 5 µm Roscovitine. (c) Relative protein level of SWI1 according to (b). The intensity of all bands between 100 and 40 kDa was measured and plotted on the graph. The solid lines represent the relative protein level of SWI1 shown in (b) and the dashed lines

depict the results of the second biological replicate. The large subunit of Rubisco stained by CBB verifies the equal loading of the samples. The red and black arrowheads indicate the protein marker at 70 and 55 kDa, respectively.

Discussion

The precise establishment, maintenance, and removal of sister chromatid cohesion is essential for faithful chromosome segregation in both mitosis and meiosis. In contrast to the well-described mechanisms of cohesion regulation in mitosis (Nishiyama *et al*, 2010; Ladurner *et al*, 2016; Yamada *et al*, 2017), much less is known about the control of cohesion in meiosis. Our study in Arabidopsis provides evidence that the prophase pathway of cohesion regulation exists in meiosis including the inhibition of the cohesin remodeler WAPL by a new type of inhibitor represented by the previously identified protein SWI1 that functions and is regulated in an amazingly similar fashion as Sororin in animals. Given that both animals and plants have WAPL homologs and that the lineage that led to plants and to animals were very early separated in eukaryotic evolution, much earlier than the separation of the predecessors of animals and yeast, it is likely that a basic prophase pathway of cohesin removal is very ancient and was probably present in the last common ancestor of animals and plants.

However, the repression of WAPL appears to have evolved independently in animals and plants and hence is likely younger in evolutionary terms. Remarkably, the two independent WAPL regulators, Sororin and SWI1, target the same cohesin subunit, i.e., PDS5, and are themselves controlled by a similar mechanisms, i.e., Cdk phosphorylation. Our finding that SWI1 from Arabidopsis can also bind to PDS5 from maize and rice indicates that the function of SWI1 as a WAPL antagonist is conserved in flowering plants. Moreover, the presence of *SWI1* homologs in moss gives rise to the hypothesis that *SWI1* appeared very early in the plant lineage.

A model of the regulation of the prophase pathway in plant meiosis

Based on our results, we propose the following model of how SWI1 prevents the premature removal of sister chromatid cohesion in Arabidopsis (Fig. 10): SWI1 starts to be expressed and is recruited onto chromosomes by interacting with PDS5 proteins during very early meiosis, likely already during the premeiotic S phase. The recruitment of SWI1 is dependent, at least partially, on the formation of the cohesin

complex (Fig. 2c). After entry into meiosis, cohesin needs to be maintained until late prophase to facilitate multiple processes of meiosis, e.g., double-strand break (DSB) repair, chromosome pairing, and homologous recombination (Cai *et al*, 2003; Bhatt *et al*, 1999). The maintenance of cohesin is achieved by SWI1 that has a higher affinity towards PDS5 than WAPL, thereby displacing WAPL from PDS5, consistent with the dispersed localization of WAPL at early stages in prophase I (Fig. 1d). Given the stronger interaction strength between SWI1 and PDS5 versus WAPL and PDS5, it seems likely that both complexes do not co-exist or that at least the SWI1-PDS5 complex is much more prominent than a WAPL-PDS5 complex if all three proteins are equally present.

While a protein sequence-based alignment of the first 300 amino acids of the Arabidopsis SWI1 with its othologs in other plant species including Brachypodium, bean, maize, sorghum, rapeseed, and rice revealed three conserved domains, no clear motif is emerging and further work will be required to address whether one of these domains or a specific combination mediates the interaction with PDS5. Including Sororin in this alignment did also not pinpoint to a PDS5 binding domain making it likely that the interaction between WAPL inhibitors and PDS5 is complex.

SWI1 is released from chromatin by CDKA;1-dependent phosphorylation and subjected to degradation, likely in an APC/C-mediated manner (Fig. 10). However, CDKA;1 phosphorylation of SWI1 does not appears to be sufficient for degradation and possibly, the degradation machinery needs to be activated as well, perhaps depending on CDKA;1 phosphorylation as well. The removal of SWI1 allows the interaction of WAPL with PDS5 as indicated by the tight chromosome association of WAPL at late prophase (Fig. 1d, Supplementary Fig. S1c), thereby activating the prophase pathway of cohesin removal.

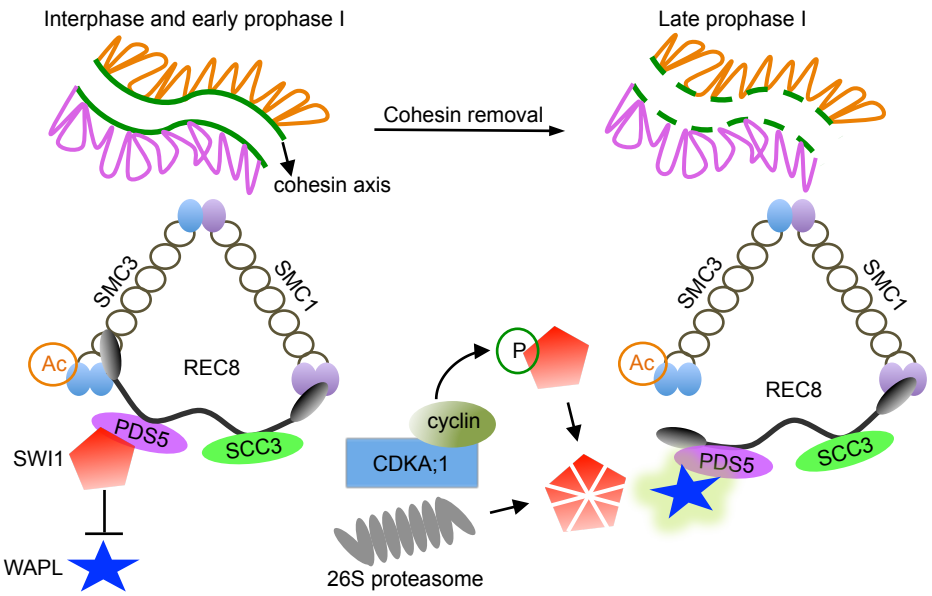

Figure 10. Model for the role of SWI1 in the regulation of cohesin during prophase I of meiosis. During interphase and early prophase I, SWI1 is highly expressed and is recruited to chromatin through interacting with PDS5 family proteins, which in turn inhibits the action of WAPL by dislodging WAPL from PDS5. In late prophase I, SWI1 is phosphorylated by CDKA;1. This phosphorylation of SWI1 then promotes its release from chromatin by facilitating the ubiquitination by APC/C, and subsequent degradation by the 26S proteasome. The release of SWI1 allows the binding of WAPL to PDS5 resulting in the release of cohesin from chromatin.

The complex nature of the cohesin complex in plants

The retained signal of SWI1-GFP in *rec8* mutants suggests that SWI1 might also localize to other cohesin complexes that do not contain REC8. Unlike most other organisms that have only one mitotic *RAD21* gene, three paralogs of the kleisin subunit, *RAD21.1*/*SYN2*, *RAD21.2*/*SYN3*, and *RAD21.3*/*SYN4*, have been identified in Arabidopsis next to the meiotic paralog REC8/SYN1. Similarly rice and other plants also have several *SCC1*/*RAD21* genes (Bolaños-Villegas *et al*, 2017). Among the Arabidopsis RAD21 genes, especially RAD21.2 has been found to play an important role in reproduction, i.e., meiosis and subsequent gametogenesis, next to a function in vegetative growth since knockdown of RAD21.2 in meiocytes impaired chromosome synapsis and SC formation (Jiang *et al*, 2007; Yuan *et al*, 2012). This together with the observation that sister chromatids are still bound at centromeres in the absence of

REC8 until metaphase I indicates that at least two different kleisins contribute to sister chromatid cohesion. However, RAD21.2 was unexpectedly detected to be predominantly present in the nucleolus of meiocytes and not along chromatin (Jiang *et al*, 2007). Thus, the function of this putative kleisin is still obscure and it is also not clear whether SWI1 can regulate different types cohesin complexes in meiosis. Conversely, *wapl* and *swi1* mutants do not show any mitotic defects raising the question whether there is a prophase pathway in mitosis in Arabidopsis.

SWI1 function beyond the control of cohesion

Although the premature removal of REC8 and with that the REC8-dependent cohesion loss are suppressed by the absence of *WAPL1* and *WAPL2*, *swi1 wapl1 wapl2* plants are still completely sterile similarly to the *swi1* single mutants and much more affected than *wapl1 wapl2* double mutants (Supplementary Fig. S14). This implies that SWI1 might have further roles in meiosis and/or might be involved in other biological processes after meiosis. Indeed, in addition to the cohesion defects, *swi1* mutants are also compromised in the specification of meiocytes resulting in the formation of multiple rather than a single female meiocytes (Agashe *et al*, 2002; Siddiqi *et al*, 2000). These defects are specific to *swi1* in Arabidopsis and have not been reported for *am1* mutants in maize and rice (Pawlowski *et al*, 2009; Che *et al*, 2011). However, *AM1* also appears to regulate the entry into meiosis and very early meiotic events.

Interestingly, we found that the number of ovules with a single female meiocyte is significantly higher in the *swi1 wapl1 wapl2* mutants (14.3%, n=126) than in *swi1* mutants (3.9%, n=128) (Chi-squared test, p=0.00395, Supplementary Fig. S15). Whether the loss of cohesin contributes to the formation of multiple meiocytes is not clear as yet. The germline in plants has to be established post-embryonically and there is accumulating evidence that the specification of meiocytes also involves a substantial reprogramming of chromatin possibly contributing to the repression of mitotic regulators and stem cell genes (Zhao *et al*, 2017; Schmidt *et al*, 2015; Olmedo-Monfil *et al*, 2010). In this context it is interesting to note that the pattern of histone modifications is altered in *swi1* mutants (Boateng *et al*, 2008). Our finding that SWI1 binds to PDS5 opens a new perspective here given that PDS5 plays a broad role in regulating plant growth and development (Pradillo *et al*, 2015). Thus, it is tempting to speculate that PDS5 is also involved in meiocyte specification in

Arabidopsis. Further work is required to explore the role of SWI1 as a regulator of PDS5 containing complexes.

Methods

Plant material and growth conditions

The *Arabidopsis thaliana* accession Columbia (Col-0) was used as wild-type reference throughout this study. The T-DNA insertion lines SAIL_654_C06 (*swi1-4*), SAIL_423H01 (*asy3-1*) (Ferdous *et al*, 2012), SALK_146172 (*spo11-1-3*) (Stacey *et al*, 2006), SAIL_807_B08 (*rec8*) and SALK_046272 (*asy1-4*) (Crismani *et al*, 2013) were obtained from the collection of T-DNA mutants at the Salk Institute Genomic Analysis Laboratory (SIGnAL, http://signal.salk.edu/cgi-bin/tdnaexpress) and GABI_206H06 (*swi1-3*) (Schubert *et al*, 2009) was obtained from GABI-Kat T-DNA mutant collection (http://www.GABI-Kat.de) via NASC (http://arabidopsis.info/). The mutant *swi1-2* has a premature stop codon induced by EMS (ethyl methanesulfonate) and was kindly provided by Raphaël Mercier from INRA Centre de Versailles-Grignon. If not mentioned otherwise, *swi1* denotes *swi1-3*. All plants were grown in growth chambers with a 16 h light/21°C and 8 h/18°C dark photoperiod and 60% humidity.

Plasmid construction and plant transformation

To create the *SWI1* reporters, the genomic sequence of *SWI1* was amplified by PCR and inserted into *pDONR221* vector by gateway BP reactions (Supplemental Table 2). The *SmaI* restriction site was then introduced in front of the stop codon by PCR. All constructs were then linearized by *SmaI* restriction and ligated to GFP or RFP fragments, followed by gateway LR reactions with the destination vector *pGWB501* (Nakagawa *et al*, 2007). WAPL1-GFP and ASY3-RFP reporters were created by using same strategy as described above. For the ZYP1b-GFP reporter, the *AscI* restriction site was inserted into *pDONR221-ZYP1b* between the 464-465aa of ZYP1b by PCR. Following the linearization by *AscI*, the mEGFP fragment was inserted into *pDONR221-ZYP1b*. The resulting ZYP1b-GFP expressing cassette was integrated into the destination vector *pGWB501* by a gateway LR reaction. Primers used for the creation of these constructs are shown in Supplementary Table S2. All constructs were transformed into *Arabidopsis thaliana* plants by floral dipping.

Yeast two-hybrid assay

The coding sequences of the respective genes were amplified by PCR from cDNA with primers flanking the *attB* recombination sites and subcloned into *pDONR223* vector by gateway BP reactions (Supplementary Table S2). The resulting constructs were then integrated into the *pGADT7-GW* or *pGBKT7-GW* vectors by gateway LR reactions. Yeast two-hybrid assays were performed according to the Matchmaker Gold Yeast two-hybrid system manual (Clontech). Different combinations of constructs were co-transformed into yeast strain AH109 using the polyethylene glycol/lithium acetate method as described in the manual of Clontech. Yeast cells harboring the relevant constructs were grown on the SD/-Leu -Trp and SD/-Leu -Trp -His plates to test for protein-protein interactions.

Protein expression and purification

To generate HisMBP-SWI1$^{1-300}$, HisMBP-SWI1$^{301-639}$, HisGST-PDS5A$^{1-809}$ and HisMBP-WAPL1 constructs, the respective coding sequences were amplified by PCR and subcloned into *pDONR223* vector by gateway BP reactions (Table S2). The resulting constructs were integrated by gateway LR reactions into *pHMGWA* or *pHGGWA* vectors for the His MBP- or HisGST- tagged fusions, respectively. For the heterologous expression, the constructs were transformed into the *E. coli* BL21 (DE3)pLysS cells and grown at 37°C in the presence of 100 mg/l ampicillin until the OD_{600} of 0.6. Protein expression was induced by adding IPTG to a final concentration of 0.3 mM, and the cells were incubated at 37°C for 3 h (HisMBP-SWI1$^{301-639}$) or 18°C overnight (HisMBP-SWI1$^{1-300}$, HisGST-PDS5A$^{1-809}$ and HisMBP-WAPL1). All proteins were purified under native conditions by using Ni-NTA sepharose (QIAGEN) according to the manual.

For the purification of PDS5A$^{1-809}$ - WAPL1 heterodimers, the ampicillin resistance gene of *WAPL1-pHMGWA* was first replaced by the kanamycin resistance gene and co-transformed into BL21 (DE3)pLysS cells containing the vector *PDS5A$^{1-809}$-pHGGWA*. The cells harboring both constructs were grown at 37°C in the presence of 100 mg/l ampicillin and 50 mg/l kanamycin until the OD_{600} to 0.6 and induced with 0.3 mM IPTG at 18°C for overnight. Cells were harvested and PDS5A$^{1-809}$ and WAPL1 heterodimers were purified using GST agarose beads (Novogene). Coomassie Brilliant Blue (CBB) stained gels of all purified proteins used in this study

are shown in Supplementary Fig. S15. The protease inhibitor cocktail (Roche) was always used in the purification procedures.

***In vitro* protein binding affinity assay**

For the GST pull-down assay, 1 μg of HisGST-PDS5A$^{1-809}$, HisMBP-SWI1$^{1-300}$ and HisMBP-SWI1$^{301-639}$ protein, purified as described above, were added to the pull-down buffer system containing 25 mM Tris-HCl, pH 7.5, 100 mM NaCl , 10% glycerol, and 20 μl GST agarose beads (Chromotek) as indicated in Fig. 3C. After incubation for 1 h at 4°C, the GST beads were rinsed 5 times by the washing buffer containing 25 mM Tris-HCl, pH 7.5, 200 mM NaCl , 10% glycerol and 0.1% Triton X-100. The beads-bound proteins were eluted by boiling in an equal volume of 1X SDS protein loading buffer and subjected to immunoblotting.

For the WAPL removal assay, 50 ng/μl HisGST-PDS5A$^{1-809}$- HisMBP-WAPL1 heterodimers were bound to anti-GST agarose beads and incubated with different amounts of HisMBP-SWI1$^{1-300}$ (40, 80, 120 or 200 ng/μl) in a buffer containing 25 mM Tris-HCl, pH 7.5, 100 mM NaCl , 10 mM $MgCl_2$, 2 mM DTT, 10% glycerol and 0.1% Triton X-100 for 1 h at 4°C. After incubation, the proteins in supernatant and from the beads-bound fraction were separated and subjected to immunoblot analysis.

Chromosome spread analysis

Chromosome spreads were performed as described previously (Wijnker *et al*, 2012). In brief, fresh flower buds were fixed in 75% ethanol and 25% acetic acid for 48 h at 4°C, followed by two washing steps with 75% ethanol and stored in 75% ethanol at 4°C. For chromosome spreading, flower buds were digested in an enzyme solution (10mM citrate buffer containing 1.5% cellulose, 1.5% pectolyase, and 1.5% cytohelicase) for 3 h at 37°C and then transferred onto a glass slide, followed by dispersing with a bended needle. Spreading was performed on a 46°C hotplate by adding an approximately 10 μl drop of 45% acetic acid. The slide was then rinsed by ice-cold ethanol/acetic acid (3:1) and mounted in Vectashield with DAPI (Vector Laboratories) to observe the DNA.

In vitro kinase assay

CDKA;1-SDS complexes were expressed and purified as described in Harashima and Schnittger (Harashima & Schnittger, 2012) with slight modification using Strep-Tactin agarose (iba) instead of Ni-NTA agarose for the purification. Briefly, the CDKA;1-SDS complexes were first purified by Strep-Tactin agarose (iba), followed by desalting with PD MiniTrap G-25 (GE Healthcare). The quality of purified kinase complexes was checked by CBB staining and immunoblotting (Supplementary Fig. S15). Kinase assays were performed by incubating the kinase complexes with HisMBP-SWI1$^{1-300}$ or HisMBP-SWI1$^{301-639}$ in the reaction buffer containing 50 mM Tris-HCl, pH 7.5, 10mM $MgCl_2$, 0.5 mM ATP and 5mM DTT for 90 min. The CBB stained gel after kinase reaction is shown in Fig. S9.

Cell free degradation assay

Wild-type Arabidopsis flower buds were freshly harvested and immediately grounded into powder in liquid nitrogen. Subsequently, total soluble proteins were extracted in the degradation buffer containing containing 25 mM Tris-HCl (pH 7.5), 10 mM NaCl, 10 mM MgCl2, 4 mM PMSF, 5 mM DTT, and 10 mM ATP as previously described (Yang *et al*, 2016). The supernatant was harvested after two 10-min centrifugations at 16,000 g at 4°C and protein concentration was measured using the Bio-Rad protein assay. Two hundred nanograms of recombinant proteins (HisGST-SWI1$^{301-639}$ or HisGST-SWI1$^{301-639/9A}$) were mixed with 150 μL protein extracts (600 μg in total) containing either DMSO, 50 μm MG132, or 5 μm Roscovitine. The reactions were incubated at 22°C and protein samples were collected at the indicated intervals followed by western blot analysis.

Bimolecular Fluorescence Complementation Assay

The coding sequences of *SWI1*, *PDS5* paralogs and *WAPl1* were amplified from cDNA and subcloned into *pDONR221-P3P2* or *pDONR221-P1P4*. The resulting constructs were subsequently integrated into the *pBiFC-2in1-NN* destination vector using a gateway LR reaction (Grefen & Blatt, 2012). All genes were under the control of the *35S* promoter. The relevant proteins were transiently expressed in tobacco leaves by *Agrobacterium* infiltration at a concentration of OD600. The fluorescence of YFP was imaged 2 days after infiltration using a Leica SP8 laser-scanning confocal microscope. For the competitive interaction BiFC assay in tobacco, *SWI1-mTurquiose2* and *WAPL1-mTurquiose2*, both driven by *35S* promoter, were generated

by integrated their coding sequences into *pGWB502* vector. The resulting constructs were then brought into *Agrobacterium*. Co-infiltration was performed by mixing the *Agrobacterium* of *SWI1-mTurquiose2* and *WAPL1-mTurquiose2* with the *pBiFC-2in1-NN* harboring relevant combinations. YFP fluorescence was imaged 2 days after infiltration using a Leica SP8 laser-scanning confocal microscope with the same setup.

Immunolocalization

For immunolocalization analyses, freshly harvested young flower buds were sorted by different size and the intact anthers were macerated in 10 µl enzyme mix (0.4% cytohelicase with 1% polyvinylpyrrolidone) for 5 min in a moisture chamber at 37°C followed by a squashing. Subsequently, 10 µl enzyme mix was added onto the Poly-Prep slides (Sigma) that were incubated for further 7 min in a moisture chamber. Afterwards, a fine smashing of the anthers was performed in 20 µl 1% Lipsol for 2 min. Cell fixation was then performed by incubating 35 µl 4% (w/v) paraformaldehyde for 2-3 h until dry. After 3 times washing with PBST buffer (PBS with 1% Triton X-100), slides were then blocked in PBS buffer with 1% BSA (PBSA) for 30 min at 37°C in a moisture chamber followed by an incubation with anti-GFP (1:100 in PBSA) antibody at 4°C for 72 h (Takara 632381/JL-8)). After three times of washing (10 min each) in PBST, fluorescein-conjugated horse anti-mouse antibody (FI-2000, Vector Laboratories) were added onto the slides (1:500 dilution) followed by 2 h incubation at 37°C in a moisture chamber. After three times washing in PBST, the chromosomes were counterstained with anti-fade DAPI solution (Vector Laboratories). The images were captured using the Leica SP8 laser scanning microscopy.

Sample preparation and LC-MS/MS data acquisition

The protein mixtures were reduced with dithiothreitol, alkylated with chloroacetamide, and digested with trypsin. These digested samples were desalted using StageTips with C18 Empore disk membranes (3 M) (Rappsilber *et al*, 2003), dried in a vacuum evaporator, and dissolved in 2% ACN, 0.1% TFA. Samples were analyzed using an EASY-nLC 1200 (Thermo Fisher) coupled to a Q Exactive Plus

mass spectrometer (Thermo Fisher). Peptides were separated on 16 cm frit-less silica emitters (New Objective, 0.75 µm inner diameter), packed in-house with reversed-phase ReproSil-Pur C18 AQ 1.9 µm resin (Dr. Maisch GmbH). Peptides were loaded on the column and eluted for 50 min using a segmented linear gradient of 5% to 95% solvent B at a flow rate of 300 nL/min (0 min : 5%B; 0-5 min -> 5%B; 5-25 min -> 20%B; 25-35 min ->35%B; 35-40 min -> 95%B; 40-50 min ->95%B; solvent A 0% ACN, 0.1% FA; solvent B 80% ACN, 0.1%FA). Mass spectra were acquired in data-dependent acquisition mode with a TOP15 method. MS spectra were acquired in the Orbitrap analyzer with a mass range of 300–1500 m/z at a resolution of 70,000 FWHM and a target value of 3×10^6 ions. Precursors were selected with an isolation window of 1.3 m/z. HCD fragmentation was performed at a normalized collision energy of 25. MS/MS spectra were acquired with a target value of $5x10^5$ ions at a resolution of 17,500 FWHM, a maximum injection time of 120 ms and a fixed first mass of m/z 100. Peptides with a charge of 1, greater than 6, or with unassigned charge state were excluded from fragmentation for MS^2; dynamic exclusion for 20s prevented repeated selection of precursors.

MS data analysis

Raw data were processed individually using MaxQuant software (version 1.5.7.4, http://www.maxquant.org/) (Cox & Mann, 2008). MS/MS spectra were searched by the Andromeda search engine against a database containing the respective proteins used for the *in vitro* reaction and a background *E. coli* database (*E.coli* (K12) database, UniProt). Sequences of 244 common contaminant proteins and decoy sequences were added during the search. Trypsin specificity was required and a maximum of two missed cleavages allowed. Minimal peptide length was set to seven amino acids. Carbamidomethylation of cysteine residues was set as fixed, phosphorylation of serine, threonine and tyrosine, oxidation of methionine and protein N-terminal acetylation as variable modifications. Peptide-spectrum-matches and proteins were retained if they were below a false discovery rate of 1%.

Confocal microscopy and sample preparation

For protein localization analyses, young anthers or ovules were dissected and imaged using an Leica TCS SP8 inverted confocal microscope. For tracing the dynamics of cohesin in *swi1 wapl1 wapl2* mutants, live cell imaging was performed as described

by Prusicki et al.[29]. Briefly, one single fresh flower bud was detached from the flower and dissected with two anthers exposed. Subsequently, the isolated bud including the pedicel and a short part of the floral stem was embedded into the Arabidopsis Apex Culture Medium (ACM) and then covered by one drop of 2% agarose. The sample was then subjected to constant image capture with 15 min intervals by using an upright Zeiss LSM880 confocal microscope with Airyscan.

For analyzing the dynamics of cohesin during meiosis, live cell imaging was performed with the anthers of the wildtype and *wapl1 wapl2* mutant plants harboring a functional REC8-GFP reporter. To quantify the dynamics of the REC8-GFP signal, the metaphase I was denoted as 0 h and the REC8-GFP signal from at least 20 meiocytes was calculated for every one hour prior to metaphase I by using the image processing software Fiji (Schindelin *et al*, 2012). Representative videos for the wildtype and *wapl1 wapl2* mutants are shown in the supplementary Video S1 and S2, respectively.

Pollen viability assay

The Peterson staining method was used to analyze the pollen viability (Peterson *et al*, 2010). For counting of pollen, three mature flower buds containing dehiscent anthers were collected and dipped in 13 µl Perterson staining solution (10% ethanol, 0.01% malachite green, 25% glycerol, 0.05% acid fuchsin, 0.005% orange G, 4% glacial acetic acid) for 10 seconds on a microscope slide, which was then covered by a cover-slip; for the staining of entire anthers, 8 non-dehiscent anthers from mature flower buds were dissected under a binocular, immersed in 30 µl Perterson staining solution on a microscope slide, and stained for overnight. Subsequently, slides were heated on a hotplate at 80°C for 10 minutes (for pollen counting) or 60 minutes (for entire anther staining) to distinguish aborted and non-aborted pollen grains. Slides were analyzed and imaged using a light microscope.

Data availability

The mass spectrometry proteomics data have been deposited to the ProteomeXchange Consortium via the PRIDE (Vizcaíno *et al*, 2016) partner repository with the dataset identifier PXD009959.

References

Agashe B, Prasad CK & Siddiqi I (2002) Identification and analysis of DYAD: a gene required for meiotic chromosome organisation and female meiotic progression in Arabidopsis. *Development* **129:** 3935–3943

Ben-Shahar TR, Heeger S, Lehane C, East P, Flynn H, Skehel M & Uhlmann F (2008) Eco1-Dependent Cohesin Acetylation During Establishment of Sister Chromatid Cohesion. *Science* **321:** 563–566

Bhatt AM, Lister C, Page T, Fransz P, Findlay K, Jones GH, Dickinson HG & Dean C (1999) The DIF1 gene of Arabidopsis is required for meiotic chromosome segregation and belongs to the REC8/RAD21 cohesin gene family. *Plant J* **19:** 463–472

Boateng KA, Yang X, Dong F, Owen HA & Makaroff CA (2008) SWI1 is required for meiotic chromosome remodeling events. *Molecular Plant* **1:** 620–633

Bolaños-Villegas P, De K, Pradillo M, Liu D & Makaroff CA (2017) In Favor of Establishment: Regulation of Chromatid Cohesion in Plants. *Front. Plant Sci.* **8:** 846

Brieño-Enríquez MA, Moak SL, Toledo M, Filter JJ, Gray S, Barbero JL, Cohen PE & Holloway JK (2016) Cohesin Removal along the Chromosome Arms during the First Meiotic Division Depends on a NEK1-PP1γ-WAPL Axis in the Mouse. *CellReports* **17:** 977–986

Cai X, Dong F, Edelmann RE & Makaroff CA (2003) The Arabidopsis SYN1 cohesin protein is required for sister chromatid arm cohesion and homologous chromosome pairing. *Journal of Cell Science* **116:** 2999–3007

Challa K, Fajish G V, Shinohara M, Klein F, Gasser SM & Shinohara A (2019) Meiosis-specific prophase-like pathway controls cleavage-independent release of cohesin by Wapl phosphorylation. *PLoS Genet* **15:** e1007851

Challa K, Lee M-S, Shinohara M, Kim KP & Shinohara A (2016) Rad61/Wpl1 (Wapl), a cohesin regulator, controls chromosome compaction during meiosis. *Nucleic Acids Research* **44:** 3190–3203

Che L, Tang D, Wang K, Wang M, Zhu K, Yu H, Gu M & Cheng Z (2011) OsAM1 is required for leptotene-zygotene transition in rice. *Nature Publishing Group* **21:** 654–665

Ciosk R, Shirayama M, Shevchenko A, Tanaka T, Toth A & Nasmyth K (2000) Cohesin's binding to chromosomes depends on a separate complex consisting of Scc2 and Scc4 proteins. *Molecular Cell* **5:** 243–254

Cox J & Mann M (2008) MaxQuant enables high peptide identification rates, individualized p.p.b.-range mass accuracies and proteome-wide protein quantification. *Nat. Biotechnol.* **26:** 1367–1372

Crawley O, Barroso C, Testori S, Ferrandiz N, Silva N, Castellano-Pozo M, Jaso-

Tamame AL & Martinez-Perez E (2016) Cohesin-interacting protein WAPL-1 regulates meiotic chromosome structure and cohesion by antagonizing specific cohesin complexes. *Elife* **5:** e10851

Crismani W, Portemer V, Froger N, Chelysheva L, Horlow C, Vrielynck N & Mercier R (2013) MCM8 is required for a pathway of meiotic double-strand break repair independent of DMC1 in Arabidopsis thaliana. *PLoS Genet* **9:** e1003165

De K, Sterle L, Krueger L, Yang X & Makaroff CA (2014) Arabidopsis thaliana WAPL Is Essential for the Prophase Removal of Cohesin during Meiosis. *PLoS Genet* **10:** e1004497

Dissmeyer N, Nowack MK, Pusch S, Stals H, Inzé D, Grini PE & Schnittger A (2007) T-loop phosphorylation of Arabidopsis CDKA;1 is required for its function and can be partially substituted by an aspartate residue. *Plant Cell* **19:** 972–985

Dreier MR, Bekier ME 2nd & Taylor WR (2011) Regulation of sororin by Cdk1-mediated phosphorylation. *Journal of Cell Science* **124:** 2976–2987

Ferdous M, Higgins JD, Osman K, Lambing C, Roitinger E, Mechtler K, Armstrong SJ, Perry R, Pradillo M, Cuñado N & Franklin FCH (2012) Inter-homolog crossing-over and synapsis in Arabidopsis meiosis are dependent on the chromosome axis protein AtASY3. *PLoS Genet* **8:** e1002507

Gandhi R, Gillespie PJ & Hirano T (2006) Human Wapl Is a Cohesin-Binding Protein that Promotes Sister-Chromatid Resolution in Mitotic Prophase. *Current Biology* **16:** 2406–2417

Goto Y, Yamagishi Y, Shintomi-Kawamura M, Abe M, Tanno Y & Watanabe Y (2017) Pds5 Regulates Sister-Chromatid Cohesion and Chromosome Bi-orientation through a Conserved Protein Interaction Module. *Curr. Biol.* **27:** 1005–1012

Gómez R, Felipe Medina N, Ruiz Torres M, Berenguer I, Viera A, Pérez S, Barbero JL, Llano E, Fukuda T, Alsheimer M, Pendás AM, Losada A & Suja JA (2016) Sororin loads to the synaptonemal complex central region independently of meiotic cohesin complexes. *EMBO reports* **17:** 695–707

Grefen C & Blatt MR (2012) A 2in1 cloning system enables ratiometric bimolecular fluorescence complementation (rBiFC). *BioTechniques* **53:** 311–314

Hara K, Zheng G, Qu Q, Liu H, Ouyang Z, Chen Z, Tomchick DR & Yu H (2014) Structure of cohesin subcomplex pinpoints direct shugoshin-Wapl antagonism in centromeric cohesion. *Nature Publishing Group* **21:** 864–870

Harashima H & Schnittger A (2012) Robust reconstitution of active cell-cycle control complexes from co-expressed proteins in bacteria. *Plant Methods* **8:** 23

Jiang L, Xia M, Strittmatter LI & Makaroff CA (2007) The Arabidopsis cohesin protein SYN3 localizes to the nucleolus and is essential for gametogenesis. *Plant J* **50:** 1020–1034

Kanke M, Tahara E, Huis In't Veld PJ & Nishiyama T (2016) Cohesin acetylation and Wapl-Pds5 oppositely regulate translocation of cohesin along DNA. *EMBO J.* **35:** 2686–2698

Kueng S, Hegemann B, Peters BH, Lipp JJ, Schleiffer A, Mechtler K & Peters J-M (2006) Wapl controls the dynamic association of cohesin with chromatin. *Cell* **127:** 955–967

Ladurner R, Kreidl E, Ivanov MP, Ekker H, Idarraga Amado MH, Busslinger GA, Wutz G, Cisneros DA & Peters J-M (2016) Sororin actively maintains sister chromatid cohesion. *EMBO J.* **35:** 635–653

Lengronne A, McIntyre J, Katou Y, Kanoh Y, Hopfner K-P, Shirahige K & Uhlmann F (2006) Establishment of Sister Chromatid Cohesion at the S. cerevisiae Replication Fork. *Molecular Cell* **23:** 787–799

Litwin I, Pilarczyk E & Wysocki R (2018) The Emerging Role of Cohesin in the DNA Damage Response. **9:** 581

Liu H, Rankin S & Yu H (2013) Phosphorylation-enabled binding of SGO1-PP2A to cohesin protects sororin and centromeric cohesion during mitosis. *Nat. Cell Biol.* **15:** 40–49

Liu Z, Yuan F, Ren J, Cao J, Zhou Y, Yang Q & Xue Y (2012) GPS-ARM: computational analysis of the APC/C recognition motif by predicting D-boxes and KEN-boxes. *PLoS ONE* **7:** e34370

Makrantoni V & Marston AL (2018) Cohesin and chromosome segregation. *Curr. Biol.* **28:** R688–R693

Mercier R (2003) The meiotic protein SWI1 is required for axial element formation and recombination initiation in Arabidopsis. *Development* **130:** 3309–3318

Mercier R, Vezon D, Bullier E, Motamayor JC, Sellier A, Lefèvre F, Pelletier G & Horlow C (2001) SWITCH1 (SWI1): a novel protein required for the establishment of sister chromatid cohesion and for bivalent formation at meiosis. *Genes & Development* **15:** 1859–1871

Nakagawa T, Suzuki T, Murata S, Nakamura S, Hino T, Maeo K, Tabata R, Kawai T, Tanaka K, Niwa Y, Watanabe Y, Nakamura K, Kimura T & Ishiguro S (2007) Improved Gateway binary vectors: high-performance vectors for creation of fusion constructs in transgenic analysis of plants. *Biosci. Biotechnol. Biochem.* **71:** 2095–2100

Nishiyama T, Ladurner R, Schmitz J, Kreidl E, Schleiffer A, Bhaskara V, Bando M, Shirahige K, Hyman AA, Mechtler K & Peters J-M (2010) Sororin Mediates Sister Chromatid Cohesion by Antagonizing Wapl. *Cell* **143:** 737–749

Nishiyama T, Sykora MM, Huis in 't Veld PJ, Mechtler K & Peters J-M (2013) Aurora B and Cdk1 mediate Wapl activation and release of acetylated cohesin from chromosomes by phosphorylating Sororin. *Proc. Natl. Acad. Sci. U.S.A.* **110:** 13404–13409

Olmedo-Monfil V, Durán-Figueroa N, Arteaga-Vázquez M, Demesa-Arévalo E, Autran D, Grimanelli D, Slotkin RK, Martienssen RA & Vielle-Calzada J-P (2010) Control of female gamete formation by a small RNA pathway in Arabidopsis. *Nature* **464:** 628–632

Pawlowski WP, Wang C-JR, Golubovskaya IN, Szymaniak JM, Shi L, Hamant O, Zhu T, Harper L, Sheridan WF & Cande WZ (2009) Maize AMEIOTIC1 is essential for multiple early meiotic processes and likely required for the initiation of meiosis. *Proc. Natl. Acad. Sci. U.S.A.* **106:** 3603–3608

Petela NJ, Gligoris TG, Metson J, Lee B-G, Voulgaris M, Hu B, Kikuchi S, Chapard C, Chen W, Rajendra E, Srinivisan M, Yu H, Löwe J & Nasmyth KA (2018) Scc2 Is a Potent Activator of Cohesin's ATPase that Promotes Loading by Binding Scc1 without Pds5. *Molecular Cell* **70:** 1134–1148.e7

Peterson R, Slovin JP & Chen C (2010) A simplified method for differential staining of aborted and non-aborted pollen grains. *Int J Plant Biol* **1:** 13–e13

Pradillo M, Knoll A, Oliver C, Varas J, Corredor E, Puchta H & Santos JL (2015) Involvement of the Cohesin Cofactor PDS5 (SPO76) During Meiosis and DNA Repair in Arabidopsis thaliana. *Front. Plant Sci.* **6:** 3020

Prusicki MA, Keizer EM, van Rosmalen RP, Komaki S, Seifert F, Müller K, Wijnker E, Fleck C & Schnittger A (2018) Live cell imaging of meiosis in Arabidopsis thaliana - a landmark system. *bioRxiv***:** 446922

Rankin S (2005) Sororin, the cell cycle and sister chromatid cohesion. *Cell Cycle* **4:** 1039–1042

Rankin S, Ayad NG & Kirschner MW (2005) Sororin, a substrate of the anaphase-promoting complex, is required for sister chromatid cohesion in vertebrates. *Molecular Cell* **18:** 185–200

Rappsilber J, Ishihama Y & Mann M (2003) Stop and go extraction tips for matrix-assisted laser desorption/ionization, nanoelectrospray, and LC/MS sample pretreatment in proteomics. *Anal. Chem.* **75:** 663–670

Ravi M, Marimuthu MPA & Siddiqi I (2008) Gamete formation without meiosis in Arabidopsis. *Nature* **451:** 1121–1124

Schindelin J, Arganda-Carreras I, Frise E, Kaynig V, Longair M, Pietzsch T, Preibisch S, Rueden C, Saalfeld S, Schmid B, Tinevez J-Y, White DJ, Hartenstein V, Eliceiri K, Tomancak P & Cardona A (2012) Fiji: an open-source platform for biological-image analysis. *Nat. Methods* **9:** 676–682

Schmidt A, Schmid MW & Grossniklaus U (2015) Plant germline formation: common concepts and developmental flexibility in sexual and asexual reproduction. *Development* **142:** 229–241

Schubert V, Weißleder A, Ali H, Fuchs J, Lermontova I, Meister A & Schubert I (2009) Cohesin gene defects may impair sister chromatid alignment and genome

stability in Arabidopsis thaliana. *Chromosoma* **118:** 591–605

Siddiqi I, Ganesh G, Grossniklaus U & Subbiah V (2000) The dyad gene is required for progression through female meiosis in Arabidopsis. *Development* **127:** 197–207

Stacey NJ, Kuromori T, Azumi Y, Roberts G, Breuer C, Wada T, Maxwell A, Roberts K & Sugimoto-Shirasu K (2006) Arabidopsis SPO11-2 functions with SPO11-1 in meiotic recombination. *Plant J* **48:** 206–216

Stronghill PE, Azimi W & Hasenkampf CA (2014) A novel method to follow meiotic progression in Arabidopsis using confocal microscopy and 5-ethynyl-2'-deoxyuridine labeling. *Plant Methods* **10:** 33

Suja JA & Barbero JL (2009) Cohesin complexes and sister chromatid cohesion in mammalian meiosis. *Genome Dyn* **5:** 94–116

Sutani T, Kawaguchi T, Kanno R, Itoh T & Shirahige K (2009) Budding Yeast Wpl1(Rad61)-Pds5 Complex Counteracts Sister Chromatid Cohesion-Establishing Reaction. *CURBIO* **19:** 492–497

Taylor SL, Kinchington PR, Brooks A & Moffat JF (2004) Roscovitine, a cyclin-dependent kinase inhibitor, prevents replication of varicella-zoster virus. *J. Virol.* **78:** 2853–2862

Vaur S, Feytout AEL, Vazquez SEP & Javerzat J-P (2018) Pds5 promotes cohesin acetylation and stable cohesin–chromosome interaction. *EMBO reports* **13:** 645–652

Vizcaíno JA, Csordas A, Del-Toro N, Dianes JA, Griss J, Lavidas I, Mayer G, Perez-Riverol Y, Reisinger F, Ternent T, Xu Q-W, Wang R & Hermjakob H (2016) 2016 update of the PRIDE database and its related tools. *Nucleic Acids Research* **44:** 11033–11033

Wang Y, Wu H, Liang G & Yang M (2004) Defects in nucleolar migration and synapsis in male prophase I in the ask1-1 mutant of Arabidopsis. *Sexual Plant Reproduction* **16:** 273–282

Watrin E, Schleiffer A, Tanaka K, Eisenhaber F, Nasmyth K & Peters J-M (2006) Human Scc4 is required for cohesin binding to chromatin, sister-chromatid cohesion, and mitotic progression. *CURBIO* **16:** 863–874

Wijnker E, van Dun K, de Snoo CB, Lelivelt CLC, Keurentjes JJB, Naharudin NS, Ravi M, Chan SWL, de Jong H & Dirks R (2012) Reverse breeding in Arabidopsis thaliana generates homozygous parental lines from a heterozygous plant. *Nat. Genet.* **44:** 467–470

Yamada T, Tahara E, Kanke M, Kuwata K & Nishiyama T (2017) Drosophila Dalmatian combines sororin and shugoshin roles in establishment and protection of cohesion. *EMBO J.* **36:** 1513–1527

Yang C, Hu H, Ren H, Kong Y, Lin H, Guo J, Wang L, He Y, Ding X,

Grabsztunowicz M, Mulo P, Chen T, Liu Y, Wu Z, Wu Y, Mao C, Wu P & Mo X (2016) LIGHT-INDUCED RICE1 Regulates Light-Dependent Attachment of LEAF-TYPE FERREDOXIN-NADP+ OXIDOREDUCTASE to the Thylakoid Membrane in Rice and Arabidopsis. *Plant Cell* **28:** 712–728

Yang X, Timofejeva L, Ma H & Makaroff CA (2006) The Arabidopsis SKP1 homolog ASK1 controls meiotic chromosome remodeling and release of chromatin from the nuclear membrane and nucleolus. *Journal of Cell Science* **119:** 3754–3763

Yuan L, Yang X, Ellis JL, Fisher NM & Makaroff CA (2012) The Arabidopsis SYN3 cohesin protein is important for early meiotic events. *Plant J* **71:** 147–160

Zhao X, Bramsiepe J, Van Durme M, Komaki S, Prusicki MA, Maruyama D, Forner J, Medzihradszky A, Wijnker E, Harashima H, Lu Y, Schmidt A, Guthörl D, Logroño RS, Guan Y, Pochon G, Grossniklaus U, Laux T, Higashiyama T, Lohmann JU, et al (2017) RETINOBLASTOMA RELATED1 mediates germline entry in Arabidopsis. *Science* **356:** eaaf6532

Acknowledgments:

The authors are grateful to Anne Harzen (Max Planck Institute for Plant Breeding Research) for technical assistance. The authors thank Maren Heese and Paul Larsen for critically reading the manuscript. We kindly acknowledge the Salk T-DNA collection, the GABI-Kat T-DNA collection, the *Arabidopsis* Biological Resource Center (ABRC) and the European *Arabidopsis* Stock Centre (NASC) for providing seeds of T-DNA lines used in this report. This work was supported by core funding of the University of Hamburg.

Author contributions

C.Y. and A.S. conceived the experiments. C.Y., Y.H., K.S., F.B. performed the experiments and statistical analyses; S.C.S. and H.N. performed the mass spectrometry experiment and data analysis. C.Y. and A.S. analyzed the data. C.Y. and A.S. wrote the manuscript.

Competing interests

Authors declare no competing interests.

SUPPLEMENTARY FIGURES

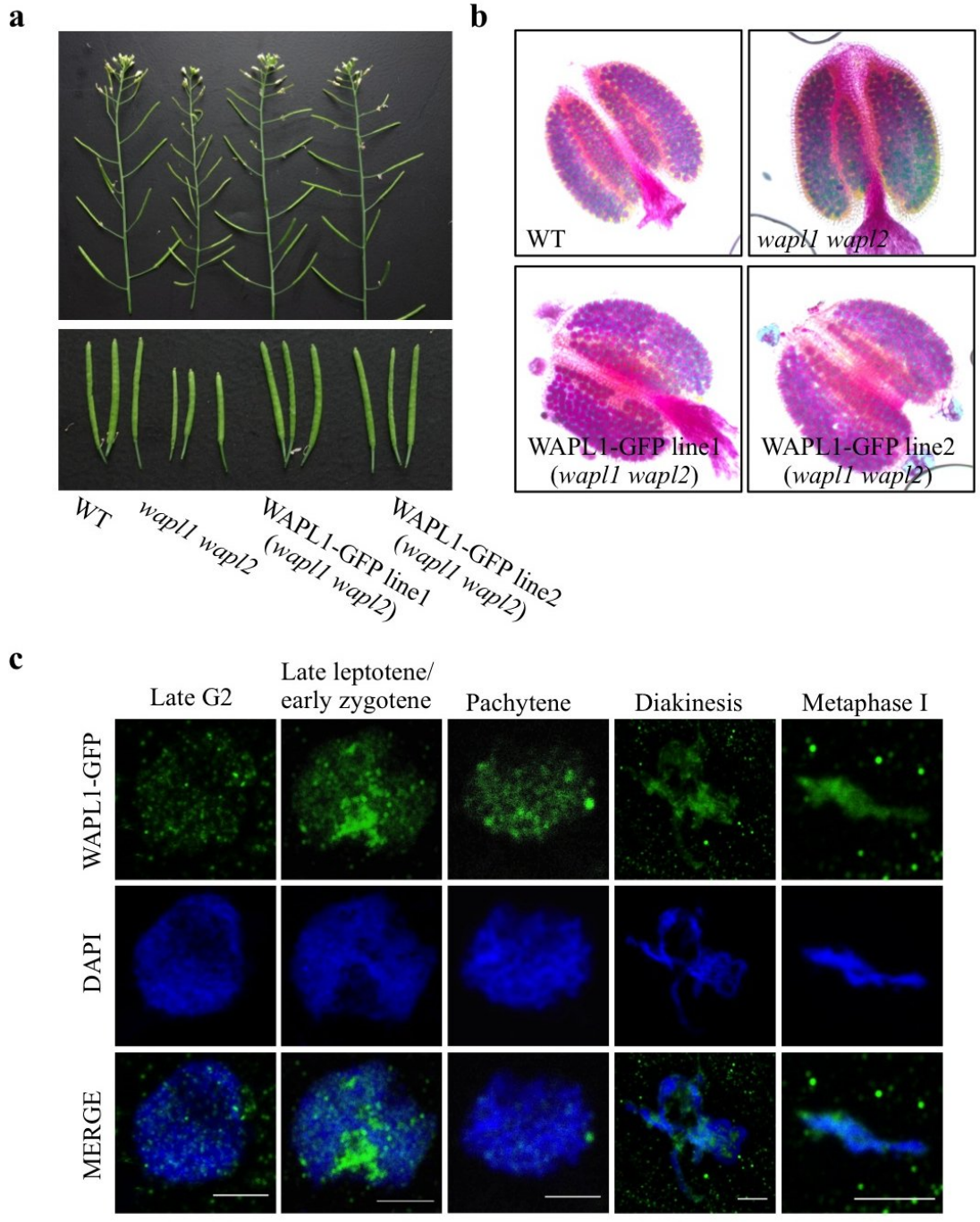

Supplementary Figure 1

WAPL1-GFP is functional and accumulates on chromatin from late leptotene/early zygotene till metaphase I. (a) Main branches (upper panel) and siliques (lower panel) of the wildtype (WT), *wapl1 wapl2*, and two lines expressing WAPL1-GFP in a *wapl1 wapl2* mutant background. (b) Peterson staining of anthers

in the wildtype (WT), *wapl1 wapl2* mutants, and two WAPL1-GFP lines. Blue staining indicates dead pollen. (c) Immunolocalization of WAPL1-GFP during meiosis I of male meiocytes. Anti-GFP antibody was used for detecting WAPL1-GFP. Bar: 5 µm.

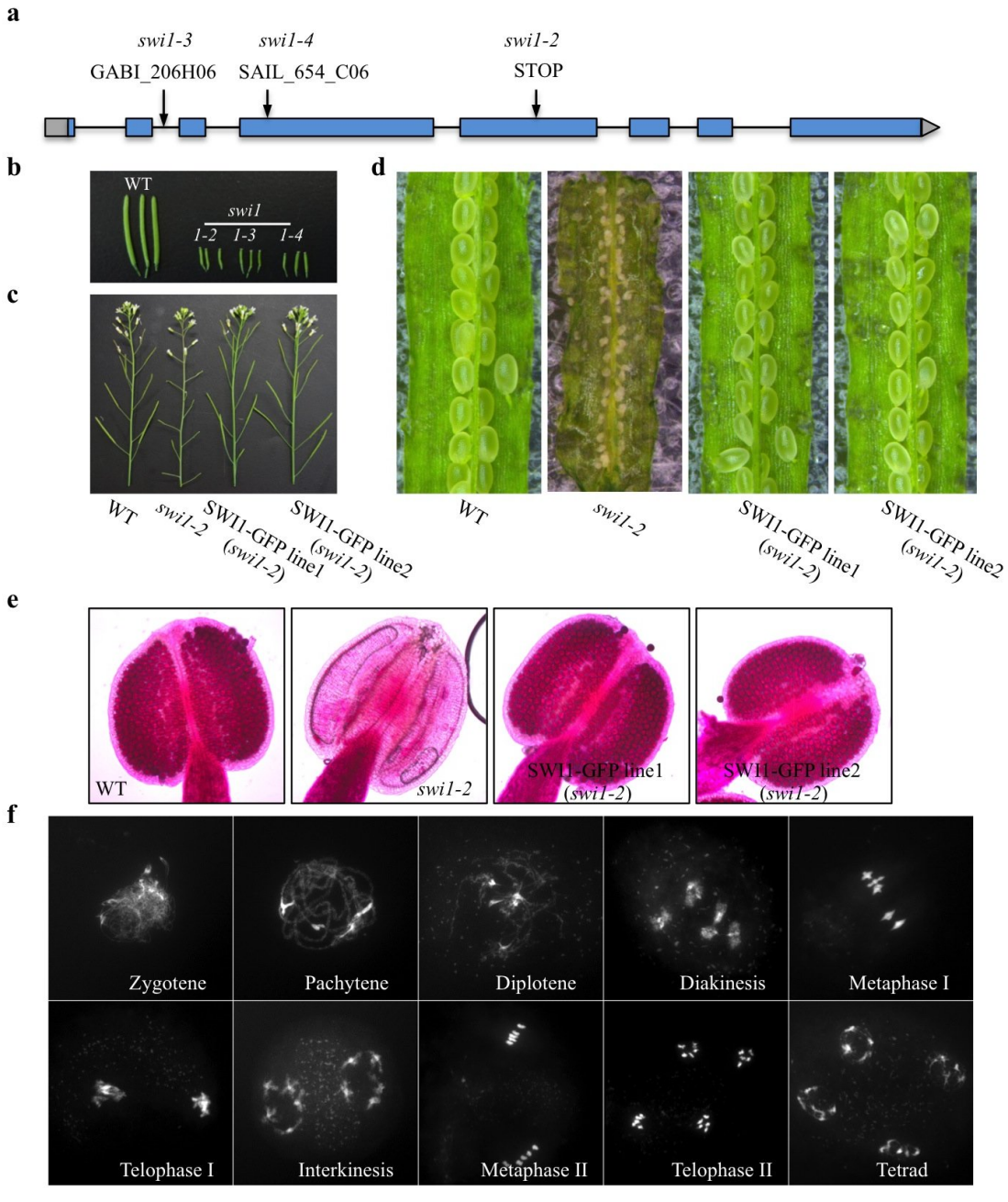

Supplementary Figure 2

SWI1-GFP fully complements the meiotic defects in *swi1* mutants. (a) Scheme of the genomic region of SWI1. Arrows denote the position of T-DNA insertions (*swi1-3*, *swi1-4*) and of a premature stop codon (*swi1-2*). (b) Siliques of the wildtype (WT)

and different *swi1* mutant alleles, which are completely sterile. (c) The main branches of the wildtype, *swi1-2* and two *SWI1-GFP* lines. (d) Seed sets in siliques of the wildtype, two *SWI1-GFP* lines and the *swi1-2* mutant. (e) Peterson staining of pollen for the wildtype, *swi1-2* and *SWI1-GFP* lines. No pollen was found in the *swi1-2* mutants. Blue staining indicates dead pollen. (f) Chromosome spread analysis of male meiocytes in *SWI1-GFP* line #2 (*swi1-2*) shows a wild-type meiotic program. **The figure (f) is kindly provided by by Kostika Sofroni using the materials prepared by Chao Yang.**

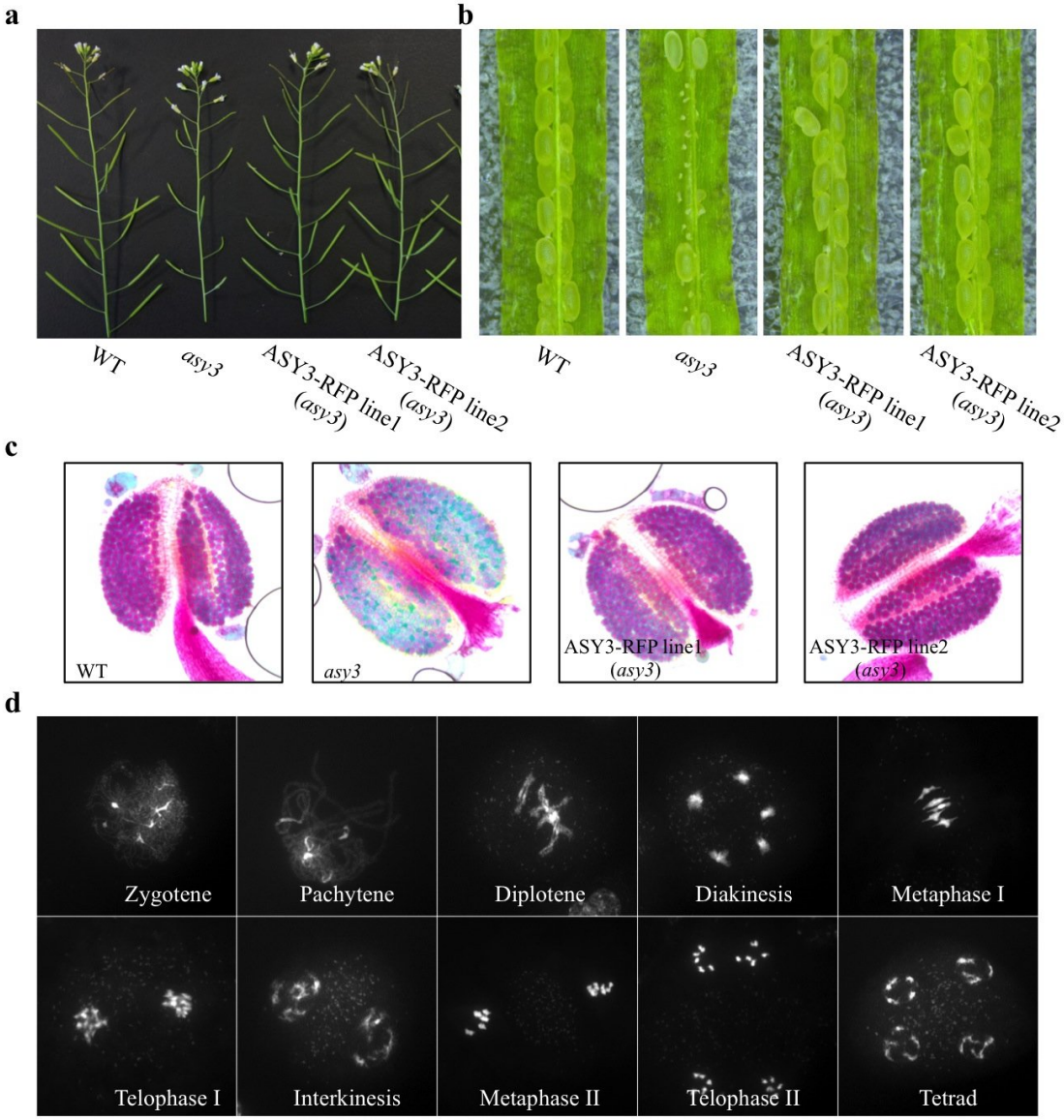

Supplementary Figure 3

ASY3-RFP fully complements the meiotic defects in *asy3* mutants. (a) The main branches of the wildtype (WT) and two *ASY3-RFP* lines. (b) Seed sets in siliques of

the wildtype (WT) and two *ASY3-RFP* complementary lines. (c) Peterson staining of pollens for the wildtype (WT), *asy3* and *ASY3-RFP* lines. (d) Chromosome spread analysis of male meiocytes in *ASY3-RFP* line #1 (*asy3*) reveals a normal meiotic program. **The figure (d) is kindly provided by by Kostika Sofroni using the materials prepared by Chao Yang.**

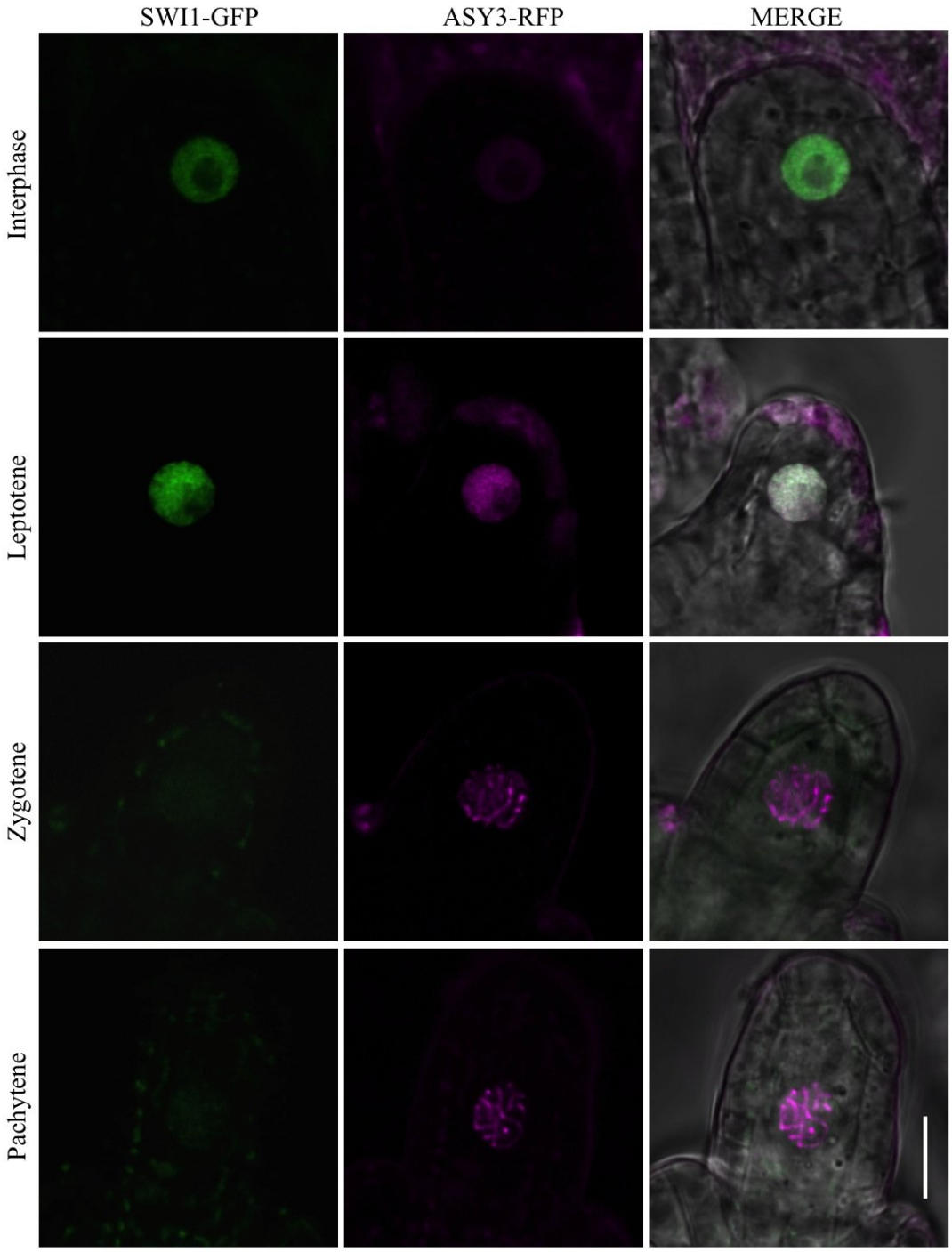

Supplementary Figure 4

Co-localization of SWI1 with ASY3 in female meiocytes. Co-localization analysis of SWI1-GFP (green) with ASY3-RFP (red) during interphase and prophase I in female meiocytes by using confocal laser scanning microscopy. Bar: 10 μm.

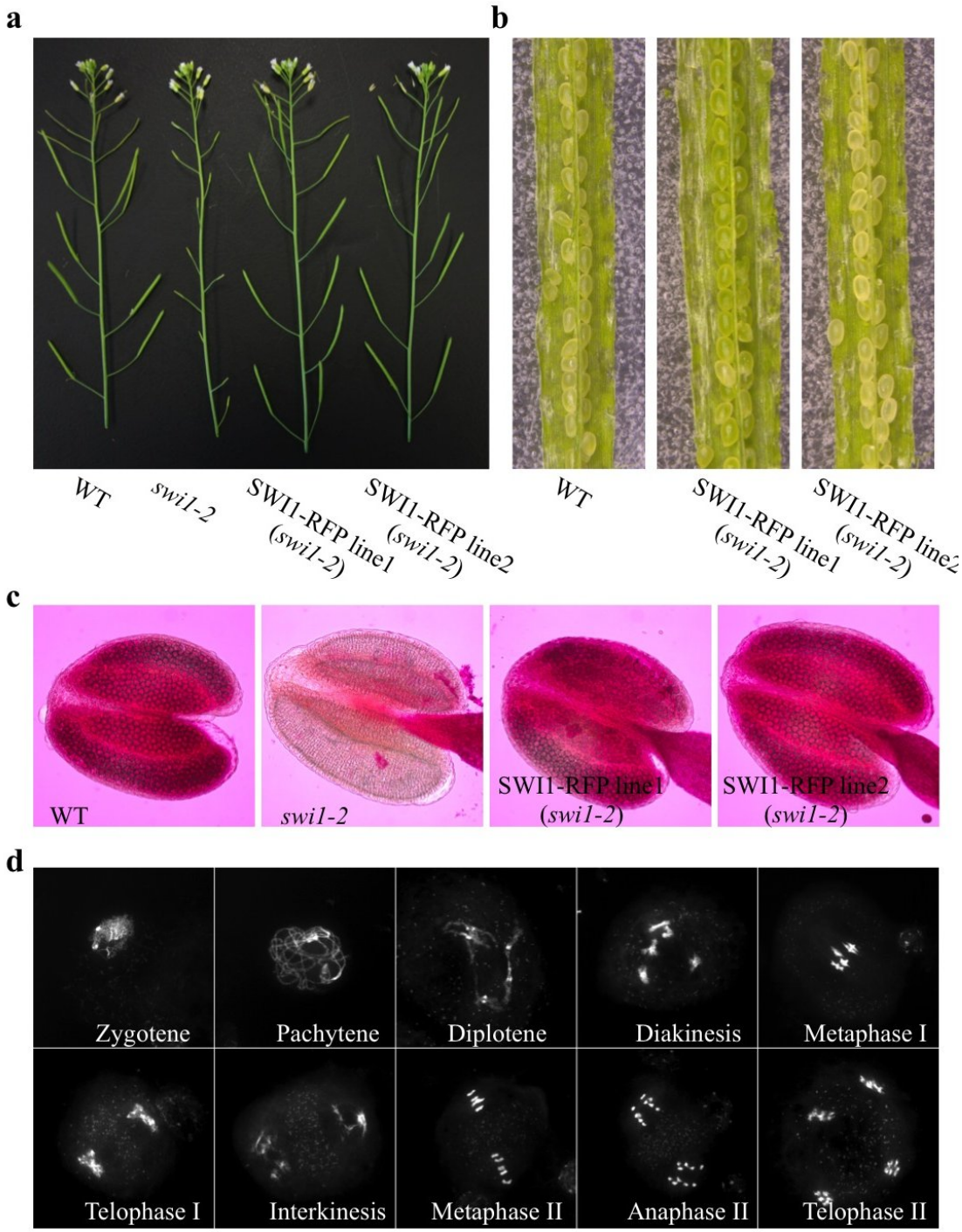

Supplementary Figure 5

SWI1-RFP fully complements the meiotic defects in *swi1* mutants. (a) Main branches of the wildtype (WT), *swi1-2* and two *SWI1-RFP* lines. (b) Seed sets in siliques of the wildtype (WT) and two *SWI1-RFP* lines. (c) Peterson staining of anthers for the wildtype (WT), *swi1-2* and *SWI1-GFP* lines. (d) Chromosome spread analysis of male meiocytes in *SWI1-RFP* line #1 (*swi1-2*) reveals a wild-type meiotic

program. **This figure (d) is kindly provided by Kostika Sofroni using the materials prepared by Chao Yang.**

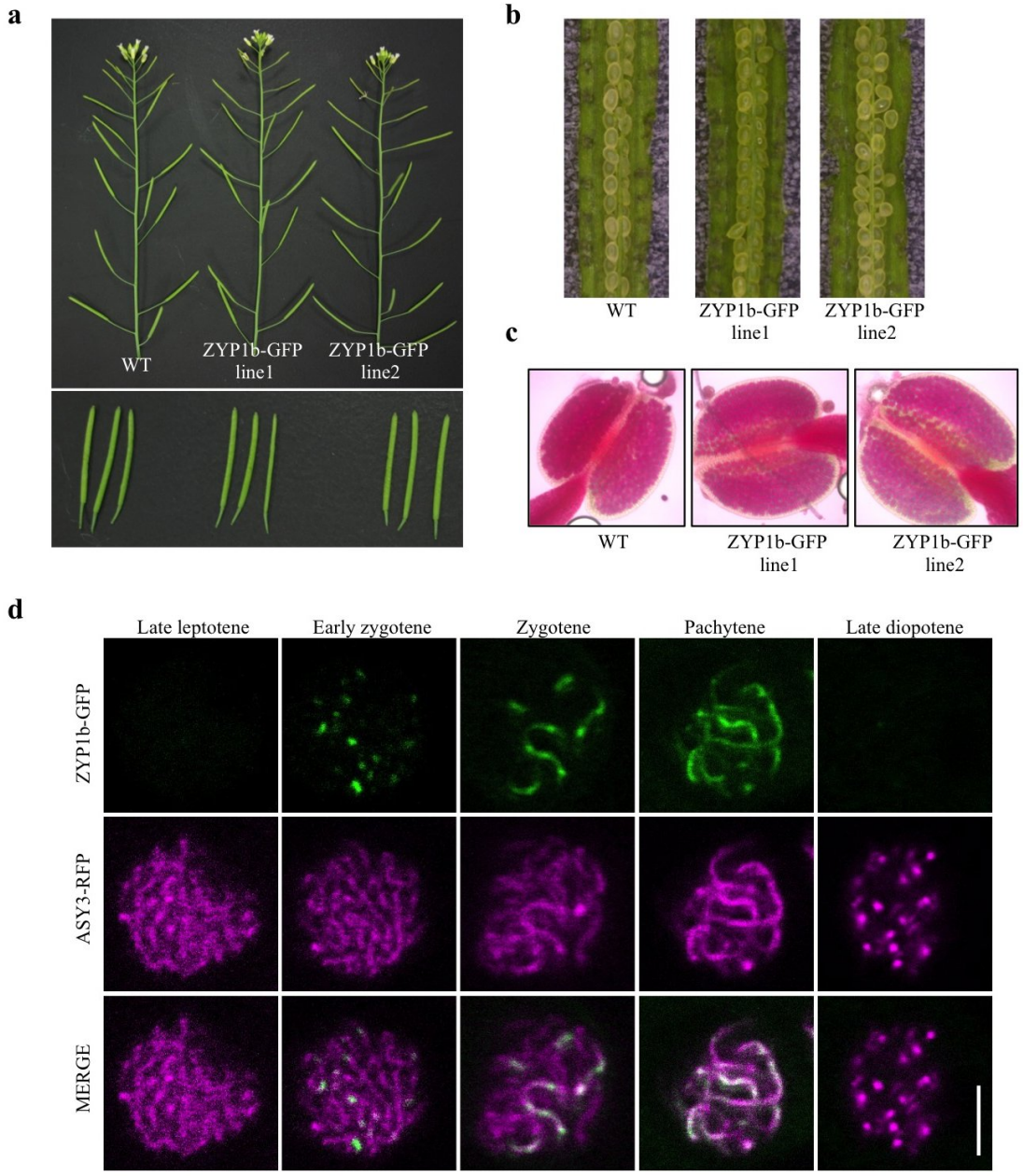

Supplementary Figure 6

ZYP1b-GFP is a good reporter for staging and has no dominant effect on plants. (a) Main branches of the wildtype (WT) and two *ZYP1b-GFP* lines in wildtype bacground. (b) Seed sets in siliques of the WT and two *ZYP1b-GFP* lines. (c) Peterson staining of anthers for the WT and and two *ZYP1b-GFP* lines. (d) Co-localization of ZYP1b-GFP with ASY3-RFP in the male meiocytes of wildtype shows

that ZYP1b-GFP specifically localizes to synaptic regions during prophase I. Bar: 5 µm.

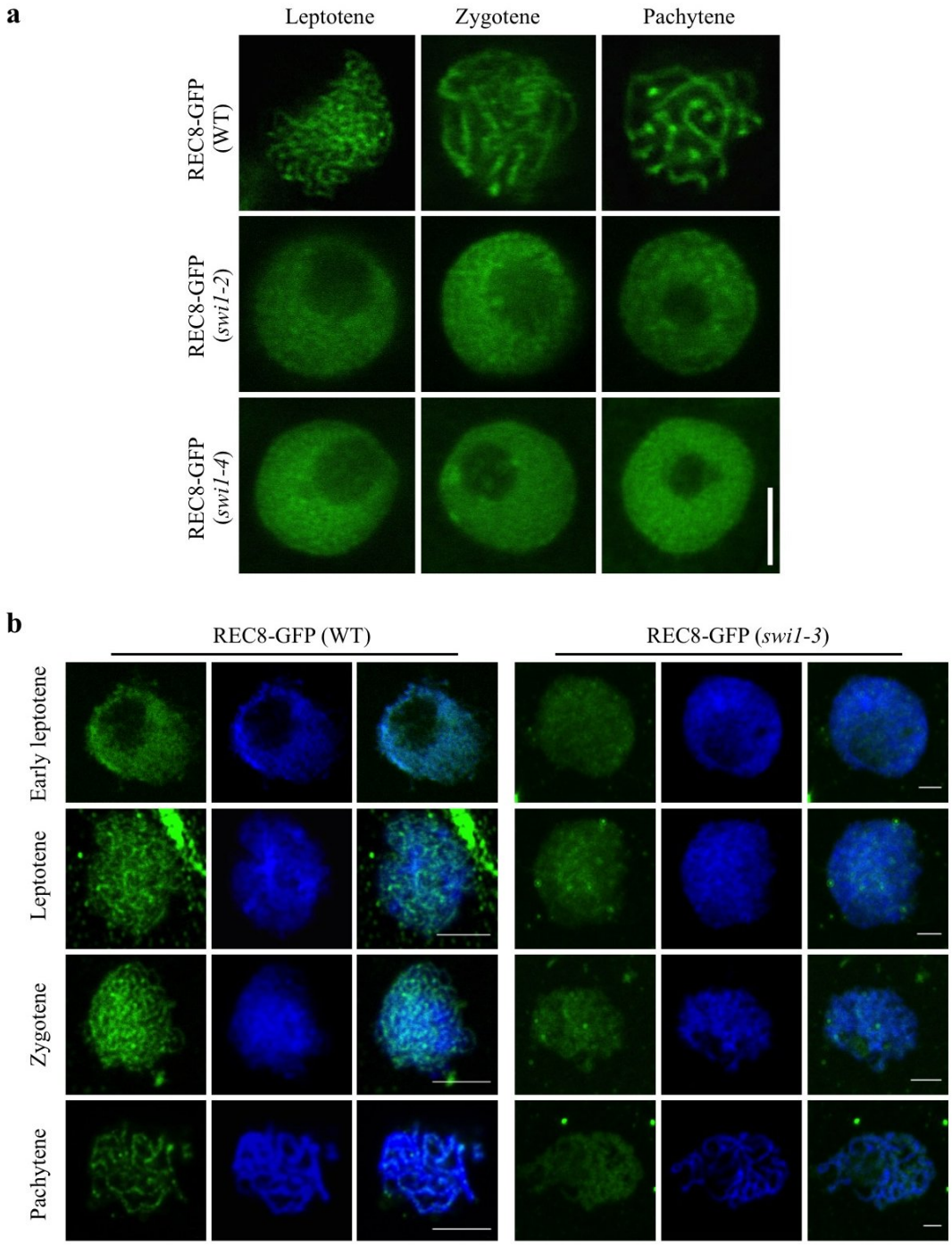

Supplementary Figure 7

Cohesion establishment is compromised in different *swi1* alleles. (a) Localization of REC8-GFP was analyzed by using laser confocal microscopy during prophase I of male meiocytes in the wildtype (WT), *swi1-2 and swi1-4*. Bar: 5 µm. (b)

Immunolocalization of REC8-GFP in the male meiocytes of the wildtype and *swi1-3* mutants during prophase I. Anti-GFP antibody was used for detecting REC8-GFP. Bar: 5 μm. **The figure (b) was obtained by the joint contributions of Fanziska Böwer, Kostika Sofroni and Chao Yang.**

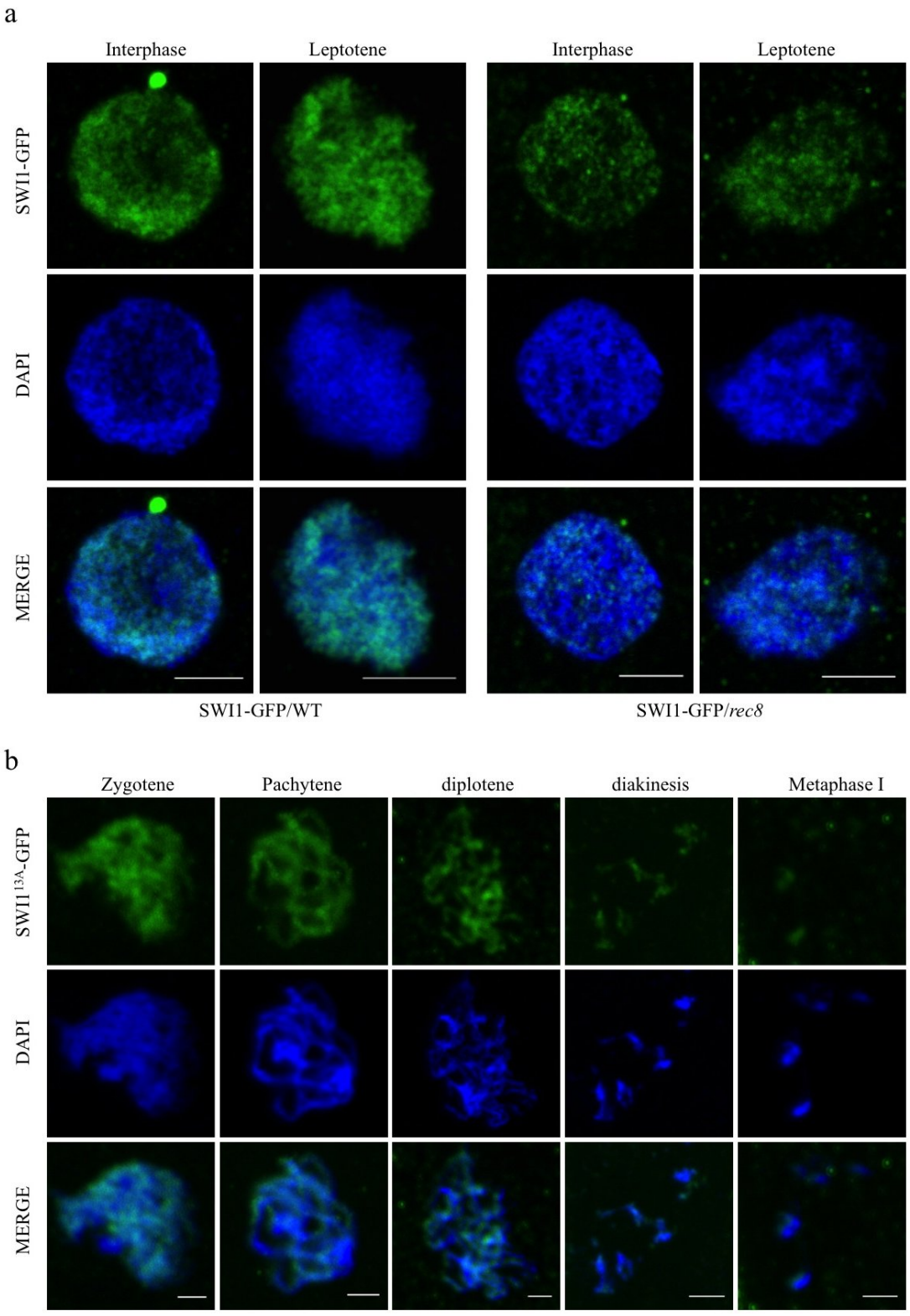

Supplementary Figure 8

Immunolocalization of SWI1-GFP and SWI1^{13A}-GFP. (a) Immunolocalization of SWI1-GFP in the wildtype (WT) and *rec8* mutants. Bar: 5 µm. (b) Immunolocalization of SWI1^{13A}-GFP in the wildtype. Bar: 5 µm. Anti-GFP antibody

was used for detecting SWI1. **This figure was obtained by the joint contributions of Fanziska Böwer, Kostika Sofroni and Chao Yang.**

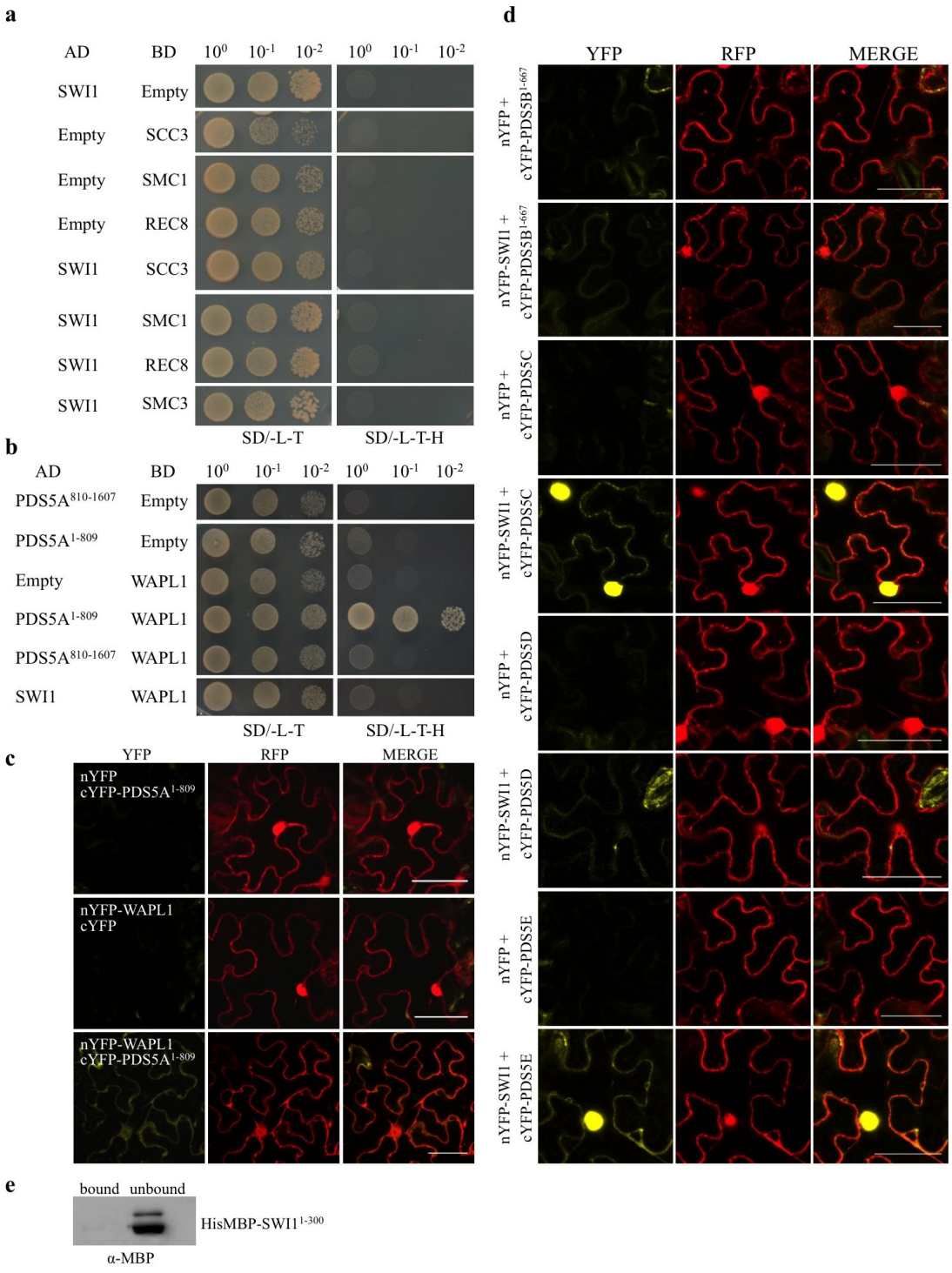

Supplementary Figure 9

Interaction analyses of SWI1, PDS5, and WAPL. (a) Yeast two-hybrid interaction assay of SWI1 with the core cohesin subunits SMC1, SMC3, REC8 and SCC3. (b) Yeast two-hybrid analysis of the interactions of WAPL1 with PDS5 and SWI1. (c)

BiFC interaction assay of WAPL1 with PDS5A. Bar: 50 μm. (d) BiFC interaction assay of SWI1 with PDS5B, PDS5C, PDS5D, and PDS5E. (e) Immunoprecipitation for HisMBP-SWI1$^{1-300}$ only using GST binding beads showing no unspecific binding.

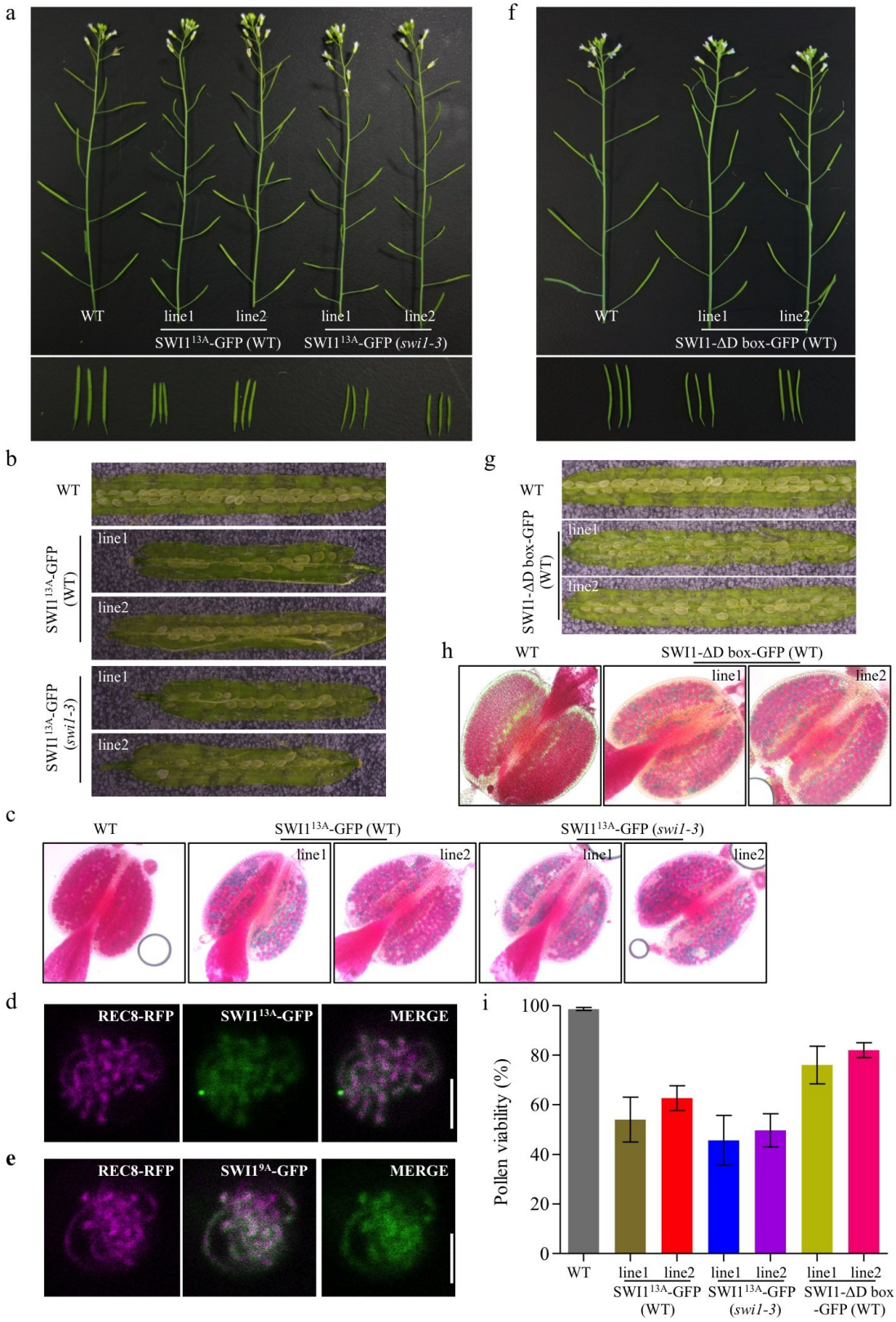

Supplementary Figure 10

Fertility of plants harboring the SWI1^{13A}-GFP and SWI1-ΔD box-GFP constructs. (a) Main branches (upper panel) and siliques (lower panel) of the wildtype (WT) and two *SWI1^{13A}-GFP* lines in both WT and *swi1-3* muatnt

background. (b) Seed sets in siliques of the WT and two *SWI1*^{13A}*-GFP* lines in both WT and *swi1-3* muatnt background. (c) Peterson staining of anthers for the WT and and two *SWI1*^{13A}*-GFP* lines in both WT and *swi1-3* muatnt background. (d, e) Co-localization of REC8-RFP and SWI1^{13A}-GFP (d) and SWI1^{9A}-GFP (e) in the male meiocytes of *swi1-3* mutant at pachytene. Bar: 5 μm. (f) Main branches (upper panel) and siliques (lower panel) of the wildtype (WT) and two *SWI1-ΔD box-GFP* lines in WT background. (g) Seed sets in siliques of the WT and two *SWI1-ΔD box-GFP* lines in WT background. (h) Peterson staining of anthers for the WT and and two *SWI1-ΔD box-GFP* lines in WT background. (i) Quantification of the pollen viability for the plants shown in (a) and (f).

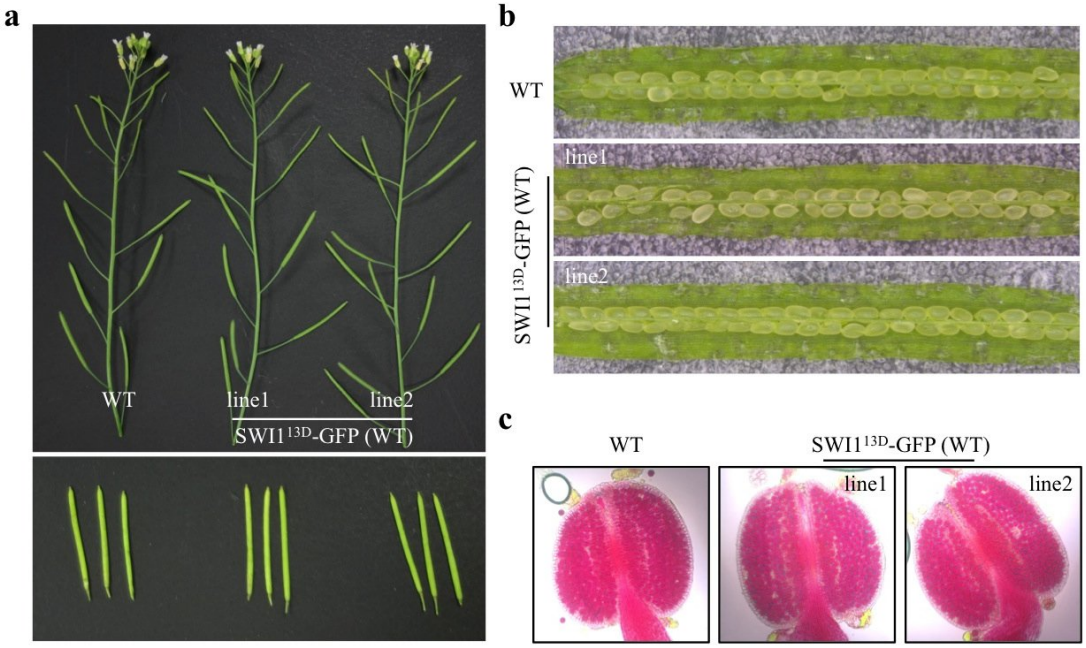

Supplementary Figure 11

Fertility of plants harboring the SWI1^{13D}-GFP construct. (a) Main branches (upper panel) and siliques (lower panel) of the wildtype (WT) and two *SWI1*^{13D}*-GFP* lines in wildtype (WT) background. (b) Seed sets in siliques of the WT and two *SWI1*^{13D}*-GFP* lines. (c) Peterson staining of anthers for the WT and and two *SWI1*^{13D}*-GFP* lines.

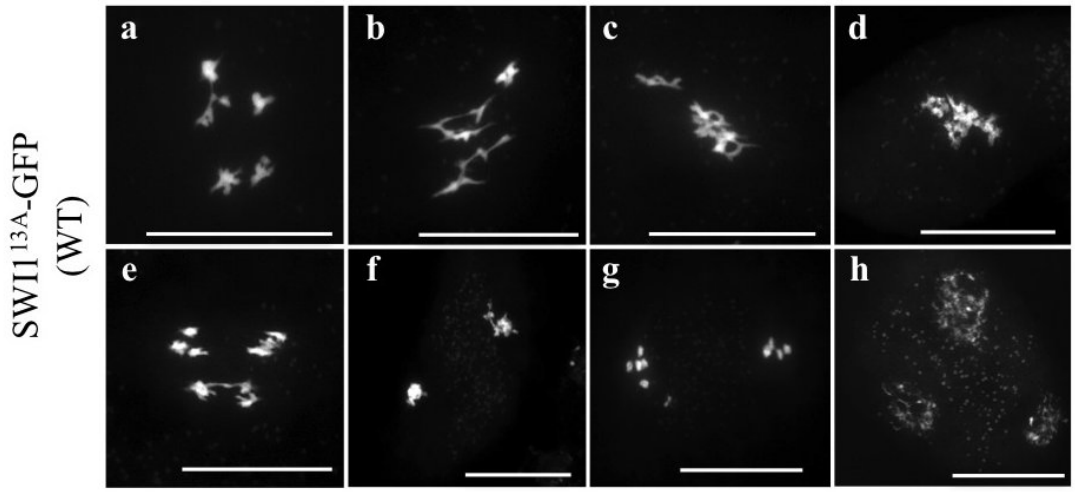

Supplementary Figure 12

Chromosome spread analysis of male meiocytes in *SWI1*^{13A}*-GFP*/WT plants. (a, b) diakinesis-like stage; (c, d) metaphase I-like stage; (e) anaphase I; (f, g) late telophase I or interkinesis; (h) Tetrad-like stage. Bar: 20 μm. **This figure is kindly provided by Kostika Sofroni using the materials prepared by Chao Yang.**

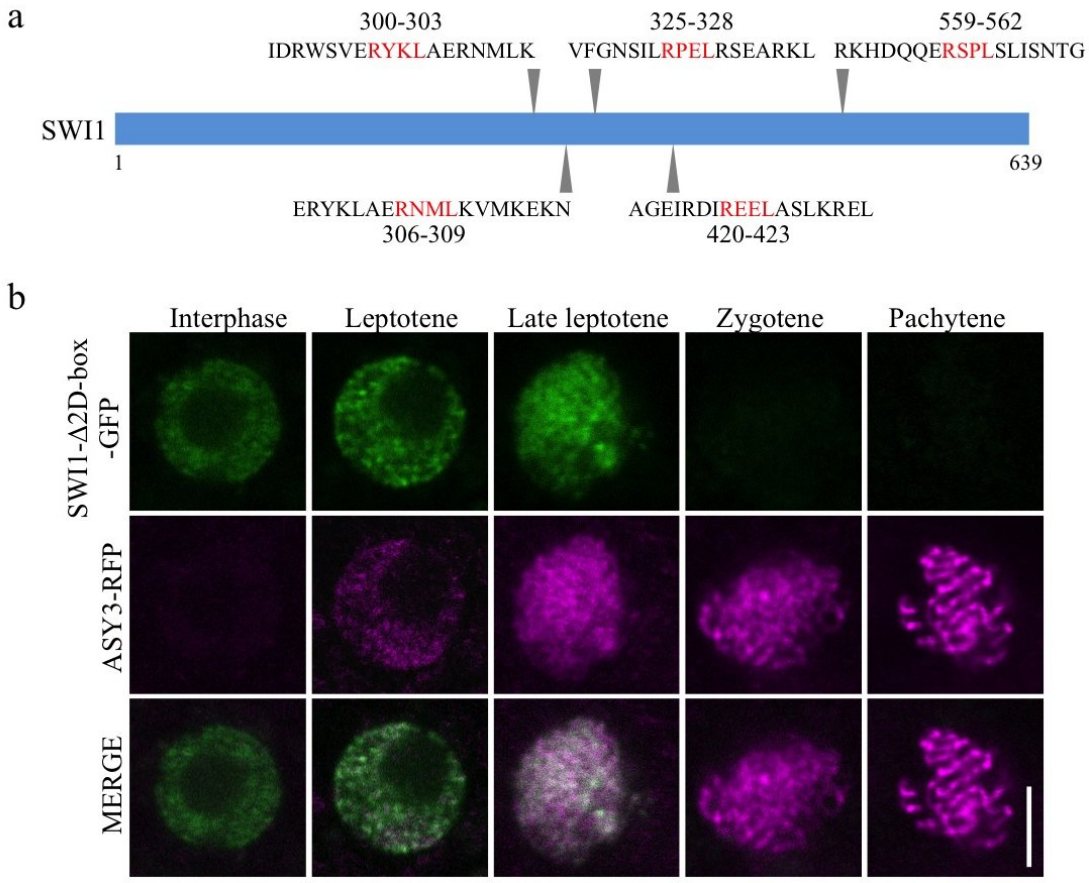

Supplementary Figure 13

Mutation of two conserved destruction box (D-box) has no impact on the localization pattern of SWI1. (a) Scheme of SWI1 coding region. Arrowheads indicate the positions of five putative D-boxes. (b) Localization analysis of SWI1-Δ2D-box-GFP (306-309 and 559-562) in the male meiocytes during prophase I. Bar: 5 µm.

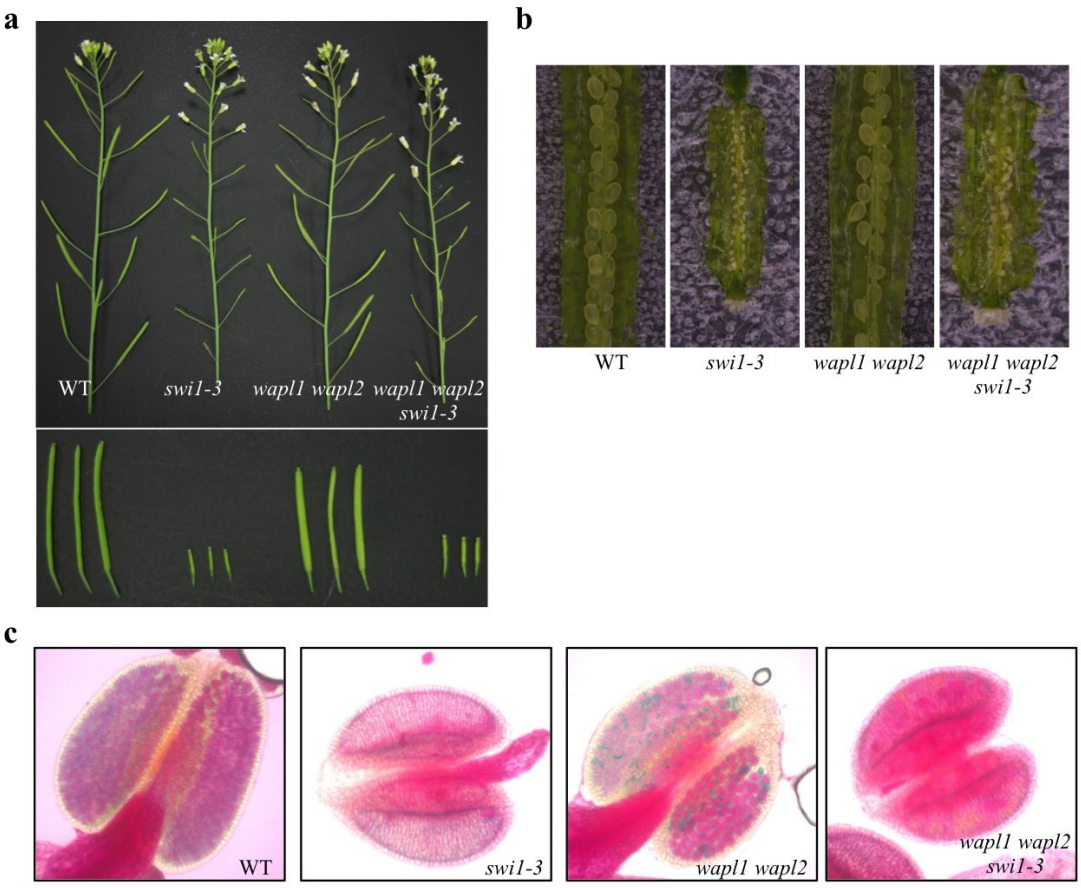

Supplementary Figure 14

The absence of *WAPL1 WAPL2* does not restore the fertility of *swi1-3* mutants.

(a) Main branches (upper panel) and siliques (lower panel) of the wildtype (WT), *swi1-3*, *wapl1 wapl2* and *wapl1 wapl2 swi1-3* mutants. (b) Seed sets in siliques of the wildtype (WT), *swi1-3*, *wapl1 wapl2* and *wapl1 wapl2 swi1-3* mutants. (h) Peterson staining of anthers for the wildtype (WT), *swi1-3*, *wapl1 wapl2* and *wapl1 wapl2 swi1-3* mutants.

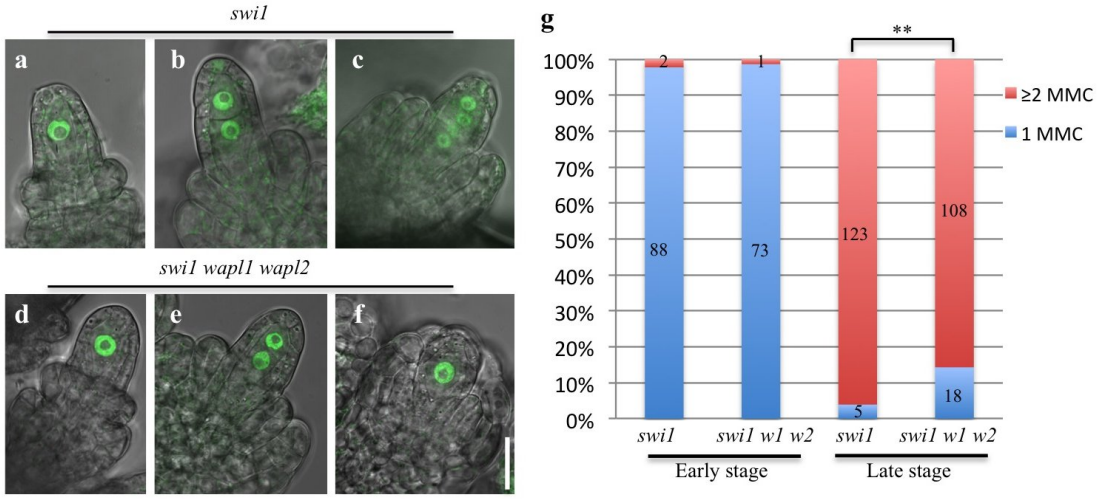

Supplementary Figure 15

The formation of single megaspore mother cell (MMC) in *swi1* mutants is partially rescued by depletion of WAPL. REC8-GFP was used as a maker for the counting of MMC. (a, d) Early premeiotic ovule with short integument primordia harboring one MMC. (b, e) Further developed ovules with elongated integuments containing two MMCs. (c) Older ovules than shown in (b) encompassing four MMCs. (f) Ovule at the similar stages as shown in (b, e) with only one MMC. Bar: 20 μm. (g) Statistical analysis of the number of MMCs at early (as in a, d) and late stages (as in b, c, e, f) in *swi1* and *swi1 wapl1 wapl2* (*swi1 w1 w2*) mutants. The numbers on the columns denote the amount of ovules counted. **, P< 0.01 (Chi-squared test).

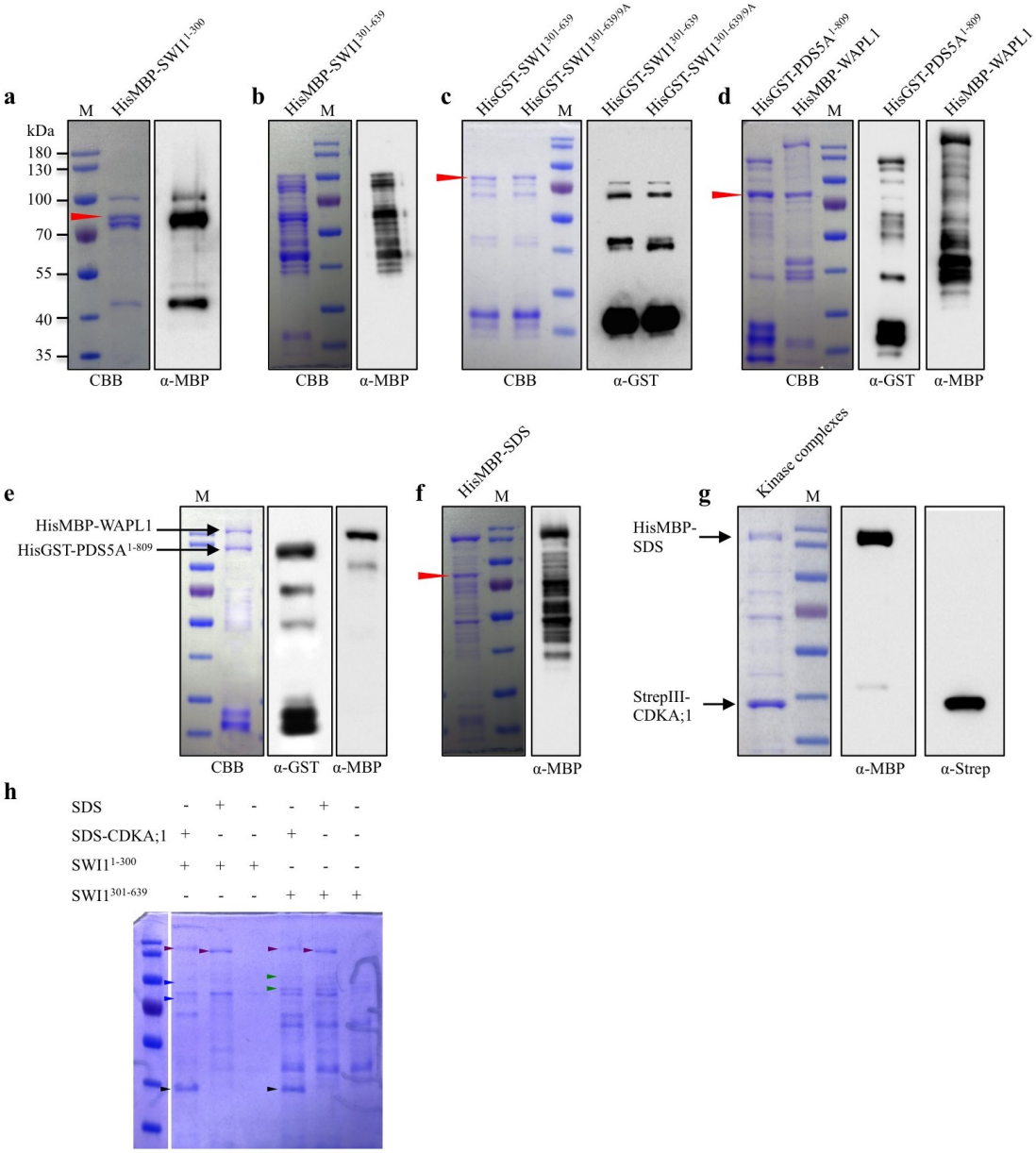

Supplementary Figure 16

CBB stained gels of all purified proteins from *Escherichia Coli* used in this research. (a-c) CBB staining and western blot confirmation of purified HisMBP-SWI1$^{1-300}$ (a), HisMBP-SWI1$^{301-639}$ (b), HisGST-SWI1$^{301-639}$ and HisMBP-SWI1$^{301-639/9A}$ (c), HisMBP-PDS5A$^{1-809}$ and HisMBP-WAPL1 (d), HisMBP-PDS5A$^{1-809}$-HisMBP-WAPL1 heterodimers (e), HisMBP-SDS (f) and CDKA;1-SDS complexes (g) from *E.coli*. The arrowheads indicate the bands of unspecific protein binding generally to Ni-NTA beads. (h) CBB staining of the proteins after kinase reaction of SWI1 with CDKA;1-SDS complexes. The purple, blue, green or black arrowheads

denote the main bands of SDS, SWI1$^{1-300}$, SWI1$^{301-639}$ or CDKA;1 proteins, respectively.

Supplementary table 1. Phosphorylated sites in SWI1.

Experiments	Proteins	Positions	Amino acid	Localization probabilities	peptides and Phospho Probabilities
replicate 1	SWI1 1-300; AT5G51330.1	22	S	0,99989	ISS(1)PSSPTLNVAVAHIR
	SWI1 1-300; AT5G51330.1	166	T	0,998469	REVVSQPAY(0.002)NT(0.998)R
	SWI1 301-639; AT5G51330.1	395	T	1,00000	EAGVKDPYWT(1)PPPGWK
	SWI1 301-639; AT5G51330.1	447	T	0,89016	KEEEELVIMT(0.11)T(0.89)PNSCVTSQNDNLMTPAK
	SWI1 301-639; AT5G51330.1	544	S	0,99992	VVNKGNQITES(1)PQNR
	SWI1 301-639; AT5G51330.1	560	S	1,00000	KHDQQERS(1)PLSLISNTGFR
	SWI1 301-639; AT5G51330.1	597	S	0.34000	ICRPVGMFAWPQLPALAAATDT(0.037)NAS(0.478)S(0.34)PS(0.117)HR
	SWI1 301-639; AT5G51330.1	606	S	1,00000	QAYPS(1)PFPVKPLAAK
replicate 2	SWI1 1-300; AT5G51330.1	22	S	0,99998	ISS(1)PSSPTLNVAVAHIR
	SWI1 1-300; AT5G51330.1	166	T	0,893899	REVVS(0.001)QPAY(0.106)NT(0.894)R
	SWI1 301-639; AT5G51330.1	395	T	1,00000	EAGVKDPYWT(1)PPPGWK
	SWI1 301-639; AT5G51330.1	447	T	0,60282	KEEEELVIMT(0.354)T(0.603)PNS(0.035)CVTSQNDNLMTPAK
	SWI1 301-639; AT5G51330.1	544	S	0,99997	VVNKGNQITES(1)PQNR
	SWI1 301-639; AT5G51330.1	560	S	0,98042	KHDQQERS(0.98)PLS(0.02)LISNTGFR
	SWI1 301-639; AT5G51330.1	597	S	0,70145	ICRPVGMFAWPQLPALAAATDTNAS(0.073)S(0.701)PS(0.225)HR
	SWI1 301-639; AT5G51330.1	606	S	0,99999	QAYPS(1)PFPVKPLAAK

Phosphorylated peptides of SWI1 were identified by mass spectrometry analysis after subjecting SWI1 to *in vitro* kinase assays with CDKA;1-SDS complexes, as shown in Fig. S9d. No phosphorylated peptides were found in reactions without CDKA;1. Results from two independent biological replicates are shown. Data are available via ProteomeXchange Consortium with the identifier PXD009959. **The kinase assay was performed by Chao Yang and the subsequent mass spectrometry analysis was kindly performed by Sara Christina Stolze and Hirofumi Nakagami.**

Supplementary Table 2. Primers used in this research.

Purpose	Prmer name	sequence
SWI1 reporter	gSWI1-F	TTGACATTGTGAGAGTAACG
	gSWI1-R	AACTAGTCTAGAGAACGGGT
	gSWI1-attB1-F	GGGGACAAGTTTGTACAAAAAAGCAGGCTTAGCACTTTATGGTTTTTCCG
	gSWI1-attB2SmaI-R	GGGGACCACTTTGTACAAGAAAGCTGGGTTTCACCCGGGAACGTTGAAGAGATTCTTGG
ASY3 reporter	gASY3-F	TTTGAGAACTCCACTTTACTGCGT
	gASY3-R	CTGCTACTATCTTGTCGTCTTCTC
	gASY3-attB1-F	GGGGACAAGTTTGTACAAAAAAGCAGGCTTAAAAACATTACTTCCCCTACCAAA
	gASY3-attB2-SmaI-R	GGGGACCACTTTGTACAAGAAAGCTGGGTTTCACCCGGGATCATCCCTCAAACATTCTGCGA
ZYP1b reporter	gZYP1b-F	GAAATCAGATGAGCCCTTCCTTAA
	gZYP1b-R	GGGAACTGACTTTGTGTGGTAGAC
	gZYP1b-attB1-F	GGGGACAAGTTTGTACAAAAAAGCAGGCTTAGAAATCAGATGAGCCCTTCC
	gZYP1b-attB2-R+T	GGGGACCACTTTGTACAAGAAAGCTGGGTTTTATCAATCAAATGCATAGGGATC
	gZYP1b-AscI-F	AAGCATGGCGCGCCGGTAATAAGAGAAGCGAGCA
	gZYP1b-AscI-R	AAGCATGGCGCGCCACCAAGACGAGATTCTTTCA
	GFP-AscI-F	AAGCATGGCGCGCCAGGTGGCGGTGGATCAGGCGG
	GFP-AscI-R	AAGCATGGCGCGCCCAGACCCTCCACCTCCCTTGT
Y2H	SMC1-EcoRI-F	CCGGAATTCATGCCTGCGATACAATCCCCATCG
	SMC1-SalI-R	ACGCGTCGACTCACGATTCTTGGTAGTTCCTAAGG
Y2H	SMC3-NcoI-F	CATGCCATGGGAATGTTTATCAAGCAGGTTATAATCG
	SMC3-BamHI-R	CGCGGATCCTCAGGTATCGTGGGACTGATCTTTC
Y2H	REC8-EcoRI-F	CCGGAATTCATGTTGAGACTGGAGAGTTTGATAG
	REC8-SalI-R	ACGCGTCGACTTACATGTTGGGTCCTCTTGCAATG
Y2H	SCC3-EcoRI-F	CCGGAATTCATGGAAGACAGTCCTCAAGGCCTTA
	SCC3-SalI-R	ACGCGTCGACTCAGTGTCCCTTGGACCGTTCACCC
Y2H	SWI1-EcoRI-F	CCGGAATTCATGAGTAGTACGATGTTCGTGAAAC
	SWI1-XhoI-R	CCGCTCGAGTCAAACGTTGAAGAGATTCTTGG
Y2H and protein expression	SWI1-attB1-F	GGGGACAAGTTTGTACAAAAAAGCAGGCTTCATGAGTAGTACGATGTTCGTGAAA
	SWI1-300aa-attB2-R	GGGGACCACTTTGTACAAGAAAGCTGGGTTTCACCTCTCAACAGACCATCTATCA
	SWI1-301aa-attB1-F	GGGGACAAGTTTGTACAAAAAAGCAGGCTTCTACAAACTAGCTGAGAGGAACATG
	SWI1-639aa-attB2-R	GGGGACCACTTTGTACAAGAAAGCTGGGTTTCAAACGTTGAAGAGATTCTTGGG
Y2H and protein expression	AtPDS5A 1-809aa-F	ATGGCTCAGAAGCCGGAGGAACAGTTGAAAG
	AtPDS5A 1-809aa-R	CTACTTAACCAACGTCTTGATCCCATATATCTTC
	AtPDS5A 810-1607aa-F	CTGAAGATATATGGGATCAAGACGTTGGTT
	AtPDS5A 810-1607aa-R	CTATATTGCTGTCCTCGAGATTGACTTACCCAC
	AtPDS5A 1-809-attB1 F	GGGGACAAGTTTGTACAAAAAAGCAGGCTTCATGGCTCAGAAGCCGGAGGAACAG
	AtPDS5A 1-809-attB2 R	GGGGACCACTTTGTACAAGAAAGCTGGGTTCTACTTAACCAACGTCTTGATCCCA
	AtPDS5A 810-1607-attB1 F	GGGGACAAGTTTGTACAAAAAAGCAGGCTTCCTGAAGATATATGGGATCAAGAC
	AtPDS5A 810-1607-attB2 R	GGGGACCACTTTGTACAAGAAAGCTGGGTTCTATATTGCTGTCCTCGAGATTGAC
Y2H and protein expression	WAPL1-CDS-F	ATGATAATTGTAAAACTAACGGCCAATCGC
	WAPL1-CDS-R	CTACGGTGATTTGCAGGATTCAATCACTCCC
	WAPL1-CDS-attB1-F	GGGGACAAGTTTGTACAAAAAAGCAGGCTTCATGATAATTGTAAAACTAACGGCC
	WAPL1-CDS-attB2-R	GGGGACCACTTTGTACAAGAAAGCTGGGTTCTACGGTGATTTGCAGGATTCAATC
Y2H	OsAM1-CDS F	ATGGACGCGGAGATGGCGGCTCCTGCGCTTG

Y2H	OsAM1-CDS R	TCAGCAGTAGGACGGAGTGGCCAGTGCCAGCTC
	OsAM1-attB1-F	GGGGACAAGTTTGTACAAAAAAGCAGGCTTCATGGACGCGGAGATGGCGGCTCC
	OsAM1-attB2-R	GGGGACCACTTTGTACAAGAAAGCTGGGTTTCAGCAGTAGGACGGAGTGGCCAG
	ZmAM1-CDS F	ATGGACGTAGAGACGGTGCAGGCGGGTCCTG
	ZmAM1-CDS R	TCAGCAGTAGGATGGAGTAGCCAGGGCCAGCTC
	ZmAM1-attB1-F	GGGGACAAGTTTGTACAAAAAAGCAGGCTTCATGGACGTAGAGACGGTGCAGGC
	ZmAM1-attB2-R	GGGGACCACTTTGTACAAGAAAGCTGGGTTTCAGCAGTAGGATGGAGTAGCCAG
Dephospho mutagenesis	SWI1 S22/25A-F	GCTCCGTCGGCTCCGACTTTGAATGgtaaactactga
	SWI1 S22/25-R	AGAGATTTTCCCGGCGGTGGTTTCT
	SWI1 S52A-F	GCTCCGGAAAATCTTAAATCGATTAGAG
	SWI1 S52-R	TCTCTGAGGAAGAATCGAAGCATCG
	SWI1 S173A-F	GCTCCGGAGGGAAAGTGCTCGTCTGAG
	SWI1 S173-R	AGCAGCGCGACAGAGACGAGTATTG
	SWI1 T242A-F	GCTAAACAAGAGGCAAAGGAGATAACTA
	SWI1 T242-R	GCCTCCTATTTCATTCCCATCATCA
	SWI1 S261A-F	GCTAGTACTGAGAGACTCGCTCAGAAAG
	SWI1 S261-R	TTCAATCAGCTTTCTCTTACGATT
	SWI1 T395A-F	GCTCCTCCACCTGGTTGGAAGCTTGGTG
	SWI1 T395-R	CCAGTAAGGATCTTTAACTCCTGCT
	SWI1 T447A-F	GCTCCTAATTCTTGTGTTACTAGTCAG
	SWI1 T447-R	AGTCATGATAACAAGCTCCTCCTCT
	SWI1 T461A-F	GCTCCAGCAAAGgtaagagctcgaaaca
	SWI1 T461-R	CATCAGATTATCATTCTGACTAGTA
	SWI1 T515A-F	GCTCCTTTGCTACTAGAGGATTCACCAC
	SWI1 T515-R	CTCTGTTGAGTCTGGCTTTTTAGGA
	SWI1 S522A-F	GCTCCACCAATACAGACACTAGAAGGAG
	SWI1 S522-R	ATCCTCTAGTAGCAAAGGTGTCTCT
	SWI1 S544A-F	GCTCCTCAAAACAGAGAAAAAGGAAGGA
	SWI1 S544-R	CTCTGTGATTTGGTTACCCTTGTTC
	SWI1 S560A-F	GCTCCACTTTCACTAATAAGCAACACTG
	SWI1 S560-R	TCTTTCTTGTTGATCATGCTTCCTT
	SWI1 S597A-F	GCTCCAAGTCACAGACAAGCCTACCCAT
	SWI1 S597-R	AGAAGCATTAGTATCAGTAGCAGCA
	SWI1 S606A-F	GCTCCTTTTCCAGTCAAGCCACTTGCAG
	SWI1 S606-R	TGGGTAGGCTTGTCTGTGACTTGGC
genotyping for *swi1-2*	SWI1-CAPS-F	AACAAGAGGCAAAGGAGATAAC
	SWI1-CAPS-R	TTTTCAGCAGATCAGCCGTAGA
genotyping for *swi1-3*	SAIL_654_C06 LP	ACTCATCACCGCTTGATTCTG
	SAIL_654_C06 RP	TGATACTGCACACGCAATCTC
genotyping for *swi1-4*	GABI_206H06 LP	CTCCCAGATTCATTAAATGCG
	GABI_206H06 RP	CTAGAAACCCAGAAACCCCAG
Phosphomimic mutagenesis	SWI1 S22/25D-F	GACCCGTCGGACCCGACTTTGAATGgtaaactactga
	SWI1 S22/25-R	AGAGATTTTCCCGGCGGTGGTTTCT
	SWI1 S52D-F	GACCCGGAAAATCTTAAATCGATTAGAG
	SWI1 S52-R	TCTCTGAGGAAGAATCGAAGCATCG
	SWI1 S173D-F	GACCCGGAGGGAAAGTGCTCGTCTGAG
	SWI1 S173-R	AGCAGCGCGACAGAGACGAGTATTGTAC
	SWI1 T395D-F	GACCCTCCACCTGGTTGGAAGCTTGGTG

Phosphomimic mutagenesis	SWI1 T395-R	CCAGTAAGGATCTTTAACTCCTGCT
	SWI1 T447D-F	GACCCTAATTCTTGTGTTACTAGTCAG
	SWI1 T447-R	AGTCATGATAACAAGCTCCTCCTCT
	SWI1 T461D-F	GACCCAGCAAAGgtaagagctcgaaaca
	SWI1 T461-R	CATCAGATTATCATTCTGACTAGTA
	SWI1 T515D-F	GACCCTTTGCTACTAGAGGATTCACCAC
	SWI1 T515-R	CTCTGTTGAGTCTGGCTTTTTAGGA
	SWI1 S544D-F	GACCCTCAAAACAGAGAAAAAGGAAGGA
	SWI1 S544-R	CTCTGTGATTTGGTTACCCTTGTTC
	SWI1 S560D-F	GACCCACTTTCACTAATAAGCAACACTG
	SWI1 S560-R	TCTTTCTTGTTGATCATGCTTCCTT
	SWI1 S597D-F	GACCCAAGTCACAGACAAGCCTACCCAT
	SWI1 S597-R	AGAAGCATTAGTATCAGTAGCAGCA
	SWI1 S522D-F	GACCCACCAATACAGACACTAGAAGGAG
	SWI1 S522-R	ATCCTCTAGTAGCAAAGGTGTCTCT
	SWI1 S606D-F	GACCCTTTTCCAGTCAAGCCACTTGCAG
	SWI1 S606-R	TGGGTAGGCTTGTCTGTGACTTGGC
BiFC constructs	AtPDS5A-attB1 F1	GGGGACAAGTTTGTACAAAAAAGCAGGCTTCATGGCTCAGAAGCCGGAGGAACAG
	AtPDS5A-attB4 R1-T 809aa	GGGGACAACTTTGTATAGAAAAGTTGGGTGCTTAACCAACGTCTTGATCCCA
	AtPDS5B-CDSattB1-F1	GGGGACAAGTTTGTACAAAAAAGCAGGCTTCATGGAGAAAACTCCGACGCAG
	AtPDS5B-CDSattB4-R1_T	GGGGACAACTTTGTATAGAAAAGTTGGGTGGCCACAAAGCTGATTCAAAAG
	AtPDS5C-CDSattB1-F	GGGGACAAGTTTGTACAAAAAAGCAGGCTTCATGTCGGATTCTGATAAAGAG
	AtPDS5C-CDSattB4-R_T	GGGGACAACTTTGTATAGAAAAGTTGGGTGTCGCTTCCTCTTCTTACCGG
	AtPDS5D-CDSattB1-F	GGGGACAAGTTTGTACAAAAAAGCAGGCTTCATGCAAAGTGCCCTAATTCCATC
	AtPDS5D-CDSattB4-R_T	GGGGACAACTTTGTATAGAAAAGTTGGGTGTGACTTTCTCTTCTCTTCATC
	AtPDS5E-CDSattB1-F	GGGGACAAGTTTGTACAAAAAAGCAGGCTTCATGGGTCCTCTTGTCGAAGCG
	AtPDS5E-CDSattB4-R_T	GGGGACAACTTTGTATAGAAAAGTTGGGTGTGGATCAACCTCAAGCACC
	AtSWI1-CDS-attB3-F	GGGGACAACTTTGTATAATAAAGTTGTAATGAGTAGTACGATGTTCGTGAAA
	AtSWI1-639-attB2-R-T	GGGGACCACTTTGTACAAGAAAGCTGGGTTAACGTTGAAGAGATTCTTGGG
	AtSWI1-300-attB2-R-T	GGGGACCACTTTGTACAAGAAAGCTGGGTTCCTCTCAACAGACCATCTATCA
	WAPL1-attB3-F	GGGGACAACTTTGTATAATAAAGTTGTAATGATAATTGTAAAACTAACGGCC
	WAPL1-attB2-R-T	GGGGACCACTTTGTACAAGAAAGCTGGGTTCGGTGATTTGCAGGATTCAATC

The Supplementary videos are kindly provided by Yuki Hamamura (Universität Hamburg) using the materials prepared by Chao Yang.

Supplementary Video 1

Dynamics of REC8-GFP in wild-type plants. Live cell imaging of REC8-GFP was performed in male meiocytes of wild-type plants. Video starts at leptotene stage and runs for 25 h with scan intervals of 30 mins. Bar: 10 μm.

Supplementary Video 2

Dynamics of REC8-GFP in *wapl1 wapl2* mutants. Live cell imaging of REC8-GFP was performed in male meiocytes of *wapl1 wapl2* mutants. Video starts at leptotene stage and runs for 25 h with scan intervals of 30 mins. Bar: 10 μm.

Supplementary Video 3

Dynamics of REC8-GFP in *swi1* mutants. Live cell imaging of REC8-GFP was performed in male meiocytes of *swi1* mutants. Video starts at early zygotene-like stage and runs for 21 h with scan intervals of 15 mins. Bar: 10 μm.

Supplementary Video 4

Dynamics of REC8-GFP in *swi1 wapl1 wapl2* mutants. Live cell imaging of REC8-GFP was performed in male meiocytes of *swi1 wapl1 wapl2* mutants. Video starts at early zygotene-like stage and runs for 21 h with scan intervals of 15 mins. Bar: 10 μm.

Supplementary Video 5

Dynamics of REC8-GFP in wild-type plants. Live cell imaging of REC8-GFP was performed in male meiocytes of wild-type plants. Video starts at early leptotene stage and runs for 30 h with scan intervals of 15 mins. Bar: 10 μm.

Supplementary Video 6

Dynamics of REC8-GFP in *SWI1*^{13A}*-GFP*/WT plants. Live cell imaging of REC8-GFP was performed in male meiocytes of *SWI1*^{13A}*-GFP*/WT plants. Video starts at early leptotene stage and runs for 35 h with scan intervals of 15 mins. Bar: 10 μm.

1.2 Additional results on SWI1 function

The absence of SWI1 results in successive meiosis-like divisions

In chapter 1.1, a novel function and mechanism of SWI1 for the regulation of sister chromatid cohesion is unraveled. In addition, I observed a very interesting phenomenon in *swi1* mutants besides the compromised establishment of sister chromatid cohesion. In early meiosis, as seen by the squared cell shape, a strong signal of REC8-GFP, a meiosis specific protein, was observed in nucleus of the male meiocytes, where a similar size of nucleus was present, indicating that the meiocytes are in an early stage of meiosis I-like as that in wildtype (Figure 1). However, while as the progression of meiosis, REC8-GFP signal was not detectable any longer and tetrads, products of meiosis, were formed in wildtype at late meiosis, a strong signal of REC8-GFP, which highlights many nucleuses with varied sizes, was observed in the cells that were in a very round shape suggesting an late meiotic stage (Figure 1). The different sizes of nucleus suggest that the cells expressing REC-GFP are the daughter cells from the last round of cell division. This observation strongly suggest that following the first round of meiosis I-like division, instead of entering meiosis II the male meiocytes reprogram and restart a new round of meiosis I-like division highlighting by the reappearance of REC8-GFP (Figure 1). This strongly indicates a successive meiosis-like cell division in *swi1* mutants, a previously unrecognized phenotype. This successive meiosis-like cell division is more clearly manifested by a constant observation of the expression of REC8-GFP for 45 h in the male meiocytes of *swi1 wpal1 wapl2* mutants in which the establishment of the sister chromatid cohesion is rescued thus showing the clear cell divisions (Figure 2, supplemental movie 7).

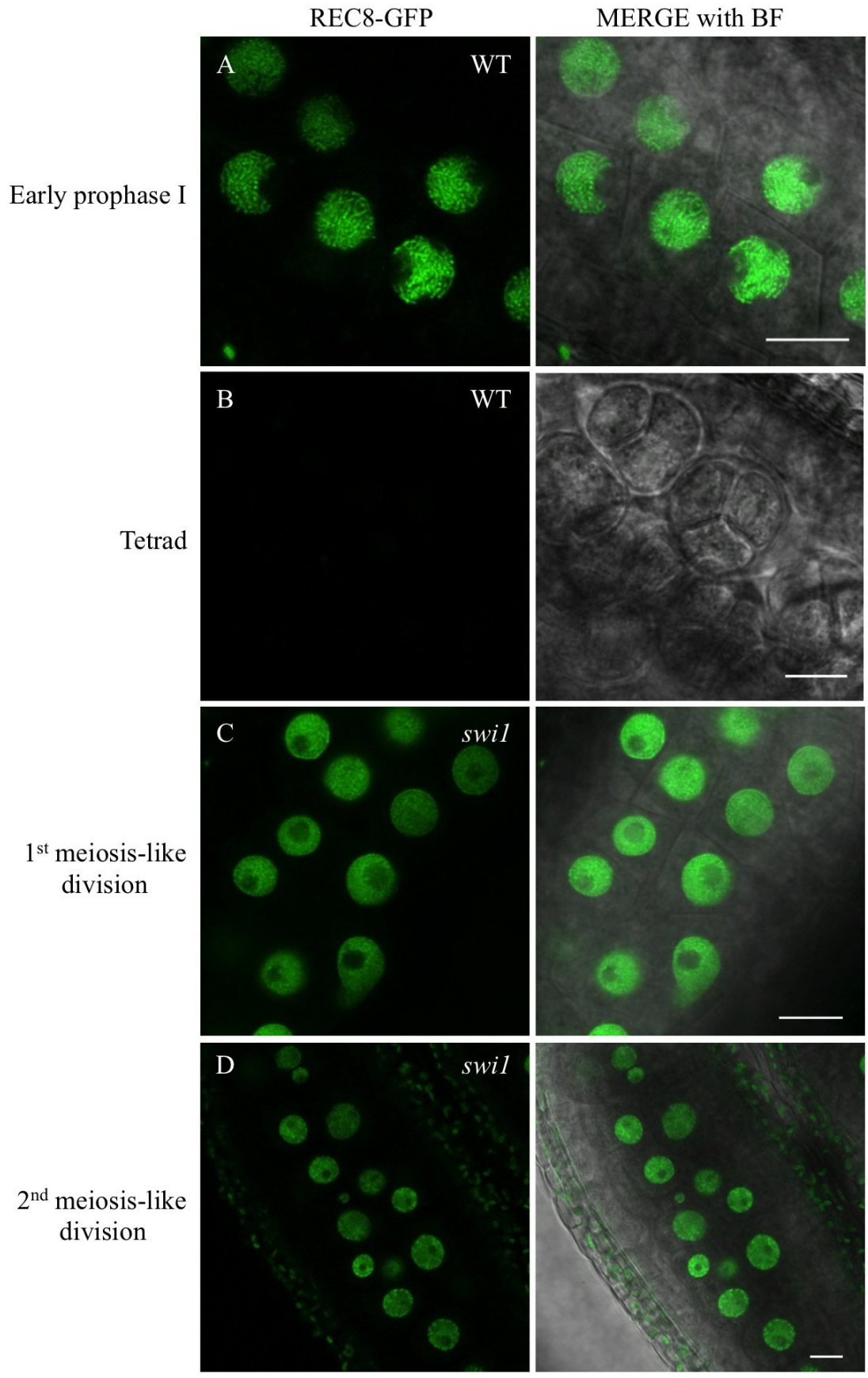

Figure 1. The absence of SWI1 leads to successive meiosis-like cell divisions. (A and B) Confocal laser scanning micrographs of REC8-GFP at early prophase I (A)

and tetrad stage (B) of the male meiocytes of wildtype. (C and D) Confocal laser scanning micrographs of REC8-GFP at the 1st- (C) and 2nd meiosis-like divisions (D) of the male meiocytes of *swi1* mutants. Bars: 10 μm.

In addition, the successive meiosis-like cell division was also observed in the female meiocytes (chapter 3 Fig. S15A-F). For example, when the very short integument primordia of the ovule was observed, only one meiocyte expressing REC8-GFP was usually observed (88 out of 90) (chapter 3 Fig. S15A). However, when the integuments were further elongated indicating a later stage, two meiocytes expressing REC8-GFP were detected (65 out of 68), which suggests that the daughter cells generated from the last mitosis-like meiotic cell division restart a meiosis I-like cell program (chapter 3 Fig. S15B). Moreover, as the further development of the ovule where the meiosis has been finished in wildtype, in *swi1* mutants four meiocytes expressing REC8-GFP were present in one ovule (58 out of 60), which suggests that the cells expressing REC8-GFP are still performing meiosis-like program (chapter 3 Fig. S15C).

REC8-GFP in *swi1 wapl1 wapl2*

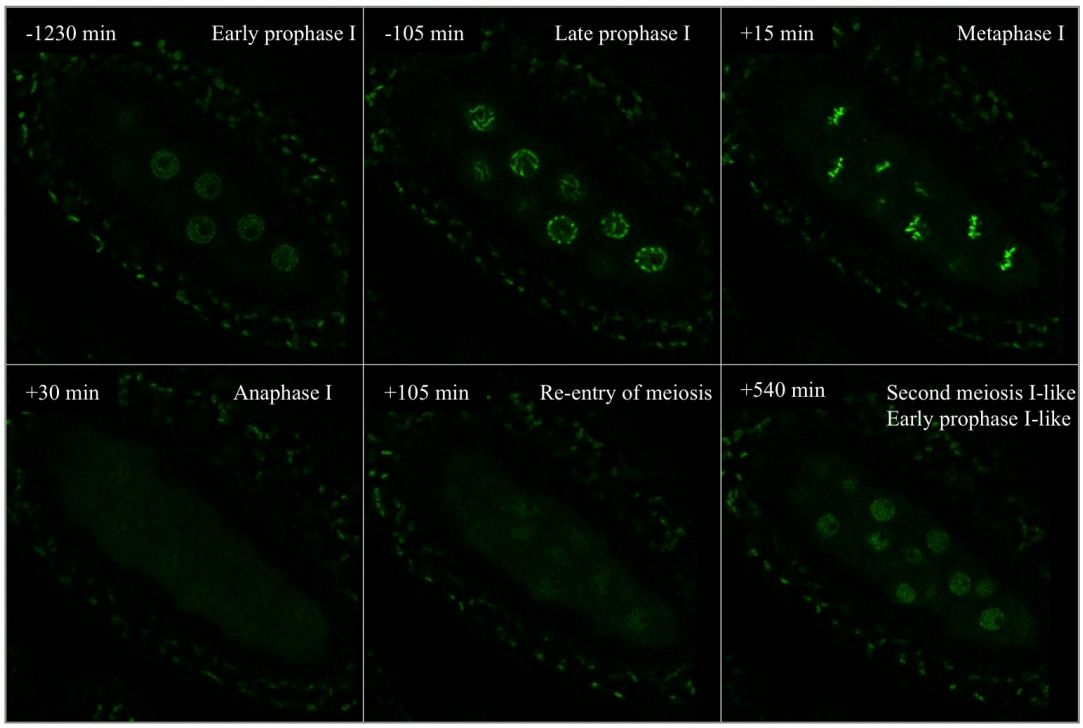

Figure 2. Expression patterns of REC8-GFP in the same anther of the *swi1 wapl1 wapl2* mutants at different time points of cell division using live cell imaging. The

time point of the first nuclear envelope breakdown was defined as 0 min. The complete movie was shown in supplemental movie 7. **This figure is provided kindly by Yuki Hamamura using the materials generated by Chao Yang.**

1.3 Additional discussion on SWI1 function

Beyond the regulation of sister chromatid cohesion by SWI1

The successive meiosis-like cell division in *swi1* mutants shown above suggests that, in addition to regulating sister chromatid cohesion, SWI1 might be involved either in defining the identity of germ cells, or in the regulation of the transition from sporogenesis to gametogenesis (from spores to gametes). Since the restoration of sister chromatid cohesion in *swi1* mutants by the depletion of WAPL does not rescue this successive meiosis-like dividing defect (Figure 2), it suggests that SWI1 might regulate this process by forming different complexes with PDS5 family proteins, which includes five functional redundant paralogs in *Arabidopsis*, or by interacting with other factors, e.g., chromatin remodeling proteins including the nucleosome remodeling complex SWI/SNF and histone modifying enzymes, to regulate the chromatin structure and/or the relevant gene expression. Interestingly, Boateng et al. found that in *swi1* mutants the patterns of histone 3 acetylation and dimethylation of H3-K4me2 were affected, which supports the latter possibility (Boateng *et al*, 2008). Further investigations will be needed to determine how SWI1 affects this process. For example, identifying new interactors of SWI1 could shed light on this question. One possibility would be to perform the immunoprecipitation (IP) experiments followed by mass spectrometry using *35S:AP1-GR* (*ap1 cal*) plants harboring a stabilized version of SWI1, i.e., the version described in chapter 1 with inactivated phospho-sites (SWI1^{13A}-GFP). The reason to use the *35S:AP1-GR* (*ap1 cal*) plants is that the floral development could be induced and therefore largely synchronized by the dexamethasone treatment, and thus that massive flower buds within the progression of meiosis can be obtained to overcome the material limitation (Wellmer *et al*, 2006). In addition, using the stabilized SWI1^{13A}-GFP for the IP, which is largely functional and does not show localization defect, would largely avoid the degradation issue during the experimental operation (chapter 1 Figure 6c and S10d). These studies will contribute to understand the multiple functions of SWI1 in the regulation of meiosis besides the role in maintaining sister chromatid cohesion.

Chapter 2

2.1 Manuscript under revision

The *Arabidopsis* Cdk1/Cdk2 homolog CDKA;1 controls chromosome axis assembly in meiosis

Authors: **Chao Yang**[1], Kostika Sofroni[1], Erik Wijnker[1,2], Yuki Hamamura[1], Lena Carstens[1,3], Hirofumi Harashima[4,5], Sara Christina Stolze[6], Daniel Vezon[7], Liudmila Chelysheva[7], Zsuzsanna Orban-Nemeth[8,9], Gaëtan Pochon[1], Hirofumi Nakagami[6], Peter Schlögelhofer[8], Mathilde Grelon[7] and Arp Schnittger[1,*]

[1] University of Hamburg, Department of Developmental Biology, Ohnhorststr. 18, D-22609 Hamburg, Germany

[2] Current affiliation: Laboratory of Genetics, Wageningen University & Research, P.O. Box 16 6700 AA Wageningen, The Netherlands

[3] Current affiliation: Kiel University, Plant Developmental Biology & Plant Physiology, Am Botanischen Garten 5, 24118 Kiel, Germany

[4] RIKEN Center for Sustainable Resource Science, 1-7-22 Suehiro, Tsurumi, Yokohama, Kanagawa, 230-0045, Japan

[5] Current affiliation: Solution Research Laboratory, AS ONE Corporation, 3-25-22, Tonomachi, Kawasakiku, Kawasaki, Kanagawa, 210-0821, Japan

[6] Max-Planck-Institute for Plant Breeding Research, 50829 Cologne, Germany.

[7] Institut Jean-Pierre Bourgin, INRA, AgroParisTech, CNRS, Université Paris-Saclay, 78000, Versailles, France

[8] Department of Chromosome Biology, Max F. Perutz Laboratories, University of Vienna, Vienna Biocenter, 1030 Vienna, Austria

[9] Current affiliation: Institute of Molecular Pathology, Vienna Biocenter, 1030 Vienna, Austria

[*] For correspondence: arp.schnittger@uni-hamburg.de

The *Arabidopsis* Cdk1/Cdk2 homolog CDKA;1 controls chromosome axis assembly in meiosis

Abstract

Meiosis is key to sexual reproduction and genetic diversity. Here, we show that the *Arabidopsis* cyclin-dependent kinase Cdk1/Cdk2 homolog CDKA;1 is an important regulator of meiosis needed for several aspects of meiosis such as chromosome synapsis. We identify the chromosome axis protein ASYNAPTIC 1 (ASY1), the *Arabidopsis* Homolog pairing 1 (Hop1) homolog, which is required for synaptonemal complex formation, as a target of CDKA;1. Phosphorylation of ASY1 is required for its recruitment to the chromosome axis via ASYNAPTIC 3 (ASY3), the *Arabidopsis* Reductional division 1 (Red1) homolog, counteracting the disassembly activity of the AAA+ ATPase PACHYTENE CHECKPOINT 2 (PCH2). Furthermore, we have identified the closure motif in ASY1, typical for HORMA domain proteins, and provide evidence that the phosphorylation of ASY1 regulates the putative self-polymerization of ASY1 along the chromosome axis. Hence, the phosphorylation of ASY1 by CDKA;1 appears to be a two-pronged mechanism to initiate chromosome axis formation in meiosis.

Introduction

Cell division relies on a highly orchestrated order of events to allow the faithful distribution of chromosomes to daughter cells. Progression through the cell cycle is controlled by the activity of cyclin-dependent kinases (Cdks) (Morgan, 1997; Malumbres *et al*, 2009; Harashima *et al*, 2013). Eukaryotes usually contain several different families of cyclins that are thought to provide substrate specificity to Cdk-cyclin complexes and guide their intracellular localization (Miller & Cross, 2001; Pagliuca *et al*, 2011). However, the absolute levels of kinase activity have been found to be of key importance for cell cycle control and, at least in fission yeast, a single Cdk-cyclin complex has been found to be sufficient to drive both mitosis and meiosis (Coudreuse & Nurse, 2010; Gutiérrez-Escribano & Nurse, 2015).

In comparison to mitosis, much less is known about how Cdks control the progression of the two consecutive division events of meiosis. Meiosis II leads to the separation of sister chromatids that, at least formally, resembles a mitotic division and

is thought to largely rely on similar control mechanisms as mitosis. In contrast, meiosis I holds many features that are not known from mitosis, foremost recombination between homologous chromosomes. Nonetheless, Cdk-cyclin complexes have been shown to control several aspects of meiosis I such as the formation of DNA double strand breaks (DSBs) at the beginning of the meiotic recombination process by phosphorylating Mer2/Rec107 (Meiotic recombination 2/ Recombination 107) (Rockmill & Roeder, 1990; Li *et al*, 2006; Henderson *et al*, 2006).

Furthermore, the repair of DSBs through meiotic recombination has been found to involve Cdks, namely to phosphorylate the nuclease Sae2/Com1 (Sporulation in the absence of spo eleven 2/Completion of meiotic recombination 1) and by that promote its activity to generate 3' overhangs at the DSB site (Huertas & Jackson, 2009; Anand *et al*, 2016; Cannavo *et al*, 2018). These DNA ends are further processed by the MRN/MRX complex comprising the subunits Mre11 (Meiotic recombination 11), Rad50 (Radiation 50) and Nbs1/Xrs2 (Nijmegen Breakage Syndrome 1/X-ray sensitive 2) (Mimitou and Symington, 2009; Manfrini *et al.*, 2010). Subsequently, the single DNA strands are bound by the recombinases Rad51 (Radiation 51) and Dmc1 (Disrupted meiotic cDNA1) to promote strand invasion and formation of heteroduplex DNA (Shinohara *et al*, 1997; Kurzbauer *et al*, 2012; Da Ines *et al*, 2013). Depending on how the subsequently resulting double Holliday junctions are resolved, meiotic crossovers (COs) can be formed that lead to the reciprocal exchange of DNA segments between homologous chromosomes (Zickler & Kleckner, 2015; Lambing *et al*, 2017). Cdks were found to partially co-localize with Rad51 as well as other components acting downstream of Rad51 involved in CO formation (Baker *et al.*, 1996, 1996; Zhu *et al.*, 2010). This, together with the observation that inhibition of Cdk activity in early meiosis abolished the formation of RAD51 foci, led to the conclusion that the activity of Cdk is essential for DSB formation and/or processing (Henderson *et al*, 2006; Huertas *et al*, 2008; Zhu *et al*, 2010).

In many species, the synaptonemal complex (SC) stabilizes the pairing of homologous chromosomes and plays an important role in promoting the inter-homolog bias during recombination and in maturation of recombination intermediates into COs (Zickler & Kleckner, 1999; Mercier *et al*, 2015). The SC is formed by the two proteinaceous axes of homologous chromosomes that will become then the lateral

elements of the SC after synapsis. A number of proteins have been identified that are required for the correct formation of the chromosome axis. These include Red1 in yeast and its orthologs such as ASY3 in *Arabidopsis* (Smith & Roeder, 1997; Rockmill & Roeder, 1990; Ferdous *et al*, 2012). Another key protein of the chromosome axis is the HORMA domain protein Hop1 in yeast and its ortholog ASY1 in *Arabidopsis* (Hollingsworth *et al*, 1990; Armstrong, 2002). Phosphorylation of Hop1 at an [S/T]Q cluster domain by Tel1 (Telomere maintenance 1) and Mec1 (Mitosis entry checkpoint 1), the ATM (Ataxia-telangiectasia mutated) and ATR (Ataxia-telangiectasia and Rad3-related) orthologs, is essential for the inter-homolog biased recombination, but not for the chromosomal loading of Hop1 (Carballo *et al*, 2008).

For the correct assembly of the SC, Hop1/ASY1 is recruited to the axis by direct interaction with Red1/ASY3 (Smith & Roeder, 1997; Ferdous *et al*, 2012). Furthermore, it was recently proposed that Hop1 might build a homopolymer through its C-terminal closure motif and it was thought that this polymerization is likely crucial for its function and axis association since the point mutation K593A in the closure motif of Hop1 causes an 11-fold reduction in CO number and results in high spore lethality (Niu *et al*, 2015; West *et al*, 2018).

In wildtype, the chromosome axes (lateral elements) of homologs become connected in the SC via central elements formed by dimers of the Zip1/ZYP1 family of proteins along with other components (Zickler and Kleckner, 2015). SC assembly goes along with the coordinated release of Hop1/ASY1 from the chromosome axis, catalyzed by the triple AAA+ ATPase PCH2 (Wojtasz *et al*, 2009; Chen *et al*, 2014; Lambing *et al*, 2015). However, it is not clear how the dynamic localization Hop1/ASY1 on chromosomes is regulated.

Cdks have also been implicated in the assembly of the SC since Cdk2 mutations in mice as well as inactivation of Cdc28 (Cdk1 homolog) in budding yeast resulted in defects in SC formation (Ortega *et al*, 2003; Zhu *et al*, 2010). However, although Zip1 has been shown to be phosphorylated by Cdk *in vitro*, the molecular details of Cdk function for SC formation are still obscure since the SC is assembled normally in *zip1* mutants in which the Cdk phosphorylation sites were exchanged with amino acids that cannot be phosphorylated (Zhu *et al*, 2010).

The model plant *Arabidopsis*, similar to other multicellular eukaryotes, has several Cdks and cyclins with some of them having been assigned a function in

meiosis (Wijnker & Schnittger, 2013). Six out of the ten A- and one out of the nine B-type cyclins are expressed in meiosis including SOLO DANCERS (SDS), an atypical cyclin that has similarities to both A- and B-type cyclins (Bulankova *et al*, 2013; Azumi *et al*, 2002). However, of these eight cyclins potentially involved in meiosis, only the loss of either *CYCA1;2*, also known as *TARDY ASYNCHRONOUS MEIOSIS* (*TAM*), *CYCB3;1* or *SDS* was found to result in meiotic defects (Prusicki *et al*, 2019; Magnard *et al*, 2001; Azumi *et al*, 2002; d'Erfurth *et al*, 2010; Bulankova *et al*, 2013). TAM is required for the timely progression through meiosis I and for progression into meiosis II. SDS is necessary for crossover (CO) formation after DSBs have been induced, and the meiotic recombinase DMC1 does not localize to chromosomes in *sds* mutants (De Muyt *et al*, 2009). Mutants in *CYCB3;*1 have only a weak mutant phenotype and occasionally show premature and ectopic cell wall formation during meiosis I, a phenotype, however, that can be strongly enhanced in double mutants with *sds* demonstrating a redundant function of at least some of the meiotic cyclins in *Arabidopsis* (Bulankova *et al*, 2013).

SDS and TAM build active kinase complexes with CDKA;1, the *Arabidopsis* Cdk1/Cdk2 homolog, that is the main cell cycle regulator in *Arabidopsis* (Cromer *et al*, 2012; Harashima & Schnittger, 2012; Nowack *et al*, 2012; Cifuentes *et al*, 2016). A function of CDKA;1 in meiosis is supported by the analysis of weak loss-of-function mutants, which are completely sterile (Dissmeyer *et al*, 2009; 2007). Next to CDKA;1, CDKG has been implicated in meiosis by controlling synapsis at ambient but not low temperatures (Zheng *et al*, 2014). However, CDKG, which is related to human Cdk10, is likely involved in transcriptional and posttranscriptional control of gene expression and presumably does not control structural components of chromosomes directly (Zabicki *et al*, 2013; Tank & Thaker, 2011; Huang *et al*, 2013; Doonan & Kitsios, 2009).

Here, we demonstrate by detailed cytological and genetics studies that CDKA;1 is an important regulator of meiosis especially for chromosome synapsis and bivalent formation. We show that ASY1 is a phosphorylation target of CDKA;1 and that phosphorylation of ASY1 is crucial for chromosomal axis formation in *Arabidopsis* by two, possibly interconnected mechanisms, involving the binding to ASY3 as well as to itself leading to ASY1 polymers assembling along the chromosome axis.

Results

Changes of subcellular distribution of CDKA;1 during meiosis

For a detailed understanding of the role of CDKA;1 in meiosis, we first analyzed its localization pattern in male meiocytes. Previous studies using a functional fusion of CDKA;1 to mVenus have shown that CDKA;1 is present in both female and male meiosis (Nowack *et al*, 2007; Bulankova *et al*, 2010; Zhao *et al*, 2012). Since the previous reporter was subject to frequent silencing effects, a new *CDKA;1* reporter was generated not relying on the cDNA, as in the previous construct. Instead, a 7kb genomic fragment into which mVenus was introduced before the stop codon of *CDKA;1* was used. Expression of this construct fully rescued the *cdka;1* mutant phenotype and gave rise to stable CDKA;1:mVenus expression (Fig EV1A-C).

By using this reporter, the subcellular localization pattern of CDKA;1 during male meiosis was revealed (Fig 1A and B, and Appendix Movie S1). In early prophase, CDKA;1:mVenus is equally distributed between nucleus and cytoplasm. As prophase progresses, CDKA;1 accumulates more strongly in the nucleus. Then, towards the end of prophase, CDKA;1 becomes more cytoplasmically localized. After nuclear envelope breakdown, CDKA;1 decorates the first meiotic spindle and later accumulates in the two forming nuclei. In metaphase II, CDKA;1 is uniformly present in the entire cell, then is enriched at the spindle, and subsequently accumulates in the nuclei of the four meiotic products, i.e., the microspores (Fig 1A).

Due to a strong accumulation in the nucleoplasm, the presence of CDKA;1 at chromosomes, as reported for its mouse homolog Cdk2 or its yeast homolog Cdc28 (Ashley *et al*, 2001; Zhu *et al*, 2010), was difficult to judge. To address the chromosomal localization pattern of CDKA;1, we used plants that express a *StrepIII-tag-CDKA;1* fusion construct known to completely rescue the *cdka;1* mutant phenotype (Pusch *et al*, 2012), and followed the CDKA;1 localization in meiosis by immuno-localization using ASY1, a key component of the chromosome axis, for staging of meiosis. While Cdk2 and Cdc28 show a distinct punctuate staining in meiosis (Ashley *et al*, 2001; Zhu *et al*, 2010), our experiments revealed that CDKA;1 co-localizes with ASY1 and forms a continuous signal along the chromosomes at leptotene. At zygotene, when homologous chromosomes start to synapse and ASY1 is removed, CDKA;1 was no longer detectable on synapsed chromosome regions (Fig 1C). These data suggest that CDKA;1 physically interacts with the chromosome axis

during early meiotic prophase and might be important for chromosome pairing and synapsis.

Meiosis is severely affected in hypomorphic *cdka;1* mutants

To assess the requirement of CDKA;1 for early stages of meiosis, we compared meiotic progression by chromosome spreads between wild-type plants and two previously described weak loss-of-function *cdka;1* mutants (Fig 1D and Fig EV1D). These alleles resulted from the complementation of a *cdka;1* null mutant with *CDKA;1* expression constructs, in which conserved amino acids have been replaced resulting in CDKA;1 variants with strongly reduced kinase activity: *cdka;1* $PRO_{CDKA;1}$*: CDKA;1*^{T161D} (in the following designated *CDKA;1*^{T161D}) and *cdka;1* $PRO_{CDKA;1}$*:CDKA;1*$^{T14D;Y15E}$ (in the following referred to as *CDKA;1*$^{T14D;Y15E}$ (Dissmeyer *et al*, 2009; 2007). Both mutants were found to exhibit similar meiotic phenotypes during male meiosis, because of which we focus on the description of one allele (*CDKA;1*^{T161D}) in the following (Fig 1D and Fig EV1D).

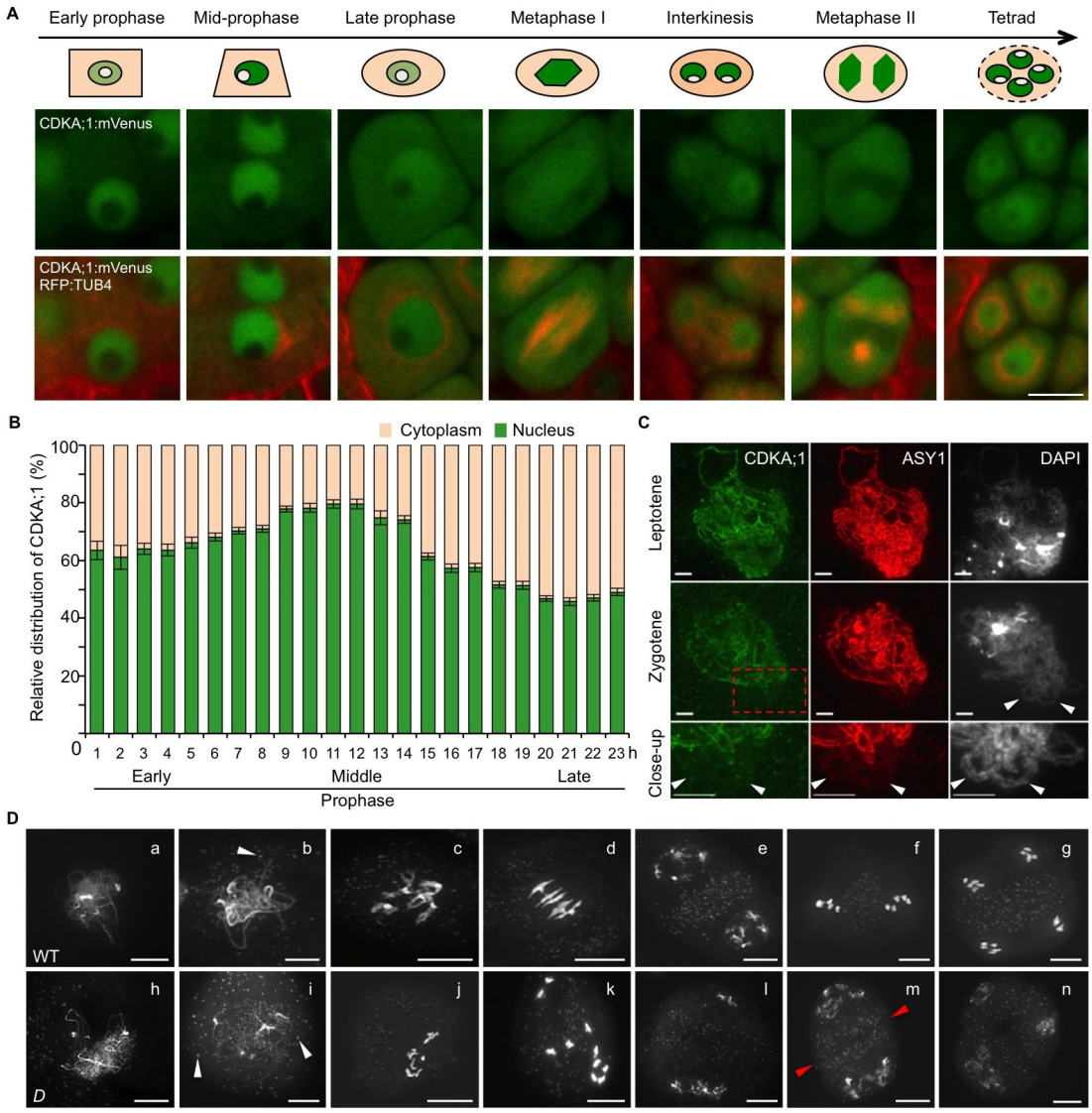

Figure 1. Changes in CDKA;1 distribution and meiotic defects in hypomorphic *cdka;1* mutants in male meiocytes. (A) Confocal laser scanning micrographs showing the localization of a functional CDKA;1:mVenus fusion protein in the wildtype (WT) and cartoons on top highlighting the changes in abundance of CDKA;1:mVenus in the nucleus and cytoplasm during the course of meiosis. The region colored in beige represents the cytoplasm, in green the nucleoplasm, and in white the nucleolus. (B) Quantitative analysis of the signal distribution of the nuclear versus cytoplasmic fraction of CDKA;1:mVenus during prophase I of meiosis as revealed by live cell imaging (Appendix Movie S1). (C) Immunolocalization of CDKA;1 (green) and ASY1 (red) on spread chromsomes in leptotene and zygotene of wild-type plants expressing a functional $PRO_{CDKA;1}$*:CDKA;1:Strep* construct. The last lane shows a magnification of the region marked by the red rectangle. Arrowheads indicate synapsed regions of homologous chromosomes where CDKA;1 is no longer

present. Bar: 5 μm. (D) Chromosome spread analysis of the wildtype and the hypomorphic *cdka;1* mutant *CDKA;1*^{T161D}. (a, h) zygotene or zygotene-like stages; (b, i) pachytene or pachytene-like stages; (c, j, k) diakinesis or dikinesis-like stages; (d) metaphase I; (e, i, m, n) end of meiosis I with two (e, m) or three (i) pools of chromosomes; (f) metaphase II; (g) tetrad. Red arrowheads indicate the initiated formation of a phragmoplast. White arrowheads depict mitochondria. Bars: 10 μm. **This Figure is made from the data provided kindly by Kostika Sofroni (Universität Hamburg), Erik Wijnker (Universität Hamburg, current in Wageningen University & Research), Mathilde Grelon (Université Paris-Saclay).**

In wild-type meiosis, chromosomes start to condense during early prophase, and initiate chromosome synapsis during zygotene, leading to full homolog synapsis at pachytene. Chromosome morphology becomes diffuse at diplotene followed by chromosome re-condensation towards diakinesis when bivalents become visible (Fig 1D a-c).

In *CDKA;1*^{T161D}, the first difference from the wildtype becomes notable at zygotene-like stage when no homolog synapsis is observed (Fig 1D h) (58%; n=120). Absence of synapsis was confirmed by the failure of ZYP1, a component of the central region of the synaptonemal complex, to localize to chromosomes of male meiocytes of *CDKA;1*^{T161D} mutants as revealed by immunofluorescence analysis (Fig EV1E). Pachytene-like stages of *CDKA;1*^{T161D} meiocytes show the characteristically even distribution of mitochondria as that in wildtype through the cell, but have largely unpaired chromosomes (Fig 1D i). Like in the wildtype, chromosomes in *CDKA;1*^{T161D} then decondense at diplotene and recondense towards diakinesis with a major difference being the appearance of 10 univalents instead of 5 bivalents (Fig 1D d and k), which is the result of an achiasmatic meiosis (No bivalents found in 9 out of 9 meiocytes analyzed). These univalents are rod shaped and often show fuzzy borders that may indicate problems in chromosome condensation.

The absence of synapsis and chiasmata can have several reasons, with one of the potentially earliest causes being the absence of SPO11 induced DSBs. However, the DSB repair recombinase DMC1 was localized correctly onto chromosomes with no significant reduction of foci, i.e. 138.5±9.8 in *CDKA;1*^{T161D} (n=10) versus 169.9±15.7 (n=7) in WT (p=0.09, two-tailed *t*-test). This suggested that DSBs are formed along the chromosome axis and that the achiasmatic meiosis in *CDKA;1*^{T161D}

results from defects in later steps of meiosis (Fig EV1F). The formation of DSBs was corroborated by the finding that a double mutant of *CDKA;1*^{T161D} with *rad51*, which is required for DSB repair, showed chromosome fragmentation (44 out of 45 meiocytes analyzed) similar to the *rad51* single mutant (39 out of 39 meiocytes) (Fig EV1G). Therefore, we conclude that DSB processing, at least up to the loading of DMC1, is functional in *CDKA;1*^{T161D}. With this, we conclude that the phenotype of the hypomorphic *CDKA;1*^{T161D} mutants manifests after the meiotic DSB formation and initiation of repair but before synapsis.

Meiotic progression in *cdka;1* hypomorphic mutants is highly disturbed during meiotic stages after pachytene indicating additional roles of CDKA;1 in meiosis (Fig 1D j-n). At least a part of the cells give rise to interkinesis-like stages where two or more daughter nuclei are separated by a clear organelle band (Fig 1D l and m) (19%; n=39). In such nuclei, up to 10 partially decondensed chromosomes are visible in two or more loosely organized groups, or as single chromosomes (Fig 1D l-n). A clear second meiotic division has not been observed in any cell (n=206) and a phragmoplast occasionally becomes visible within the organelle band at interkinesis (in 8 out of 39 cells), indicating that cytokinesis already begins at this stage (Fig 1D m). Taken together, these data suggest that CDKA;1 is an important regulator of meiosis especially for chromosome synapsis and bivalent formation.

Phosphorylation of ASY1 by CDKA;1 promotes its recruitment to the chromosome axis

Since in particular chromosome synapsis was affected in the weak loss-of-function *cdka;1* mutants, we searched for possible phosphorylation targets of CDKA;1 involved in early chromosome engagement. Several meiotic regulators in yeast have been found to contain [S/T]P Cdk consensus phosphorylation sites (Zhu *et al*, 2010). Many of these regulators have homologs in *Arabidopsis* also harboring Cdk consensus sites.

At the top of our list of putative CDKA;1 substrates was the *Arabidopsis* Hop1 homolog ASY1, especially also since *asy1* mutants are known to be asynaptic, hence partially resembling the phenotype of the hypomorphic *cdka;1* mutants (Armstrong, 2002). Moreover, a previous study identified the ASY1 orthologue of Brassica oleracea as a potential *in vivo* ATM/ATR and CDK phosphorylation target (Osman *et al*, 2017). In addition, Hop1 was found to be phosphorylated by Cdc28 in an *in vitro*

screen for Cdk substrates in budding yeast (Ubersax *et al*, 2003), but the functional importance of the phosphorylation in both *Brassica* and yeast has remained unknown.

The above-shown spatiotemporal co-localization of ASY1 with CDKA;1 on chromosomes revealed by immuno-localization is consistent with the idea that ASY1 could be a phosphorylation target of CDKA;1 (Fig 1C). To further test this, we generated two functional reporters for *ASY1* (*PRO$_{ASY1}$:ASY1:GFP* and *PRO$_{ASY1}$:ASY1:RFP*), which both restored a wild-type like meiotic program when expressed in homozygous *asy1* mutants (Appendix Fig S1A and C). As expected, and confirming our above-presented and previous immuno-detection studies (Ferdous *et al*, 2012; Lambing *et al*, 2015), ASY1 localizes to the chromosome axis at leptotene and is depleted during zygotene when the synaptonemal complex is formed as revealed by the concomitant analysis of ASY1:RFP together with a *PRO$_{ZYP1B}$:ZYP1B:GFP* reporter (Fig 2A and Fig EV2A).

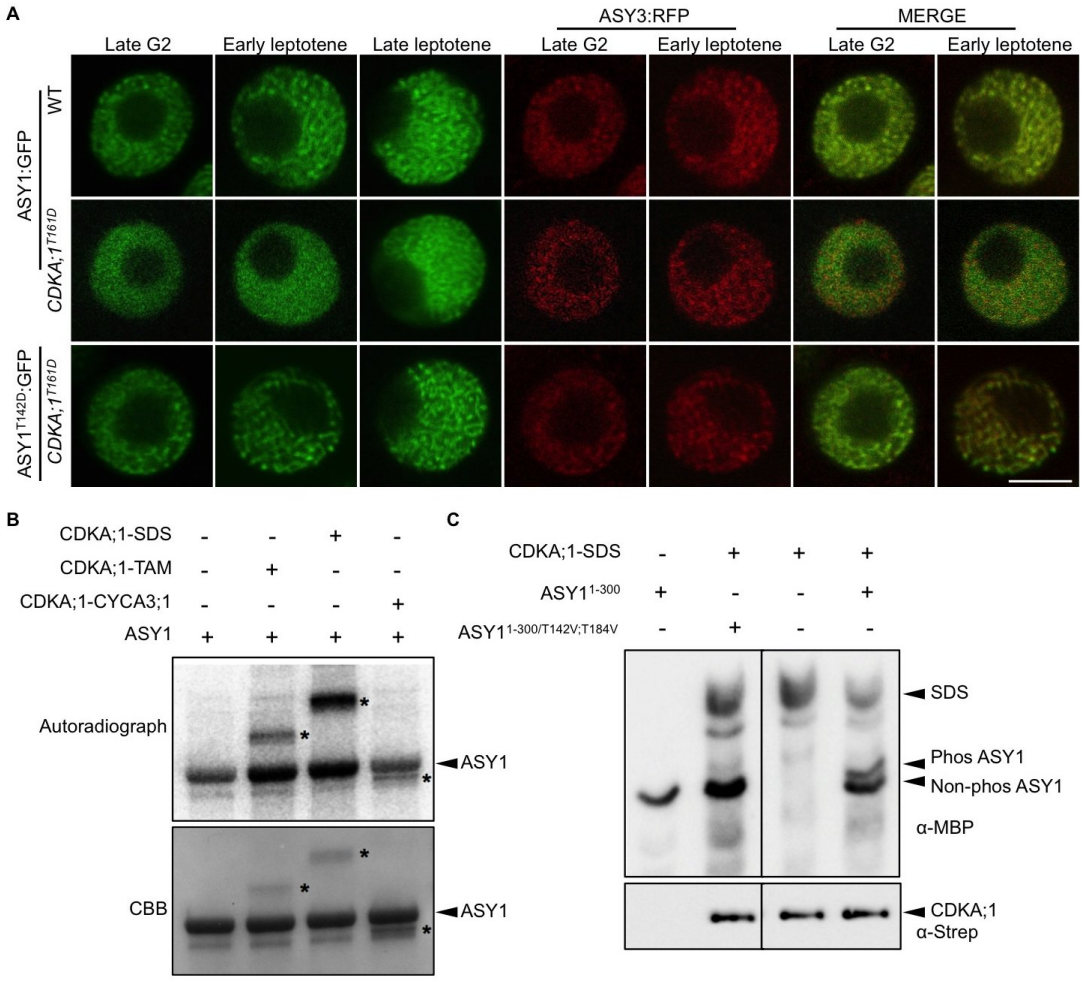

Figure 2. ASY1 is a phosphorylation target of CDKA;1. (A) ASY1:GFP and ASY1^{T142D}:GFP localization in late G2 and leptotene of male meiocytes of the

wildtype and *CDKA;1*^{T161D} mutants. ASY3:RFP, highlighting chromsomes, was used as a marker for the staging of meiosis. Bar: 5 μm. (B) Kinase assays of CDKA;1-SDS, -TAM, and -CYCA3;1 complexes using ASY1 puried from baculovirus-infected insect cells as a substrate. The upper panel shows the autoradiograph. The control reaction without CDKA;1-cyclin complex indicates a background activity co-purified from insect cells. The lower panel indicates protein loading by coomassie briliant blue (CBB) staining. Arrowheads indicate ASY1 proteins and asterisks depict the relevant cyclin used which also gets phosphorylated in the assay. (C) The upper panel shows a phos-tag gel analysis of ASY1$^{1\text{-}300}$ and ASY1$^{1\text{-}300/T142V;T184V}$ with and without CDKA;1-SDS kinase complexes using an anti-MBP antibody. The lower panel denotes loading of CDKA;1 using an anti-Strep antibody. Arrowheads represent the proteins as indicated. **The Figure (C) is kindly provided by Hirofumi Harashima from RIKEN Center for Sustainable Resource Science, Japan (current in Solution Research Laboratory, AS ONE Corporation, Japan).**

To explore a possible regulation of ASY1 by CDKA;1, we introgressed the ASY1:GFP reporter into the weak *cdka;1* loss-of-function allele *CDKA;1*^{T161D}. In wild-type male meiocytes at late G2, numerous foci and short stretches of ASY1 signal were present (n=18 out of 20 male meiocytes analyzed). The meiotic stage was determined by four morphological criteria: the squared cell shape of meiocytes, the centered position of the nucleolus, the chromosome axis being labeled by a previously generated functional *ASY3* reporter (*PRO*$_{ASY3}$*:ASY3:RFP*), and the finding that tapetum cells were still single-nucleated (Prusicki *et al*, 2019; Wang *et al*, 2004; Yang *et al*, 2006; Stronghill *et al*, 2014). In contrast, only a diffuse ASY1:GFP signal without any foci could be detected in the nuclei of meiocytes of *CDKA;1*^{T161D} plants (25 out of 25) at a moment when ASY3 forms foci and short stretches (Fig 2A). This diffuse signal of ASY1:GFP in *CDKA;1*^{T161D} persisted until early leptotene (19 out of 21), as judged by the beginning of the migration of the nucleolus towards one side of the nucleus and the appearance of ASY3 in threads. At this stage, a linear ASY1 signal co-localizes with ASY3 along chromosomes in the wildtype (23 out 23) (Fig 2A). In late leptotene, as seen by docking of the nucleolus to one side of the nucleus, the ASY1:GFP signal in *CDKA;1*^{T161D} (30 out of 30), was found to associate with chromosomes indistinguishable from the wildtype (28 out 28), indicating a delayed assembly of ASY1 on chromosomes in *CDKA;1*^{T161D} (Fig 2A).

To test whether ASY1 can be directly phosphorylated by CDKA;1, we performed *in vitro* kinase assays. To this end, we expressed and purified ASY1 from baculovirus-infected insect cells and incubated it with three meiotic CDK-cyclin complexes. This revealed that ASY1 is phosphorylated by CDKA;1-SDS and CDKA;1-TAM but not by CDKA;1-CYCA3;1 *in vitro* (Fig 2B). Since the kinase reaction without added CDK-cyclin complexes showed background phosphorylation, likely due to co-purification of kinases from insect cells, we expressed ASY1 in *E. coli* and subjected the purified protein to CDKA;1-SDS complexes. Subsequent mass spectrometry analyses showed that two sites (T142 and T535) out of the five CDKA;1 consensus phosphorylation sites in ASY1 are targeted by CDKA;1-SDS; in this case no phosphorylated peptides were found in the reactions without CDKA;1 (Fig 3A and Appendix Fig S2A).

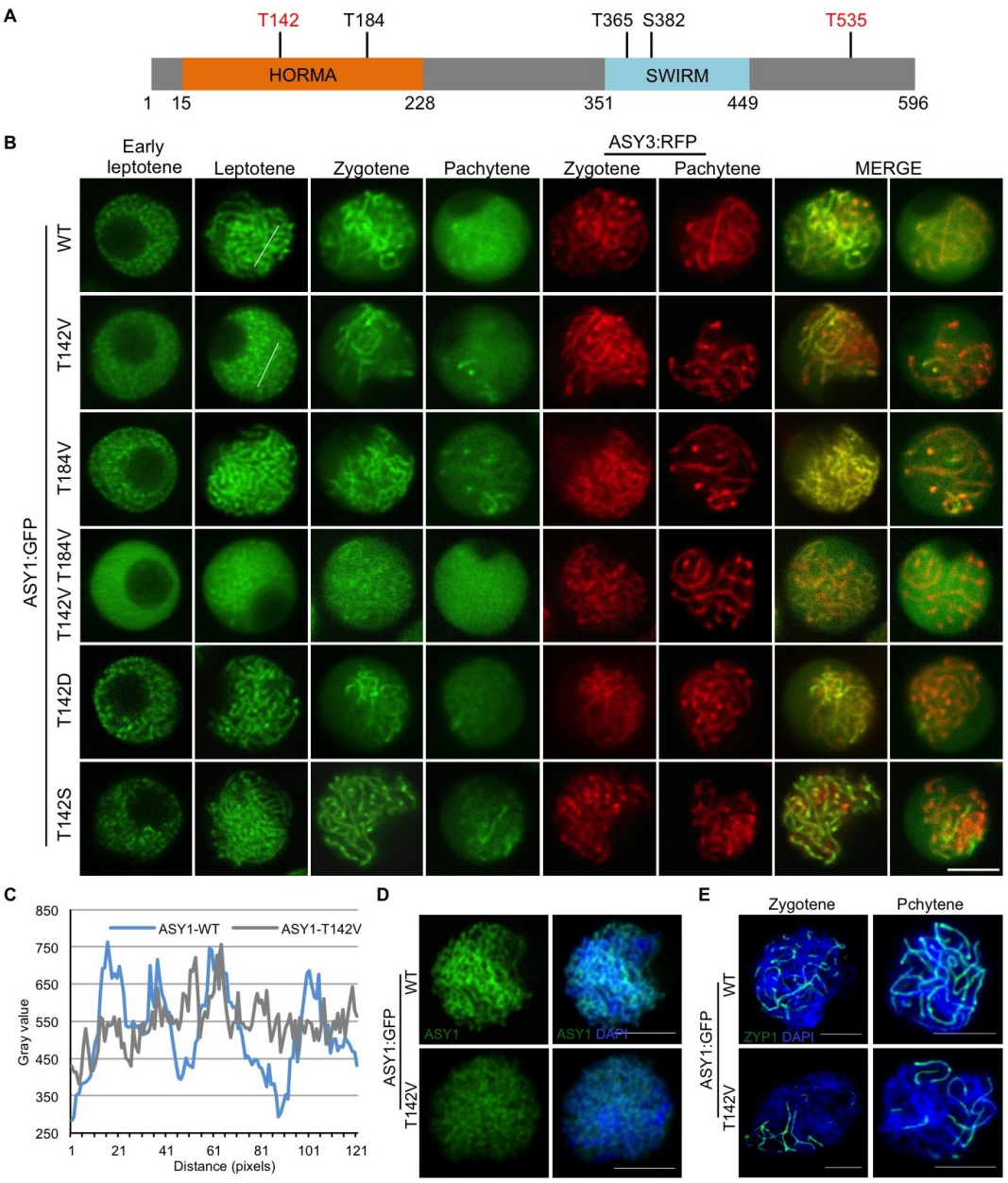

Figure 3. Phosphorylation of ASY1 is essential for its chromosomal localization. (A) Schematic representation of ASY1 with the five predicted consensus Cdk phosphorylation sites. The sites found to be phosphorylated *in vitro* by CDKA;1-SDS complexes are highlighted in red (Appendix Fig S4A). (B) Localization patterns of different ASY1:GFP variants together with ASY3:RFP (for staging of zygotene and pachytene) in a *asy1* mutant background during prophase I. Bar: 5 µm. (C) Signal distribution profiles of ASY1:GFP and ASY1^{T142V}:GFP at leptotene as shown in (B). The regions used for analysis are highlighted by white lines in respective panels in (B). The many small peaks with low amplitude in *ASY1^{T142V}:GFP* indicate diffused localization as opposed to the clear peaks seen in the wildtype. (C and D)

Immunolocalization of ASY1 (C) and ZYP1 (D) in *ASY1:GFP* (*asy1*) and *ASY1^{T142V}:GFP* (*asy1*) plants using anti-GFP and anti-ZYP1 antibodies, respectively. DNA was stained with DAPI (blue). Bars: 5 μm. **The mass spectrometry analysis of phosphorylation sites of ASY1 in (A) is done by Sara Christina Stolze and Hirofumi Nakagami in Max-Planck-Institute for Plant Breeding Research, Cologne.**

Table 1. Summary of the phenotypic analysis of ASY1 variants.

Construct	Chromosome association	Background	Seed/silique	Pollen viability (%)
-	-	wildtype	58.35 ± 1.75^{a}	99.32 ± 0.49^{a}
-	-	*asy1*	9 ± 1.2^{b}	55.57 ± 2.55^{b}
ASY1	Correct	*asy1*	58.75 ± 2.32^{a}	99.26 ± 0.63^{a}
ASY1^{T142V}	Compromised	*asy1*	41 ± 2.5^{c}	81.87 ± 2.35^{c}
ASY1^{T184V}	Correct	*asy1*	57.78 ± 2.5^{a}	99.24 ± 0.27^{a}
ASY1$^{T142V;T184V}$	Largely lost	*asy1*	9.78 ± 1.8^{b}	59.72 ± 2.27^{b}
ASY1^{3V}	Correct	*asy1*	57.75 ± 1.83^{a}	99.38 ± 0.4^{a}
ASY1^{4V}	Correct	*asy1*	58.15 ± 1.96^{a}	99.04 ± 0.25^{a}
ASY1^{5V}	Largely lost	*asy1*	9 ± 1.41^{b}	55.86 ± 3.57^{b}
ASY1^{T142D}	Correct	*asy1*	57.95 ± 2.3^{a}	99.21 ± 0.23^{a}
ASY1^{T142S}	Correct	*asy1*	56 ± 2.96^{a}	98.19 ± 0.9^{a}

Table 1. Summary of the phenotypic analysis of ASY1 variants. The level of significance ($p<0.05$) is indicated by different letters between the wildtype and ASY1 variants as determined by the one-way ANOVA followed by Turkey's test.

To address the relevance of the phosphorylation sites *in vivo*, we then generated different non-phosphorylatable and phosphorylation-mimicking variants of these five CDKA;1 consensus phosphorylation sites based on the ASY1:GFP construct. These constructs were then introduced into *asy1* mutants harboring the *ASY3:RFP* reporter (*PRO$_{ASY3}$:ASY3:RFP*) (Table 1 and Fig EV3A). ASY3 is known to be recruited to the chromosome axis prior to ASY1 and present on chromosomes from early leptotene until pachytene (Ferdous *et al*, 2012). Consistent with its chromosomal loading being independent of ASY1, the expression and localization of ASY3 was unaffected in plants harboring different ASY1 variants and hence, was used in the following as a marker for staging of meiosis (Fig 3B).

Similar to wild-type ASY1, the triple non-phosphorylatable mutant (ASY1^{3V}), i.e., ASY1 harboring the three amino acid substitutions T365V, S382V, T535V, and even the quadruple non-phosphorylatable mutant ASY1^{4V} (T184V, T365V, S382V,

T535V) fully complemented the defects of *asy1*, e.g., pollen abortion, short silique length, and reduced seed set (Table1 and Fig EV3B-F). Matching their complementing functionality, ASY1^{3V}:GFP and ASY1^{4V}:GFP localized on chromosomes similar to ASY1:GFP that associated with chromosomes at leptotene and progressively dissociated again upon synapsis during zygotene and pachytene while ASY3 still remained localized to the chromosomes (Fig EV2B).

In contrast, the quintuple non-phosphorylatable mutant ASY1^{5V} (T142V, T184V, T365V, S382V, T535V) did not properly localize to chromatin (Fig EV2B). Resembling *asy1* null mutants, no clear chromosomal threads were observed in *ASY1^{5V}* plants, which were also strongly reduced in fertility (Table1, Fig EV2B and EV3B-F). This result suggested that the *in vitro* identified CDKA;1 phosphorylation site T142 in the HORMA domain is crucial for the chromosome association of ASY1. In support of this hypothesis, we found that the single non-phosphorylatable mutant (*ASY1^{T142V}* in *asy1*) only partially complemented *asy1*, and in contrast with the wild-type version of ASY1, ASY1^{T142V}:GFP showed compromised chromosome association during leptotene and exhibited a diffuse and nucleoplasmic signal (Fig 3B-D, Table 1 and Fig EV3B-F). We also frequently observed only partially synapsed homologous chromosomes in *ASY1^{T142V}* plants (Fig 3E and Appendix Fig S3).

An exchange of T142 to Serine (ASY1^{T142S}), that maintains the CDKA;1 phosphorylation site, did not result in compromised ASY1 function and expression of this construct fully rescued *asy1* mutants (Fig 3B and Fig EV3B-F). Moreover, the expression of the phosphorylation-mimicking variant ASY1^{T142D} fully restored meiosis and fertility of *asy1* mutants indicating that most likely the charge and not the structure of the amino acid at position 142 is important for ASY1 function (Fig 3B and Fig EV3B-F). Furthermore, the delayed assembly of ASY1 in *CDKA;1^{T161D}* was reverted to a wild-type pattern when the phosphorylation-mimicking mutation ASY1^{T142D} was expressed in *CDKA;1^{T161D}* (Fig 2A).

Exploring the regulation of ASY1 phosphorylation further, we found that the double non-phosphorylatable mutant T142V, T184V (*ASY1$^{T142V;T184V}$*) enhanced the *ASY1^{T142V}* mutant phenotype and was indistinguishable from *asy1* indicating a complete loss of function reminiscent of *ASY1^{5V}* (Fig 3B, Fig EV3B-F and Appendix Fig S7). Consistently, the N-terminal half of ASY1 in which the phosphorylation sites T142 and T184 were mutated (ASY1$^{1\text{-}300/T142V;T184V}$) was no longer phosphorylated by

a CDKA;1-SDS complex *in vitro* confirming their specificity as CDKA;1 phosphorylation sites (Fig 2D).

Since no obvious localization defects, especially in leptotene, and no mutant phenotype was found in *asy1* mutants expressing the single non-phosphorylatable mutant $ASY1^{T184V}$ (Fig 3B and Fig EV3B-F), we conclude that T142 in the HORMA domain is the major site of ASY1 phosphorylation-regulation with the site T184 likely having an ancillary role.

Phosphorylation of ASY1 increases its binding affinity with ASY3

The failure of the double non-phosphorylatable mutant protein $ASY1^{T142V;T184V}$ to associate with chromosomes is reminiscent of the localization defects of ASY1 in *asy3* mutants (Fig 3B and Fig EV2C) (Ferdous *et al*, 2012). Therefore, we reasoned that phosphorylation of ASY1 may control its interaction with ASY3. The first 300 amino acids of ASY1 ($ASY1^{1-300}$), which include the HORMA domain, essential for the protein-protein interaction of Hop1 with Red1 (Muniyappa *et al*, 2014; Rosenberg & Corbett, 2015), were found to interact with ASY3 in a yeast two-hybrid assay consistent with earlier results (Ferdous *et al*, 2012). While no obvious effect of $ASY1^{1-300/T184V}$ on the interaction capacities with ASY3 was observed, we found that the binding of $ASY1^{1-300/T142V}$ to ASY3 was strongly decreased, yet not fully abolished, since yeast cells harboring $ASY1^{1-300/T142V}$ and ASY3 cannot grow on the stringent selection media (without histidine and adenine) but do survive on the less stringent media (without histidine) (Fig 4A). The interaction with ASY3 was even further reduced in the $ASY1^{1-300/T142V;T184V}$ variant (Fig 4A). Conversely, the phosphorylation site exchange mutant $ASY1^{1-300/T142S}$ and the phosphorylation-mimicking mutant $ASY1^{1-300/T142D}$ interacted with ASY3 to a similar extent as the non-mutated version of ASY1 (Fig 4A). These findings were not due to protein expression levels since we found that non-phosphorylatable mutant versions of ASY1 were even more abundantly present in yeast cells than the non-mutated version (Appendix Fig S2C). These results also suggested that ASY1 was phosphorylated in yeast cells, likely on residue T142. Indeed, phosphorylation of ASY1 in yeast was confirmed by phos-tag SDS-PAGE (Appendix Fig S2D).

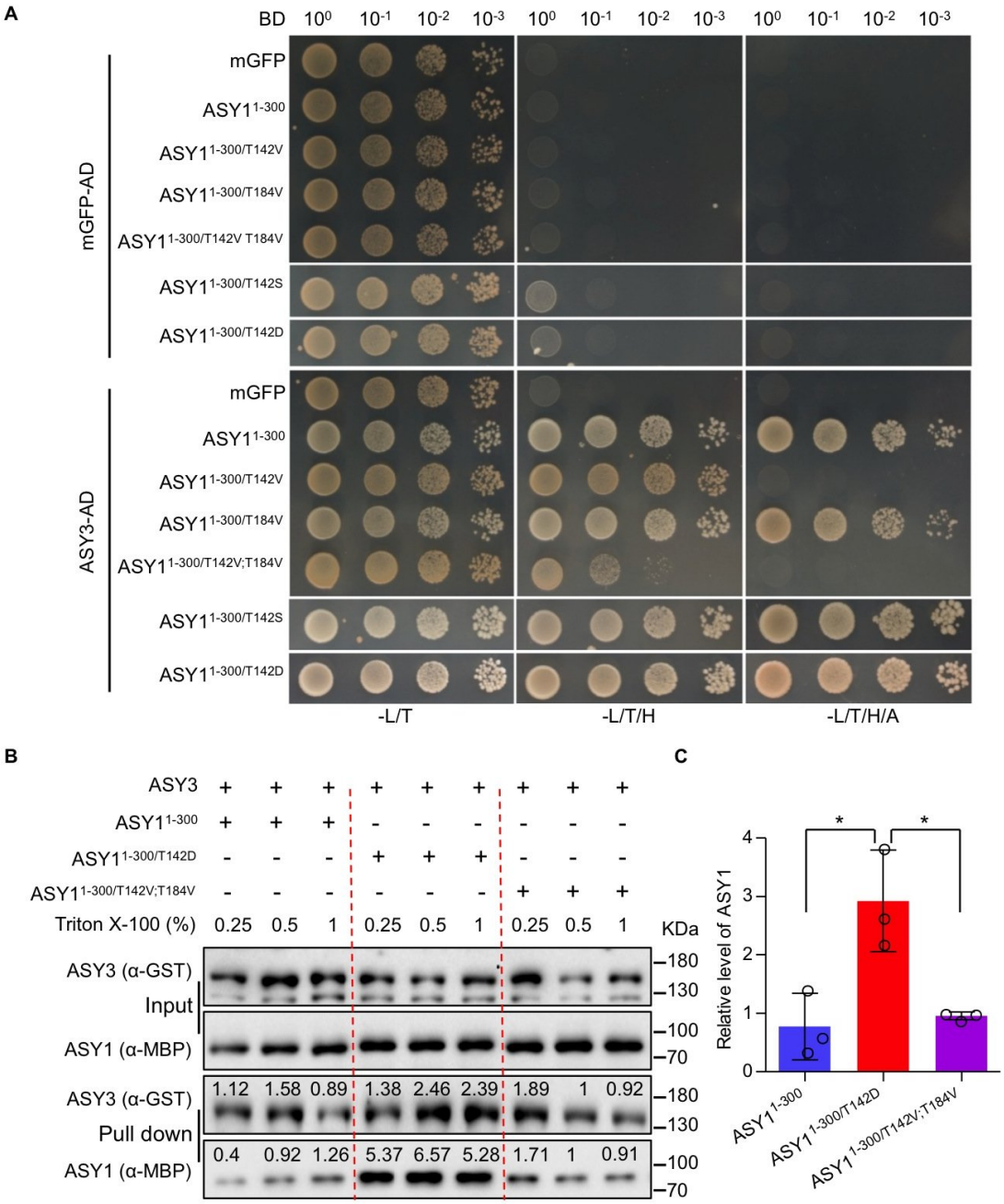

Figure 4. A negative charge at T142 in the HORMA domain of ASY1 promotes its interaction with ASY3. (A) Yeast two-hybrid interaction assays of ASY3 with different ASY1 variants. Monomeric GFP (mGFP) fused with AD (activating domain) and BD (binding domain) was used as controls. Yeast cells harboring both the AD and BD plasmids were grown on synthetic medium supplied with glucose in the absence of Leu and Trp (-L/T, left panel), on Synthetic Drop-put (SD) medium in the absence of Leu, Trp, and His (-L/T/H, middle panel), and on SD medium in the absence of Leu,Trp, His and Ade (-L/T/H/A, right panel). Yeast cells were incubated until OD_{600} = 1 and then diluted 10-, 100- and 1000-fold for the assays. (B) GST pull

down of ASY3 with different ASY1 variants. The numbers above the bands show the relative intensity of the bands. The input and pull down fractions were analyzed by immuno-blotting with the anti-GST (ASY3) and anti-MBP (ASY1) antibodies. (C) The quantification of the pull down fractions of ASY1 as shown in (B). The band intensity in the pull down of $ASY1^{1\text{-}300/T142V;T184V}$ at a Triton X-100 concentration of 0.5% was defined as 1. The relative amount of ASY1 in the pull down fractions was normalized by the band intensity of the pulled-down ASY3 fraction. The average band intensity of ASY1 at different concentrations of Triton X-100 used was plotted. Asterisks indicate significant difference (two-tailed *t*-test, $p < 0.05$). Bars represent standard deviations.

The importance of T142 phosphorylation in ASY1 for the interaction with ASY3 was confirmed by GST pull-down assay using recombinant proteins purified from *E.coli*. Similar to the results from yeast two-hybrid assay, we found that the non-phosphorylated ASY1 ($ASY1^{1\text{-}300}$ and $ASY^{1\text{-}300/T142V;T184V}$) had only a residual interaction capacity with ASY3. However, the phosphorylation-mimicking version $ASY1^{1\text{-}300/T142D}$ showed enhanced affinity towards ASY3 (Fig 4B and C).

Finally, we addressed whether and if so to what degree the altered interaction of $ASY1^{1\text{-}300/T142V}$ with ASY3 in our yeast two-hybrid experiment depends on the exchanged amino acid, i.e., Val, itself. To this end, we tested additional ASY1 variants in which we substituted T142 and T184 with Gly and Ala. Consistent with the Val substitution at T142, we found that the mutations of both $ASY1^{1\text{-}300/T142A}$ and $ASY1^{1\text{-}300/T142G}$ strongly reduced the interaction with ASY3 (Fig EV4A). The mutation of $ASY1^{1\text{-}300/T142A;T184A}$ further reduced the interaction of $ASY1^{1\text{-}300/T142A}$ similarly to the $ASY1^{1\text{-}300/T142V;T184V}$ mutant (Fig EV4A). These findings show that a reduced interaction between ASY1 and ASY3 in a yeast two-hybrid system does not depend on a specific amino acid used for substitution and corroborates that phosphorylation of ASY1 at T142 is important for its binding to ASY3.

Notably, while $ASY1^{1\text{-}300/T184V}$ does not show any obvious reduction in binding with ASY3, the substitution of T184 to A ($ASY1^{1\text{-}300/T184A}$) largely reduced the interaction, and $ASY1^{1\text{-}300/T184G}$ did not interact at all with ASY3 in our assays anymore (Fig EV4A). Since we did not find T184 to be phosphorylated *in vitro*, we cannot judge at the moment whether T184 is structurally a very important position

and does not tolerate small amino acids and/or whether T184 is, possibly very transiently, phosphorylated *in vivo*.

Phosphorylation of ASY1 counteracts the action of PCH2 in early but not late prophase

For the synaptonemal complex to be formed, ASY1 has to be depleted from synaptic regions at zygotene mediated by the conserved AAA+ ATPase PCH2 (Ferdous *et al*, 2012; Lambing *et al*, 2015). Therefore, we asked whether the phosphorylation status of ASY1 also affects its removal by PCH2. However, the phosphorylation-mimicking version ASY1^{T142D} was equally well depleted from chromatin as the non-mutated version of ASY1 (Fig 3B). Conversely, we introduced the non-phosphorylatable version ASY1$^{T142V;T184V}$ into *pch2* mutants to ask whether the loss of the chromosomal association of the ASY1$^{T142V;T184V}$ was affected by PCH2.

Strikingly, while ASY1$^{T142V;T184V}$ could not properly localize to chromosomes in both *asy1* mutant and in a wild-type background (see above, Fig 3B and 5A), the localization pattern of ASY1$^{T142V;T184V}$:GFP in *pch2* was nearly identical to the pattern of the non-mutated version of ASY1 in leptotene (Fig 5A). This observation suggests a so far not recognized function of PCH2 in counteracting the recruitment of ASY1 to ASY3 in leptotene when ASY1 needs to assemble on the chromosomes (see below). This early function of PCH2 for the regulation of the chromosome assembly of ASY1 at leptotene was further corroborated by the finding that, although ASY1$^{T142V;T184V}$:GFP could not rescue the fertility reduction of *asy1* mutants, it largely complemented the fertility of *asy1 pch2* double mutants to the level of *pch2* single mutants (Fig 5B). This result also suggested that ASY1$^{T142V;T184V}$:GFP is largely functional as long as it can be localized on chromosomes. The finding that ASY1$^{T142V;T184V}$ in a *pch2* mutant background stays tightly associated with the chromosomes at both zygotene and pachytene when ASY1 in wild-type plants is already largely removed from the synaptic chromosomes, underlines the key role of PCH2 for the late release, which we conclude is independent of the CDKA;1-dependent phosphorylation status of ASY1 (Fig 3B and 5A).

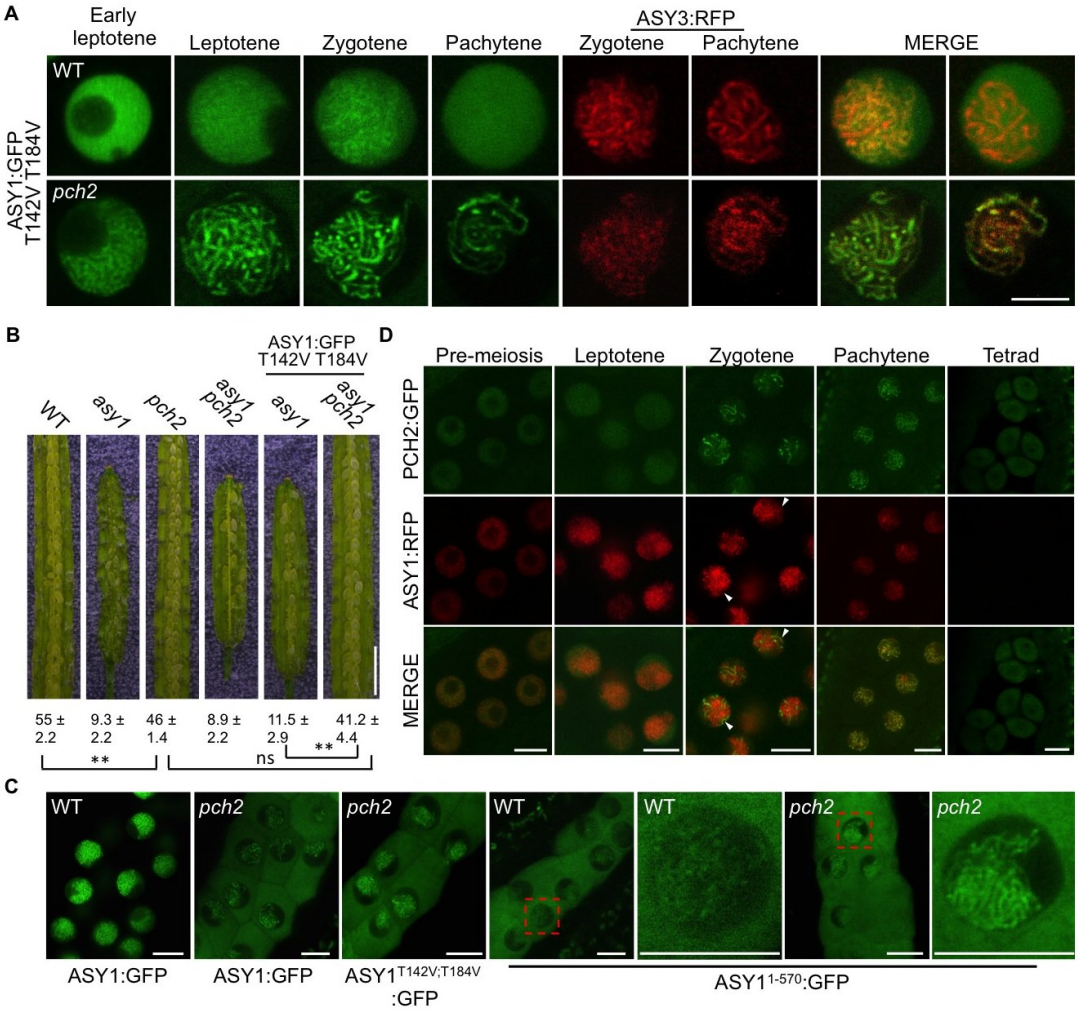

Figure 5. Phosphorylation of ASY1 counteracts the action of PCH2 in early prophase. (A) Localization patterns of ASY1$^{T142V;T184V}$:GFP together with ASY3-RFP in the wildtype and *pch2* mutants. Please note that images of ASY1$^{T142V;T184V}$:GFP in *pch2* mutants were taken with increased sensitivity for a better visibility. Bar: 5 µm. (B) Seed sets (mean ± SD, n = 5) of WT, *asy1*, *pch2*, *asy1 pch2*, *ASY1$^{T142V;T184V}$:GFP* (*asy1*) and *ASY1$^{T142V;T184V}$:GFP* (*asy1 pch2*) plants. Asterisks indicate significant differences (two-tailed *t*-test, $P < 0.01$). ns depict no significant difference. Bar: 2 mm. (C) Localization patterns of ASY1:GFP, ASY1$^{T142V;T184V}$:GFP, and ASY1$^{1-570}$:GFP in the wildtype (WT) and/or in *pch2* mutant plants at early prophase I. Bars: 5 µm. (D) Localization pattern of PCH2:GFP together with ASY1:RFP in the male meiocytes of wildtype. Arrowheads indicate the chromosomal regions where the ASY1 removal was concomitant with the localization of PCH2. Bar: 10 µm.

To further explore the new finding of an early function of PCH2, we generated a functional genomic reporter line for PCH2 (*PRO$_{PCH2}$:PCH2:GFP*) which revealed that that PCH2 is already present in male meiocytes from pre-meiosis throughout prophase I (Fig 5D, Appendix S1B and D). This observation implies the necessity of a mechanism for counteracting the releasing force of PCH2 on ASY1 at early leptotene, which we speculate to be the here-discovered phosphorylation of ASY1.

To elaborate on a possible early function of PCH2, we introduced the non-mutated functional *ASY1:GFP* reporter into *pch2* mutants. While ASY1:GFP is exclusively localized to the nucleus and chromatin in a wild-type background, we found that the same reporter was not only present in the nucleus but also strongly accumulated in the cytoplasm in *pch2* mutants (Fig 5C). Revisiting the non-phosphorylatable mutant localization ASY1$^{T142V;T184V}$:GFP in *pch2*, we also observed that it accumulates cytoplasmically (Fig 5C). Interestingly, we noted that the signal intensities of both ASY1:GFP and ASY1$^{T142V;T184V}$:GFP in the nucleus of *pch2* mutants appeared to be weaker than that of ASY1:GFP in the wildtype (Fig 5C). Thus, we conclude that PCH2 directly or indirectly facilitates the nuclear accumulation of ASY1 in early meiosis, a function that is consistent with the presence of PCH2 in the cytoplasm at that time (Fig 5D).

Taken together, these observations suggest that PCH2 has at least three, possibly interconnected functions. In early leptotene, it promotes the release of the non-phosphorylated ASY1 from chromosomes and ASY1 phosphorylation in the HORMA domain antagonizes this PCH2 activity by increasing the binding affinity of ASY1 with ASY3. At the same time PCH2 helps ASY1 to accumulate in the nucleus. Later in zygotene and pachytene, PCH2 removes ASY1, as shown in previous publications, in a fashion that appears to not depend on its phosphorylation (Lambing *et al*, 2015).

Self-assembly of ASY1 through its C-terminal closure motif is affected by the phosphorylation in the HORMA domain

The chromosomal localization of the meiotic HORMA domain proteins (HORMADs) including the budding yeast Hop1, mammalian HORMAD1 and HORMAD2, and *C. elegans* HORMADs (HTP-1, HTP-2, HTP-3, and HIM3), was recently shown to depend on at least two mechanisms, the initial recruitment by its binding partners such as Red1 in yeast, and the putative self-assembly through its N-terminal HORMA

domain-C-terminal closure motif interactions (Smith & Roeder, 1997; Wojtasz *et al*, 2009; Kim *et al*, 2014; West *et al*, 2018). Hence, we asked whether phosphorylation by CDKA;1 would also affect a possible self-assembly mechanism of ASY1.

To explore this possibility, we first tested whether the self-assembly is also conserved in *Arabidopsis* by using yeast two-hybrid assays. We found that ASY1 binds to itself and mapped this interaction to the HORMA domain of ASY1 making contact with the very C-terminus of ASY1 (residues 571-596), strongly suggesting that ASY1 likely possesses a C-terminal closure motif as its orthologs in yeast, *C. elegans*, and mammals (Fig 6A and B). While this work was in progress, West et al. (2019) also independently identified the closure motif of ASY1 as being located in the same region as here revealed by us. Deletion of the closure motif of ASY1 in the *ASY1:GFP* reporter construct (ASY1$^{1\text{-}570}$:GFP) almost abolished its chromosome association, indicating the necessity of the closure motif for its correct localization pattern (Fig 5C). At the same time, we also observed that ASY1$^{1\text{-}570}$:GFP accumulated in the cytoplasm demonstrating that the nuclear targeting of ASY1 is also compromised in this version. Next, we asked whether the compromised chromosome association of ASY1$^{1\text{-}570}$:GFP depends on PCH2. Remarkably, the chromosome localization of ASY1$^{1\text{-}570}$:GFP was largely recovered (Fig 5C), when the *ASY1$^{1\text{-}570}$:GFP* reporter was introduced into *pch2* mutant. This suggests that the closure motif is also important for antagonizing the releasing force of PCH2, presumably via the self-oligomerization during chromosome axis formation.

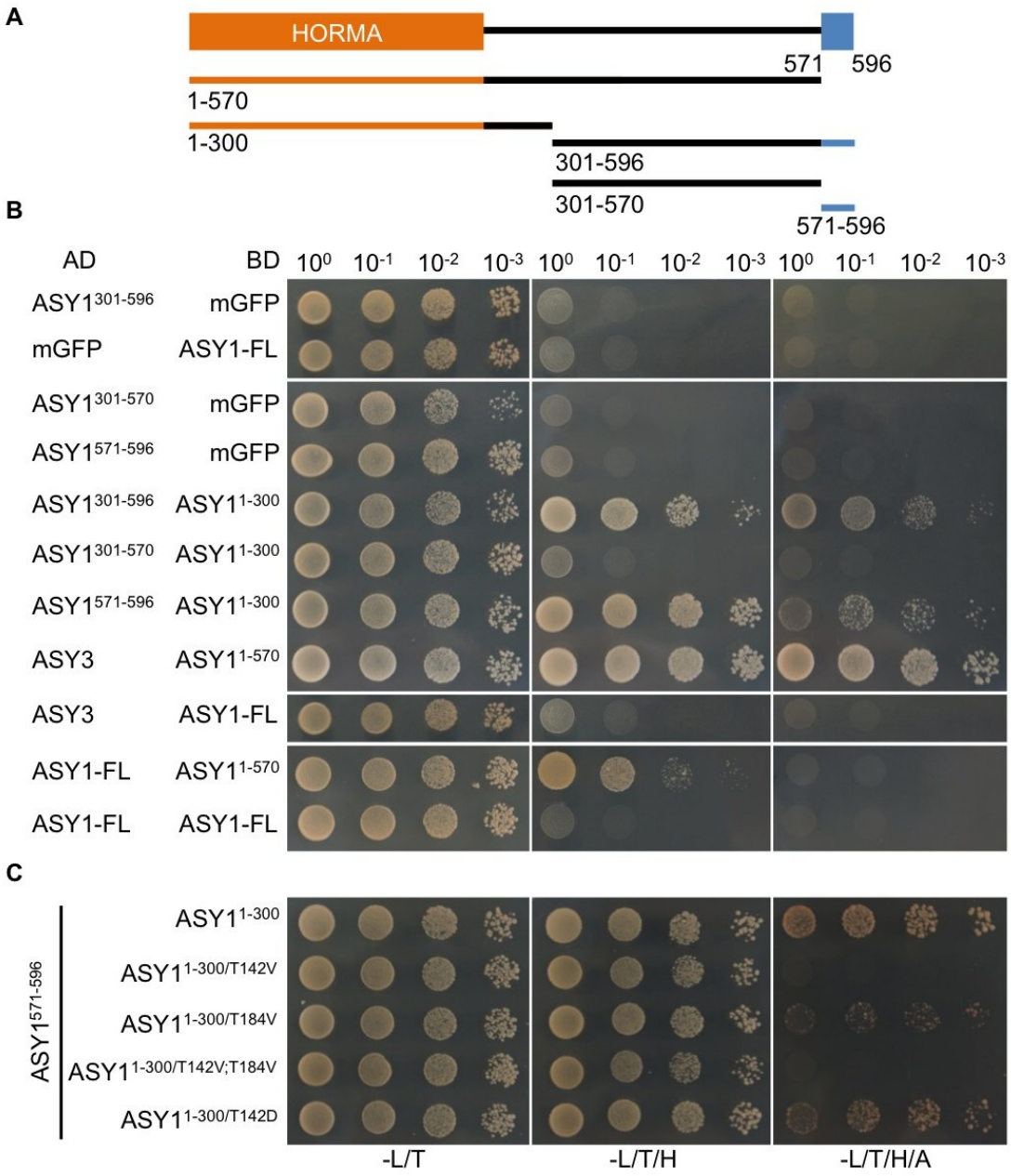

Figure 6. Phosphorylation of ASY1 affects its self-assembly. (A) Schematic graph of ASY1 full-length protein (aa 1 to 596). The HORMA domain is depicted in orange, the presumptive closure motif is highlighted in blue. The lines below indicate the constructs used for yeast two-hybrid interaction assays. (B) Interaction assays of different ASY1 fragments (with and without the closure motif). (C) Interaction analysis of the ASY1 closure motif ($ASY1^{571-596}$) with different ASY1 HORMA domain variants.

We also noticed in our yeast two-hybrid assays that the full length ASY1 could not interact with ASY3 (Fig 6B). This is consistent with previous studies that

show that full length Hop1 has a very low affinity towards Red1 *in vitro* (West *et al*, 2018). However, strong interaction with ASY3 was found when the closure motif was depleted ($ASY1^{1-570}$) (Fig 6B).

Finally, we tested the interaction of the different mutant variants of the ASY1 HORMA domain with the above-identified closure motif and found that the affinity of $ASY1^{1-300/T142V}$ and $ASY1^{1-300/T142V;T184V}$ to the closure motif was dramatically reduced. Conversely, the phosphorylation-mimicking version $ASY1^{T142D}$ showed higher interaction strength despite a slight decrease compared to that of the non-mutated ASY1 version (Fig 6C). These data suggest that phosphorylation of the ASY1 HORMA domain regulates its chromosomal assembly not only by enhancing the affinity to ASY3 but also by promoting the potential self-assembly along the chromosomes. Thus, phosphorylation of ASY1 by CDKA;1 appears to represent a two pronged mechanism for the faithful loading of ASY1 to the chromosome axis.

Discussion

Cdks are known to be the major driving force of cell divisions (Morgan, 1997). Due to their requirement in mitosis, the study of Cdks in meiosis is challenging in multicellular organisms since meiosis usually takes place late during embryonic or postembryonic development, i.e., after several mitotic divisions. This is exemplified by the early embryonic lethality of Cdk1 mutants that precludes a straightforward functional analysis of Cdk1 in mouse meiocytes (Santamaría *et al*, 2007). By replacing Cdk1 with Cdk2 and by using conditional Cdk1 knock out mice, it was shown that Cdk1 is indeed key for meiosis in mammalian oocytes and cannot be substituted by Cdk2 (Satyanarayana *et al*, 2008; Adhikari *et al*, 2012). However, it is still largely not clear how Cdk1 controls meiotic progression and what the phenotypic consequences of the loss of Cdk1 activity in meiosis are at the cellular level.

Since weak-loss-of-function mutants in the *Arabidopsis* Cdk1/Cdk2 homolog CDKA;1 are viable and produce flowers containing meiocytes (Dissmeyer *et al*, 2009; 2007), they represent a unique tool to study the requirement of Cdks in meiosis of a multicellular eukaryote. Exploiting these mutants, we find that in particular chromosome synapsis and bivalent formation is affected by reduced Cdk activity. Our data furthermore reveal ASY1 as an important phosphorylation target of CDKA;1.

So far, the ASY1 homolog Hop1 has been found to be phosphorylated by Mec1/ATR and Tel1/ATM in budding yeast, which promotes DMC1-dependent interhomolog recombination without affecting the chromosomal association of Hop1 (Carballo *et al*, 2008). Orthologs of Hop1 in plants, e.g., ASY1 in *Arabidopsis* and PAIR2 in rice, harbor also ATM/ATR consensus phosphorylation sites ([S/T]Q), but whether an ATM/ATR-dependent phosphorylation is functionally conserved in plants is still unclear. Given the finding that Hop1 can be also phosphorylated by Cdk complexes in budding yeast (Ubersax *et al*, 2003) and the presence of Cdk consensus phosphorylation sites in both HORMAD1 and HORMAD2 proteins of human and mouse, it is tempting to speculate that the here-revealed phosphorylation regulation of ASY1, needed for its chromosome localization, is conserved among eukaryotes.

The role of ASY1 phosphorylation by CDKA;1

Combining our CDKA;1 localization data with the molecular and biochemical analysis of ASY1 phosphorylation, we propose a model of how CDKA;1 regulates ASY1 (Fig 7). At early prophase I, CDKA;1 changes from an equal distribution in the cytoplasm and nucleus to a prominently nuclear localization, likely promoted by a meiotic cyclin such as SDS. In the nucleus, CDKA;1 phosphorylates ASY1 and by that enhances its binding affinity with ASY3. It is possible that CDKA;1 acts directly at the chromatin based on our immuno-localization data (Fig 1C). The related kinases Cdk2 from mammals and Cdc28 from budding yeast have both been found to localize to chromatin, too (Ashley *et al*, 2001; Zhu *et al*, 2010). However, these two kinases show a punctuate localization pattern while CDKA;1 has more continuous appearance along chromatin resembling the localization of ASY3 and ASY1 itself (Ashley *et al*, 2001; Armstrong, 2002; Ferdous *et al*, 2012).

Phosphorylation of ASY1 has several consequences. First, it enhances the affinity towards ASY3 promoting the recruitment of ASY1 to the chromosome axis. Second, it antagonizes a releasing force executed by PCH2, which is already present very early in meiosis. At the same time PCH2 promotes the nuclear accumulation of ASY1 (Fig 7).

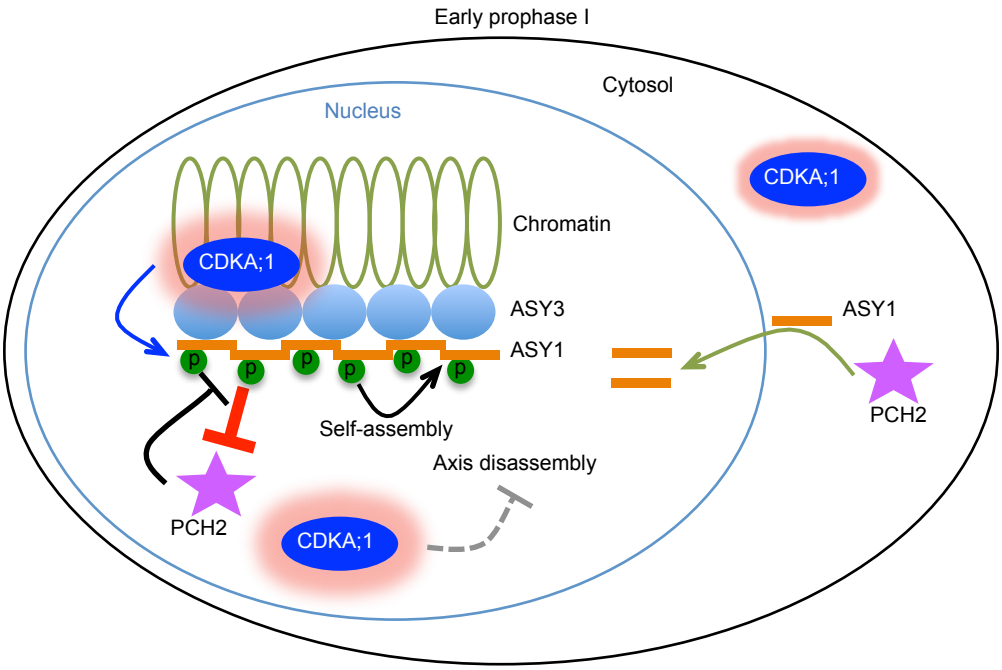

Figure 7. Model for the regulation of the chromosomal assembly of ASY1. In early prophase I, ASY1 is expressed and imported into nucleus, facilitated by PCH2. Concomitantly, CDKA;1 becomes enrichted in the nucleus, localizes on chromosomes, and phosphorylates ASY1. The phosphorylation enhances the binding affinity of ASY1 to ASY3 and the self-assembly and thus, in turn antagonizes the releasing force of PCH2. At the same time, high CDKA;1 activity in the nucleus may block other axis disassembling factors that will be activated later in synapsed regions where CDKA;1 is not present.

Moreover, the phosphorylation of ASY1 likely promotes the formation of ASY1 polymers similar to the proposed Hop1/HORMADs polymers in budding yeast *S. cerevisiae* and *C. elegans*, that is likely essential for its chromosome localization (Kim *et al*, 2014; Rosenberg & Corbett, 2015; West *et al*, 2018). HORMA domain proteins, such as Hop1, have been shown to bind to closure motifs in partner proteins (West *et al*, 2018). This interaction is stabilized by the folding of the C-terminal safety belt region of the HORMA domain protein around this binding motif from the respective partner resulting in a so-called closed state. Meiotic HORMA domain proteins such as Hop1 contain themselves closure motifs and have been shown to bind to other HORMAD molecules and by that likely leading to HORMAD polymers along the non-synaptic chromosome axes (Kim *et al*, 2014; West *et al*, 2018). These polymers are presumably anchored by binding to cohesin and/or axis proteins such as

Red1/ASY3. However, the full-length *Arabidopsis* ASY1 ($ASY1^{FL}$) showed a very low affinity towards ASY3 in our yeast two-hybrid assays (Fig 6B). Similar findings were recently reported for Hop1 and Red1 *in vitro* (West *et al*, 2018). The binding capacity of ASY1 to ASY3 was strongly enhanced when the short C-terminal region of ASY1 including the presumptive closure motif was deleted (Fig 6B). These results argue that a full-length ASY1, at least when being expressed in yeast cells, is in a closed conformation being bound by its own closure motif in the C-terminus or by the closure motif from another ASY1. However, we could not detect any interaction of $ASY1^{FL}$-to-$ASY1^{FL}$ using the yeast two-hybrid assay, suggesting that ASY1 tends to fold in a closed state though binding to its own closure motif at least when being expressed in yeast (Fig 6B). Assuming that the same holds true *in planta*, one needs to postulate that there is a factor that regulates the close-to-open state switch of ASY1. Our finding that ASY1 accumulates in the cytoplasm in *pch2* mutants suggests that PCH2 could have a function in converting ASY1 from the closed to the open state and at the same time probably avoiding the premature polymerization (in the cytoplasm) and providing a pool of available and reactive ASY1.

Mapping the ASY1 protein sequence onto the structure of *C. elegans* HIM-3 (c4trkA) using Phyre2 protein folding prediction shows that the T142 residue is likely located at the N-terminus of the alpha-C helix, a position just at the terminus of the long loop between beta-5 and alpha-C (Fig EV4B) (Kim *et al*, 2014). Since this loop anchors the C-terminal safety belt in place, one idea might be that phosphorylation of T142 imparts greater flexibility to the loop, and thereby may allow the safety belt to disengage, i.e., to "open" the protein and thus, allow the closure motif binding/dissociation (Kim *et al*, 2014; West *et al*, 2018).

When homologs synapse at zygotene and pachytene, ASY1 is displaced from chromatin by PCH2 and this removal is essential for completing chromosome synapsis and recombination (Lambing *et al*, 2015). Concomitantly with the ASY1 removal, the nuclear levels of CDKA;1 drop and CDKA;1 is also evicted from chromatin of synapsed regions (Fig 1A-C). Whether a possible drop in CDKA;1 activity in the nucleus is relevant for the removal of ASY1 is not clear. At least the phosphorylation-mimicking mutant $ASY1^{T142D}$ can be released from chromatin indicating that the removal of ASY1 functions independently from its phosphorylation. This suggests either that an unknown regulator/cofactor of PCH2 exists, which enhances the activity of PCH2, or that PCH2 has a higher activity at

synaptic regions. The latter is supported by the observation that, while the PCH2 signal shows a diffuse nuclear localization before zygotene when ASY1 is assembled on the chromosome axis, it starts to accumulate specifically at the synaptic regions at zygotene coinciding with ASY1 removal. After that, PCH2 is largely present along the entire chromosomes at pachytene (Fig 5D). It is tempting to speculate that CDKA;1 might phosphorylate and by that inhibit an ASY1 disassembly factor (Fig 7). Hence, a reduction of CDKA;1 in the nucleus as seen here by live cell imaging could also throw the switch for this removal step. Although PCH2 has a Cdk phosphorylation site, it seems unlikely that PCH2 itself could be the target of this potential mechanism since we found here that at a phase of presumed high CDKA;1 activity, PCH2 is able to displace ASY1 from the chromosome axis as seen by the restoration of this interaction in a *pch2* mutant background (Fig 5A and B). On the other hand, the removal of ASY1 at zygotene may be regulated through other post-translational modifications. Consistent with this hypothesis, Osman et al. (2017) have identified several other phosphorylation sites on ASY1, notably ATM/ATR phosphorylation sites. Thus, further work is required to understand the mechanisms of how ASY1 is removed from the chromosome axis.

Beyond ASY1 phosphorylation

Here, we have shown that CDKA;1 works together with SDS and TAM. However, the *sds* mutant phenotype is not a subset of the phenotype of the weak loss-of-function *cdka;1* mutants as seen by the apparently correct localization of DMC1 in *cdka;1* and the localization failure in *sds* (De Muyt *et al*, 2009). One possible explanation is that SDS can work with additional Cdks, such as CDKB1;1, which have been recently shown to have function in somatic homologous recombination repair (Weimer *et al*, 2016). However, at least *in vitro* neither CDKB1;1 nor the related kinase CDKB2;2 built an active kinase complex with SDS (Harashima & Schnittger, 2012). Thus, it seems more likely that the residual Cdk activity in the hypomorphic mutants is sufficient to operate together with SDS to promote DMC1 loading/stabilization. Notably, the localization of ASY1 to chromatin is also only delayed and not completely absent in weak loss-of-function mutants.

Earlier work has already indicated that TAM, the other meiotic cyclin used in our assays, is needed to promote the timely progression through meiosis I and entry into meiosis II (d'Erfurth *et al*, 2010). At the same time CDK-dependent

phosphorylation of THREE DIVISION MUTANT 1 (TDM1) has been shown to be crucial for the exact timing of meiotic exit. Mutation of the CDK phosphorylation site in TDM1 also results in termination of meiosis after anaphase I (Cifuentes *et al*, 2016). Furthermore, the loss of the APC/C inhibitor OMISSION OF SECOND MEIOTIC DIVISION1 (OSD1), also known as GIGAS CELL 1 (GIG), and the presumed increase in APC/C activity also caused a premature termination of meiosis after anaphase I (Iwata *et al*, 2011; Cromer *et al*, 2012). Consistently with these studies, we found that weak loss-of-function mutants of *cdka;1* often terminated meiosis shortly after the first meiotic division.

In addition, we observed in the weak loss-of-function *cdka;1* mutants several other defects, e.g., in chromosome condensation. While we cannot exclude that these defects are an indirect consequence of for instance altered ASY1 dynamics, it seems plausible that CDKA;1 has many more roles in meiosis than the here-revealed function in assembling the chromosome axis. Indeed, MLH1 was recently found to be an *in vitro* target of CDKA;1 activity and in *cdka;1* hypomorphic mutants, in which kinase activity is only mildly reduced, an altered recombination pattern with fewer crossovers than in the wildtype was observed (Wijnker *et al*, 2019). Interestingly, an alleged increase in CDKA;1 activity also caused an elevation in recombination events hinting at a dosage dependency of CDKA;1 for crossover formation. A key role of Cdks in meiosis is further supported by the large number of meiotic regulators that have Cdk consensus phosphorylation sites and/or a predicted cyclin binding site (Zhu *et al*, 2010). Thus, it seems very likely that we are still at the beginning to understand the phosphorylation-control of meiosis by Cdk1-type proteins.

Authors Contributions

C.Y. and A.S. conceived the experiments. C.Y., K.S., E.W.,Y.H., L.C., H.H., S.C.S., D.V., L.C., Z.O., G.P., P.S., M.G., performed the experiments and statistical analyses; S.C.S. and H.N. performed the mass spectrometry experiment and data analysis. C.Y., K.S., E.W.,Y.H., L.C., H.H., S.C.S., D.V., L.C., Z.O., G.P., P.S., M.G. and A.S. analyzed the data. C.Y. and A.S. wrote the manuscript.

Acknowledgment

We acknowledge the Salk T-DNA collection, the GABI-Kat T-DNA collection, the *Arabidopsis* Biological Resource Center (ABRC) and the European *Arabidopsis* Stock Centre (NASC) for providing seeds of T-DNA lines used in this report. We thank the reviewers for their comments and constructive feedback on this manuscript. This work was supported by core funding of the University of Hamburg. The IJPB benefits from the support of the LabEx Saclay Plant Sciences-SPS (ANR-10-LABX-0040-SPS).

Declaration of Interests

The authors declare that they have no conflict of interest.

REFERENCES

Adhikari D, Zheng W, Shen Y, Gorre N, Ning Y, Halet G, Kaldis P & Liu K (2012) Cdk1, but not Cdk2, is the sole Cdk that is essential and sufficient to drive resumption of meiosis in mouse oocytes. *Hum. Mol. Genet.* **21:** 2476–2484

Anand R, Ranjha L, Cannavo E & Cejka P (2016) Phosphorylated CtIP Functions as a Co-factor of the MRE11-RAD50-NBS1 Endonuclease in DNA End Resection. *Molecular Cell* **64:** 940–950

Armstrong SJ (2002) Asy1, a protein required for meiotic chromosome synapsis, localizes to axis-associated chromatin in Arabidopsis and Brassica. *Journal of Cell Science* **115:** 3645–3655

Ashley T, Walpita D & de Rooij DG (2001) Localization of two mammalian cyclin dependent kinases during mammalian meiosis. *Journal of Cell Science* **114:** 685–693

Azumi Y, Liu D, Zhao D, Li W, Wang G, Hu Y & Ma H (2002) Homolog interaction during meiotic prophase I in Arabidopsis requires the SOLO DANCERS gene encoding a novel cyclin-like protein. *EMBO J.* **21:** 3081–3095

Bulankova P, Akimcheva S, Fellner N & Riha K (2013) Identification of Arabidopsis meiotic cyclins reveals functional diversification among plant cyclin genes. *PLoS Genet* **9:** e1003508

Bulankova P, Riehs-Kearnan N, Nowack MK, Schnittger A & Riha K (2010) Meiotic progression in Arabidopsis is governed by complex regulatory interactions between SMG7, TDM1, and the meiosis I-specific cyclin TAM. *Plant Cell* **22:** 3791–3803

Cannavo E, Johnson D, Andres SN, Kissling VM, Reinert JK, Garcia V, Erie DA, Hess D, Thomä NH, Enchev RI, Peter M, Williams RS, Neale MJ & Cejka P (2018) Regulatory control of DNA end resection by Sae2 phosphorylation. *Nat Commun* **9:** 4016

Carballo JA, Johnson AL, Sedgwick SG & Cha RS (2008) Phosphorylation of the Axial Element Protein Hop1 by Mec1/Tel1 Ensures Meiotic Interhomolog Recombination. *Cell* **132:** 758–770

Chen C, Jomaa A, Ortega J & Alani EE (2014) Pch2 is a hexameric ring ATPase that remodels the chromosome axis protein Hop1. *Proc. Natl. Acad. Sci. U.S.A.* **111:** E44–53

Cifuentes M, Jolivet S, Cromer L, Harashima H, Bulankova P, Renne C, Crismani W, Nomura Y, Nakagami H, Sugimoto K, Schnittger A, Riha K & Mercier R (2016) TDM1 Regulation Determines the Number of Meiotic Divisions. *PLoS Genet* **12:** e1005856

Coudreuse D & Nurse P (2010) Driving the cell cycle with a minimal CDK control

network. *Nature* **468:** 1074–1079

Cromer L, Heyman J, Touati S, Harashima H, Araou E, Girard C, Horlow C, Wassmann K, Schnittger A, De Veylder L & Mercier R (2012) OSD1 promotes meiotic progression via APC/C inhibition and forms a regulatory network with TDM and CYCA1;2/TAM. *PLoS Genet* **8:** e1002865

d'Erfurth I, Cromer L, Jolivet S, Girard C, Horlow C, Sun Y, To JPC, Berchowitz LE, Copenhaver GP & Mercier R (2010) The cyclin-A CYCA1;2/TAM is required for the meiosis I to meiosis II transition and cooperates with OSD1 for the prophase to first meiotic division transition. *PLoS Genet* **6:** e1000989

Da Ines O, Degroote F, Goubely C, Amiard S, Gallego ME & White CI (2013) Meiotic Recombination in Arabidopsis Is Catalysed by DMC1, with RAD51 Playing a Supporting Role. *PLoS Genet* **9:** e1003787

De Muyt A, Pereira L, Vezon D, Chelysheva L, Gendrot G, Chambon A, Lainé-Choinard S, Pelletier G, Mercier R, Nogué F & Grelon M (2009) A high throughput genetic screen identifies new early meiotic recombination functions in Arabidopsis thaliana. *PLoS Genet* **5:** e1000654

Dissmeyer N, Nowack MK, Pusch S, Stals H, Inzé D, Grini PE & Schnittger A (2007) T-loop phosphorylation of Arabidopsis CDKA;1 is required for its function and can be partially substituted by an aspartate residue. *Plant Cell* **19:** 972–985

Dissmeyer N, Weimer AK, Pusch S, De Schutter K, Alvim Kamei CL, Nowack MK, Novak B, Duan G-L, Zhu Y-G, De Veylder L & Schnittger A (2009) Control of cell proliferation, organ growth, and DNA damage response operate independently of dephosphorylation of the Arabidopsis Cdk1 homolog CDKA;1. *Plant Cell* **21:** 3641–3654

Doonan JH & Kitsios G (2009) Functional evolution of cyclin-dependent kinases. *Mol. Biotechnol.* **42:** 14–29

Ferdous M, Higgins JD, Osman K, Lambing C, Roitinger E, Mechtler K, Armstrong SJ, Perry R, Pradillo M, Cuñado N & Franklin FCH (2012) Inter-homolog crossing-over and synapsis in Arabidopsis meiosis are dependent on the chromosome axis protein AtASY3. *PLoS Genet* **8:** e1002507

Gutiérrez-Escribano P & Nurse P (2015) A single cyclin-CDK complex is sufficient for both mitotic and meiotic progression in fission yeast. *Nat Commun* **6:** 6871

Harashima H & Schnittger A (2012) Robust reconstitution of active cell-cycle control complexes from co-expressed proteins in bacteria. *Plant Methods* **8:** 23

Harashima H, Dissmeyer N & Schnittger A (2013) Cell cycle control across the eukaryotic kingdom. *Trends in Cell Biology* **23:** 345–356

Henderson KA, Kee K, Maleki S, Santini PA & Keeney S (2006) Cyclin-dependent kinase directly regulates initiation of meiotic recombination. *Cell* **125:** 1321–1332

Hollingsworth NM, Goetsch L & Byers B (1990) The HOP1 gene encodes a meiosis-specific component of yeast chromosomes. *Cell* **61:** 73–84

Huang X-Y, Niu J, Sun M-X, Zhu J, Gao J-F, Yang J, Zhou Q & Yang Z-N (2013) CYCLIN-DEPENDENT KINASE G1 Is Associated with the Spliceosome to Regulate CALLOSE SYNTHASE5 Splicing and Pollen Wall Formation in Arabidopsis. *Plant Cell* **25:** 637–648

Huertas P & Jackson SP (2009) Human CtIP mediates cell cycle control of DNA end resection and double strand break repair. *J. Biol. Chem.* **284:** 9558–9565

Huertas P, Cortés-Ledesma F, Sartori AA, Aguilera A & Jackson SP (2008) CDK targets Sae2 to control DNA-end resection and homologous recombination. *Nature* **455:** 689–692

Iwata E, Ikeda S, Matsunaga S, Kurata M, Yoshioka Y, Criqui M-C, Genschik P & Ito M (2011) GIGAS CELL1, a novel negative regulator of the anaphase-promoting complex/cyclosome, is required for proper mitotic progression and cell fate determination in Arabidopsis. *Plant Cell* **23:** 4382–4393

Kim Y, Rosenberg SC, Kugel CL, Kostow N, Rog O, Davydov V, Su TY, Dernburg AF & Corbett KD (2014) The Chromosome Axis Controls Meiotic Events through a Hierarchical Assembly of HORMA Domain Proteins. *Developmental Cell* **31:** 487–502

Kurzbauer MT, Uanschou C, Chen D & Schlogelhofer P (2012) The Recombinases DMC1 and RAD51 Are Functionally and Spatially Separated during Meiosis in Arabidopsis. *Plant Cell* **24:** 2058–2070

Lambing C, Franklin FCH & Wang C-JR (2017) Understanding and Manipulating Meiotic Recombination in Plants. *Plant Physiol.* **173:** 1530–1542

Lambing C, Osman K, Nuntasoontorn K, West A, Higgins JD, Copenhaver GP, Yang J, Armstrong SJ, Mechtler K, Roitinger E & Franklin FCH (2015) Arabidopsis PCH2 Mediates Meiotic Chromosome Remodeling and Maturation of Crossovers. *PLoS Genet* **11:** e1005372

Li J, Hooker GW & Roeder GS (2006) Saccharomyces cerevisiae Mer2, Mei4 and Rec114 form a complex required for meiotic double-strand break formation. *Genetics* **173:** 1969–1981

Magnard JL, Yang M, Chen YC, Leary M & McCormick S (2001) The Arabidopsis gene tardy asynchronous meiosis is required for the normal pace and synchrony of cell division during male meiosis. *Plant Physiol.* **127:** 1157–1166

Malumbres M, Harlow E, Hunt T, Hunter T, Lahti JM, Manning G, Morgan DO, Tsai L-H & Wolgemuth DJ (2009) Cyclin-dependent kinases: a family portrait. *Nat. Cell Biol.* **11:** 1275–1276

Mercier R, Mézard C, Jenczewski E, Macaisne N & Grelon M (2015) The Molecular Biology of Meiosis in Plants. *Annu. Rev. Plant Biol.* **66:** 297–327

Miller ME & Cross FR (2001) Cyclin specificity: how many wheels do you need on a unicycle? *Journal of Cell Science* **114:** 1811–1820

Morgan DO (1997) Cyclin-dependent kinases: engines, clocks, and microprocessors. *Annu. Rev. Cell Dev. Biol.* **13:** 261–291

Muniyappa K, Kshirsagar R & Ghodke I (2014) The HORMA domain: an evolutionarily conserved domain discovered in chromatin-associated proteins, has unanticipated diverse functions. *Gene* **545:** 194–197

Niu B, Wang L, Zhang L, Ren D, Ren R, Copenhaver GP, Ma H & Wang Y (2015) Arabidopsis Cell Division Cycle 20.1 Is Required for Normal Meiotic Spindle Assembly and Chromosome Segregation. **27:** 3367–3382

Nowack MK, Harashima H, Dissmeyer N, Zhao X, Bouyer D, Weimer AK, De Winter F, Yang F & Schnittger A (2012) Genetic framework of cyclin-dependent kinase function in Arabidopsis. *Developmental Cell* **22:** 1030–1040

Nowack MK, Shirzadi R, Dissmeyer N, Dolf A, Endl E, Grini PE & Schnittger A (2007) Bypassing genomic imprinting allows seed development. *Nature* **447:** 312–315

Ortega S, Prieto I, Odajima J, Martín A, Dubus P, Sotillo R, Barbero JL, Malumbres M & Barbacid M (2003) Cyclin-dependent kinase 2 is essential for meiosis but not for mitotic cell division in mice. *Nat. Genet.* **35:** 25–31

Osman K, Yang J, Roitinger E, Lambing C, Heckmann S, Howell E, Cuacos M, Imre R, Dürnberger G, Mechtler K, Armstrong S & Franklin FCH (2017) Affinity proteomics reveals extensive phosphorylation of the Brassica chromosome axis protein ASY1 and a network of associated proteins at prophase I of meiosis. *Plant J* **93:** 17–33

Pagliuca FW, Collins MO, Lichawska A, Zegerman P, Choudhary JS & Pines J (2011) Quantitative proteomics reveals the basis for the biochemical specificity of the cell-cycle machinery. *Molecular Cell* **43:** 406–417

Prusicki MA, Keizer EM, van Rosmalen RP, Komaki S, Seifert F, Müller K, Wijnker E, Fleck C & Schnittger A (2019) Live cell imaging of meiosis in Arabidopsis thaliana. *Elife* **8:** 141

Pusch S, Harashima H & Schnittger A (2012) Identification of kinase substrates by bimolecular complementation assays. *Plant J* **70:** 348–356

Rockmill B & Roeder GS (1990) Meiosis in asynaptic yeast. *Genetics* **126:** 563–574

Rosenberg SC & Corbett KD (2015) The multifaceted roles of the HORMA domain in cellular signaling. *J. Cell Biol.* **211:** 745–755

Santamaría D, Barrière C, Cerqueira A, Hunt S, Tardy C, Newton K, Cáceres JF, Dubus P, Malumbres M & Barbacid M (2007) Cdk1 is sufficient to drive the mammalian cell cycle. *Nature* **448:** 811–815

Satyanarayana A, Berthet C, Lopez-Molina J, Coppola V, Tessarollo L & Kaldis P (2008) Genetic substitution of Cdk1 by Cdk2 leads to embryonic lethality and loss of meiotic function of Cdk2. *Development* **135:** 3389–3400

Schmidt TGM, Batz L, Bonet L, Carl U, Holzapfel G, Kiem K, Matulewicz K, Niermeier D, Schuchardt I & Stanar K (2013) Development of the Twin-Strep-tag® and its application for purification of recombinant proteins from cell culture supernatants. *Protein Expr. Purif.* **92:** 54–61

Shinohara A, Gasior S, Ogawa T, Kleckner N & Bishop DK (1997) Saccharomyces cerevisiae recA homologues RAD51 and DMC1 have both distinct and overlapping roles in meiotic recombination. *Genes Cells* **2:** 615–629

Smith AV & Roeder GS (1997) The yeast Red1 protein localizes to the cores of meiotic chromosomes. *J. Cell Biol.* **136:** 957–967

Stronghill PE, Azimi W & Hasenkampf CA (2014) A novel method to follow meiotic progression in Arabidopsis using confocal microscopy and 5-ethynyl-2'-deoxyuridine labeling. *Plant Methods* **10:** 33

Tank JG & Thaker VS (2011) Cyclin dependent kinases and their role in regulation of plant cell cycle. *Biologia Plantarum* **55:** 201–212

Ubersax JA, Woodbury EL, Quang PN, Paraz M, Blethrow JD, Shah K, Shokat KM & Morgan DO (2003) Targets of the cyclin-dependent kinase Cdk1. *Nature* **425:** 859–864

Wang Y, Wu H, Liang G & Yang M (2004) Defects in nucleolar migration and synapsis in male prophase□I in the ask1-1 mutant of Arabidopsis. *Sexual Plant Reproduction* **16:** 273–282

Weimer AK, Biedermann S, Harashima H, Roodbarkelari F, Takahashi N, Foreman J, Guan Y, Pochon G, Heese M, Van Damme D, Sugimoto K, Koncz C, Doerner P, Umeda M & Schnittger A (2016) The plant-specific CDKB1-CYCB1 complex mediates homologous recombination repair in Arabidopsis. *EMBO J.* **35:** 2068–2086

West AM, Rosenberg SC, Ur SN, Lehmer MK, Ye Q, Hagemann G, Caballero I, Usón I, MacQueen AJ, Herzog F & Corbett KD (2019) A conserved filamentous assembly underlies the structure of the meiotic chromosome axis. *Elife* **8:** 213

West AMV, Komives EA & Corbett KD (2018) Conformational dynamics of the Hop1 HORMA domain reveal a common mechanism with the spindle checkpoint protein Mad2. *Nucleic Acids Research* **46:** 279–292

Wijnker E & Schnittger A (2013) Control of the meiotic cell division program in plants. *Plant Reprod* **26:** 143–158

Wijnker E, Harashima H, Müller K, Parra-Nuñez P, de Snoo CB, van de Belt J, Dissmeyer N, Bayer M, Pradillo M & Schnittger A (2019) The Cdk1/Cdk2 homolog CDKA;1 controls the recombination landscape in Arabidopsis. *Proc. Natl. Acad. Sci. U.S.A.* **116:** 12534–12539

Wojtasz L, Daniel K, Roig I, Bolcun-Filas E, Xu H, Boonsanay V, Eckmann CR, Cooke HJ, Jasin M, Keeney S, McKay MJ & Tóth A (2009) Mouse HORMAD1 and HORMAD2, two conserved meiotic chromosomal proteins, are depleted from synapsed chromosome axes with the help of TRIP13 AAA-ATPase. *PLoS Genet* **5:** e1000702

Yang C, Hamamura Y, Sofroni K, Böwer F, Stolze SC, Nakagami H & Schnittger A (2019) SWITCH 1/DYAD is a WINGS APART-LIKE antagonist that maintains sister chromatid cohesion in meiosis. *Nat Commun* **10:** 1755

Yang X, Timofejeva L, Ma H & Makaroff CA (2006) The Arabidopsis SKP1 homolog ASK1 controls meiotic chromosome remodeling and release of chromatin from the nuclear membrane and nucleolus. *Journal of Cell Science* **119:** 3754–3763

Zabicki P, Kuta E, Tuleja M, Rataj K & Malec P (2013) Arabidopsis Cyclin-Dependent Kinase Gene Cdkg;2 Is Involved in Organogenic Responses Induced in Vitro. *Acta Biologica Cracoviensia Series Botanica* **55:** 37–48

Zhao X, Harashima H, Dissmeyer N, Pusch S, Weimer AK, Bramsiepe J, Bouyer D, Rademacher S, Nowack MK, Novak B, Sprunck S & Schnittger A (2012) A general G1/S-phase cell-cycle control module in the flowering plant Arabidopsis thaliana. *PLoS Genet* **8:** e1002847

Zheng T, Nibau C, Phillips DW, Jenkins G, Armstrong SJ & Doonan JH (2014) CDKG1 protein kinase is essential for synapsis and male meiosis at high ambient temperature in Arabidopsis thaliana. *Proc. Natl. Acad. Sci. U.S.A.* **111:** 2182–2187

Zhu Z, Mori S, Oshiumi H, Matsuzaki K, Shinohara M & Shinohara A (2010) Cyclin-dependent kinase promotes formation of the synaptonemal complex in yeast meiosis. *Genes Cells* **15:** 1036–1050

Zickler D & Kleckner N (1999) Meiotic chromosomes: integrating structure and function. *Annu. Rev. Genet.* **33:** 603–754

Zickler D & Kleckner N (2015) Recombination, Pairing, and Synapsis of Homologs during Meiosis. *Cold Spring Harb Perspect Biol* **7:** a016626

SUPPLEMENTAL FIGURES

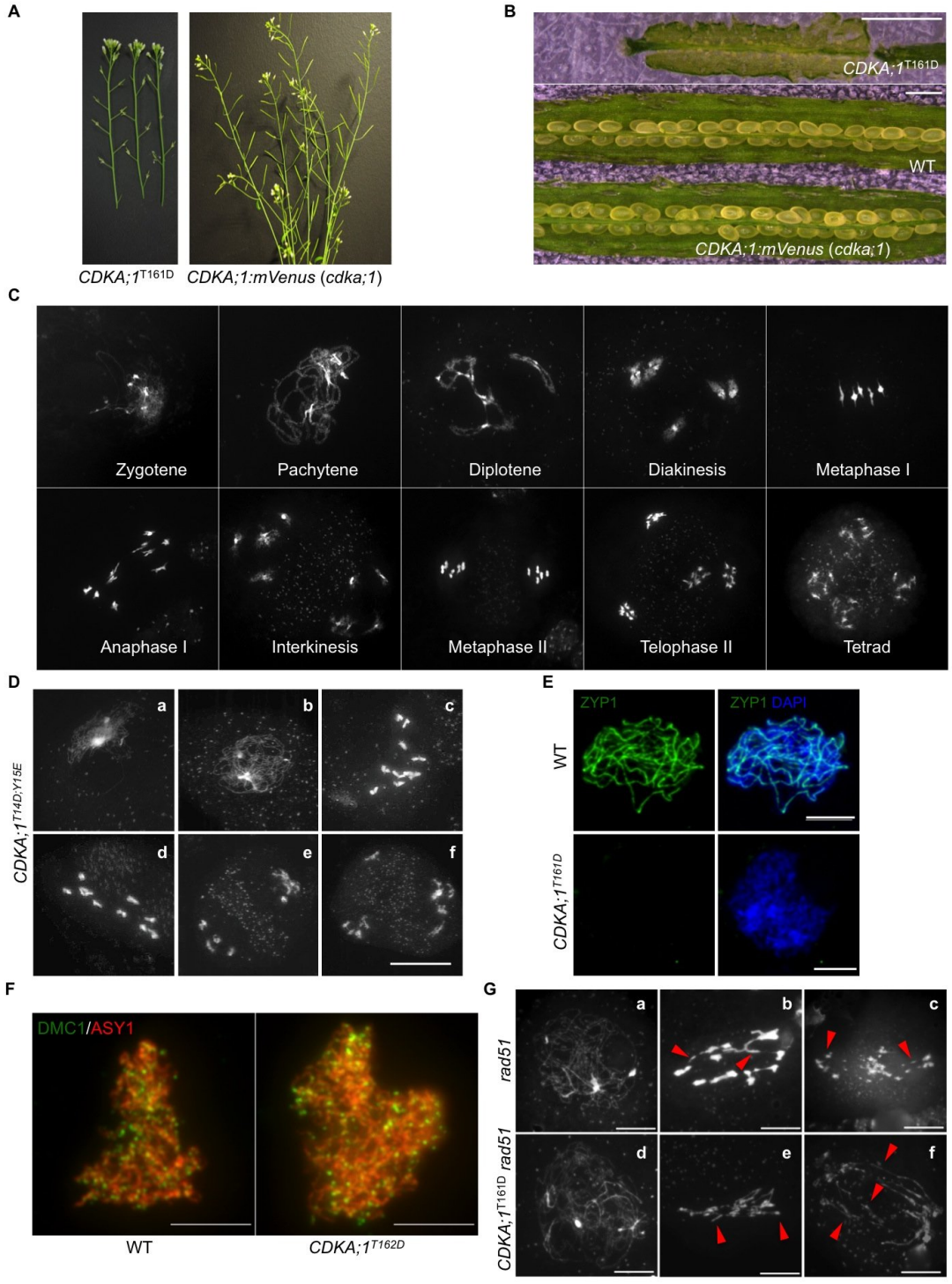

Figure EV1. CDKA;1-mVenus fully complements the *cdka;1* mutant phenotype. (A) The stems of a hypomophic *cdka;1* mutant *CDKA;1*^{T161D} are completely sterile as indicated by short siliques in contrast to homozygous *cdka;1* mutant expressing the *CDKA;1:mVenus* reporter construct that form long siliques and are full fertile. (B) The siliques of hypomophic *CDKA;1*^{T161D} do not harbor viable seeds in contrast to

homozygous *cdka;1* mutant expressing CDKA;1:mVenus that develop healthy and plump seeds. Bars: 1 mm. (C) Chromosome spread analysis of male meiocytes of a homozygous *cdka;1* mutant expressing a functional *CDKA;1:mVenus* reporter reveals a wild-type like meiotic program. Bar: 10µm. (D) Chromosome spread analysis of the hypomorphic *cdka;1* mutant $CDKA;1^{T14D;Y15E}$. (a) zygotene-like stage; (b) pachytene-like stage; (c, d) diakinesis-like stages; (e, f) end of meiosis I with two or three pools of chromsomes. (E) Immunolocalization of ZYP1 (green) in wildtype (WT) and and $CDKA;1^{T161D}$ mutants. Chromosomes are stained with DAPI (blue). Bars: 5µm. (F) Immunolocalization analysis of DMC1 (green) together with ASY1 (red) in late leptotene of male meiocytes of wildtype (WT) and $CDKA;1^{T161D}$ mutants. Bars: 5µm. (G) Chromosome spread analysis of *rad51* and *rad51* $CDKA;1^{T161D}$ mutants. (a, d) pachytene-like stage; (b, c, e and f) anaphase I-like stage. Red arrowheads indicate the chromosomal fragments. Bars: 10µm. **This Figure except for the first image of Fig A and B, and Fig E is made from the data provided kindly by Kostika Sofroni (Universität Hamburg), Erik Wijnker (Universität Hamburg, current in Wageningen University & Research), Mathilde Grelon (Université Paris-Saclay).**

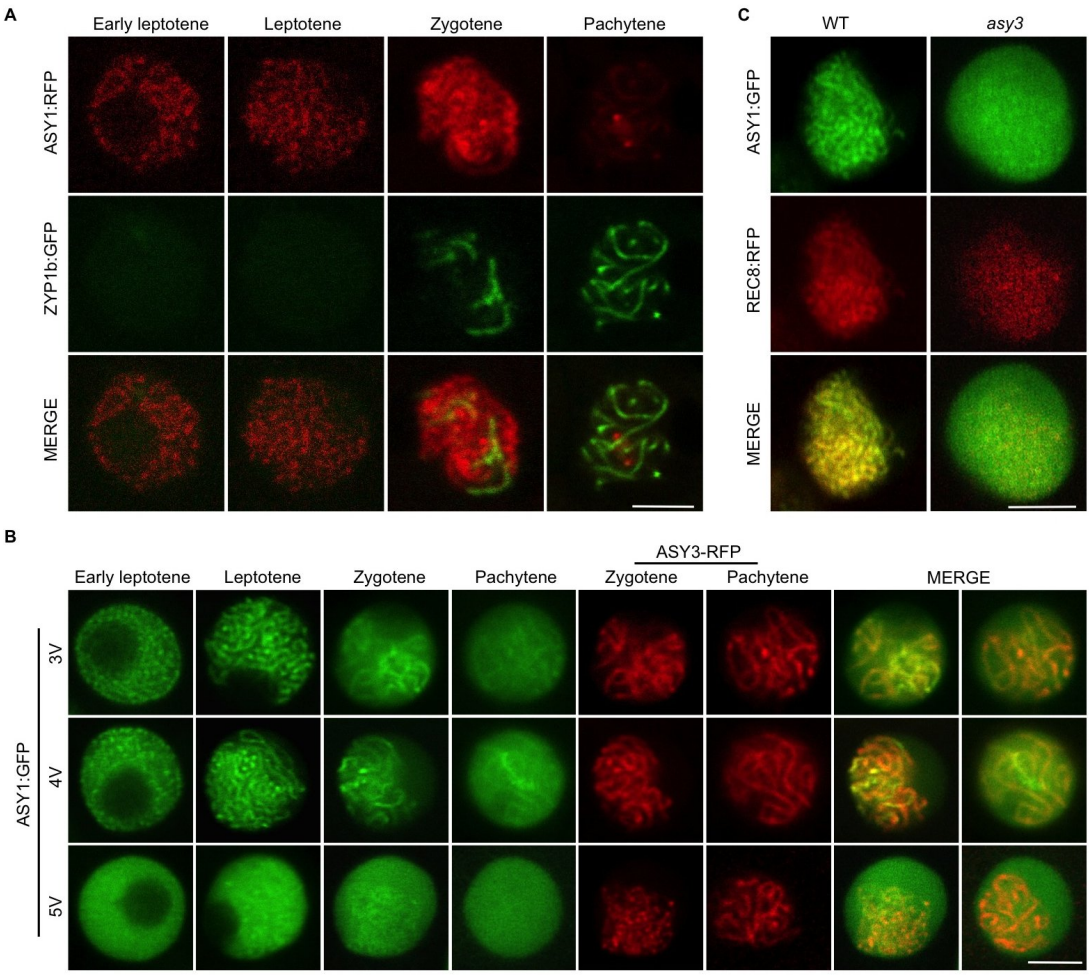

Figure EV2. Localization of ASY1 variants in the wildtype and *asy3* mutants. (A) Co-localization analysis of ASY1-RFP with ZYP1b-GFP at different meiotic stages in male meiocytes of the wildtype. Bars: 5µm. (B) Localization of ASY1^{3V}:GFP (T365V S382V T535V), ASY1^{4V}:GFP (T184V T365V S382V T535V), and ASY1^{5V}:GFP (T142V T184V T365V S382V T535V) together with ASY3:RFP (for staging of zygotene and pachytene) at different meiotic stages in male meiocytes of *asy1* mutants. Bars: 5µm. (C) Localization of ASY1:GFP in male meiocytes of the wildtype and *asy3* mutants at leptotene. REC8-RFP was used for staging and to highlight chromosomes. Bars: 5µm.

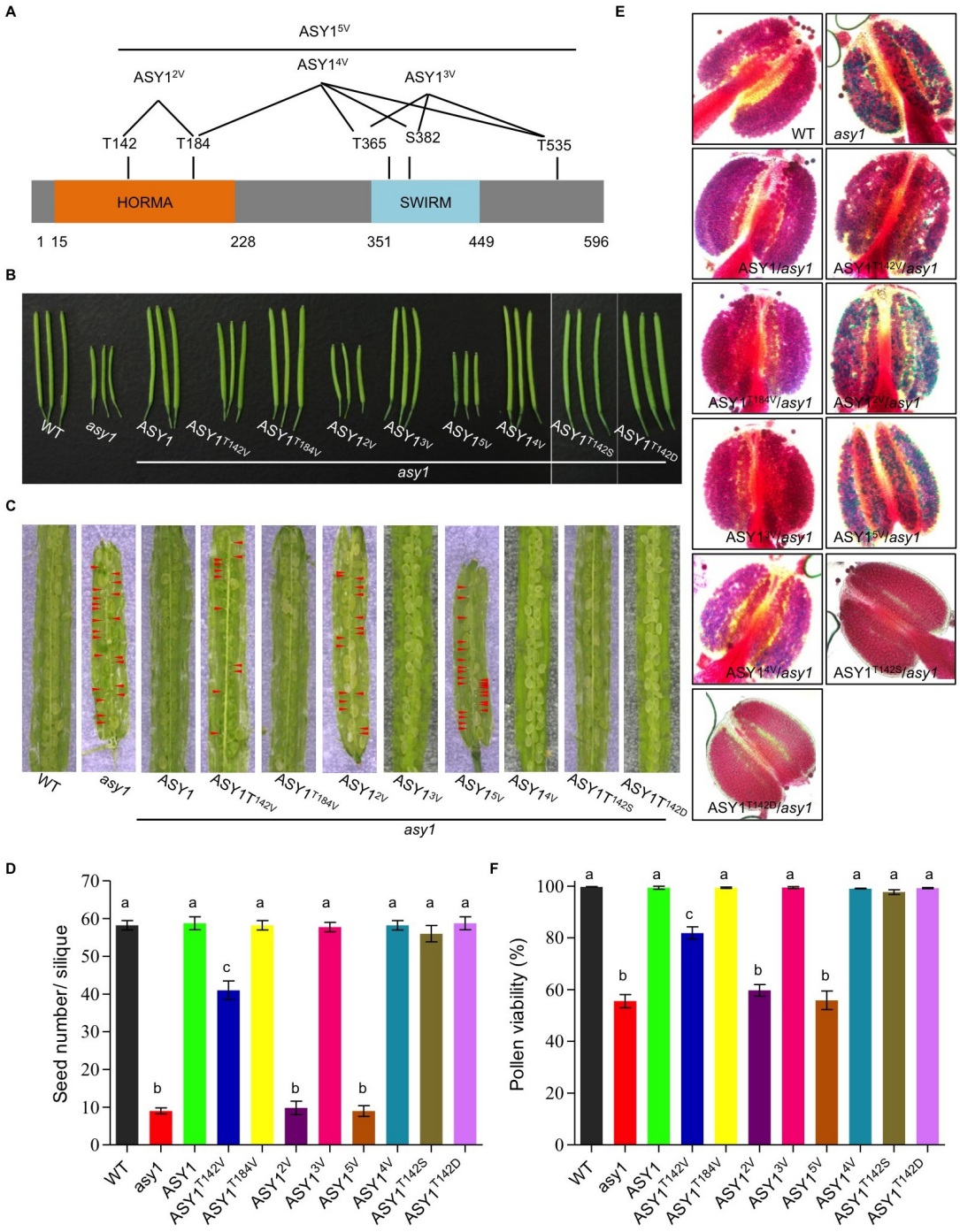

Figure EV3. Phenotypic characterization of different ASY1:GFP variants. (A) Schematic graph showing different ASY1 non-phosphorylatable mutants. Siliques (B) and seed set (C) of the wildtype (WT), *asy1*, $ASY1^{T142V}$, $ASY1^{T184V}$, $ASY1^{2V}$, $ASY1^{3V}$, $ASY1^{4V}$, $ASY1^{5V}$, $ASY1^{T142S}$, and $ASY1^{T142D}$. Red arrow heads indicate aborted seeds. (D) Quantification of the seed set shown in (C) from at least 5 siliques. (E) Peterson staining of anthers for the wildtype (WT), *asy1*, $ASY1^{T142V}$, $ASY1^{T184V}$, $ASY1^{2V}$, $ASY1^{3V}$, $ASY1^{4V}$, $ASY1^{5V}$, $ASY1^{T142S}$, and $ASY1^{T142D}$. Red indicates viable pollen grains and blue denotes aborted pollen grains. (F) Quantification of the pollen viability assay

shown in (E) using at least 9 flower buds. Level of significance ($P < 0.05$) is indicated by different letters as determined by the one-way ANOVA followed by Tukey's test.

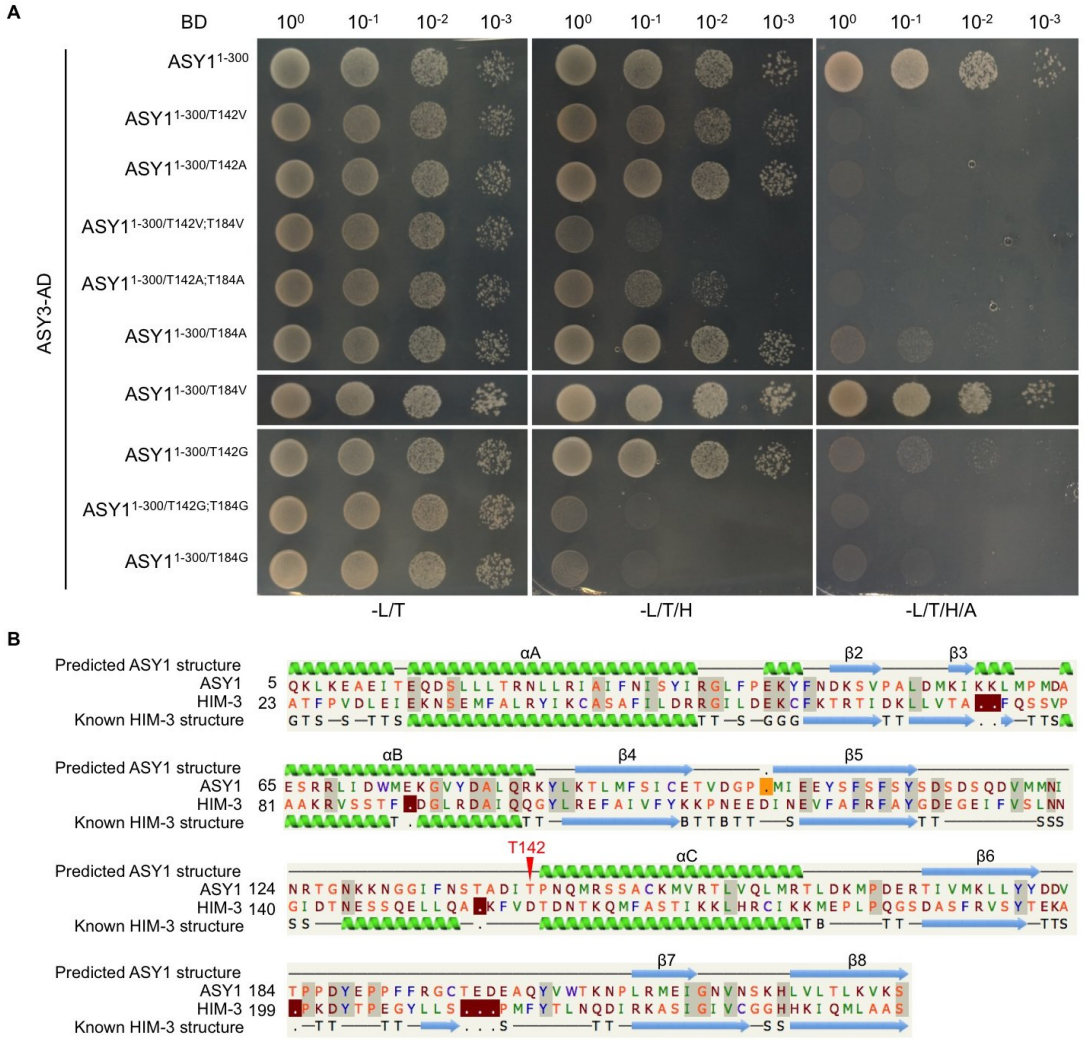

Figure EV4. Non-phosphorylatable substitutions of T142 in ASY1 reduce its interaction strength with ASY3. (A) Yeast two-hybrid interaction assays of ASY3 with different ASY1 variants. Yeast cells harboring both the AD and BD plasmids were grown on synthetic medium supplied with glucose in the absence of Leu and Trp (-L/T, left panel), on SD medium in the absence of Leu, Trp, and His (-L/T/H, middle panel), and on SD medium in the absence of Leu,Trp, His and Ade (-L/T/H/A, right panel). Yeast cells were incubated until OD_{600} = 1 and then diluted 10-, 100- and 1000-fold for the assays. (B) The predicted structure of ASY1 HORMA domain based on the known structure of *C. elegans* HIM-3 (c4trkA) using Phyre2 protein structure prediction. Red arrowhead indicates the T142 site of ASY1.

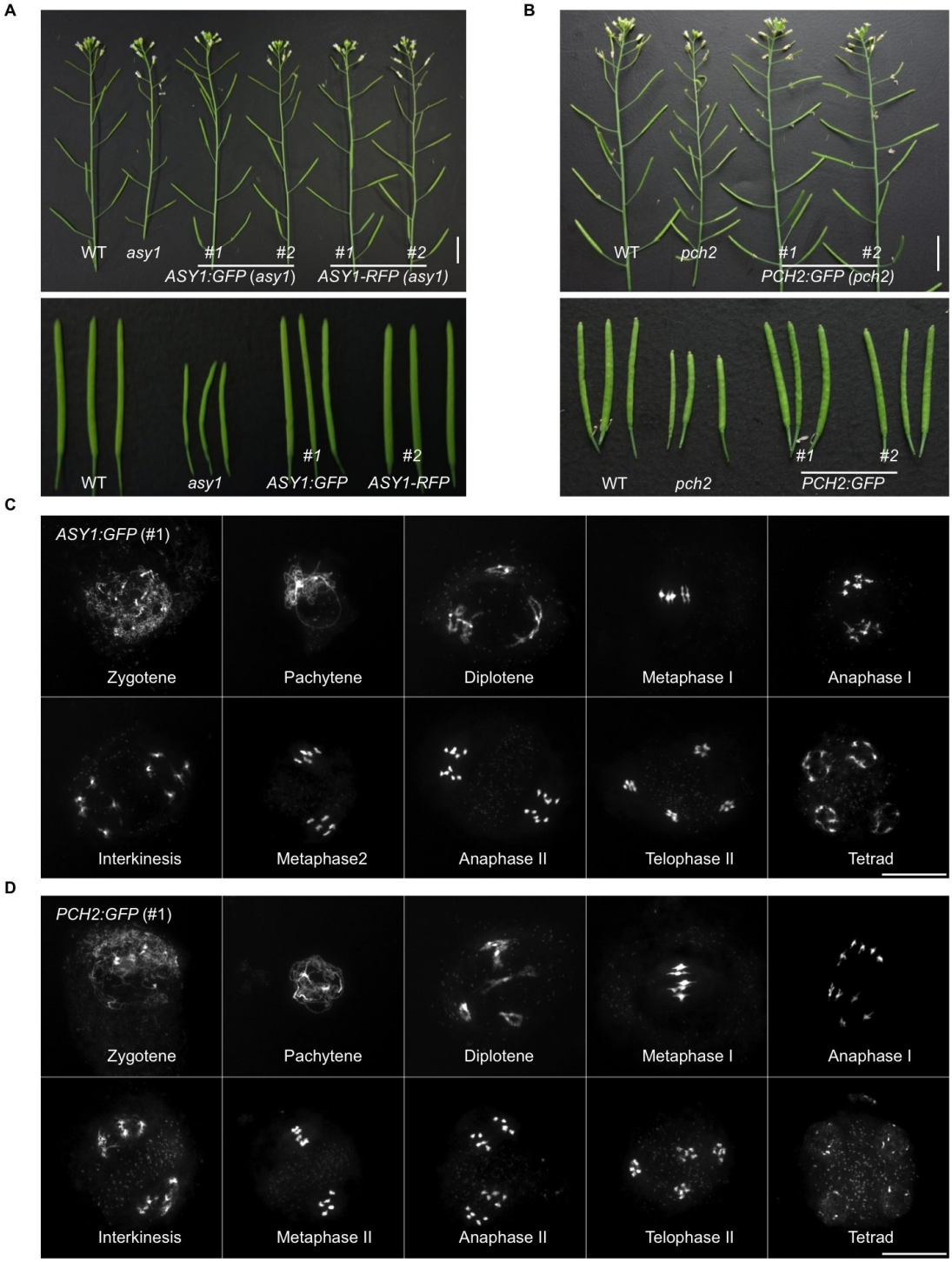

Appendix Figure S1. The ASY1 and PCH2 reporters are fully functional. (A) The main stems (upper panel) and siliques (lower panel) of the wildtype (WT) , *asy1* and two *ASY1:GFP/RFP* lines are shown. (B) The main stems (upper panel) and siliques (lower panel) of the wildtype (WT), *pch2* and two *PCH2:GFP* lines. (C) Chromosome spread analysis of male meiocytes in ASY1:GFP line *#1* shows a wild-type like meiotic program. (D) Chromosome spread analysis of male meiocytes in PCH2:GFP *#1* shows a wild-type like meiotic program. **The Figures (C) and (D) are**

kindly provided by Kostika Sofroni (Universität Hamburg) using the materials collected by Chao Yang.

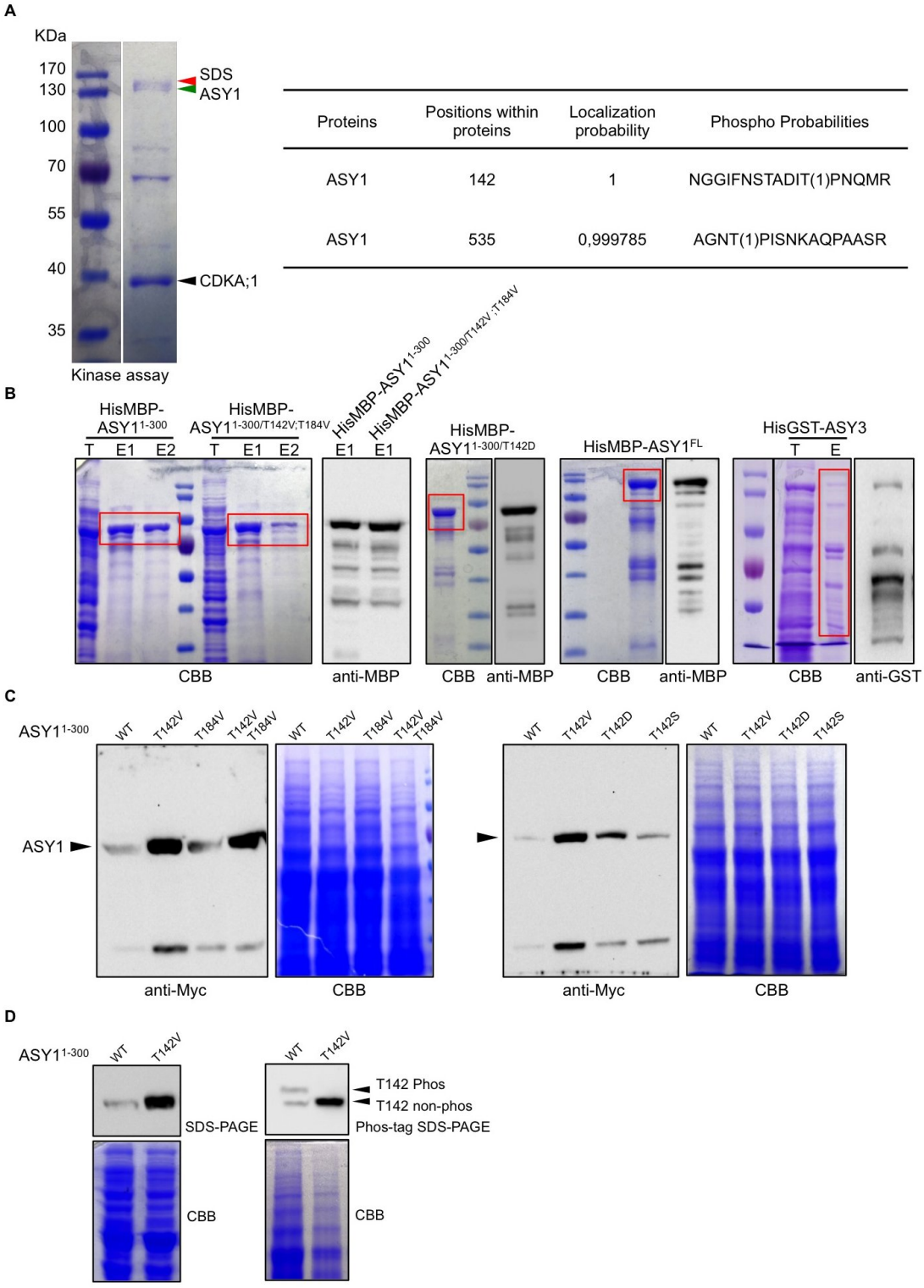

Proteins	Positions within proteins	Localization probability	Phospho Probabilities
ASY1	142	1	NGGIFNSTADIT(1)PNQMR
ASY1	535	0,999785	AGNT(1)PISNKAQPAASR

Appendix Figure S2. Mass spectrometry analysis and coomassie brilliant blue (CBB) stained gels of all purified proteins from *Escherichia coli* used in this research. (A) CBB staining of the proteins after kinase reaction of ASY1 with

CDKA;1-SDS complexes. The red, green and black arrowheads denote the SDS, ASY1, or CDKA;1 proteins, respectively. The table depicts identified ASY1 phosphorylation sites by mass spectrometry, their positions, their localization probabilities and the actual peptides. (B) CBB staining and western blot of purified HisMBP-ASY1$^{1\text{-}300}$, HisMBP-ASY1$^{1\text{-}300/T142V;T184V}$, HisMBP-ASY1$^{1\text{-}300/T142D}$, HisMBP-ASY1 and His-GST-ASY3 proteins. (C) Protein abundance analysis of ASY1 variants expressed in yeast. Total protein extracts of yeast cells expressing binding domain-Myc-tagged ASY1$^{1\text{-}300}$, ASY1$^{1\text{-}300/T142V}$, ASY1$^{1\text{-}300/T184V}$, ASY1$^{1\text{-}300/T142V;T184V}$, ASY1$^{1\text{-}300/T142D}$, and ASY1$^{1\text{-}300/T142S}$ were subjected to western blot analysis using an anti-Myc antibody. The protein loading were shown by CBB staining. (D) The left panel shows the SDS-PAGE analysis of the extracts of yeast cells expressing ASY1$^{1\text{-}300}$ and ASY1$^{1\text{-}300/T142V}$ and the right panel denotes the phos-tag gel analysis using an anti-Myc antibody. The CBB staining shows the protein loading.

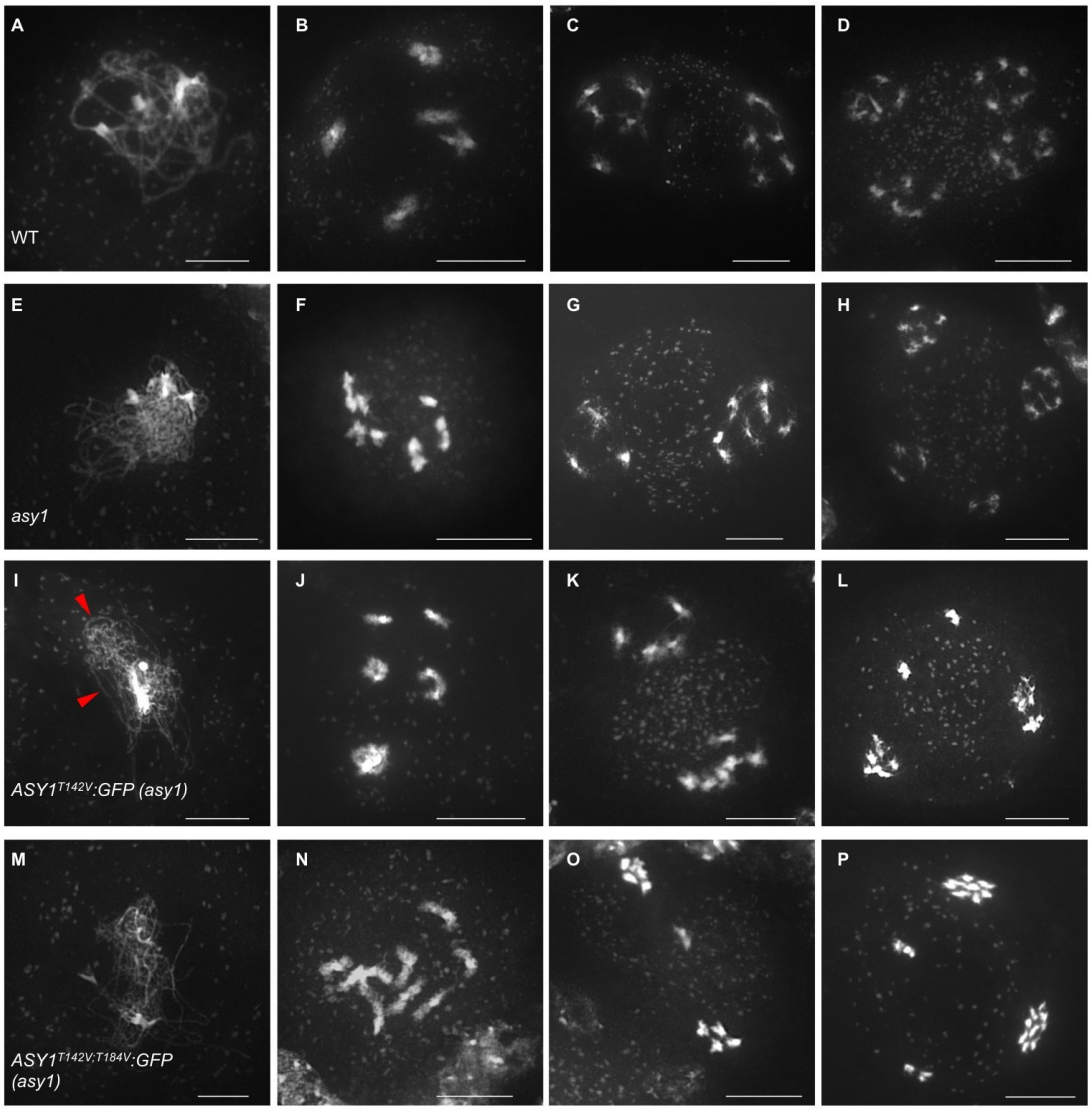

Appendix Figure S3. Chromosome spread analysis of male meiocytes in the wildtype (WT) (A-D), *asy1* mutant (E-H), ASY1^{T142V}:GFP (*asy1*) (I-L), and ASY1$^{T142V;T184V}$:GFP (*asy1*) (M-P) plants. (A, E, I, M) pachytene or pachytene-like stages; (B, F, J, N) diakinesis or diakinesis-like stages; (C, G, K, O) interkinesis or interkinesis-like stages; (D, H, L, P) tetrad or tetrad-like stages. Red arrowheads indicate the partially synaptic chromosomes. Bars: 5μm. **This Figures is kindly provided by Lev Böttger (Universität Hamburg) using the materials collected by Chao Yang.**

Appendix Movie 1: Distribution of CDKA;1:mVenus in *cdka;1* mutant background. Live cell imaging of CDKA;1:mVenus was performed in male meiocytes of *cdka;1* mutants. Video starts at early leptotene stage and runs for 26 h with scaning intervals of 7 mins.

Appendix table 1. Primers used in this research

Purpose	Primer name	Sequence
CDKA;1:mVenus reporter	gCDKA;1-F	ACCAAGACACCAAGCGCAA
	gCDKA;1-R	CAGAATGGAAGCGTCTTTGCTT
	pENTR2B-CDKA;1-F	AAGCAAAGACGCTTCCATTCTGCGCGGCCGCACTCGAGATA
	pENTR2B-CDKA;1-F	TTGCGCTTGGTGTCTTGGTGGATCCAGTCGACTGAATTG
	gCDKA;1-SmaISTOP-F	GGGATCTTTCCGTATTTTGGTCATT
	gCDKA;1-SmaISTOP-R	GGGAGGCATGCCTCCAAGATCCTTG
ASY1:GFP and ASY1:RFP reporters	gASY1-F	CAGGGTGGGGTCCAGTTAAG
	gASY1-R	TGTCCACGTAATCCAACGGT
	gASY1-smaISTOP- F	GGGTGAAGACACCACCTCTA
	gASY1-smaISTOP- R	GGGATTAGCTTGAGATTTCTG
	pENTR2B-ASY1-F	TATCAACCGTTGGATTACGTGGACAG CGGCCGCACTCGAGATATC
	pENTR2B-ASY1-R	CTCTTCTTAACTGGACCCCACCCTGG GATCCAGTCGACTGAATTG
ASY1:GFP dephospho- and phospho-mimicry variants	gASY1-T142V-F	GTCCCAAATCAAATGAGGTGC
	gASY1-T142V-R	AATGTCAGCAGTGGAGTTA
	gASY1-T184V-F	GTGGTATGATTACAGCCTTCC
	gASY1-T184V-R	CACATCATCGTAGTACAGAA
	gASY1-T365V-F	GTACCAGAGAGCGAATTCACC
	gASY1-T365V-R	CTGAAATTTTGGGGTAAGTA
	gASY1S382V -F	GTTCCAGGGAAATCTGTTGCT
	gASY1-S382V-R	AATTTGACCATCGGCTTCCT
	gASY1-T535V-F	GTTCCCATTAGCAACAAGGCA
	gASY1-T535V-R	GTTCCCAGCTTTAGAGATAG
	gASY1-T142S-F	TCACCAAATCAAATGAGgtgcagtgttg
	gASY1-T142D-F	GATCCAAATCAAATGAGgtgcagtgttg
ASY1$^{1-570}$:GFP	gASY1-570aa-R	CTGTGAGGCTTGGCTACAGTTGACTGTC
	mGFP-F	CCCGGGGGTGGCatggtgagcaagggcgaggagc
Y2H and/or protein expression	ASY1-attB1-F	GGGGACAAGTTTGTACAAAAAAGCAGGCTTCATGGTGATGGCTC AGAAGCT
	ASY1-attB1-R	GGGGACCACTTTGTACAAGAAAGCTGGGTTTCAATTAGCTTGAG ATTTCTG
	ASY1 1-300 attB2-R	GGGGACCACTTTGTACAAGAAAGCTGGGTTTCACTCAGCCGGAT CCTGTGTGT
	ASY1 T142V CDS-F	GTCCCAAATCAAATGAGGAGTTCAG
	ASY1 T142V CDS-R	AATGTCAGCAGTGGAGTTAAATATT
	ASY1 T184V CDS-F	GTGCCACCAGATTACGAGCCACCTT
	ASY1 T184V CDS-R	CACATCATCGTAGTACAGAAGCTTC
	ASY1-571aa-F	GACAGACGTGGCAGGAAAACCAGCATGG
	attL1-R2	GAAGCCTGCTTTTTTGTACAAAGTTGG
	ASY1-570attB2-R	GGGGACCACTTTGTACAAGAAAGCTGGGTTTCACTGTGAGGCTT GGCTACAGTTG
	ASY1 T142S CDS-F	TCACCAAATCAAATGAGGAGTTCAG
	ASY1 T142D CDS-F	GACCCAAATCAAATGAGGAGTTCAG
PCH2:GFP reporter	gPch2-F	TACATGGAAGCTAAAGTCGTCGTCAG
	gPch2-R	GGGGACAAGTTTGTACAAAAAAGCAGGCTTCACACGGATACTGC CTTCAAGACAA
	gPch2-attB1-F	GGGGACCACTTTGTACAAGAAAGCTGGGTTgatcagatgacttggttgctg ac
	gPch2-interAscI-F	AAGCATGGCGCGCCGCGACTATTCCAGTGCAAATAGCCG
	gPch2-interAscI-R	AAGCATGGCGCGCCTGCTTCAATGGGGTTTTGGTAAGAG

Genotyping of *cdka;1*	CDKA;1-WT-F	AAAAAACTATAACATAATTGGCAAC
	CDKA;1-WT/mut-R	TGTACAAGCGAATAAAGACATTTGA
	CDKA;1-mut-F	GCGTGGACCGCTTGCTGCAACTCTCTCAGG
Genotyping of *asy1*	N546272L	AGGTGGCTCGTAATCTGGTGGCTGC
	N546272U	TCTATGTTTGTTACGCGTTAATCAG
	SALK LBb1.3	ATTTTGCCGATTTCGGAAC
	GenotypeT1 WT allele	CTGGGTTGGGCTGTAACATT

Materials and Methods

Plant materials

The *Arabidopsis thaliana* accession Columbia (*Col-0*) was used as wild-type reference throughout this study. The T-DNA insertion lines SALK_046272 (*asy1-4*) (Crismani and Mercier, 2013), SALK_031449 (*pch2-2*) (Lambing *et al.*, 2015) and SAIL_423H01 (*asy3-1*) (Ferdous *et al.*, 2012), and SALK_106809 (*cdka;1-1*) (Nowack *et al.*, 2006) were obtained from the T-DNA mutant collection at the Salk Institute Genomics Analysis Laboratory (SIGnAL, http://signal.salk.edu/cgi-bin/tdnaexpress) via NASC (http://arabidopsis.info/). The mutants *cdka;1* $PRO_{CDKA;1}$*:CDKA;1*^{T161D} and *cdka;1* $PRO_{CDKA;1}$*:CDKA;1*$^{T14D;Y15E}$, the PRO_{ZYP1B}*:ZYP1B:GFP* reporter as well as the PRO_{ASY3}*:ASY3:RFP* reporter plants were described previously (Yang *et al*, 2019; Dissmeyer *et al*, 2009; 2007). The *StrepIII-tag-CDKA;1* (*cdka;1*) line was also generated previously. The StrepIII tag is a Twin-strep-tag® developed by the IBA GmbH, which consists of two tandem Strep II tag moieties separated by a short linker and shows better binding characteristics in comparison to Strep II tag (Pusch *et al*, 2012; Schmidt *et al*, 2013). The protein sequence of StrepIII/Twin-strep-tag is WSHPQFEK-GGGSGGGSGGSA-WSHPQFEK (the Strep II tag moieties are underlined). All plants were grown in growth chambers with a 16 h light/21°C and 8 h/18°C dark cycle at 60% humidity.

Plasmid construction and plant transformation

To generate the *ASY1* reporters, a 6013bp genomic sequence of *ASY1* was amplified by PCR and subsequently integrated into *pENTR2B* vector by SLICE reaction. A *SmaI* restriction site was then introduced in front of the stop codon by PCR. The constructs obtained were then linearized by *SmaI* restriction and ligated with GFP, RFP or mVenus fragments, followed by gateway LR reaction with the destination vector *pGWB501*. The *CDKA;1:mVenus* reporter was generated by using the same strategy as described above. For the *PCH2:GFP* reporter, a 5837bp genomic sequence of *PCH2* was amplified by PCR and subsequently integrated into *pDONR221* vector by gateway BP reaction. Subsequently, an *AscI* restriction site was inserted into *pDONR221-PCH2* between the 35-36aa of PCH2 by PCR. Following the linearization by *AscI*, a GFP fragment was inserted into *pDONR221-PCH2*. The resulting *PCH2:GFP* expression cassette was integrated into the destination vector *pGWB501*

by the gateway LR reaction. For creating variants of the *ASY1:GFP* constructs including *ASY1*$^{1\text{-}570}$*:GFP*, a PCR-based mutagenesis was performed using *pENTR2B-ASY1:GFP* as a template followed by gateway LR reactions for integration into the destination vector. All constructs were transformed into *Arabidopsis thaliana* plants by floral dipping.

To make the constructs for the yeast two-hybrid assays, the coding sequences of the respective genes were amplified by PCR with primers flanked by *attB* recombination sites and subcloned into *pDONR223* vector by gateway BP reactions. The resulting constructs were subsequently integrated into the *pGADT7-GW* or *pGBKT7-GW* vectors by gateway LR reactions. Primers used for generating all constructs mentioned above are shown in Table S1.

Microscopy and live cell imaging

Light microscopy was performed with an Axiophot microscope (Zeiss). To study protein localization, young anthers harboring the relevant reporters were dissected and imaged immediately using an Leica TCS SP8 inverted confocal microscope. The meiotic stages were determined by combining the criteria of the chromosome morphology, nucleolus position (mainly for pre-meiosis to leptotene), and cell shape. For tracing the dynamics of ASY1:GFP/RFP variants in *asy1* mutants and/or wild-type plants, live cell imaging was performed as described by Prusicki et al. (2019) under controlled temperature (18 - 20°C) and humidity (60%) conditions. In brief, one single fresh flower bud was detached from the stem and dissected with two anthers exposed. Subsequently, the isolated bud including the pedicel and a short part of the floral stem was embedded into the *Arabidopsis* Apex Culture Medium (ACM) and then covered by one drop of 2% agarose. The sample was then subjected to constant image capture with 7 mins intervals by using an upright Zeiss LSM880 confocal microscope.

To analyze the distribution of the nucleus versus cytoplasm localized CDKA;1, live cell imaging was performed with two anthers of *cdka;1* mutants harboring a fully functional *CDKA;1:mVenus* reporter for 26h (Movie S1). To quantify the subcellular distribution of the CDKA;1:mVenus, the signal intensities in the nucleus and cytoplasm were calculated every hour by segmenting the respective regions using the image processing software Fiji.

Yeast two-hybrid assay

Yeast two-hybrid assays were performed according to the Matchmaker Gold Yeast two-hybrid system manual (Clontech). Different combinations of constructs were co-transformed into yeast strain AH109 using the polyethylene glycol/lithium acetate method as described in the manual. Yeast cells harboring the relevant constructs were grown on the SD/-Leu -Trp, SD/-Leu -Trp -His, and SD/-Leu -Trp -His -Ade plates to test protein-protein interactions.

Protein expression and purification

To generate the HisMBP-ASY1, HisMBP-ASY1$^{1\text{-}300}$, HisMBP-ASY1$^{1\text{-}300/T142V;T184V}$ and HisGST-ASY3 constructs, the respective coding sequences were amplified by PCR and subcloned into *pDONR223* vector by gateway BP reactions. The resulting constructs were integrated by gateway LR reactions into *pHMGWA* or *pHGGWA* vectors for the HisMBP- and the HisGST-tagged fusions, respectively. For heterologous expression, the constructs were transformed into the *E. coli* BL21 (DE3) pLysS cells, which were grown at 37°C in the presence of 100 mg/l ampicillin until the OD_{600} of 0.6, followed by protein induction by adding IPTG to a final concentration of 0.3 mM. The cells were further incubated at 37°C for 3 h (HisMBP-ASY1, HisMBP-ASY1$^{1\text{-}300}$ and HisMBP-ASY1$^{1\text{-}300/T142V;T184V}$) or 18°C overnight (HisGST-ASY3). All proteins were purified under native conditions by using Ni-NTA sepharose (QIAGEN) according to the manual.

GST pull-down assays

For GST pull-down assay, 4 µg of HisMBP-ASY1$^{1\text{-}300}$, HisMBP-ASY1$^{1\text{-}300/T142V;T184V}$ and 2 µg HisGST-ASY3 were added to the pull-down buffer system containing 25 mM Tris-HCl, pH 7.5, 100 mM NaCl , 10% glycerol, and 20 µl GST agarose beads (Chromotek) as indicated in Fig 4B. After incubation for 1 h at 4°C, GST beads were collected by centrifugation and washed 3 times with the washing buffer (25 mM Tris-HCl, pH 7.5, 200 mM NaCl , 10% glycerol and 0.25/0.5/1% Triton X-100). Beads-bound proteins were eluted by boiling in an equal volume of 1X SDS protein loading buffer and subjected to immuno-blotting analysis.

Protein blots

For SDS-PAGE, protein samples were subjected to the gel electrophoresis at room temperature (12% acrylamide, 375mM Tris-HCl, pH 8.8, and 0.1% SDS) followed by transfer blotting onto nitrocellulose membrane. For Phos-tag SDS-PAGE, proteins from kinase assays were subjected to Phos-tag gel electrophoresis (6% acrylamide, 375mM Tris-HCl, pH 8.8, 50 μM Phos-tag (Wako), and 100μM $MnCl_2$) at 4°C followed by transfer blotting. After incubation with the primary and secondary antibodies, the immuno-blots were exposed and observed using a Bio-Rad Image Analyzer. Relative protein levels were quantified with the Image Lab software (Bio-Rad).

Chromosome spreads

Chromosome spreads was performed as described previously (Wijnker *et al.*, 2012). In brief, fresh flower buds were fixed in 75% ethanol and 25% acetic acid for 48 h at 4°C, washed two times with 75% ethanol and stored in 75% ethanol at 4°C. For spreading, flower buds were digested in an enzyme solution (10mM citrate buffer containing 1.5% cellulose, 1.5% pectolyase, and 1.5% cytohelicase) for 3 h at 37°C and then transferred onto a glass slide, followed by mashing with a bended needle. Spreading was performed on a 46°C hotplate by adding 10 μl of 45% acetic acid. The slide was then rinsed with ice-cold ethanol/acetic acid (3:1) solution and mounted in Vectashield with DAPI (Vector Laboratories).

***In vitro* kinase assays**

CDKA;1-SDS, CDKA;1-TAM and CDKA;1-CYCA3;1 complexes were expressed as described by Harashima and Schnittger (Harashima and Schnittger, 2012). The kinase complexes were purified by Strep-Tactin Agarose (IBA), followed by desalting with PD MiniTrap G-25 (GE Healthcare). The kinase assay in Fig 2C was performed by incubating the kinase complexes with the ASY1 proteins purified from baculovirus-infected insect cells in the kinase buffer containing 50 mM Tris-HCl, pH 7.5, 10mM $MgCl_2$, 5% (V/V) [γ-^{32}P]ATP (9.25 MBq, GE Healthcare) for 30 min. The reaction was then inactivated by boiling at 95 °C for 5 min after adding 5X SDS protein loading solution, and autoradiography was subsequently performed following the SDS-PAGE. The kinase assay in Fig 2D was performed by incubating the kinase complexes with HisMBP-ASY1 in the reaction buffer containing 50 mM Tris-HCl, pH 7.5, 10mM $MgCl_2$, 0.5 mM ATP and 5mM DTT for 90 min. The phosphorylation

of ASY1 was then verified by Phos-tag SDS-PAGE. The CBB stained gel after kinase reaction is shown in Appendix Fig S2A.

Sample preparation and LC-MS/MS data acquisition

The protein mixtures after kinase assays were reduced with dithiothreitol, alkylated with chloroacetamide, and digested with trypsin. Subsequently, the digested samples were desalted using StageTips with C18 Empore disk membranes (3 M) (Rappsilber et al, 2003), dried in a vacuum evaporator, and dissolved in 2% ACN, 0.1% TFA. Samples were analyzed using an EASY-nLC 1200 (Thermo Fisher) coupled to a Q Exactive Plus mass spectrometer (Thermo Fisher). Peptides were separated on 16 cm frit-less silica emitters (New Objective, 0.75 μm inner diameter), packed in-house with reversed-phase ReproSil-Pur C18 AQ 1.9 μm resin (Dr. Maisch). Peptides were loaded on the column and eluted for 50 min using a segmented linear gradient of 5% to 95% solvent B (0 min : 5%B; 0-5 min -> 5%; 5-25 min -> 20%; 25-35 min ->35%; 35-40 min -> 95%; 40-50 min ->95%) (solvent A 0% ACN, 0.1% FA; solvent B 80% ACN, 0.1%FA) at a flow rate of 300 nL/min. Mass spectra were acquired in data-dependent acquisition mode with a TOP15 method. MS spectra were acquired in the Orbitrap analyzer with a mass range of 300–1500 m/z at a resolution of 70,000 FWHM and a target value of 3×10^6 ions. Precursors were selected with an isolation window of 1.3 m/z. HCD fragmentation was performed at a normalized collision energy of 25. MS/MS spectra were acquired with a target value of $5x10^5$ ions at a resolution of 17,500 FWHM, a maximum injection time of 120 ms and a fixed first mass of m/z 100. Peptides with a charge of 1, greater than 6, or with unassigned charge state were excluded from fragmentation for MS^2; dynamic exclusion for 20s prevented repeated selection of precursors.

For targeted analysis, samples were resolved using the segmented linear gradient as mentioned above. The acquisition method consisted of a full scan method combined with a non-scheduled PRM method. The 16 targeted precursor ions were selected based on the results of DDA peptide search in Skyline. MS spectra were acquired in the Orbitrap analyzer with a mass range of 300–2000 m/z at a resolution of 70,000 FWHM and a target value of 3×10^6 ions, followed by MS/MS acquisition for the 16 targeted precursors. Precursors were selected with an isolation window of 2.0 m/z. HCD fragmentation was performed at the normalized collision energy of 27. MS/MS

spectra were acquired with a target value of $2x10^5$ ions at a resolution of 17,500 FWHM, a maximum injection time of 120 ms and a fixed first mass of m/z 100.

MS data analysis and PRM method development

Raw data from DDA acquisition were processed using MaxQuant software (version 1.5.7.4, http://www.maxquant.org/) (Cox and Mann, 2008). MS/MS spectra were searched by the Andromeda search engine against a database containing the respective proteins used for the *in vitro* reaction. Trypsin specificity was required and a maximum of two missed cleavages allowed. Minimal peptide length was set to seven amino acids. Carbamidomethylation of cysteine residues was set as fixed, phosphorylation of serine, threonine and tyrosine, oxidation of methionine and protein N-terminal acetylation as variable modifications. The match between runs option was disabled. Peptide-spectrum-matches and proteins were retained if they were below a false discovery rate of 1% in both cases.

The DDA approach only enabled the identification of T142. To analyze the putative phosphorylation sites at T184 and T535, a targeted approach was employed. Raw data from the DDA acquisition were analyzed on MS1 level using Skyline (Version 4.1.0.18169, https://skyline.ms) (MacLean *et al.*, 2010) and a database containing the respective proteins used for the *in vitro* reaction. Trypsin specificity was required and a maximum of two missed cleavages allowed. Minimal peptide length was set to seven maximum length to 25 amino acids. Carbamidomethylation of cysteine, phosphorylation of serine, threonine and tyrosine, oxidation of methionine and protein N-terminal acetylation were set as modifications. Results were filtered for precursor charges of 2, 3 and 4. For each phosphorylated precursor ion a respective non-phosphorylated precursor ion was targeted as a control, and several precursor ions from the backbone of ASY1 recombinant protein were chosen as controls between the different samples. In total 16 precursors were chosen to be targeted with a PRM approach. After acquisition of PRM data the raw data were again processed using MaxQuant software, with above-mentioned parameters. Peptide search results were analyzed using Skyline using above-mentioned parameters, additionally data were filtered for b- and y-ions and ion charges +1 and +2.

Quantification and statistical analysis

The Student's *t*-test (two-tailed) was used to evaluate the significance of the difference between two groups. * denotes $P < 0.05$, and ** $P < 0.01$. The significance of the differences in more than two groups was determined by one-way ANOVA followed by Turkey's test. Level of significance is indicated by different letters. The numbers of samples are indicated in the figure legends.

Data availability

The mass spectrometry proteomics data have been deposited to the ProteomeXchange Consortium via the PRIDE partner repository with the dataset identifier PXD011035. The results of the mass spectrometry with a targeted approach analyzed using Skyline have been deposited to the Panorama Public (dataset link: https://panoramaweb.org/ASY_phosphorylation.url).

Reviewer accounts for the mass spectrometry data:

ProteomeXchange
Username: reviewer98402@ebi.ac.uk
Password: 7iziGIqA

Panorama Public:
Email: panorama+mpipz@proteinms.net
Password: sc&K6QeL

Chapter 3

How are the meiotic HORMADs assembled on chromosomes?

Dissecting the function of the closure motif of ASY1

3.1 Introduction

Current model for the assembly of meiotic HORMADs onto chromosomes

As mentioned in chapter 2, the chromosomal localization of the meiotic HORMA domain proteins (HORMADs) including the budding yeast Hop1, mammalian HORMAD1 and HORMAD2 as well as the *C. elegans* HORMADs HTP-1, HTP-2, HTP-3, and HIM3, was thought to depend on at least two mechanisms, the initial recruitment by its binding partners (linker proteins) such as Red1 in yeast or ASY3 in *Arabidopsis*, and the self-assembly through its N-terminal HORMA domain with C-terminal closure motif interactions (Fig. 1) (West *et al*, 2018; Kim *et al*, 2014). While the localization dependency of the HORMADs on the linker proteins was extensively studied and confirmed in different species including plants, yeast and mammals, the self-assembly of HORMADs through the head-to-tail oligomerization is a model only recently proposed by West and colleagues (2018) based on the observations that yeast Hop1 shows binding between the N-terminal HORMA domain and the C-terminal closure motif *in vitro*, and that the binding is aborted by a mutation (*K593A*) in the closure motif of Hop1 (West *et al*, 2018; Niu *et al*, 2005). However, there is a previous publication, reporting that the *K593A* mutation results in an asynaptic phenotype but does not affect the chromosome localization of Hop1, which indicates that although the C-terminal closure motif is essential for Hop1 function, it is not required for its chromosome association (Niu *et al*, 2005). Also, the observations that Red1/ASY3 has a stronger binding affinity for Hop1/ASY1 in comparison to the N-terminal Hop1/ASY1-to-closure motif interaction, at least *in vitro,* and that Red1/ASY3 and the closure motif compete for a common binding site in HORMA domain, make the self-assembly model vulnerable (chapter 3 Fig. 5B) (West *et al*, 2018). Moreover, an explanation for the physical basis of HOP1/ASY1 oligomerization is missing, which is somehow contradictory to the principle of mechanics. For example, it is not convincing that one intermolecular interaction of ASY1 with ASY3 could hold a long chain of ASY1 oligomers if no additional mechanism supports this interaction.

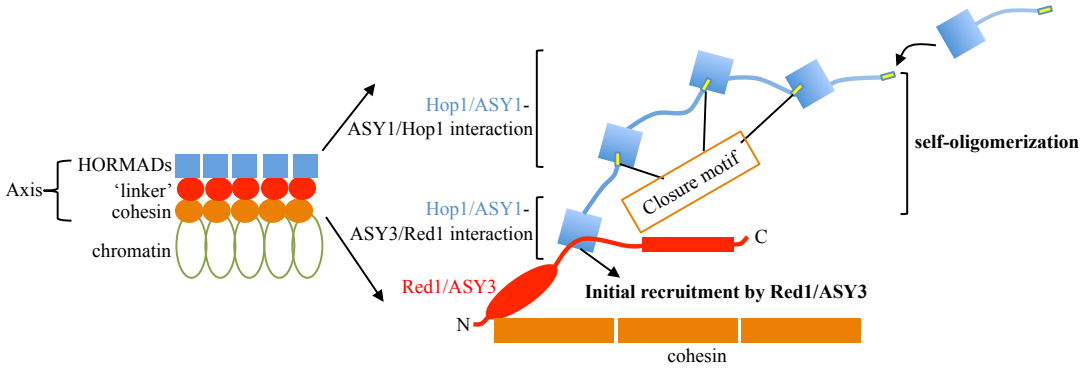

Figure 1. Current model of the chromosome assembly of meiotic HORMADs. Cohesin complexes constitute the physical basis for the chromosome axis formation. Meiotic HORMADs (Hop1/ASY1, blue) are initially recruited to the chromosome by interacting with the linker proteins Red1/ASY3 (red). Then the closure motif (yellow) of Hop1/ASY1 serves to recruit additional molecules of Hop1/ASY1 to form a chain by self-oligomerization. This model is drawn according to West et al. (2018).

3.2 Results

The closure motif of ASY1 plays a role as a nuclear localization signal, but it is not essential for chromosome localization

To check whether the closure motif/self-oligomerization is required for the chromosome association of ASY1, a genomic construct with a deletion of the C-terminal 26 aa of ASY1 (ASY1$^{1-570}$:GFP) which largely eliminates, at least in yeast two-hybrid assays, the intermolecular interaction ASY1-to-ASY1, was generated and transformed into *asy1* mutants (chapter 2 Figure 5B). While the full length ASY1:GFP shows an exclusive nuclear localization, ASY1$^{1-570}$:GFP was only expressed in the cytoplasm of the male meiocytes and no signal was detected in the nucleus of *asy1* mutants, indicating that the C-terminal closure motif might act as a nuclear localization signal (NLS) (Fig. 2A). To confirm this, I generated a GFP-tagged closure motif construct driven by the ASY1 promoter (ASY1$^{571-596}$:GFP) which was subsequently transformed into wildtype plants. Although no signal was detected in male meiocytes, the ASY1$^{571-596}$:GFP signal was observed in the connective tissue of the anther where it localizes exclusively to the nucleus, substantiating that the closure motif of ASY1 functions as a NLS (Fig. 2B).

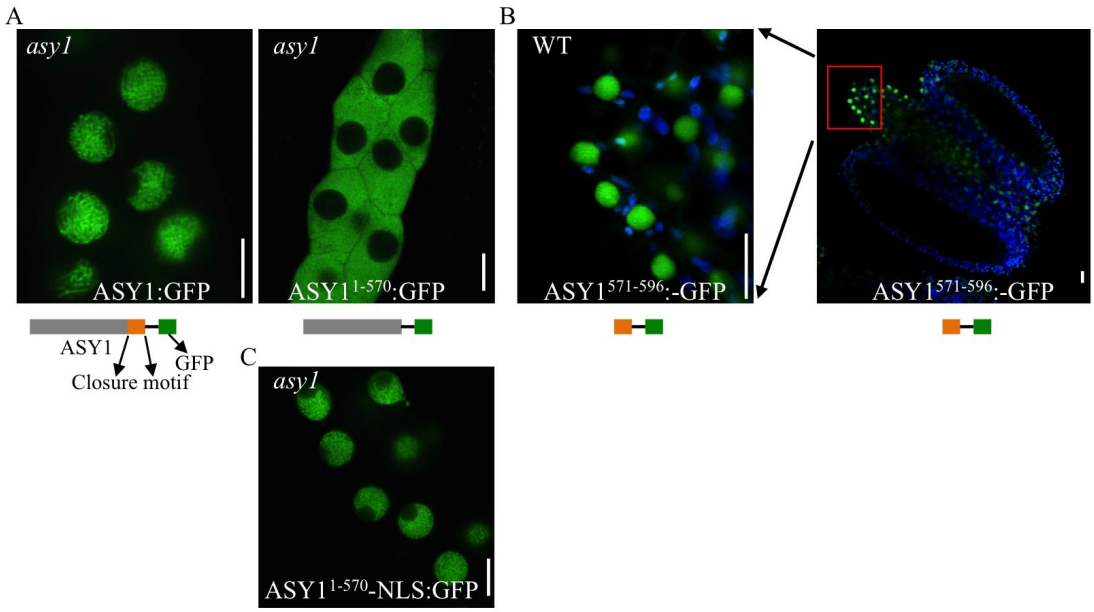

Figure 2. The closure motif of ASY1 serves as a nuclear localization signal.
(A) Localization of ASY1:GFP and ASY1$^{1\text{-}570}$:GFP at early prophase I in male meiocytes of *asy1* mutants. (B) Localization of ASY1$^{571\text{-}596}$:GFP in the connective tissue of the anther. (C) Localization of ASY1$^{1\text{-}570}$-NLS:GFP at early prophase I in male meiocytes of *asy1* mutant. Bar: 10 μm.

Since the NLS function of the closure motif precludes the possibility of using ASY1$^{1\text{-}570}$:GFP to test whether the putative head-to-tail self-oligomerization is required for chromosome localization of ASY1, I introduced a SV40 NLS sequence (PKKKRKV) right in front of the GFP tag of the ASY1$^{1\text{-}570}$:GFP (ASY1$^{1\text{-}570}$-NLS:GFP) to complement the NLS role of the closure motif, thus allowing the functional verification of the closure motif for the chromosome association of ASY1. As expected, the SV40 NLS gives rise to a nuclear localization of ASY1$^{1\text{-}570}$-NLS:GFP (Fig. 2C). Subsequently, a detailed analysis of this separation of function allele revealed an indistinguishable chromosome localization between ASY1$^{1\text{-}570}$-NLS:GFP and ASY1:GFP in male meiocytes at early prophase I, which indicates that the closure motif is dispensible for the chromosome localization of ASY1 (Fig. 3). This is consistent with the previous finding in yeast that HOP1 with a *K593A* mutation which abolishes the head-to-tail interaction, localizes on chromosomes normally (West *et al*, 2018; Niu *et al*, 2005). However, I cannot exclude the possibility of a slight localization defect due to the current limitation in optical resolution. Also, it is possible that the ASY3/Red1-dependent assembly and the

closure motif-dependent self-oligomerization of ASY1/Hop1 are two independent but synergistic pathways to concentrate ASY1 at the chromosome axis, i.e., the latter might contribute to the chromosome localization of ASY1/HORMADs, but the ASY3/Red1-dependent assembly might be sufficient for the proper chromosome localization at least in *Arabidopsis*.

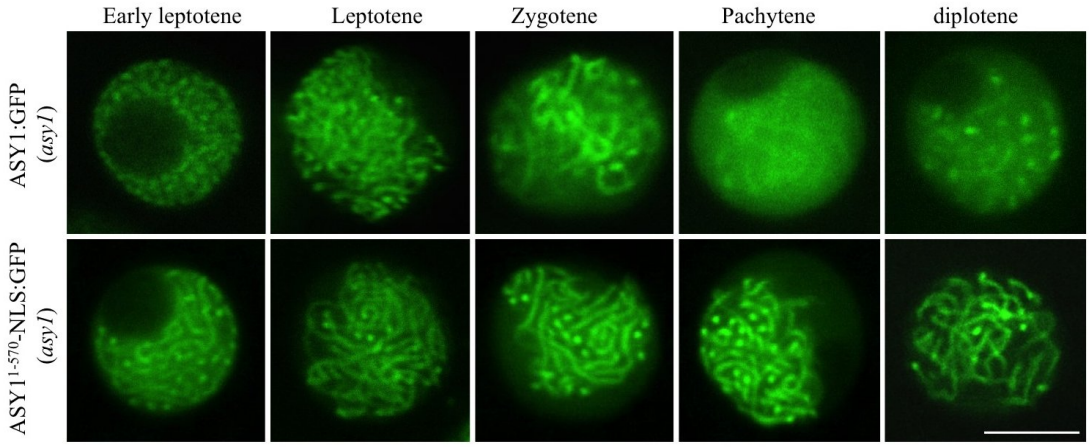

Figure 3. Closure motif of ASY1 is not required for its chromosome localization. Localization of ASY1:GFP and ASY1$^{1\text{-}570}$-NLS:GFP at different meiotic stages in male meiocytes of *asy1* mutants. Bar: 5 μm.

In addition, ASY1$^{1\text{-}570}$-NLS:GFP remains on chromosomes even in diplotene at a time point when the wild-type ASY1:GFP is already largely removed from the synaptic chromosomes, suggesting a failure of synapsis in *asy1* mutants harboring ASY1$^{1\text{-}570}$-NLS:GFP (Fig. 3). Also, despite an unaffected chromosome localization, ASY1$^{1\text{-}570}$-NLS:GFP is not functional since it does not complement the fertility defect of *asy1* mutants, indicating that the closure motif of ASY1 is essential for its function, especially for chromosome synapsis, resembling the situation of Hop1 in yeast (Fig. 4A) (Niu *et al*, 2005). Moreover, I observed that when transformed into wildtype, ASY1$^{1\text{-}570}$-NLS:GFP resulted in a fertility reduction of plants (Fig. 4B). This is likely due to the competition of the nonfunctional ASY1$^{1\text{-}570}$-NLS:GFP with the wild-type version, also suggesting that the closure motif is required for ASY1 function.

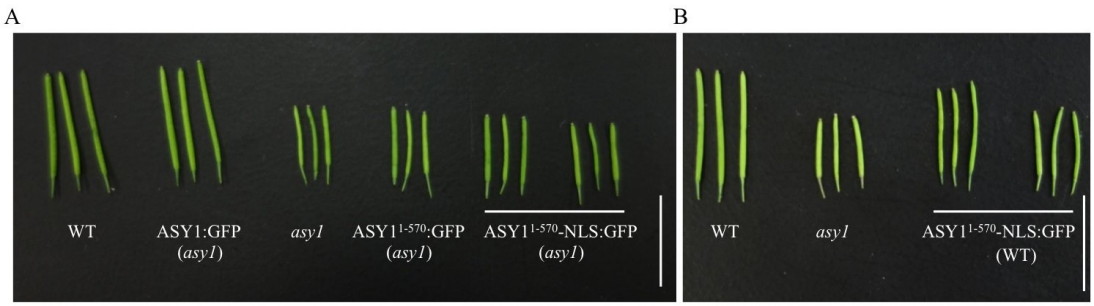

Figure 4. Closure motif of ASY1 is necessary for its function. Siliques of wildtype (WT), *ASY1:GFP* (*asy1*), *asy1*, *ASY1$^{1-570}$:GFP* (*asy1*), *ASY1$^{1-570}$-NLS:GFP* (*asy1*) and *ASY1$^{1-570}$-NLS:GFP* (WT) plants. Bar: 1 cm.

PCH2 is essential for the nuclear targeting of ASY1

PCH2, an AAA+ ATPase protein, mediates the removal of ASY1 and its orthologues from the synaptic axes during meiosis in many species studied including *Arabidopsis*, yeast and mammals. In chapter 2, by applying the live cell imaging technique to the male meiocytes expressing a functional ASY1 reporter, we observed that despite a weak expression in nucleus, ASY1 remains largely in cytoplasm of male meiocytes in *pch2* mutants which contrasts the primarily nuclear localization of ASY1 in wildtype (Fig. 5A). This observation suggests that PCH2 is essential for the efficient nuclear targeting of ASY1 by an unknown molecular mechanism.

To test whether this cytoplasmic retention of ASY1 in the absence of PCH2 involves an interplay between PCH2 and the closure motif, the ASY1$^{1-570}$-NLS:GFP construct of separation-of-function was transformed into the *pch2* mutants. Interestingly, differ from the cytoplasmic retention of ASY1:GFP in *pch2* mutants, I found that ASY1$^{1-570}$-NLS:GFP was exclusively present in nucleus of the male meiocytes in *pch2* mutants (Fig. 5C). To further confirm that the rescue of the nuclear targeting of ASY1 in *pch2* mutants by the deletion of the closure motif (ASY1$^{1-570}$-NLS:GFP) is not simply due to the SV40 NLS added, but due to the absence of the closure motif, I added the SV40 NLS to the wild-type version of ASY1 (ASY1-NLS:GFP) which was then introgressed into the *pch2* mutants. While there is a higher nucleus to cytoplasm signal ratio of ASY1-NLS:GFP in comparison to ASY1:GFP, showing a clear effect of the SV40 NLS on ASY1 nuclear localization, lots of signal are still present in the cytoplasm of the male meiocytes in *pch2* mutants,

which corroborates a PCH2 dependent necessity of the closure motif for complete nuclear targeting of ASY1 (Figure 5D).

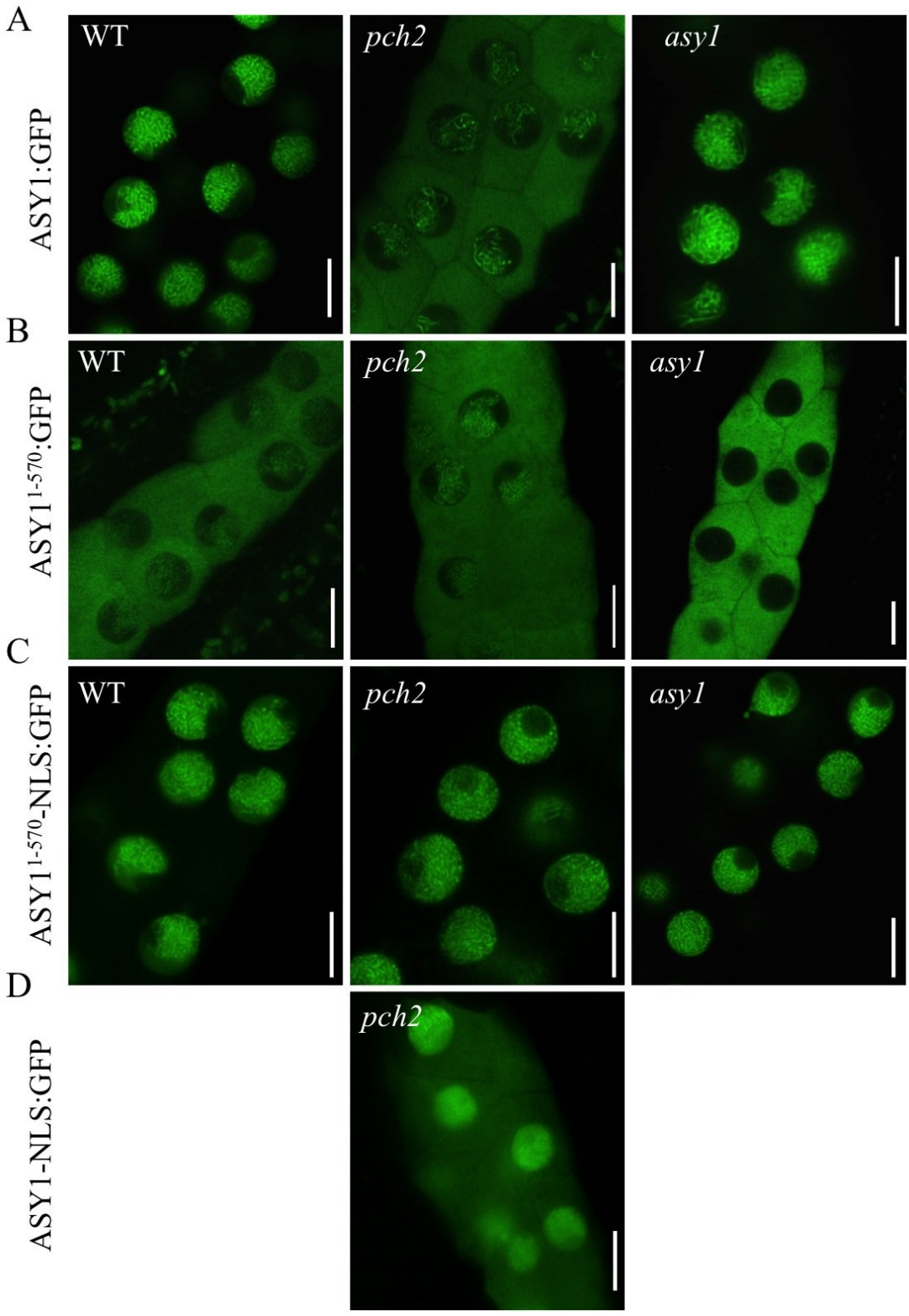

Figure 5. PCH2 regulates the nuclear targeting of ASY1 through the closure motif. Localization of ASY1:GFP (A), ASY1$^{1-570}$:GFP (B), ASY1$^{1-570}$-NLS:GFP (C),

and ASY1-NLS:GFP (D) in the male meiocytes of wildtype (WT), *pch2* and *asy1* mutants using confocal laser scanning microscope. Bar: 10 μm.

3.3 Discussion

Function of the closure motif of meiotic HORMADs

The above-presented results reveal that the C-terminal closure motif of Hop1/ASY1 is not essential for its localization, but is required for its function, especially for synapsis. In yeast, the closure motif of Hop1 seems to function to promote the dimerization of Mek1, a meiosis-specific kinase, thereby enabling Mek1 to phosphorylate targets and thus to promote the interhomologous recombination and synapsis (Niu *et al*, 2005). However, no protein sequence homologs of yeast Mek1 exist in *Arabidopsis*. Since Arabidopsis ASY1 without the closure motif shows an indistinguishable chromosome localization pattern compared to the wild-type version, but a failure of chromosome synapsis, the closure motif of ASY1 might function to recruit other essential components to facilitate DSB repair, homologous recombination and synapsis. Therefore, identifying new partners of ASY1, especially partners interacting with the closure motif, will promote our understanding of the molecular role of ASY1 and of the regulation of meiotic recombination and synapsis. To achieve this aim, a yeast two-hybrid screening could be performed using a library made from the reproductive tissue. Alternatively a GFP pull-down assay using flowers of the ASY1:GFP (*asy1*) plants could be performed. In addition, detailed analyses of the wild-type plants harboring the non-functional ASY1$^{1\text{-}570}$-NLS:GFP that leads to a dominant negative effect, should be done, which will shed light on the understanding of the function and mechanism of the closure motif of ASY1 in chromosome synapsis and recombination. In this context, it is interesting to investigate the chromosome behavior during meiosis by the chromosome spreads trying to pinpoint the exact moment when the dominant effect of the missing closure motif manifests. Moreover, immunofluorescence and live cell imaging experiments should be performed to check the functionality of the homologous recombination process, especially for the processing and repair of DSB, namely to check the expression and localization patterns of the key recombination regulators involved, e.g., MRE11, HOP2, MND1, RAD51, RAD51, DMC1, ZYP1, MLH1, and HEI10.

PCH2 is essential for the nuclear targeting of ASY1

The function of PCH2 for the chromosome removal of meiotic HORMADs has been extensively studied in different species including plants, yeast and mammals (Chen *et al*, 2014; Lambing *et al*, 2015; Wojtasz *et al*, 2009). Here, I found a novel role of PCH2 in *Arabidopsis*, namely to regulate the nuclear targeting of ASY1, which likely requires a functional interaction between PCH2 and the closure motif of ASY1. However, the underlying molecular mechanism is still largely obscure, but might be one of the following possibilities.

First, assuming that Hop1/ASY1 forms intermolecular Hop1/ASY1-to-Hop1/ASY1 interactions mediated by the closure motif which are essential for its function and that PCH2 putatively disassembles these Hop1/ASY1-containing complexes localized at the synaptic chromosome axes (West *et al*, 2018; Lambing *et al*, 2015), one likely possibility is that PCH2 also prevents a premature multimerization of ASY1 in cytoplasm thereby allowing the nuclear import of ASY1 monomer and/or short oligomer. This hypothesis is supported not only by the cytoplasmic localization of PCH2 (chapter 2 Fig. 5D), but also by the observation that a deletion of the ASY1 oligomerization/closure motif ($ASY1^{1-570}$-NLS:GFP) rescues the cytoplasmic retention of ASY1:GFP and ASY1-NLS:GFP in *pch2* mutants (Fig. 5B-D). In addition, ASY1 without the closure motif ($ASY1^{1-570}$:GFP) which is exclusively localized in the cytoplasm in *asy1* mutant background, is partially imported into nucleus when the endogenous ASY1 is present (Fig. 5B). This suggests an intermolecular interaction between the $ASY1^{1-570}$:GFP and the endogenous ASY1 facilitating the nuclear localization of $ASY1^{1-570}$:GFP. Nonetheless, further evidence is needed to confirm this hypothesis, e.g., it has to be tested whether there really is a premature oligomerization of ASY1 in cytoplasm in the absence of PCH2.

Second, the cytoplasmic retention of ASY1 in *pch2* mutants might be due to the fact that in the absence of PCH2, the interaction profile between ASY1 and its partners, that might be essential for its nuclear localization, is affected, e.g., the recognition and binding of the nuclear import protein complex importin to ASY1, likely through the closure motif, might be compromised. Even if this recognition and binding turns out not to be affected, there are likely other factors, which are involved in the nuclear import of ASY1 and might be regulated by PCH2.

Third, there is the possibility that PCH2 might regulate the turnover of ASY1. However, the fact that the presence of ASY1 in the nucleus of *pch2* mutants is reduced compared to that in wildtype, does not support this argument (Fig. 5A).

To test these different hypotheses, several experiments could be performed in the future. **First**, to answer whether ASY1 forms premature multimerization in the cytoplasm of *pch2* mutants, I have generated *pch2* mutants harboring both ASY1:mVenus and ASY1:mTurquiose2 reporters. With these materials an *in vivo* Förster Resonance Energy Transfer (FRET) experiment is ongoing to confirm the intermolecular interactions of ASY1 likely through the head-to-tail mechanism mediated by the closure motif. In this sense, if the cytoplasmic interaction would be observed to take place, *pch2* mutants co-expressing ASY1$^{1\text{-}570}$:mVenus and ASY1$^{1\text{-}570}$:mTurquiose2 that I have generated, should be analyzed to check whether this interaction really requires the closure motif. To complement the FRET experiment, I sought to perform an *in vivo* Bimolecular Fluorescence Complementation (BiFC) assay. Therefore, *pch2* mutants co-expressing either the ASY1:mVenus^{Nter} and ASY1:mVenus^{Cter} (split at 172-173 aa of mVenus) or ASY1$^{1\text{-}570}$:mVenus^{Nter} and ASY1$^{1\text{-}570}$:mVenus^{Cter} were generated. Next step would be to check whether there is an mVenus fluorescence complementation from the ASY1 intermolecular interactions, and if so whether the closure motif is involved. In addition, by taking using of the materials I have generated combing with FRET and BiFC analyses, it is possible to answer the long-standing questions of whether ASY1 really forms multi-intermolecular interactions at the chromosome axis and if so, of when and where this takes place during meiosis. **Second**, with the development of the higher sensitivity of confocal microscopy, the fluctuations of fluorescence intensity of ASY1:GFP and ASY1$^{1\text{-}570}$:GFP in the cytoplasm of living male meiocytes of *pch2* mutants can be measured using the Fluorescence Correlation Spectroscopy (FCS) technique, which reveals the concentrations and sizes of the fluorescent molecules thus reflecting the molecular compositions and dynamics of ASY1-containing molecules. **Third**, the immunoprecipitation experiment using flowers of *pch2* mutants expressing a functional PCH2:GFP reporter is worth trying for the identification of novel interactors of PCH2. This will help to understand the functional interplay of the ASY1 closure motif with PCH2. Once these different possibilities have been addressed experimentally, our understanding of the role of PCH2 and the mechanism

of the nuclear localization and chromosome assembly of ASY1 will be significantly broadened.

References

Allers T & Lichten M (2001) Differential timing and control of noncrossover and crossover recombination during meiosis. *Cell* **106:** 47–57

Armstrong SJ (2002) Asy1, a protein required for meiotic chromosome synapsis, localizes to axis-associated chromatin in Arabidopsis and Brassica. *Journal of Cell Science* **115:** 3645–3655

Armstrong SJ, Franklin FCH & Jones GH (2003) A meiotic time-course for Arabidopsis thaliana. *Sexual Plant Reproduction* **16:** 141–149

Barakate A, Higgins JD, Vivera S, Stephens J, Perry RM, Ramsay L, Colas I, Oakey H, Waugh R, Franklin FCH, Armstrong SJ & Halpin C (2014) The synaptonemal complex protein ZYP1 is required for imposition of meiotic crossovers in barley. *Plant Cell* **26:** 729–740

Bleuyard J-Y, Gallego ME & White CI (2004) Meiotic defects in the Arabidopsis rad50 mutant point to conservation of the MRX complex function in early stages of meiotic recombination. *Chromosoma* **113:** 197–203

Boateng KA, Yang X, Dong F, Owen HA & Makaroff CA (2008) SWI1 is required for meiotic chromosome remodeling events. *Molecular Plant* **1:** 620–633

Bolaños-Villegas P, De K, Pradillo M, Liu D & Makaroff CA (2017) In Favor of Establishment: Regulation of Chromatid Cohesion in Plants. *Front. Plant Sci.* **8:** 846

Bolcun-Filas E & Handel MA (2018) Meiosis: the chromosomal foundation of reproduction. *Biol. Reprod.* **99:** 112–126

Chambon A, West A, Vezon D, Horlow C, De Muyt A, Chelysheva L, Ronceret A, Darbyshire AR, Osman K, Heckmann S, Franklin FCH & Grelon M (2018) Identification of ASYNAPTIC4, a component of the meiotic chromosome axis. *Plant Physiol.***:** pp.01725.2017

Chelysheva L, Diallo S, Vezon D, Gendrot G, Vrielynck N, Belcram K, Rocques N, Márquez-Lema A, Bhatt AM, Horlow C, Mercier R, Mézard C & Grelon M (2005) AtREC8 and AtSCC3 are essential to the monopolar orientation of the kinetochores during meiosis. *Journal of Cell Science* **118:** 4621–4632

Chen C, Jomaa A, Ortega J & Alani EE (2014) Pch2 is a hexameric ring ATPase that remodels the chromosome axis protein Hop1. *Proc. Natl. Acad. Sci. U.S.A.* **111:** E44–53

Da Ines O, Degroote F, Goubely C, Amiard S, Gallego ME & White CI (2013) Meiotic Recombination in Arabidopsis Is Catalysed by DMC1, with RAD51 Playing a Supporting Role. *PLoS Genet* **9:** e1003787

de los Santos T & Hollingsworth NM (1999) Red1p, a MEK1-dependent phosphoprotein that physically interacts with Hop1p during meiosis in yeast. *J. Biol. Chem.* **274:** 1783–1790

Ferdous M, Higgins JD, Osman K, Lambing C, Roitinger E, Mechtler K, Armstrong SJ, Perry R, Pradillo M, Cuñado N & Franklin FCH (2012) Inter-homolog crossing-over and synapsis in Arabidopsis meiosis are dependent on the chromosome axis protein AtASY3. *PLoS Genet* **8:** e1002507

Geelen D (2016) Chromosome segregation in plant meiosis. **:** 1–19

GENETICS OF MEIOTIC PROPHASE I IN PLANTS (2016) GENETICS OF MEIOTIC PROPHASE I IN PLANTS. **:** 1–39

Gorbsky GJ (2015) The spindle checkpoint and chromosome segregation in meiosis. *FEBS J* **282:** 2471–2487

Hartung F, Wurz-Wildersinn R, Fuchs J, Schubert I, Suer S & Puchta H (2007) The catalytically active tyrosine residues of both SPO11-1 and SPO11-2 are required for meiotic double-strand break induction in Arabidopsis. *Plant Cell* **19:** 3090–3099

Henderson KA & Keeney S (2005) Synaptonemal complex formation: where does it start? *BioEssays* **27:** 995–998

Higgins JD, Sanchez-Moran E, Armstrong SJ, Jones GH & Franklin FCH (2005) The Arabidopsis synaptonemal complex protein ZYP1 is required for chromosome synapsis and normal fidelity of crossing over. *Genes & Development* **19:** 2488–2500

Ji J, Tang D, Shen Y, Xue Z, Wang H, Shi W, Zhang C, Du G, Li Y & Cheng Z (2016) P31comet, a member of the synaptonemal complex, participates in meiotic DSB formation in rice. **113:** 10577–10582

Joshi N, Barot A, Jamison C & Börner GV (2009) Pch2 links chromosome axis remodeling at future crossover sites and crossover distribution during yeast meiosis. *PLoS Genet* **5:** e1000557

Kim Y, Rosenberg SC, Kugel CL, Kostow N, Rog O, Davydov V, Su TY, Dernburg AF & Corbett KD (2014) The Chromosome Axis Controls Meiotic Events through a Hierarchical Assembly of HORMA Domain Proteins. *Developmental Cell* **31:** 487–502

Kurzbauer MT, Uanschou C, Chen D & Schlogelhofer P (2012) The Recombinases DMC1 and RAD51 Are Functionally and Spatially Separated during Meiosis in Arabidopsis. *Plant Cell* **24:** 2058–2070

Lambing C, Franklin FCH & Wang C-JR (2017) Understanding and Manipulating

Meiotic Recombination in Plants. *Plant Physiol.* **173:** 1530–1542

Lambing C, Osman K, Nuntasoontorn K, West A, Higgins JD, Copenhaver GP, Yang J, Armstrong SJ, Mechtler K, Roitinger E & Franklin FCH (2015) Arabidopsis PCH2 Mediates Meiotic Chromosome Remodeling and Maturation of Crossovers. *PLoS Genet* **11:** e1005372

Lee DH, Kao Y-H, Ku J-C, Lin C-Y, Meeley R, Jan Y-S & Wang C-JR (2015) The Axial Element Protein DESYNAPTIC2 Mediates Meiotic Double-Strand Break Formation and Synaptonemal Complex Assembly in Maize. *Plant Cell* **27:** 2516–2529

Litwin I, Pilarczyk E & Wysocki R (2018) The Emerging Role of Cohesin in the DNA Damage Response. **9:** 581

Ma H (2006) A Molecular Portrait of Arabidopsis Meiosis. *The Arabidopsis Book* **4:** e0095

Makrantoni V & Marston AL (2018) Cohesin and chromosome segregation. *Curr. Biol.* **28:** R688–R693

Marston AL & Wassmann K (2017) Multiple Duties for Spindle Assembly Checkpoint Kinases in Meiosis. *Front Cell Dev Biol* **5:** 109

Mercier R, Mézard C, Jenczewski E, Macaisne N & Grelon M (2015) The Molecular Biology of Meiosis in Plants. *Annu. Rev. Plant Biol.* **66:** 297–327

MIZPAH (2018) Cohesin Complexes and Sister Chromatid Cohesion in Mammalian Meiosis. **:** 1–23

Monje-Casas F, Prabhu VR, Lee BH, Boselli M & Amon A (2007) Kinetochore orientation during meiosis is controlled by Aurora B and the monopolin complex. *Cell* **128:** 477–490

Morales C & Losada A (2018) Establishing and dissolving cohesion during the vertebrate cell cycle. **52:** 51–57

Nairz K & Klein F (1997) mre11S--a yeast mutation that blocks double-strand-break processing and permits nonhomologous synapsis in meiosis. *Genes & Development* **11:** 2272–2290

Niu H, Wan L, Baumgartner B, Schaefer D, Loidl J & Hollingsworth NM (2005) Partner choice during meiosis is regulated by Hop1-promoted dimerization of Mek1. *Mol. Biol. Cell* **16:** 5804–5818

Osman K, Higgins JD, Sanchez-Moran E, Armstrong SJ & Franklin FCH (2011) Pathways to meiotic recombination in Arabidopsis thaliana. *New Phytologist* **190:** 523–544

Otegui M & Staehelin LA (2000) Cytokinesis in flowering plants: more than one way to divide a cell. *Curr. Opin. Plant Biol.* **3:** 493–502

Pawlowski WP, Golubovskaya IN, Timofejeva L, Meeley RB, Sheridan WF & Cande WZ (2004) Coordination of meiotic recombination, pairing, and synapsis by PHS1. *Science* **303:** 89–92

Prusicki MA, Keizer EM, van Rosmalen RP, Komaki S, Seifert F, Müller K, Wijnker E, Fleck C & Schnittger A (2018) Live cell imaging of meiosis in Arabidopsis thaliana - a landmark system. *bioRxiv***:** 446922

Puizina J, Siroky J, Mokros P, Schweizer D & Riha K (2004) Mre11 deficiency in Arabidopsis is associated with chromosomal instability in somatic cells and Spo11-dependent genome fragmentation during meiosis. *Plant Cell* **16:** 1968–1978

RILEY R & CHAPMAN V (1958) Genetic Control of the Cytologically Diploid Behaviour of Hexaploid Wheat. *Nature* **182:** 713–715

Ronceret A, Doutriaux M-P, Golubovskaya IN & Pawlowski WP (2009) PHS1 regulates meiotic recombination and homologous chromosome pairing by controlling the transport of RAD50 to the nucleus. *Proc. Natl. Acad. Sci. U.S.A.* **106:** 20121–20126

Sanchez-Moran E, Santos JL, Jones GH & Franklin FCH (2007) ASY1 mediates AtDMC1-dependent interhomolog recombination during meiosis in Arabidopsis. *Genes & Development* **21:** 2220–2233

Shingu Y, Mikawa T, Onuma M, Hirayama T & Shibata T (2010) A DNA-binding surface of SPO11-1, an Arabidopsis SPO11 orthologue required for normal meiosis. *FEBS J* **277:** 2360–2374

Stacey NJ, Kuromori T, Azumi Y, Roberts G, Breuer C, Wada T, Maxwell A, Roberts K & Sugimoto-Shirasu K (2006) Arabidopsis SPO11-2 functions with SPO11-1 in meiotic recombination. *Plant J* **48:** 206–216

Sybenga J (1999) What makes homologous chromosomes find each other in meiosis? A review and an hypothesis. *Chromosoma* **108:** 209–219

Vrielynck N, Chambon A, Vezon D, Pereira L, Chelysheva L, De Muyt A, Mézard C, Mayer C & Grelon M (2016) A DNA topoisomerase VI-like complex initiates meiotic recombination. *Science* **351:** 939–943

Wang K, Wang M, Tang D, Shen Y, Qin B, Li M & Cheng Z (2011) PAIR3, an axis-associated protein, is essential for the recruitment of recombination elements onto meiotic chromosomes in rice. *Mol. Biol. Cell* **22:** 12–19

Wang M, Wang K, Tang D, Wei C, Li M, Shen Y, Chi Z, Gu M & Cheng Z (2010) The central element protein ZEP1 of the synaptonemal complex regulates the number of crossovers during meiosis in rice. *Plant Cell* **22:** 417–430

Wang Y & Copenhaver GP (2018) Meiotic Recombination: Mixing It Up in Plants. *Annu. Rev. Plant Biol.* **69:** 577–609

Watanabe Y (2012) Geometry and force behind kinetochore orientation: lessons from meiosis. *Nat Rev Mol Cell Biol* **13:** 370–382

Waterworth WM, Altun C, Armstrong SJ, Roberts N, Dean PJ, Young K, Weil CF, Bray CM & West CE (2007) NBS1 is involved in DNA repair and plays a synergistic role with ATM in mediating meiotic homologous recombination in plants. *Plant J* **52:** 41–52

Wellmer F, Alves-Ferreira M, Dubois A, Riechmann JL & Meyerowitz EM (2006) Genome-wide analysis of gene expression during early Arabidopsis flower development. *PLoS Genet* **2:** e117

West AMV, Komives EA & Corbett KD (2018) Conformational dynamics of the Hop1 HORMA domain reveal a common mechanism with the spindle checkpoint protein Mad2. *Nucleic Acids Research* **46:** 279–292

Wojtasz L, Daniel K, Roig I, Bolcun-Filas E, Xu H, Boonsanay V, Eckmann CR, Cooke HJ, Jasin M, Keeney S, McKay MJ & Tóth A (2009) Mouse HORMAD1 and HORMAD2, two conserved meiotic chromosomal proteins, are depleted from synapsed chromosome axes with the help of TRIP13 AAA-ATPase. *PLoS Genet* **5:** e1000702

Yang C, Hamamura Y, Sofroni K, Böwer F, Stolze SC, Nakagami H & Schnittger A (2019) SWITCH 1/DYAD is a WINGS APART-LIKE antagonist that maintains sister chromatid cohesion in meiosis. *Nat Commun* **10:** 1755

Zickler D & Kleckner N (2015) Recombination, Pairing, and Synapsis of Homologs during Meiosis. *Cold Spring Harb Perspect Biol* **7:** a016626

Publications and presentations

Publications

Yang, C., Hamamura, Y., Sofroni, K., Böwer, F., Stolze, S.C., Nakagami, H., Schnittegr, A. (2019) SWITCH 1/DYAD is a WINGS APART-LIKE antagonist that maintains sister chromatid cohesion in meiosis. ***Nature Communications*** 10, 1755 (2019)

Yang, C., Sofroni, K., Wijnker, E., Hamamura, Y., Carstens, L., Harashima, H. Stolze, S.C., Vezon, D., Chelysheva, L., Orban-Nemeth, Z., Pochon, G., Nakagami, H., Schlögelhofer, P., Grelon, Schnittger, A. The *Arabidopsis* Cdk1/Cdk2 homolog CDKA;1 controls the chromosome axis assembly in meiosis. (**under revision on *The EMBO Journal***)

Oral presentations

- The 29th 'International Conference on Arabidopsis Research', Turku, Finland, June 25 – 29, 2018
- The 2nd 'Biology Conference of Doctoral Candidates', Hamburg, Germany, May 4, 2018
- The 'Students and Postdocs Meiosis Workshop', Montpellier, France, Sept. 19 - 20, 2016

Poster presentations

- The 30th 'International Conference on Arabidopsis Research', Wuhan, China, June 16 – 20, 2019
- The 'Plant Cell and Developmental Biology' conference, Cold Spring Harbor Asia, China, May 22 – 26, 2017
- The 'Gordon Research Conference – Meiosis', New London, NH, USA, June 26 - July 1, 2016

Eidesstattliche Versicherung /Declaration On Oath

Hiermit erkläre ich an Eides statt, dass ich die vorliegende Dissertationsschrift selbst verfasst und keine anderen als die angegebenen Quellen und Hilfsmittel benutzt habe.

I hereby declare, on oath, that I have written the present dissertation by my own and have not used other than the acknowledged resources and aids.

Hamburg, den Unterschrift

Declaration of contributions

I hereby declare that all results shown in this thesis are obtained by my own except for the ones indicated in the respective figure legends. Here I summarize the contributions from collaborators as below.

In chapter 1:

- The Figures 1A and 8B are kindly provided by Yuki Hamamura using the materials prepared by Chao Yang.
- The Figures 8A, S2F, S3D, S5D and S12 are kindly provided by Kostika Sofroni using the materials prepared by Chao Yang.
- The Figures S1C, S7B and S8 are obtained by the joint contributions of Fanziska Böwer, Kostika Sofroni and Chao Yang.
- For Table S1, the kinase assay is performed by Chao Yang and the subsequent mass spectrometry analysis is kindly performed by Sara Christina Stolze and Hirofumi Nakagami.
- All movies are kindly generated by Yuki Hamamura using the materials prepared by Chao Yang.

In chapter 2:

- The Figure 1 is made from the data provided kindly by Kostika Sofroni, Erik Wijnker, Daniel Vezon, Liudmila Chelysheva and Mathilde Grelon.
- The Figures EV1C, Appendix Figure S2C and D are kindly provided by Kostika Sofroni.
- The Figure EV1D, F and G are kindly provided by Erik Wijnker, Daniel Vezon, Liudmila Chelysheva and Mathilde Grelon.
- The Appendix Figure 3 is kindly provided by Lev Böttger supervised by Chao Yang who prepared the materials.
- The mass spectrometry analysis in Appendix Figure 2A is kindly performed by Sara Christina Stolze and Hirofumi Nakagami.
- The Appendix Movie 1 is kindly provided by Kostika Sofroni.

_____

Chao Yang

Confirmation of correct English

7/1/19

To Whom it may concern,

I confirm, that I, John Paul Bowers II, a native english speaker have read and revised the thesis submitted by Chao Yang.

Sincerely,
John Paul Bowers II Passport # 488254766

Acknowledgements

Wow! What a wonderful journey! After more than 4 years, the exciting moment to wrap my life of Ph.D. study up is finally coming. Since March 2015, I have come to Hamburg and luckily joined in the laboratory of Prof. Dr. Arp Schnittger for my Ph.D. thesis research. During the journey of my Ph.D. study, I have received lots of help and fun supporting my life and study from all the lab members to whom I would like to deliver my cordial acknowledgements.

First of all, I thank my supervisor Prof. Dr. Arp Schnittger for giving me the opportunity to achieve my Ph.D. study in his team, which is very precious for me. He is not only an excellent advisor, but also a good friend to me. I have learned many great things from him regarding both scientific research and the development of an academic career, which will definitely guide my path for science.

Second, I thank all my colleagues and collaborators for giving so much help and fun for my research and routine life. Many thanks to Maren (secretary), Gaëtan, Dagmar, Katja, Maren, Reinhold, Yuki, Kostika, Maria, Joke, Martina, Mariana, Franzi, Lucas, Max, Poyu, Dave, Jara, Peter, Jantje, Susanne, Wojciech, Oscar, Viola, Kostas, Stephan, Vanesa, Shinichiro, Xinai and others I may forget to mention. Thanks all of you for making my journey so meaningful and memorable.

Third, I thank Dr. Maren Heese, Prof. Dr. Arp Schnittger and Prof. Dr. Sigrun Reumann for critical reading and/or examining this dissertation.

Finally, I am grateful to my parents. They are so supportive and helpful, which makes my journey go smoothly. Thanks for your great dedication.

This journey is destined to be unforgettable!